University of Oxford

Doctor of Philosophy (D.Phil) Thesis

Investigating the effects of a point mutation in the TRPC3 channel – cause of cerebellar ataxia in *Moonwalker* mice – on the Purkinje cells in mice

Anna Dulneva
Queen's College
2012

Supervisor: Prof Kay E Davies
MRC Functional Genomics Unit, Department of Physiology, Anatomy and Genetics

Abstract

The *Moonwalker* (*Mwk*) mouse is a mouse model of cerebellar ataxia that harbours a point mutation in the *Trpc3* gene. TRPC3 is a non-selective cation channel, most highly expressed in the Purkinje cells of the cerebellum. The gain-of-function mutation in the TRPC3 protein affects the development of Purkinje cell dendrites by reducing their branching, and also leads to abnormal motor coordination and cerebellar ataxia in *Mwk* mice at the age of 3 weeks. The aim of this thesis was to determine how the mutation in the TRPC3 channel results in the observed pathology.

Proper function of the TRPC3 channel relies on its interaction with other proteins, hence we investigated binding partners of TRPC3. The study revealed PI synthase and CaMKIV as novel interaction partners of TRPC3. PI synthase is implicated in the upstream signalling events leading to TRPC3 activation, whereas CaMKIV is activated by Ca^{2+}, possibly due to TRPC3 activation. We have identified alterations in phosphorylation of several key Ca^{2+} signalling proteins (CaMKII, CaMKIV, CREB and ERK), which indicates that there are changes in Ca^{2+} homeostasis in *Mwk* cerebella. Down-regulation of CaMKIV and up-regulation of CREB phosphorylation occurs as early as P21, which indicates that their abnormal activity could contribute to the *Mwk* phenotype. Microarray analysis comparing wild-type and *Mwk* Purkinje cells has revealed gene expression changes, which are likely due to abnormal Ca^{2+} signalling. Genes *Ipo5, Opn3* and *Sv2c* are up-regulated at P11; *Car2* and *Stk17b* are down-regulated at P14; and *Cntn3* is up-regulated at P18 in *Mwk* Purkinje cells. High quality RNA from Purkinje cells was extracted using an optimised laser-capture microdissection method.

Work on the *Mwk* mice points to the importance of TRPC3 activity for the proper development of Purkinje cell dendrites and depicts TRPC3 as a possible target for cerebellar ataxia treatment.

Declaration

The work presented in this thesis was performed in the Department of Physiology, Anatomy and Genetics, University of Oxford, and funded by the Medical Research Council. Except where acknowledgement is made, all the work presented is my own and has not been submitted for any other degree in this or any other university or institute of learning.

Acknowledgements

First, I would like to thank Kay for the opportunity she has given me, for her constant support and encouragement and for being an excellent role model.

I would also like to thank Esther, a brilliant scientist, with, no doubt, a bright and successful future in front, who has been by my side throughout the years, helping me every step of the way.

I am very thankful to my family, who have given me the opportunity to study abroad, and who always believed in me, sometimes too much.

A big thanks goes to Dirk and Justin, who not only helped me with various questions, but also made our lab corner the most fun to work in, not to mention the enjoyable coffee breaks. I would also like to thank other students in the unit, who were always great to talk to: Alice, Mattea, Akshay, Alistair, Tom, Grant, Ghows, Sian, James and Greg.

I would like to thank all the post docs in our lab: Emmanuelle, who is the most positive person I know; Becki, who I could talk to about anything, and who dragged me to the gym when I didn't want to go; Pete, who is always happy to help; Carmen, who is never too busy for you and who makes the best cakes; Angie, who loves dance as much as I do; Neza, who was always in the lab in the evenings; Aurelie, who is full of happiness; Janet, whose hard work is inspiring. I would also like to thank Holger, who was always interested in my work and was willing to help every time.

I would like to thank the people in the most entertaining office: Dave, Sarah, Ben, Ally and Viv, who were always there to lift my spirits. Big thanks also goes to Arran for tea chats and useful photography tips!

Thanks goes to Sergei and Kate, who brought adventure to our life, and a sense of home, while abroad.

Julian has motivated and encouraged me throughout the writing, for which I am very thankful to him.

I would like to thank Amira, who I have met on the first day of the DPhil, and we have been through the whole process together.

I am thankful to have met so many great people at Queen's college, especially Kathy, Frida, Jonathan and Young, who made my first year filled with fun.

I would also like to thank all my friends here, back home and all around the world, for being so great.

Last but not least, I would like to thank Daniil, who has been with me through the ups and downs of my DPhil and who was undoubtedly the most supportive and encouraging person by my side. I could not have done it without you!

Table of Contents

List of Figures

List of Tables

List of Abbreviations

ALS	Amyotrophic lateral sclerosis
AMPA	α-amino-3-hydroxy-5-methyl-4-isoxazolepropionic acid
BDNF	Brain-derived neurotrophic factor
Bet1	Blocked early in transport 1 homolog
CA	Carbonic anhydrase
Ca^{2+}	Calcium
CaM	Calcium/Calmodulin
CaMKII	Calcium/Calmodulin-dependent protein kinase type II
P-CaMKII	Phosphorylated CaMKII
CaMKIV	Calcium/Calmodulin-dependent protein kinase type IV
P-CaMKIV	Phosphorylated CaMKIV
CaMKK	Calcium/calmodulin-dependent protein kinase kinase
Car2	Carbonic anhydrase 2
CBP	CREB-binding protein
CIRB	Calmodulin/IP_3R binding
Cntn3	Contactin 3
CREB	Cyclic-AMP response element binding protein
P-CREB	Phosphorylated CREB
DAG	Diacylglycerol
DHPG	(S)-3,5-dihydroxyphenylglycine
DA	Dopaminergic
EGL	External granule cell layer
Elk1	ETS-like transcription factor
ENU	N-ethyl N-nitrosourea
ER	Endoplasmic Reticulum
ERK	Extracellular signal regulated kinase
P-ERK	Phosphorylated ERK
FACS	Fluorescence activated cell sorting
GABA	Gamma-aminobutyric acid
Glu	Glutamate
GST	Glutathione S-transferase
GFP	Green fluorescent protein
HEK293T	Human embryonic kidney 293T cells
Hn1l	Hematological and neurological expressed 1-like
ICC	Immunocytochemistry
IGL	Internal granule cell layer
IHC	Immunohistochemistry
IP	Immunoprecipitation

IP_3	Inositol 1,4,5-trisphosphate
IP_3R1	IP_3 receptor 1
Ipo5	Importin 5
Flt3	FMS-like tyrosine kinase 3
Fbrs	Fibrosin
LCM	Laser-capture microdissection
LTD	Long-term depression
MAPK	Mitogen-activated protein kinase
MEK	MAPK/ERK kinase
mGluR1	Metabotropic glutamate receptor 1
Mwk	Moonwalker
NFAT	Nuclear factor of activated T-cells
Nlk	Nemo-like kinase
OAG	1-oleoyl-2-acetyl-sn-glycerol
Opn3	Opsin3
PD	Parkinson's Disease
PI synthase	Phosphatidylinositol synthase
PIP_2	Phosphatidylinositol 4,5-bisphosphate
PLCβ4	Phospholipase C beta 4
PLC δ3	Phospholipase C delta 3
PLD	Phospholipase D
PLIER	Probe Logarithmic Intensity ERror
PKCγ	Protein kinase C gamma
PP2A	Protein serine/threonine phosphatase 2A
qRT-PCR	Quantitative real time PCR
RIN	RNA Integrity Number
RMA	Robust Multichip Average
RSK	Ribosomal S6 kinase
RyR	Ryanodine receptor
SCA	Spinocerebellar ataxia
SERCA	Smooth endoplasmic reticulum calcium ATPase
SNAP25	Synaptosomal-associated protein 25
Stk17b	Serine-threonine kinase 17b, apoptosis-inducing
Stx1A	Syntaxin 1A
Stx1B	Syntaxin 1B
SV2	Synaptic vesicle 2
Sv2c	Synaptic vesicle glycoprotein 2c
TESS	Transcription Element Search System
TRPC	Transient Receptor potential canonical channel
TRPC3	Transient receptor potential canonical channel, type 3
Tsg101	Tumor susceptibility gene 101

Unc13c	Unc-13 homolog C
VGCC	Voltage-gated calcium channel
WT	Wild-type
Y2H	Yeast two hybrid
Zbtb20	Zink finger and BTB domain containing 20

CHAPTER 1. Introduction

According to the World Health Organisation, up to one billion people across the world suffer from neurological disorders, and it costs the European economy billions of pounds every year (www.who.int).

A disease called cerebellar ataxia is one of the neurological disorders. It can be found in 1-4 out of 100,000 people and no treatment is currently available. Cerebellar ataxia is the disease of the cerebellum, characterised by the loss of neurons and their connections. Usually, the symptoms of the disease occur between 30 and 50 years of age. They include abnormalities in the execution of voluntary movements, lack of coordination, slurred speech, and inability to swallow and breathe smoothly, which could even lead to death (Durr 2010; Koeppen 2005; Manto 2005; Matilla-Duenas 2008; Orr 2012; Taroni & DiDonato 2004; Zoghbi & Orr 2000).

Studying the cerebellum, its development and disease mechanisms leading to ataxia would be very important in order to develop new therapies for the treatment of cerebellar ataxia.

Cerebellum

The word cerebellum means “little brain” in Latin. The cerebellum is a region in the brain important for motor control: it analyses the differences between intention and action and regulates the process of motor centres in the cortex and brain stem during a movement; the cerebellum is also important for motor learning (Ghez & Thach 2000). It allows us to move accurately and precisely, gives us the ability to learn complex movement sequences and lets us control our posture and balance (Hartmann et al 2011; Hibi & Shimizu 2012; Ito 2002; Tanaka 2009).

The cerebellum is positioned at the base of the brain, with the pons in front of it and the cerebral cortex above it. Despite it being only 10% of the total brain volume, the cerebellum contains more than half of all neurons. It has a simple structure, comprising of three layers: the innermost layer, called the granule cell layer, which consists of granule cells and the Golgi cells; the thin layer in the middle which is made up entirely of Purkinje cell bodies and is called the Purkinje cell layer; and the outermost layer, the molecular layer, which contains basket and stellate cells, as well as Purkinje cell dendrites (Miale & Sidman 1961). The schematic structure of the cerebellum is demonstrated in Figure 1-1. The input of the cerebellum is much greater than its output and provides visual, auditory, vestibular and somatosensory inputs from the spinal cord and the cerebral cortex. The only output that projects outside of the cerebellar cortex is provided by Purkinje cells, which project their axons to the deep cerebellar nuclei, located at the core of the cerebellum (Sotelo 2004). Deep cerebellar nuclei provide the cerebellar output to the thalamus, red nucleus, vestibular nucleus, etc. for motor planning, execution and balance. The whole cerebellar circuit is organised around Purkinje cells, which makes them crucial for receiving, processing and channelling the information of the cerebellar cortex (Ghez & Thach 2000).

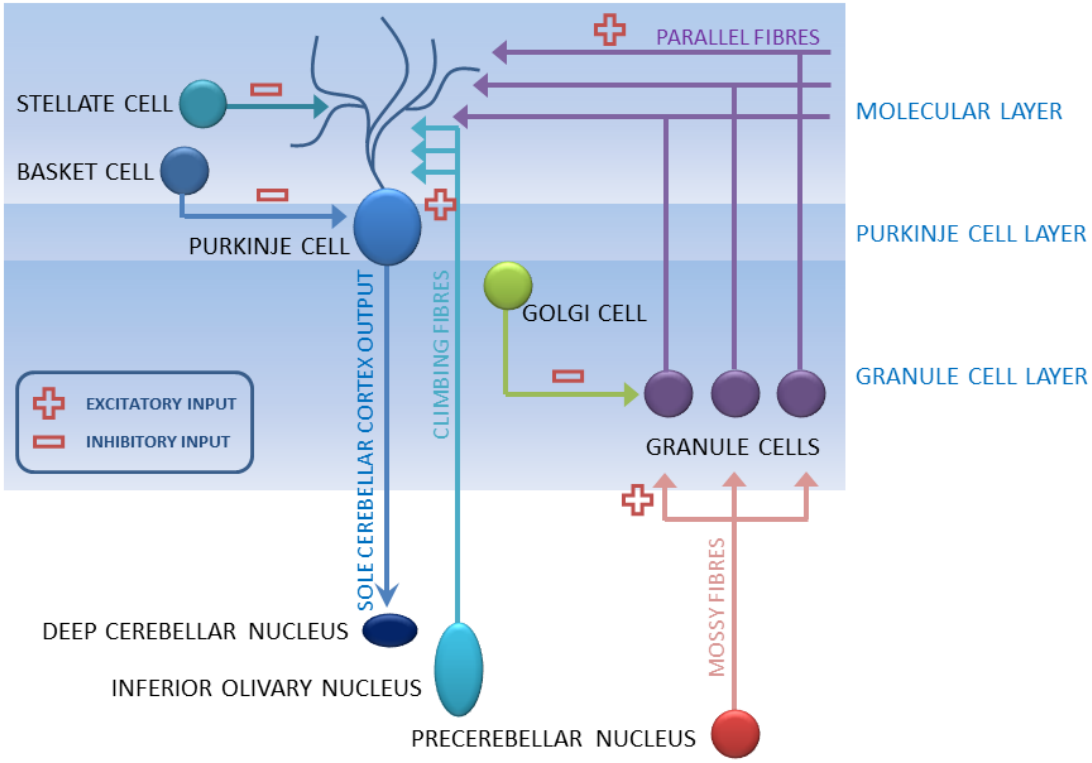

Figure 1-1. The structure of the mature cerebellum. The cerebellum consists of three layers: the granule cell layer, the Purkinje cell layer and the molecular layer. The granule cell layer is very dense and consists of a large number of granule cells as well as Golgi cells. The Purkinje cell layer is occupied by the cell bodies of Purkinje cells. The dendrites of Purkinje cells extend into the molecular layer of the cerebellum, which also contains basket and stellate cells. Purkinje cell axons connect with the deep cerebellar nuclei and form the sole output of the cerebellar cortex. Purkinje cells receive inhibitory synaptic inputs from basket and stellate cells and excitatory synaptic inputs from granule cells and inferior olive. Granule cells extend their axons – the parallel fibres – into the molecular layer and form more than 100,000 synapses with just one Purkinje cell dendritic tree. Granule cells receive their main input from precerebellar nuclei via mossy fibres and also from Golgi cells. Inferior olive is located in the medulla oblongata and extends its axon – the climbing fibre – into the cerebellum to form around 100 synapses with the proximal part of one dendritic tree.

- **Development of the mouse cerebellum**

The cerebellum undergoes a 1000 fold increase in its volume and forms a layered structure in the first three-four weeks after birth (Goldowitz & Hamre 1998; Tanaka 2009). The Purkinje cells are born early in development, but the growth of the dendritic tree only occurs after birth during the first four weeks (Kapfhammer 2004). In the first postnatal week, the Purkinje cells become aligned in the Purkinje cell layer, the initial dendritic process develops side branches, and a few more dendritic processes can form in any direction (Figure 1-2). The period between the second and the fourth postnatal weeks is when the main primary dendrite emerges and starts undergoing rapid growth and branching to form secondary and tertiary dendrites, extending into the molecular layer of the cerebellum (Kapfhammer 2004; Tanaka 2009). Most Purkinje cells have one primary dendrite, whereas some have two or even more (Tanaka 2009). It has also been demonstrated, that for the normal development of Purkinje cell dendritic tree, the dendrites not only need to extend, but also

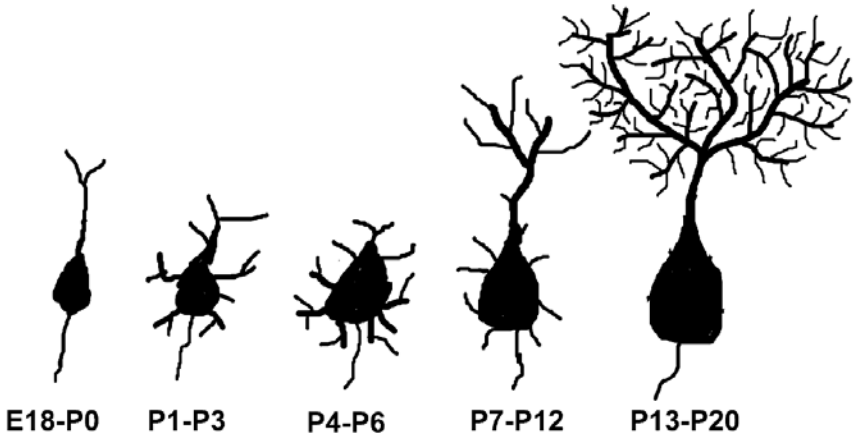

Figure 1-2. The developmental stages of the Purkinje cells of the cerebellum. The Purkinje cell body is generated during embryogenesis, but the development of its dendritic tree takes place postnatally. During the first postnatal week, several dendritic processes can form, which start to develop side branches. During the second postnatal week the primary dendrite starts to emerge and during the third and fourth postnatal weeks is when the dendrite undergoes rapid growth and branching, as well as some retraction. The development of the Purkinje cell dendritic tree takes about four weeks, after which it is considered mature. Taken with permission from Kapfhammer 2004.

retract (Tanaka et al 2006b). The process of the dendritic tree formation takes 2-3 weeks and is complete by the fourth postnatal week (Hendelman & Aggerwal 1980).

Granule cells at first are localised to the outer layer of the cerebellum, which is referred to as external granule cell layer (EGL) (Miale & Sidman 1961). The cells from the EGL then start migrating inwards through the Purkinje cell layer along Bergmann glial cells, and form an internal granule cell layer (IGL). The migration process is controlled by a molecular interaction between the granule cells and Bergman glial fibres (Hatten & Heintz 1995). The EGL disappears during the third postnatal week, and IGL remains the only granule cell layer in the developed structure (Goldowitz & Hamre 1998; Hatten & Heintz 1995). Stellate and basket cells are generated postnatally and they occupy the molecular layer of the cerebellum (Spatkowski & Schilling 2003).

The dendrites of Purkinje cells receive two different glutamatergic excitatory inputs, which are key determinants of the cerebellar function: inputs from inferior olive and inputs from granule cells (Hartmann et al 2011). Inferior olive neurons are located in the medulla oblongata and they project their axons, which are called the climbing fibres, into the cerebellum to form synapses with the Purkinje cells. Purkinje cells start receiving synaptic input from the climbing fibres during embryogenesis and continue during the first postnatal week (Morara et al 2001). Climbing fibres convey somatosensory, visual and cerebral cortical information to Purkinje cells. Several climbing fibres innervate a Purkinje cell at first, with substantial elimination occurring later, with one climbing fibre retaining approximately 100 contacts with the proximal part on the dendritic tree of only one Purkinje cell (Ito 1984). Climbing fibres generate a very powerful synaptic effect on Purkinje cells, producing a prolonged voltage-gated calcium conductance in Purkinje cells and evoking a complex spike (Ghez & Thach 2000).

Granule cells of the cerebellum are the most abundant neurons in the whole brain (Hartmann et al 2011). Granule cells receive input from mossy fibres that originate from nuclei in the spinal cord and brain stem and carry sensory information from the periphery and cerebral cortex (Ghez & Thach 2000). Mossy fibres convey information to Purkinje cells via axons of granule cells, i.e. parallel fibres. Starting from the second postnatal week, granule cells extend the parallel fibres into the molecular layer of the cerebellum to form many synapses with the dendrites of Purkinje cells (Hatten & Heintz 1995; Ito 1984; Kapfhammer 2004). Each parallel fibre forms one or a few of more than 100,000 synapses across the whole dendritic tree of just one Purkinje cell (Ito 1984; Takechi et al 1998). Parallel fibres generate a brief excitatory postsynaptic potential in Purkinje cells, which evokes a simple spike (Ghez & Thach 2000).

GABAergic inhibitory inputs to the Purkinje cells are provided by basket and stellate cells that are located in the molecular layer of the cerebellum (Spatkowski & Schilling 2003).

- **Development of dendrites in general**

Dendritic tree formation is a very dynamic and tightly controlled process. It undergoes extension and retraction of newly formed branches, formed by dynamic actin filaments,and is followed by stabilisation of existing dendrites through building of synapses. Even though dendritic morphologies of neurons vary tremendously, the process of dendritic maturation has a common mechanism among different types of neurons. The initial process of dendritic outgrowth and patterning is controlled by genetic processes inside the neurons, supported by local growth factors. It is known to significantly influence the specification of the dendritic architecture. This has been established in culture experiments, where particular neurons are isolated from extrinsic cues and still develop features of their specific morphology. The later stages of dendritic development are crucial for the full dendritic

maturation and require synaptic inputs from connecting neuronal cells, as well as some intrinsic factors (Fujishima et al 2012; Matus 2000; Metzger 2010; Sotelo & Dusart 2009).

- **Development of Purkinje cell dendrites**

Purkinje cells are some of the most distinctive neurons in the brain and can be easily identified based on their morphology (Figure 1-3). Their dendritic tree is very large, highly branched and flat, which can be revealed by staining the cerebellum with a Purkinje cell specific marker – calbindin (Celio 1990). Due to their highly elaborate dendritic tree, they have been used to study the regulation of dendritic development (Kapfhammer 2004).

Branching of Purkinje cell dendrites most of the time occurs through terminal branching, i.e. division of growing tips. In some instances, the branches are formed by extension of collaterals from the

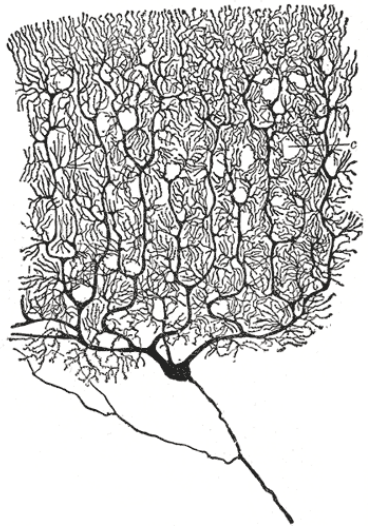

Figure 1-3. Structure of a single Purkinje cell, illustrated by Ramón y Cajal. The Purkinje cell is one of the most distinctive neurons of the brain. They have been first described in 1837 by Purkinje and were the first neurons to be discovered (Orr 2012; Tanaka 2009). Purkinje cells have very large somata. Most Purkinje cells have one primary dendrite, whereas some have more. Their primary dendrite undergoes a period of rapid branching which results in a very large, highly elaborate, yet flat dendritic tree. The illustration was taken from the book "Histology of the Nervous System", Volume II, with permission from the Oxford University Press.

dendritic shaft. In the initial stages of dendritic development, retraction of branches occurs upon contact with other growing dendrites. This not only occurs among branches of the same cell, but also between neighbouring cells of the same type. Contact-dependent retraction of dendritic branches is important for the morphogenesis of Purkinje cells and facilitates a complete coverage of the neuron's territory (Fujishima et al 2012; Grueber & Sagasti 2010; Lefebvre et al 2012).

The dendritic tree of Purkinje cells can develop a certain complexity without inputs from connecting neurons through climbing fibres or mossy/parallel fibres. This was shown in experiments in rats where granule cells were killed by X-irradiation, and Purkinje cells still developed dendritic trees, although the size and complexity of dendritic arbours was significantly reduced with no higher order dendrites and the trees lost their spatial orientation (Altman & Anderson 1972; Hamori 1969). Studies in *weaver* mice which display death of granule cells before any afferent connections are formed have shown that Purkinje cells require parallel fibre stimulation to form a sagitally-oriented dendritic tree (Rakic & Sidman 1973). Purkinje cells in slice cultures demonstrate a similar story. These results indicate that intrinsic determinants play an important role in the development of Purkinje cell dendrites. These include growth factors and neurotrophins, such as brain-derived neurotrophic factor (BDNF), although the data on BDNF involvement in Purkinje cell dendritic development is controversial (Hirai & Launey 2000; McAllister et al 1995; Schwartz et al 1997; Shimada et al 1998), and growth factors corticotropin-releasing factor (CRF) and urocortin (Palkovits et al 1987; Swinny et al 2002; Swinny et al 2004). Intrinsic factors that are also involved in Purkinje cell dendritic development include hormones: thyroid, estrogen and progesterone (Sakamoto et al 2003; Sakamoto et al 2002; Vincent et al 1982).

Other aspects of Purkinje cell development, such as formation of highly complex dendritic trees, can only be seen during normal *in vivo* development and thus require synaptic input, mainly from granule cells (Fujishima et al 2012; Metzger 2010; Sotelo & Dusart 2009).

- **Key genes responsible for Purkinje cell development**

The development of any neuron requires activation of certain molecular pathways, and alterations to these pathways could lead to developmental abnormalities. Purkinje cells have a very complex dendritic tree, which must be regulated by a precise mechanism. The molecular mechanisms that are required for Purkinje cell dendritic development are largely unknown.

One gene has been implicated in the development of Purkinje cell dendritic tree: protein kinase C γ (PKCγ). PKCγ is the most abundant PKC isoform in the Purkinje cells and is not expressed in other neurons of the cerebellum (Barmack et al 2000; Kose et al 1988; Saito et al 1988). Its expression in the Purkinje cells is developmentally regulated, as it starts increasing from birth until the third postnatal week, which suggests that it could be involved in neuronal development (Hashimoto et al 1988). Activation of PKC in slice cultures results in a severely altered dendritic tree of Purkinje cells, with shorter primary dendrites and less terminal branches; whereas PKC inhibition causes an increase in dendritic growth (Gugger et al 2012; Metzger & Kapfhammer 2000). In addition, Purkinje cells in mice lacking the PKCγ isoform have an enlarged dendritic tree with more branch points, compared to control neurons (Schrenk et al 2002). These observations lead to a conclusion that PKCγ is involved in the development of the dendritic tree of Purkinje cells by inhibiting its growth and branching, and hence is important for the normal function of the cerebellum. Another isoform – PKCα, but not PKCβ, has also been implicated in the regulation of dendritic development of Purkinje cells, but only upon its activation from a reserve pool if needed (Gundlfinger et al 2003). Recent studies have shown that inhibition of Purkinje cell dendritic growth by PKC involves calcium entry through P/Q-type and T-type

voltage-gated calcium channels (VGCCs), which highlights the importance of calcium for proper development of Purkinje cell dendrites (Gugger et al 2012).

Another gene that has been shown to influence dendritic tree development of Purkinje cells is stathmin. Unlike PKCγ, expression of stathmin is down-regulated during cerebellar development through reduced gene expression and also through deactivation by calcium/calmodulin-dependent kinases (CAMK) CaMKII and CaMKIV (Belmont et al 1996; Gradin et al 1997; Ohkawa et al 2007). In cultured neurons, over-expression of stathmin limits the growth of the dendritic tree, which occurs through destabilisation of microtubules. Interestingly, knockdown of endogenous stathmin also resulted in abnormal growth of Purkinje cell dendrites (Ohkawa et al 2007). Therefore accurate regulation of stathmin is important for dendritic arborisation of Purkinje cells, which is mediated through control of microtubule dynamics.

A serine/threonine protein kinase CaMKII is involved in calcium-dependent neuronal dendritic differentiation (Fink et al 2003; Gaudilliere et al 2004; Vaillant et al 2002; Wu & Cline 1998). In Purkinje cells, inhibition of CaMKII reduced the number of primary dendrites as well as the total dendritic length (Ohkawa et al 2007; Tanaka et al 2006b). This makes CaMKII another molecule that is important for Purkinje cell dendritic morphogenesis (Tanaka 2009).

Homer1, a scaffolding protein, can also affect Purkinje cell dendritic morphology via controlling calcium release from intracellular stores(Tanaka et al 2006a).

More studies are required to be able to better understand the complicated mechanism behind the development of the highly elaborate dendritic tree of Purkinje cells.

- **Calcium in Purkinje cell development**

Calcium (Ca^{2+}) is an essential, ubiquitous second messenger that controls important processes in brain development (Tai et al 2009). It's role in the nervous system is extremely important, as it is responsible for many mechanisms, including neuronal proliferation and survival, synaptic transmission and plasticity, dendritic development, learning and memory (Berridge 1995; 1998; Ginty 1997; Greer & Greenberg 2008; Lynch et al 1983; Malenka et al 1988; Mellstrom & Naranjo 2001; Tai et al 2008; Wojda et al 2008; Zieg et al 2008). Consequences of abnormal calcium homeostasis in neuronal cells have been implicated in neurological diseases, such as spinocerebellar ataxias (SCAs), Alzheimer's, Parkinson's, Huntington's and amyotrophic lateral sclerosis (ALS) (Bezprozvanny 2009; Wojda et al 2008).

Purkinje cells of the cerebellum express many Ca^{2+} channels, transporters and Ca^{2+} binding proteins (Liu et al 2009). They possess a powerful Ca^{2+} signalling system with a high Ca^{2+} buffering capability, which indicates that Ca^{2+} signalling is crucial for the normal function of these neurons (Vig et al 2001). Moreover, in the Purkinje cells, Ca^{2+} ions are involved in the dendritic growth, which is a complicated process that requires substantial dendritic branching (Schilling et al 1991).

Molecular events that take place downstream of Ca^{2+} signalling involve phosphorylation cascades and include some key neuronal calcium signalling pathways, such as the Ca^{2+}/calmodulin-dependent protein (CaM) kinase signalling cascade, the mitogen-activated protein (MAP) kinase signalling cascade and the nuclear factor of activated T-cells (NFAT) signalling cascade, which are involved in the regulation of gene transcription (Greer & Greenberg 2008; Zieg et al 2008).

Cerebellar ataxia

Damage to the cerebellum causes abnormalities in spatial accuracy and temporal coordination of movement, as well as impaired balance and reduced muscle tone. However, the cerebellum is not essential for movement or perception, which has been demonstrated by its removal. One of the neurodegenerative disorders of the cerebellum that results from degeneration of neurons in the cerebellum and their afferent and efferent connections is called cerebellar ataxia. The symptoms of cerebellar ataxia in humans usually appear between 30 and 50 years of age, and include delay in initiating responses with an affected body part, inaccuracy in range and direction of movement, irregular pattern of rate and regularity of movements, abnormal balance, slurred speech and could even lead to inability to swallow and breathe smoothly which is potentially lethal (Ghez & Thach 2000, Orr 2012).

More than 50 inherited forms of cerebellar ataxias have been identified (Matilla-Duenas 2008; Wojda et al 2008). An autosomal dominant form of cerebellar ataxia is referred to as spinocerebellar ataxia (SCA) (Orr 2012). Approximately 30 forms of SCAs have been described so far and for only half of them the causative genes have been identified (Matilla-Duenas 2008; Orr 2012).

Different genes are responsible for different spinocerebellar ataxia types. Some of them are implicated in glutamate, calcium and potassium signalling, while the normal function of others remains elusive (Durr 2010; Orr 2012). Even though SCAs display genetic heterogeneity, they all affect central and peripheral nervous systems in a similar way. Atrophy of cerebellum is the most prominent features of cerebellar ataxias (Durr 2010). Most common lesions in the cerebellum disrupt the cerebellar module, which involves a relationship between the cerebellar cortex, the dentate nuclei and the inferior olivary nuclei (Voogd & Glickstein 1998). Some SCAs can have pontine atrophy,

for example SCA1/2 and 7. Other structures may also degenerate in SCAs, such as spinal cord and substantia nigra (Koeppen 2005).

Purkinje cell dendritic atrophy and cell loss is common among most SCAs and is considered to be their main feature (Taroni & DiDonato 2004). However, Purkinje cell atrophy is not a necessary primary event of cerebellar ataxia. In different SCAs, degeneration of Purkinje cells, with the exception for SCA6, leads to atrophy of the inferior olivary nuclei. Other cell types, i.e. basket, stellate and granule cells, do not undergo degeneration as a result of Purkinje cell disappearance. Golgi cells are less susceptible than Purkinje cells to the effects of ataxia, however there are also SCAs which display substantial loss of granule cells, for example SCA11 (Houlden et al 2007). Loss of Purkinje cells in some SCAs, such as SCA1/2/6 and 17, does not cause disappearance of synapses in the molecular layer of the cerebellum, whereas in other SCAs (e.g. SCA2/6) it does. Death of pontine and olivary neurons, on the other hand, always causes degeneration of their afferent synapses (Koeppen 2005).

Most SCAs have an expansion of a CAG-repeat in their genes, which results in an abnormally long and unstable polyglutamine tract in the corresponding protein (Taroni & DiDonato 2004). Some SCAs, such as SCA1/2/3/6/7 and 17, have an expanded CAG-repeat in the open reading frame of their genes. Other SCAs have the insertion outside of the open-reading frame, for example, SCA8/10 and 12. Formation of inclusion bodies in CAG-repeat SCAs may be a common step in their pathogenesis (Koeppen 2005). Conventional mutations in genes also occur in SCAs and can lead to alterations in the amino acid composition of the protein, which is the case in SCA5/11/14/15/27 and 28 (Durr 2010; Matilla-Duenas 2008).

So far, the following mechanisms have been implicated in the pathogenesis of cerebellar ataxia: translocation of proteins from the cytoplasm to the nucleus, regulation of RNA translation, regulation of the ubiquitin-proteasome pathway, membrane channel activity and gene transcription (Orr 2012).

However, molecular mechanisms that lead to the degeneration or abnormal function of Purkinje cells are still poorly understood.

To understand the disease mechanism, first the normal function in basic cellular processes of the proteins mutated in ataxias need to be identified. Mutant mice have been used as successful models of human neurological diseases, cerebellar ataxia being one of them (Oliver & Davies 2005).

- **Mouse models of cerebellar ataxia with alterations in calcium signalling**

Many mouse models of cerebellar ataxias exist. The mechanism of ataxia pathogenesis is not known for many ataxia types, but some evidence suggests, that changes in neuronal Ca^{2+} signalling appears to play a significant role in the pathogenesis of many of them (Bezprozvanny 2009; Wojda et al 2008). These models of ataxia are described below.

SCA1 mouse models have a polyglutamine expansion in the ataxin-1 protein, display gait abnormalities and atrophy of Purkinje cell dendrites with a reduced molecular cell layer (Burright et al 1995; Clark et al 1997; Orr et al 1993). In SCA1 mutant mice several genes involved in Ca^{2+} signalling in neurons, including calbindin and inositol 1,4,5-trisphosphate receptor 1 (IP_3R1), have been shown to be down-regulated in the cerebellum (Lin et al 2000; Serra et al 2004). This suggests that SCA1 pathogenesis could be due to abnormalities in Ca^{2+} signalling in Purkinje cells (Vig et al 2001).

Staggerer mouse has a loss-of-function mutation in the RORα gene, encoding a transcription factor. The mutation causes gait abnormalities and abnormal development of Purkinje cells, very similar to that of SCA1 mice and RORα has been shown to interact with ataxin-1 (Hamilton et al 1996; Sidman et al 1962).

SCA2 has a polyglutamine expansion in the ataxin-2 protein, which results in the gain-of-function mutation and leads to degeneration of Purkinje cells. The mutant ataxin-2 protein has been shown to associate with the Ca^{2+} channel of intracellular stores IP_3R1, making it more sensitive to its activator IP_3, and hence cause an influx of Ca^{2+} into the cytoplasm of Purkinje cells from the intracellular stores. Interestingly, administration of a Ca^{2+} stabilising drug into the mice reduced Purkinje cell loss and alleviated age-dependent motor defects (Liu et al 2009).

SCA3 mouse model has a polyglutamine expansion in the ataxin-3 protein and displays motor abnormalities due to neuronal dysfunction, with less arborisation of Purkinje cell dendrites. Mutant ataxin-3 protein also binds and activates IP_3R1, causing the release of Ca^{2+} into the cytoplasm. Hence, similar to SCA2, abnormal activity of ataxin-3 protein could lead to the pathogenesis of SCA3 through changes in Ca^{2+} signalling in Purkinje cells of the cerebellum. Chen et al also suggested that Ca^{2+} stabilisers could be used to treat patients with SCA3, because evidence in mice showed alleviation of SCA3 symptoms when a Ca^{2+} stabilising drug was administrated (Chen et al 2008).

A polyglutamine expansion in the pore-forming α_{1A} subunit of the P/Q-type VGCC, which is encoded by the *Cacna1a* gene, is the cause of ataxia and Purkinje cell degeneration in **SCA6** (Zhuchenko et al 1997). P/Q-type VGCCs are highly enriched in the Purkinje cells of the cerebellum and are responsible for voltage-dependent Ca^{2+} influx into the neurons (Catterall 1995; Westenbroek et al 1995). Some reports suggest that SCA6 disorder is due to the channel dysfunction via abnormalities in neuronal Ca^{2+} homeostasis, although conflicting data has been reported on whether there is a decrease (Matsuyama et al 1999; Toru et al 2000), or an increase in Ca^{2+} influx (Piedras-Renteria et al 2001; Restituito et al 2000), possibly due to different structural variants of α_{1A} tested and different animal species used in the studies. There is, however, another theory as to how the mutated protein causes pathogenesis in SCA6, and it is not dependent on abnormal Ca^{2+} levels. It has been demonstrated that

the toxicity of the polyglutamine containing α_{1A} subunit depends on the nuclear localisation of its C-terminus. Both the wild-type and the mutated C-termini of the α_{1A} subunits are cleaved and translocated to the nucleus, perhaps to regulate gene transcription. But only the C terminus containing the expanded polyglutamine leads to cell death in tissue culture (Kordasiewicz et al 2006).

A loss-of-function mutation in the *Cacna1a* gene has also been found in mouse models of cerebellar ataxia, called **tottering** and **leaner** mice. Tottering mice have an amino acid substitution in the α_{1A} subunit and they display progressive loss of neurons from cerebellar cortex, including granule and Purkinje cells (Fletcher et al 1996). Leaner mice have a deletion in the C-terminus of the α_{1A} subunit and they have a more severe phenotype, with severe ataxia and death of cerebellar neurons (Herrup & Wilczynski 1982). In has been shown that in the tottering and leaner mice, there is a reduction in the Ca^{2+} influx into the Purkinje cells, so Ca^{2+} signalling could be responsible for the disease mechanism (Lorenzon et al 1998; Wakamori et al 1998).

Another type of spinocerebellar ataxia – **SCA14** – has a mutation in the PKCγ kinase (Abeliovich et al 1993; Yabe et al 2003). As mentioned before, PKCγ expression is particularly high in the Purkinje cells during their dendritic development and its proper function is crucial for the development of the dendritic tree of Purkinje cells (Barmack et al 2000; Gundlfinger et al 2003; Saito et al 1988; Schrenk et al 2002). It has been demonstrated that a mutation in PKCγ results in Ca^{2+} homeostasis dysfunction, which is mediated by a non-selective transient receptor potential canonical channel, type 3 (TRPC3) (Adachi et al 2008).

SCA15 has deletions or mutations in the IP_3R1 channel, which releases calcium from intracellular stores (Hara et al 2008; van de Leemput et al 2007). The mutation leads to a decrease in the expression levels of the mutated protein itself in the Purkinje cells, which suggests that Ca^{2+} homeostasis could be altered in SCA15 (Bezprozvanny 2011).

These mouse models clearly demonstrate that abnormal Ca^{2+} signalling could play a major role in the pathogenesis of cerebellar ataxias. And perhaps, common mechanisms that lead to different types of ataxias could occur.

Moonwalker mouse

Another mouse model of cerebellar ataxia has been discovered recently in our laboratory (Becker et al 2009). It is called the *Moonwalker* (*Mwk*) mouse and it has a point mutation in the TRPC3 ion channel, which leads to an ataxic phenotype and abnormal development (and later loss) of Purkinje cells of the cerebellum. The *Mwk* mouse has been generated by ENU mutagenesis.

- **ENU mutagenesis**

The ENU mutagenesis programme uses a chemical mutagen, called *N*-ethyl-*N*-nitrosourea (ENU), to introduce a random and, predominantly, single point mutation in male mice (Nolan et al 2000a; Nolan et al 2000b). The males with the introduced mutation are then bred with wild-type female mice. The ENU mutagenesis is a phenotype-driven approach, hence the offspring are screened for visible abnormalities at birth and weaning (such as facial, limb and tail defects); again at 5 weeks using a SHIRPA phenotype assessment protocol, which uses a number of simple tests to identify defects in spinocerebellar function, lower motor neuron function, etc.; and at 6 weeks to check for abnormal locomotor activity (Nolan et al 2000a; Rogers et al 1997). The selected mice can then be analysed for dominant mutations.

Compared to targeted mutagenesis, where a specific gene is targeted (Capecchi 1989), the ENU mutagenesis has certain advantages. First of all, it is an unbiased approach, where mutant mice are selected based on their phenotype, and no prior assumptions are made about the gene, so novel gene functions can be identified (Nolan et al 2000a; Nolan et al 2000b; Oliver & Davies 2005). The

ENU mutagenesis approach can introduce dominant-negative mutations, as well as gain-of-function mutations, which are difficult to achieve since they are impossible to predict. Knockout studies do not always help identify the function of a particular gene, hence gain-of-function mutations generated by ENU mutagenesis become very useful. Another advantage of the ENU mutagenesis approach is the possibility to generate hypomorphs, which are mutations with a partial loss of gene function due to reduced mRNA or protein expression, or reduced functional performance (Muller 1932). Finally, a large number of mutant mice can be generated relatively quickly displaying a wide range of symptoms.

The *Mwk* mouse displayed symptoms of a neurological disorder with motor and coordination problems, and was referred to our group for further investigation because of our interest in movement disorder and ataxia. When placed on smooth surface, the mice displayed retropulsion, hence they were named the *Moonwalker* mice, referring to the Michael Jackson's "moonwalk" dance move.

The subsequent characterisation of the *Mwk* mouse has been described (Becker et al 2009). The analyses were complete when I joined the laboratory and are summarised below.

Heterozygous *Mwk* mutants are approximately 60% of the size of wild-type littermates and show motor and coordination defects from around 3 weeks of age. They meander from side to side and have a much wider gait than the wild-type mice. Static rod test confirmed that the balance of *Mwk* mice is significantly impaired. Homozygous *Mwk* mice are not viable.

The general structure of the *Mwk* cerebellum is very similar to that of their wild-type littermates, with the granule layer size being indistinguishable. However, at approximately 3 weeks of age, subtle differences can be observed in the complexity of the Purkinje cell dendritic tree. Interestingly, this defect is even more profound in cerebellar organotypic slice cultures starting from 2 weeks old (in the

paper the tested age of organotypic slice cultures was P8+12, and the fact that the differences can be observed even earlier was established later), where *Mwk* Purkinje cells display less branched dendrites and decreased total dendrite length by 40% compared to wild-type littermates (Figure 1-4). The slow and progressive Purkinje cell loss is only detected from 4 months of age (Figure 1-5), which indicates that the ataxic phenotype is caused by the abnormal function of Purkinje cells, rather than their loss.

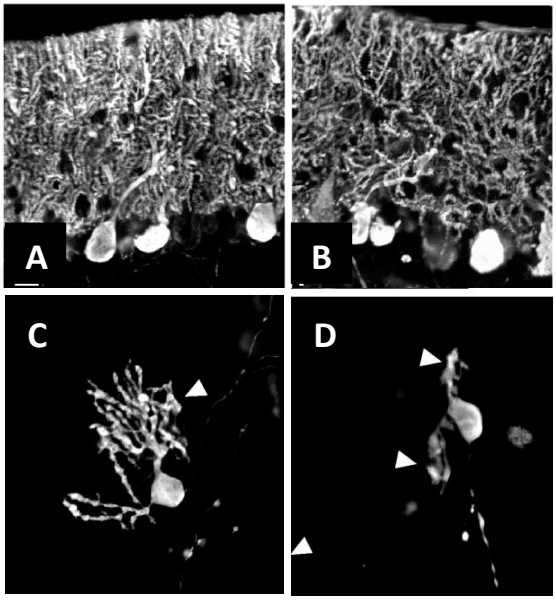

Figure 1-4. Cerebellar sections of 3 week old wild-type (**A**) and *Mwk* (**B**) mice stained with an α calbindin antibody demonstrate that the Purkinje cells of *Mwk* mice have a less branched dendritic tree. Organotypic slice cultures (P8+12) of wild-type (**C**) and *Mwk* (**D**) cerebella stained with α calbindin antibody demonstrate a smaller dendritic tree in *Mwk* Purkinje cells with less branched dendrites and a 40% shorter total dendrite length. Taken with permission from Becker et al 2009.

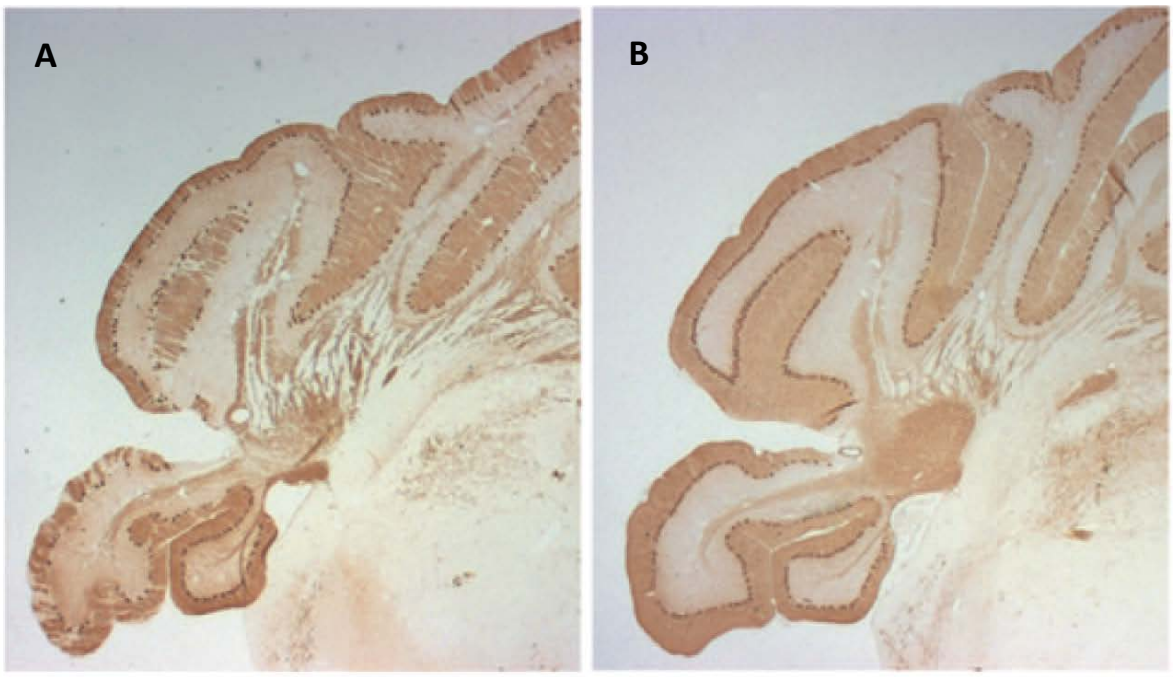

Figure 1-5. Coronal sections of *Mwk* (**A**) and wild-type (**B**) cerebella at 6 months of age stained with an α calbindin antibody. Taken with permission from Becker et al 2009.

- **TRPC3 mutation**

The *Mwk* mice have a single point mutation from A-to-G, localised to Chromosome 3, at the position 1903 of exon 7 of the *Trpc3* gene, which encodes a transient receptor potential cation channel, subfamily C, member 3 (TRPC3) and is highly enriched in the Purkinje cells of the cerebellum. The mutation causes an amino acid change from threonine to alanine (T635A), and is located in the highly conserved region of the protein. Over-expression of *Mwk* TRPC3 in various cell lines causes a significant proportion of cell death which makes it impossible to study the mutation in tissue culture experiments.

TRPC3 is an ion channel that is involved in the metabotropic glutamate receptor (mGluR)-mediated synaptic transmission in Purkinje cells (Hartmann et al 2008). Therefore, it was tested whether the *Mwk* mutation alters the inward current in cerebellar slices, when stimulated by an mGluR1 agonist (S)-3,5-dihydroxyphenylglycine (DHPG), at the age of ataxia onset P20-P22 . The differences between the inward currents of the wild-type and *Mwk* Purkinje cells were clearly observed. At a high DHPG concentration, *Mwk* Purkinje cells displayed significantly smaller spikes at a faster interval, or no spikes at all. But most interestingly, at low DHPG concentration, when the wild-type Purkinje cells had no inward current, *Mwk* Purkinje cells demonstrated a very clear inward current (Figure 1-6), meaning that the *Mwk* is a gain-of-function mutation causing the TRPC3 ion channel to open more readily upon stimulation.

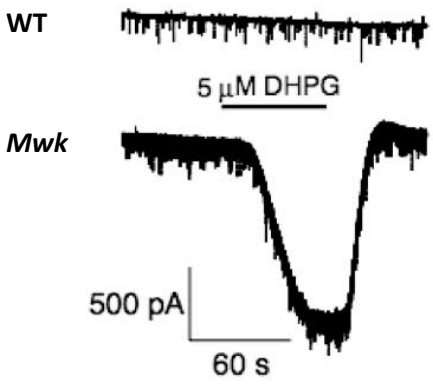

Figure 1-6. At a low concentration of an mGluR1 agonist DHPG (5 μM), wild-type Purkinje cells do not show any inward current, whereas the *Mwk* Purkinje cells show a clear inward current. Taken with permission from Becker et al 2009.

Also, the *Mwk* mutation does not cause any changes to the expression levels of the TRPC3 protein (Figure 1-7), hence the increase in TRPC3 activity in *Mwk* mice is not due to changes

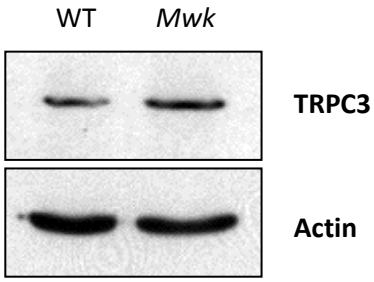

Figure 1-7. Levels of TRPC3 protein in wild-type and *Mwk* cerebella of 3 week old mice are the same. Actin was used as a loading control and its levels are the same in both samples. Taken with permission from Becker et al 2009.

in expression, but due to the gating abnormalities.

It has been demonstrated that phosphorylation of TRPC3 by protein kinase C γ (PKCγ) is a negative regulation of TRPC3 activity (Trebak et al 2005; Venkatachalam et al 2003). The threonine at position 635 in the S4/S5 linker of the protein (see Figure 1-9 further in this chapter for the structure of TRPC3) is a potential site for PKCγ phosphorylation, and in the *Mwk* mice, this threonine is replaced by alanine, which cannot be phosphorylated. Therefore, the *Mwk* TRPC3 channels could lose their mechanism of deactivation by PKCγ. An *in vitro* kinase assay, using only the S4/S5 linker of the TRPC3 protein attached to glutathione S-transferase (GST) demonstrated that PKCγ phosphorylates the wild-type S4/S5 linker, whereas it fails to phosphorylate the S4/S5 linker that contains the *Mwk* mutation (Figure 1-8). Hence, inability of PKCγ to phosphorylate the site of the *Mwk* mutation could be one of the reasons *Mwk* is a gain-of-function mutation as TRPC3 would lose its mechanism of deactivation.

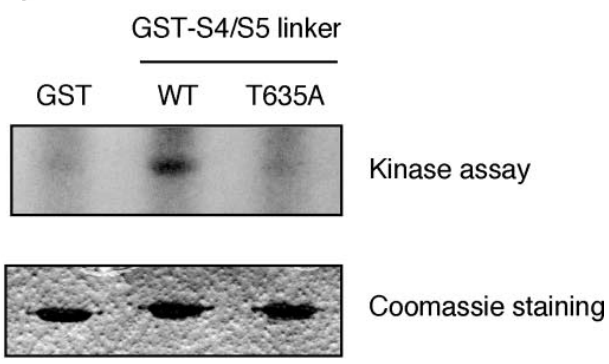

Figure 1-8. The *in vitro* kinase assay showed that PKCγ failed to phosphorylate the *Mwk* S4/S5 linker (site of the *Mwk* mutation) attached to a GST protein, whereas the wild-type S4/S5 linker was phosphorylated. GST only was used as a negative control which showed no phosphorylation by PKCγ. Coomassie staining demonstrated that equal loading was achieved. Taken with permission from Becker et al 2009.

TRPC3 channel

TRPC3 is a non-selective cation channel that acts as a sensor of cellular environment and is a member of the TRP family (Eder et al 2007; Ramsey et al 2006; Tai et al 2009; Venkatachalam & Montell 2007). TRPC3 has been previously implicated in motor coordination through the studies of knockout mice

(Hartmann et al 2008; Rodriguez-Santiago et al 2007). And the study of *Mwk* mice also demonstrates that its abnormal function leads to ataxia, as well as abnormal development of Purkinje cell dendrites (Becker et al 2009).

- **Structure**

Seven TRPC proteins are known and are divided into three groups on the basis of their sequence similarities: TRPC1/4/5, TRPC3/6/7 and TRPC2 (in humans TRPC2 is a pseudogene) (Ramsey et al 2006; Vannier et al 1999). Sometimes, TRPC1 is referred to a separate group (Putney 2005). The putative structure of the TRPC3 channels is shown in Figure 1-9.

The intracellular N-terminus of TRPC3 comprises of 4 ankyrin repeats, a coiled coil domain and a hydrophobic domain (Vannier et al 1998). Next comes the transmembrane segment of the TRPC3 protein, containing seven membrane-spanning hydrophobic regions, six out of them form the transmembrane core domains. The intracellular C-terminus has a TRP box, a proline rich region, and another coiled coil domain. TRPC3 channel topology is similar to that of voltage-gated potassium channels, and therefore it was proposed that the transmembrane segments 5 and 6 and their connecting region are part of the pore of the channel (Vannier et al 1998). Mutation studies in the putative pore region, indeed, demonstrated changes in pore properties (Hofmann et al 2002). The S4/S5 linker that is highlighted in the figure is the location of the *Mwk* mutation.

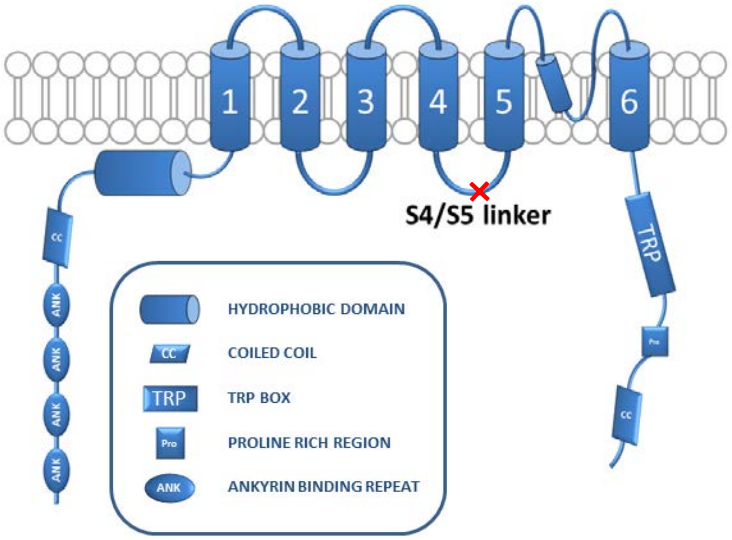

Figure 1-9. Putative structure of the TRPC3 channel. The N-terminus of the TRPC3 ion channel is intracellular and consists of ankyrin repeats, a coiled coil domain and one hydrophobic domain. TRPC3 has six transmembrane core domains, with a hydrophobic region between domains 5 and 6. The C-terminus is also intracellular and comprises of a TRP box, a proline rich region and another coiled coil domain. The site of the *Mwk* mutation (represented with a red cross) is located between transmembrane domains four and five, which is referred to as the "S4/S5 linker". Adapted with permission from Eder et al 2007.

The human protein is 848 amino acids long and runs at approximately 100 kD on an SDS-PAGE gel (Eder et al 2007). Human and mouse TRPC3 proteins have 96% homology, which make the mouse a good model to study human TRPC3 gene function (Eder et al 2007).

Similarities of the membrane topology of TRPC3 channels with other channels comprised of six transmembrane segments, such as voltage-gated potassium channels, suggested that TRPC3 channels form tetramers (Eder et al 2007). In fact, TRPC3 has been implicated in homomeric interactions with more TRPC3 proteins, as well as heteromeric interactions with TRPC1, TRPC4, TRPC6 and TRPC7 (Ambudkar & Ong 2007; Poteser et al 2006). Also, interactions with TRPC1 channels seem to make the channels become store-operated, whereas interactions with TRPC6 and TRPC7 make the complex receptor-operated (Eder et al 2007; Liu et al 2005).

- **Expression**

TRPC3 is expressed in the heart and the thalamus, and is highly enriched in the Purkinje cells of the cerebellum (Figure 1-10), being the most abundant TRPC isoform in these cells (Becker et al 2009; Hartmann et al 2008; Huang et al 2007; Riccio et al 2002). Granule cell TRPC3 staining is very low, almost invisible by *in situ* hybridisation, but western blot analysis of cultured granule cells does confirm some level of expression (Jia et al 2007).

In the cerebellum, the expression of TRPC3 increases after birth, peaks at three weeks of age and

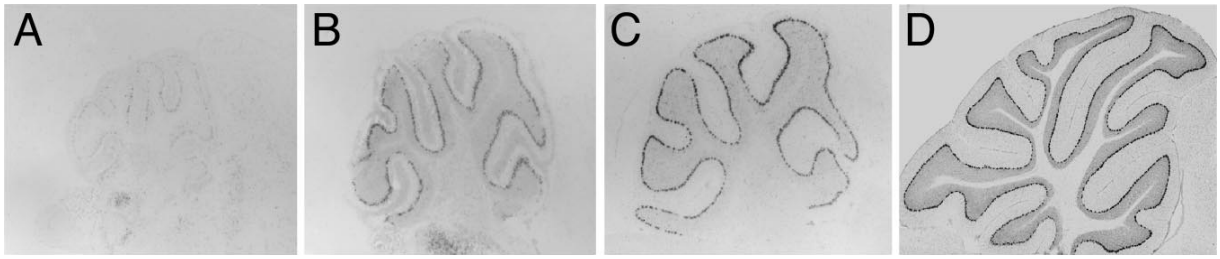

Figure 1-10. TRPC3 expression in the mouse cerebellum by *in situ* hybridisation. In the cerebellum, TRPC3 is expressed in the Purkinje cells of the cerebellum throughout its development. Relatively low expression is observed at 8 days (**A**), after which stronger expression in observed at 13 days (**B**), 18 days (**C**) and in an adult mouse at 56 days (**D**). Taken with permission from Becker et al 2009.

remains fairly constant after (Figure 1-11), which is consistent with our *in situ* hybridisation observations (Becker et al 2009; Huang et al 2007). Such expression pattern correlates with the period of extensive Purkinje cell dendritic growth and elaboration, with the formation of parallel fibre synapses and the elimination of multiple climbing fibre connections (Kapfhammer 2004).

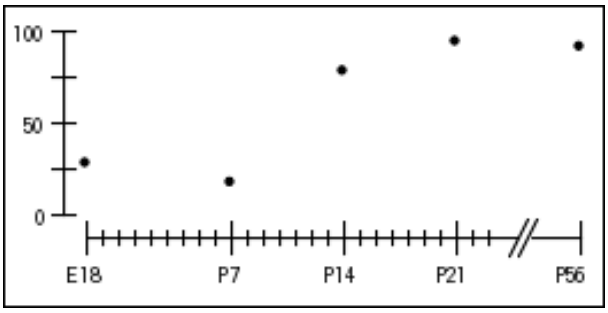

Figure 1-11. TRPC3 expression in the mouse cerebellum. TRPC3 expression starts increasing from birth and plateaus from about three weeks of age. After that, the expression of TRPC3 remains constant throughout adulthood. Taken with permission from the Cerebellar Development Transcriptome Database (CDT-DB).

- **Localisation inside the cell**

TRPC3 is located at the plasma membrane and in intracellular vesicles near the Endoplasmic Reticulum (ER) (Cayouette & Boulay 2007; Eder et al 2007). TRPC3 channels in intracellular vesicles are inactive, but when the channels are stimulated, the vesicles are rapidly translocated to the plasma membrane and fused with it through a vesicle-associated membrane protein 2 (VAMP2)-dependent exocytosis, where they become active and allow entry of positive ions into the cell (Kim et al 2006; Singh et al 2004).

- **TRPC3 signalling**

Interaction between TRPC3 and its regulatory proteins is thought to be crucial for its proper function (Ambudkar & Ong 2007; Kiselyov et al 2005). Different mechanisms of TRPC3 regulation are summarised in Figure 1-12 and are described below.

One type of TRPC3 activation is the receptor-operated activation by the metabotropic glutamate receptor 1 (mGluR1) pathway (Hartmann & Konnerth 2009; Soboloff et al 2007). G protein-coupled receptor mGluR1 is activated by a neurotransmitter glutamate (Glu), and activates the $G\alpha_q$ protein, that activates phospholipase C β4 (PLCβ4) (Batchelor & Garthwaite 1993; Exton 1996; Takechi et al 1998). PLCβ4 cleaves phosphatidylinositol 4,5-bisphosphate (PIP_2) to produce diacylglycerol (DAG) and inositol 1,4,5-trisphosphate (IP_3) (Berridge 1993). DAG directly activates TRPC3 channels, which causes them to open and let positive ions (including Ca^{2+}) enter the cell (Hofmann et al 1999). This mechanism underlies the slow excitatory postsynaptic potential which is one of the synaptic responses in the Purkinje cells to parallel fibre stimulation and is important for synaptic plasticity and motor learning (Aiba et al 1994; Batchelor & Garthwaite 1993; Hartmann et al 2008). Recent evidence also suggests that this mechanism activates P/Q-type as well as T-type VGCCs, which are the main source of calcium entry through mGluR1 activation in Purkinje cells (Gugger et al 2012).

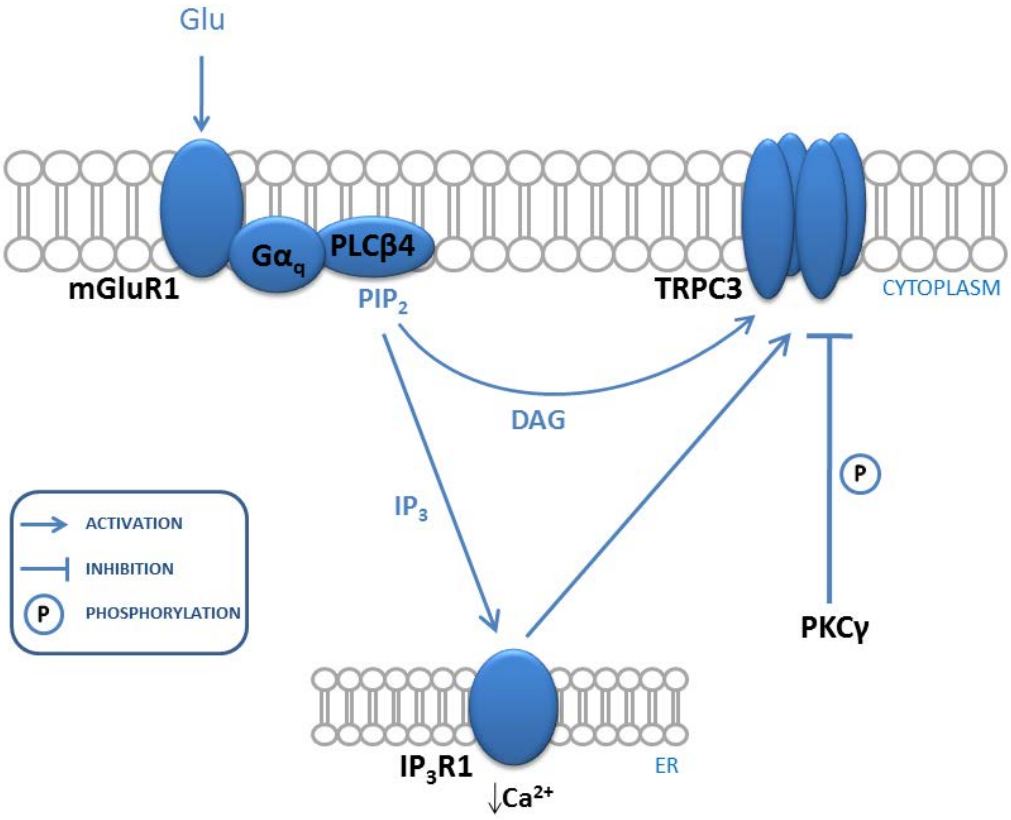

Figure 1-12. Different mechanisms of TRPC3 regulation. TRPC3 is regulated by several different mechanisms. One of the activation mechanisms involves activation of mGluR1 with a neurotransmitter glutamate (Glu). mGluR1 activates a $G\alpha_q$ protein, that activates phospholipase C β4 (PLCβ4). PLCβ4 then breaks down phosphatidylinositol 4,5-bisphosphate (PIP_2) to make diacylglycerol (DAG) and inositol 1,4,5-trisphosphate (IP_3). DAG can directly activate TRPC3, causing it to open and allow positively charged ions (including Ca^{2+}) to go through. Another mechanism of TRPC3 activation is through internal Ca^{2+} stores depletion. The IP_3 molecule, which is generated through PIP_2 breakdown, activates the IP_3 receptor 1 (IP_3R1) which releases Ca^{2+} from internal stores into the cytoplasm. When the internal stores become depleted, IP_3R1 binds TRPC3 and causes its activation. A mechanism of TRPC3 deactivation is facilitated by PKCγ. Phosphorylation of TRPC3 by PKCγ causes the channel to close.

Another mechanism of TRPC3 activation is store-operated and is triggered by Ca^{2+} store depletion from intracellular stores, such as the ER (Kiselyov et al 1998). mGluR1 is known to generate Ca^{2+} release from intracellular stores through the IP_3 Receptors (IP_3R), as a response to Purkinje cell stimulation (Berridge 1993; Takechi et al 1998). The IP_3Rs are a family of calcium channels located at the ER and their function is to release calcium from internal stores in response to activation by IP_3 (generated after mGluR1 activation as discussed above) (Mikoshiba 2011b). The IP_3R1 is known to interact with TRPC3 and control its store-dependent activation (Boulay et al 1999; Kiselyov et al 1999). In the resting state, TRPC3 is bound by a calcium sensor calmodulin. When IP_3R1 is activated by IP_3 and the internal calcium stores start being depleted, IP_3R1 displaces calmodulin by binding to the same region of the TRPC3 channel, which causes TRPC3 translocation to the plasma membrane and its activation (Tang et al 2001; Zhang et al 2001).

It has been shown *in vitro* that the activation mode of TRPC3 is dependent upon levels of its expression: when TRPC3 expression is low, it is implicated in store-dependent activation, whereas activation of TRPC3 expressed at high levels is store-independent (Vazquez et al 2003).

Another mechanism of TRPC3 regulation is through phosphorylation by PKCγ. PKCγ is known for its importance in cerebellar function and plasticity, as well as for its involvement in the development of Purkinje cell dendritic tree (Kapfhammer 2004; Metzger & Kapfhammer 2000; Schrenk et al 2002). TRPC3 channels have been shown to be deactivated by PKCγ phosphorylation *in vitro* (Trebak et al 2005; Venkatachalam et al 2003). Further studies confirming this mechanism were performed with a mutated form of PKCγ, which was unable to phosphorylate the TRPC3 protein and hence failed to inhibit the Ca^{2+} current, that the wild-type PKCγ was able to inhibit (Adachi et al 2008). As mentioned earlier, *Mwk* TRPC3 could lose its mechanism of deactivation due to inability of PKCγ to phosphorylate the site of *Mwk* mutation *in vitro*.

It is possible that phospholipase D (PLD), which is also activated through the mGluR1 signalling mechanism, could also be required for TRPC3 regulation (Glitsch 2010).

- **Calcium entry through TRPC3 channels**

TRPC3 is a non-selective cation channel, so its activation by the mechanisms described above, causes the influx of Ca^{2+} and Na^{+} ions into the cell (Clapham 2003; Li et al 1999; Soboloff et al 2007; Zhu et al 1996).

Ca^{2+} is an essential second messenger that is involved in a wide range of cellular processes. The molecular events downstream of Ca^{2+} influx are complex and mostly involve phosphorylation cascades that control gene transcription (Greer & Greenberg 2008). In the nervous system, many responses to increased intracellular Ca^{2+} levels are mediated by CaM kinases, such as CaMKII and CaMKIV (Wayman et al 2008). They also include activation of the MAP kinase, as well as the NFAT signalling cascades (Zieg et al 2008).

Since TRPC3 allows Ca^{2+} ions enter into the cell, it is very likely that these pathways could be controlled by the activity of this ion channel, and changes in TRPC3 activity in *Mwk* mice could cause alterations in these Ca^{2+} signalling pathways.

- **TRPC3 in heart and muscle**

Normal signalling of TRPC3 channels is important for proper heart and muscle function (Bush et al 2006; Nakayama et al 2006; Rosenberg et al 2004).

In skeletal muscle, it has been proposed that the influx of Ca^{2+} through activated TRPC3 ion channels regulates gene transcription via a pathway involving a phosphatase calcineurin, which de-phosphorylates an NFAT transcription factor, causing it to translocate to the nucleus where it

influences gene transcription (Rosenberg et al 2004). More studies have later confirmed that this mechanism is also true for cardiac myocytes, however up-regulation of TRPC3 activity there leads to cardiac hypertrophy (Bush et al 2006).

Cardiac hypertrophy is a disease where cardiac myocytes increase in size without dividing, which is an adaptive response to a variety of cardiovascular disorders. Cardiac hypertrophy is characterised by elevated Ca^{2+} levels which impairs heart's contractile performance through activation of calcium signalling pathways and abnormal gene expression (Frey et al 2000). It has been known that the calcineurin-NFAT pathway is activated in cardiac hypertrophy (Frey & Olson 2003). And it was later demonstrated that this activation of the calcineurin-NFAT signalling pathway in mouse models of cardiac hypertrophy occurs through the up-regulation of the TRPC3 ion channel expression and its activation (Bush et al 2006).

More recent studies in a cardiac muscle cell line also demonstrated that Ca^{2+} entry through TRPC3 channels is essential for the activation of the NFAT pathway and the NFAT-dependent gene transcription, and this process is dependent on the phosphorylation of TRPC3 by PKC. Inability of PKC to phosphorylate TRPC3 protein resulted in NFAT-dependent transcription silencing (Poteser et al 2011).

One paper could not demonstrate NFAT1 translocation to the nucleus after TRPC3 activation (Kar et al 2011). This could be explained due to the choice of the cell line for the experiment: human embryonic kidney cell line, rather than muscle or cardiac cell lines. Also, it is possible that NFAT1 is not part of TRPC3 signalling, whereas other NFAT isoforms could be. For example, Poteser and colleagues used NFAT2 to demonstrate that it is being translocated to the nucleus after Ca^{2+} entry through the TRPC3 channels (Poteser et al 2011).

One downstream pathway that is activated upon TRPC3 opening in heart and muscle has already been established. Since Ca^{2+} influences a range of signalling pathways, it is likely that TRPC3 activation controls many of them.

- **TRPC3 in cerebellum**

TRPC3 has also been implicated in cerebellar development (Becker et al 2009; Hartmann et al 2008; Jia et al 2007).

So, TRPC3 is involved in the survival of granule neurons via activation of a brain-derived neurotrophic factor (BDNF), which is important in cell survival during the development of the cerebellum (Jia et al 2007; Minichiello & Klein 1996). Jia and colleagues demonstrated that down-regulation of TRPC3 inhibits the protective effect of BDNF on cerebellar granule cells and causes apoptosis (Jia et al 2007). And blocking calcium signalling kinases CaMKII or MAPK, or introducing a dominant negative form of a transcription factor cyclic-AMP response element binding protein (CREB), or inhibiting Ca^{2+} influx, diminishes the protective effect of TRPC3. Therefore the authors concluded that Ca^{2+} influx through TRPC3 could activate CaMKII and MAPK signalling pathways, which then activate CREB that is able to regulate gene transcription. Additional studies also demonstrated that down-regulation of TRPC3 in cultured rat cerebellar granule cells stops the increase in intracellular Ca^{2+} (Li et al 2005).

TRPC3 channels are also required for normal synaptic function of Purkinje cells which has been established in knockout studies and is described below (Hartmann et al 2008).

- **TRPC3 knockout**

TRPC3 knockout mice were generated by excising exon 7 from the *Trpc3* gene. The mice appear normal, with the structure of the cerebellum and the morphology of Purkinje cells being intact. However, knockout mice display defects in motor coordination which are due to impaired cerebellar

function. Knockout mice lack the slow synaptic potential of parallel fibre – Purkinje cell synapses, and the mGluR1-mediated inward currents. Dendritic Ca^{2+} signals remained unaffected in knockout mice, because Ca^{2+} was still being released from intracellular stores. This study has demonstrated the importance of TRPC3 channels in glutamatergic synaptic transmission in Purkinje cells and its significance in motor coordination (Hartmann et al 2008). Moreover, it has been suggested, that behavioural changes in TRPC3 knockout mice could be due to altered Ca^{2+} signalling (Hartmann & Konnerth 2009).

Another TRPC3 knockout mouse model has an SV40 T antigen transgene inserted into the promoter region of the *Trpc3* gene, which stops the expression of the TRPC3 protein (Rodriguez-Santiago et al 2007). Homozygous mice develop neurological symptoms, including paralysis and progressive degeneration of spinal motor neurons, due to abnormal expansion of astrocytes in the brain (Lopez-Revilla et al 2004). These mice are considered to be a good model to study astrocytes and tumorigenesis (Lopez-Revilla et al 2004).

- **Other TRPC channels in CNS**

As stated earlier, there are seven known TRPC family members (TRPC1-7). Out of those, only TRPC1, TRPC5 and TRPC6 (along with TRPC3) have been implicated in the function of the central nervous system.

TRPC6 has been studied together with TRPC3 in knock-down studies, and just like TRPC3, it was also implicated in the survival of granule cells via the BDNF activation (Jia et al 2007). Also, in hippocampal cultures, overexpression of TRPC6 increased phosphorylation of some of the key calcium signalling proteins and promoted dendritic growth, whereas down-regulation impaired it (He et al 2012; Tai et al 2008). Interestingly, we see an opposite effect in the *Mwk* mice: the gain-of-function of TRPC3 impairs dendritic growth.

TRPC5 has been shown to control neurite extension in hippocampal neurons. Interestingly, a dominant-negative form of the protein allows formation of longer neurites (Greka et al 2003). In addition, activation of TRPC5 in hippocampal neurons leads to inhibition of neuronal dendritic growth through increase in intracellular calcium and activity of CaMKIIα (He et al 2012). This suggests that TRPC5 is a negative regulator of neurite outgrowth.

TRPC1 knockout mice display loss of dopaminergic (DA) neurons, which is consistent with Parkinson's disease (PD) pathology, and expression of TRPC1 is also reduced in patients suffering from PD. In a cell model of PD, which is induced by neurotoxin 1-methyl-4-phenyl-1,2,3,6-tetrahydropyridine (MPTP) (Przedborski et al 2004), TRPC1 channel was shown to have a decreased expression, and its over-expression protected DA neurons (Bollimuntha et al 2005; Selvaraj et al 2009). It was later discovered, that reduction of TRPC1 expression in the cell model of PD causes a loss of store-operated Ca^{2+} entry. Moreover, TRPC1 was shown to control the AKT/mTOR pathway which has a role in neuroprotection, therefore TRPC1 channel itself contributes to neuronal survival (Selvaraj et al 2012).

Single Purkinje cell studies demonstrated that expression of other TRPC channels is very low compared to TRPC3, hence it is not likely that their function is essential for the development of Purkinje cells in particular (Hartmann et al 2008).

Common mechanism

Many regulators of TRPC3 activity that are shown in Figure 1-12 have also been implicated in cerebellar ataxias. These include $G\alpha_q$, IP_3R1, mGluR1, PKCγ and PLCβ4. This suggests that different cerebellar ataxias might have a common mechanism of the disease pathogenesis. Studying this common mechanism further could lead to a therapeutic strategy, which could be effective in several types of cerebellar ataxias.

Knockout mice of $G\alpha_q$, mGluR1, and PLCβ4 proteins display cerebellar ataxia, loss of long-term depression (LTD) in Purkinje cells and impairment of climbing fibres elimination (Chen et al 1995; Hashimoto et al 2001; Ichise et al 2000; Inoue et al 1998; Kano et al 1995; Kano et al 1997; Kano et al 1998; Offermanns et al 1997). Interestingly, activation of mGluR1 inhibits dendritic growth of Purkinje cells, also suggesting that they could have the same pathogenesis mechanism as *Mwk* mice (Sirzen-Zelenskaya et al 2006).

Involvement of IP_3R1 and PKCγ in cerebellar ataxias has been mentioned earlier. Deletion of IP_3R1, an intracellular Ca^{2+} store receptor and activator of TRPC3, causes SCA15 (Boulay et al 1999; Kiselyov et al 1999; van de Leemput et al 2007). IP_3R1 is also implicated in SCA2 and SCA3, where its interaction with mutant ataxin-2 and ataxin-3 proteins causes increased Ca^{2+} release from intracellular stores via the IP_3R1 channel (Chen et al 2008; Liu et al 2009). In SCA1, levels of *Ip$_3$r1* and *Trpc3* gene expression are reduced, suggesting their possible involvement in SCA1 pathogenesis (Crespo-Barreto et al 2010; Lin et al 2000; Mitsumura et al 2011; Serra et al 2004). Mutation in PKCγ, which is a negative regulator of TRPC3 activity through phosphorylation, is implicated in SCA14, where abnormalities in Ca^{2+} homeostasis are actually mediated by TRPC3 (Abeliovich et al 1993; Adachi et al 2008; Yabe et al 2003).

This information strongly suggests that TRPC3 could be part of a signalling cascade responsible for the degeneration of Purkinje cells in different types of cerebellar ataxia, as well as for the normal development and function of Purkinje cells and their dendrites.

Summary

The study of the *Mwk* mouse that was completed before the start of this thesis demonstrated that TRPC3 ion channel is a major player in the development of Purkinje cell dendrites and is required for the normal function of the cerebellum (Becker et al 2009). The molecular mechanism through which

abnormal function of the TRPC3 protein causes reduced branching of the Purkinje cell dendrites and cerebellar ataxia was not known.

Interaction between TRPC3 and other proteins is important for the normal function of the channel (Ambudkar & Ong 2007; Kiselyov et al 2005). It is possible, that the threonine-to-alanine amino acid change could lead to alterations in their interaction, which could cause abnormal function of the TRPC3 protein or of its interactors. Also, the *Mwk* mutation is a gain-of-function mutation, so it is likely that the *Mwk* TRPC3 channel would allow more Ca^{2+} ions to enter the cell, which are important for the development of Purkinje cell dendrites (Schilling et al 1991; Wong & Ghosh 2002). Abnormal levels of Ca^{2+} inside Purkinje cells could lead to changes in Ca^{2+} signalling cascades that consequently could lead to transcriptional changes inside the cell.

Further studies using the *Mwk* mouse would help us clarify the importance of TRPC3 function for the proper development of Purkinje cell dendrites, and elucidate the molecular mechanism that causes the observed phenotype in *Mwk* mice. Also, as TRPC3 is implicated in a common signalling pathway that could be altered in several types of cerebellar ataxia, studying the mutation could lead to a potential treatment strategy for different cerebellar ataxias.

Aims of Thesis

- **Investigate the interaction partners of TRPC3 and check whether the *Mwk* mutation makes a difference to their affinity.**
- **Examine the neuronal Ca^{2+} signalling pathways and observe whether the *Mwk* mutation causes alterations in their activity.**
- **Explore changes in gene expression in the Purkinje cells of *Mwk* mice to determine the mechanism leading to the abnormal development of Purkinje cells.**

CHAPTER 2. Materials and Methods

Mice

The mouse carrying the *Moonwalker* (*Mwk*) mutation was generated in a large-scale ENU mutagenesis programme at the Medical Research Council centre in Harwell, UK. The *Mwk* colony has a C3H/HeH background. All animal studies were carried out under the ‘‘Responsibility in the Use of Animals for Medical Research’’ guidelines issued by the Medical Research Council in 1993, and Home Office Project License 30/2306. All mouse colonies were maintained by Dr Esther Becker.

Genotyping

To the ear clip, 195 µl lysis buffer (100 mM Tris pH=8.5, 5 mM ethylenediaminetetraacetic acid [EDTA] pH=8, 0.2% SDS, 200 mM NaCl) and 5 µl proteinase K (Roche) were added and incubated overnight in a 55˚C water bath. To the dissolved ear clip in the lysis buffer, 200 µl isopropanol was added and mixed by inversion. The tube was then centrifuged at 15,000 *g* for 20 min and the supernatant discarded. 500 µl of cold 70% ethanol (stored at -20˚C) was added to the DNA precipitate and centrifuged at 15,000 *g* for 20 min, the supernatant was discarded. The DNA precipitates were incubated at 37˚C with open lids for the residual ethanol to be evaporated. Then, 200 µl of nuclease free water (Ambion) was added to the pellets, vortexed, and incubated at 65˚C for 10 minutes. Before PCR, the DNA was vortexed again and centrifuged at maximum speed for 1 min.

For one genotyping PCR the following reagents were mixed:

10x RedTaq buffer (Sigma)	2.5 µl
10 mM dNTPs	0.5 µl
10 µM Forward Primer 5′ TTTCGGTCATATTCTTTCTTCTCC 3′	1 µl
10 µM Reverse Primer 5′ AGTAGTTGGTCAACACAAAAGTGTG 3′	1 µl
H_2O	17.8 µl
RedTaq polymerase (Sigma)	1.2 µl
DNA	1 µl
	Total = 25 µl

The Genotyping PCR programme:

94˚C	5 min	
94˚C	45 s	x35 cycles
58˚C	45 s	
72˚C	1 min	
72˚C	10 min	
4˚C	∞	

The PCR results were run on a 3% agarose gel with either 50 ng/ml ethidium bromide (Sigma) or 1X SYBR®Safe (Invitrogen). A single band at 300 bp represents a wild-type sample, whereas two bands represented a *Mwk* sample (due to a BALB/cAnN background in the original mouse).

Antibodies

Table 2-1. Primary Antibodies and their dilutions

Source	Antibody	Dilution			Company	Catalogue nr
		WB	IHC	ICC		
mouse	Actin	1:1000	-	-	Abcam	Ab3280
mouse	Calbindin D28K	-	1:50	-	Sigma	C7354
rabbit	Calbindin D28K	-	1:10000	-	Swant	CB-38a
rabbit	CaMKII	1:500	x	1:500	Cell Signalling	3362
rabbit	P-CaMKII	1:1000	x	1:1000	Cell Signalling	3361
rabbit	CaMKIV	1:1000	x	1:1000	Abcam	ab3557
rabbit	P-CaMKIV	1:1000	1:50	1:1000	Santa Cruz	sc-28443R
mouse	CREB	1:500	x	1:1000	Cell Signalling	9104
rabbit	P-CREB	1:1000	1:25	1:200	Cell Signalling	9198
rabbit	ERK 1/2	1:1000	x	-	Cell Signalling	9102
rabbit	P-ERK 1/2	1:1000	x	-	Cell Signalling	9101s
mouse	FLAG	1:500	-	1:500	Sigma	F3165
mouse	GFP	1:1000	-	1:1000	Invitrogen	a11120
rabbit	HA	1:500	-	1:1000	Sigma	H6908
mouse	His	1:500	-	-	Cell Signalling	2366
mouse	IP3R1	1:500	1:50	1:100	NeuroMabs	L24/18
mouse	NFATc1	x	x	-	Santa Cruz	sc-7294
mouse	NFATc2	x	x	-	Abcam	ab2722
rabbit	NFATc2	x	x	-	Santa Cruz	sc-13034
rabbit	NFATc3	x	1:50	1:1000	Santa Cruz	sc-8321
rabbit	NFATc4	x	x	-	Santa Cruz	sc-13036
rabbit	Stathmin	1:1000	x	-	Sigma	O0138
rabbit	P-Stathmin	1:500	1:50	-	Santa Cruz	sc-12948R
mouse	Stk17b	1:500	1:50	-	Santa Cruz	sc-100370
rabbit	TRPC3	1:200	x	1:100	Alomone	ACC-016

Table 2-2. Secondary Antibodies and their dilutions

Antibody	Dilution			Company	Catalogue nr
	WB	IHC	ICC		
ECL anti-rabbit IgG HRP-linked	1:10000	x	x	GE Healthcare	NA934V
ECL anti-mouse IgG HRP-linked	1:10000	x	x	GE Healthcare	NA931V
Alexa Fluor® 488 goat anti-rabbit IgG	x	1:1000	1:1000	Invitrogen	A11008
Alexa Fluor® 594 donkey anti-rabbit IgG	x	1:1000	1:1000	Invitrogen	A21207
Alexa Fluor® 488 goat anti-mouse IgG	x	1:1000	1:1000	Invitrogen	A11029
Alexa Fluor® 594 goat anti-mouse IgG	x	1:1000	1:1000	Invitrogen	A11005

Cerebellar Lysates for Western Blot

Mice were sacrificed and the cerebellum was dissected and kept on ice. Protein extracts were prepared by 30 s sonication of cerebella in 1 ml Radio-Immunoprecipitation Assay (RIPA) lysis buffer (50 mM Tris pH=8, 150 mM NaCl, 1% Nonidet P40, 0.5% sodium deoxycholate, 0.1% sodium dodecyl sulphate [SDS], 100 mM sodium fluoride, 1 x Complete Protease Inhibitors [Roche]), followed by 10 min incubation on ice and 20 min centrifugation at 14,000 *g* at 4°C. The concentration of lysates was determined using the Bradford assay, and 50 µg of lysates were used in all sodium dodecyl sulphate polyacrylamide gel electrophoresis (SDS-PAGE) experiments.

Tissue Culture Cell Lysates for Western Blot

For the western blot analysis, cells were grown in 6-well plates, transfected when 50% confluent if needed, and lysed 24 h later. To lyse the cells, the medium is removed, the cells are washed with PBS, and lysed in 200 µl RIPA buffer by scraping the cells off the plate with a cell scraper. The cells were then kept on ice for 10 min, and centrifuged for 20 min at 14,000 *g* at 4°C. The concentration of lysates was determined using the Bradford assay, and 20-30 µg of lysates were used in SDS-PAGE experiments (depending on the concentration of the sample).

Western Blot

For the western blot analysis two types of gels were used:

- A self-made acrylamide gel (for 10 ml of 10% resolving gel: 4 ml H_2O, 3.3 ml 30% acrylamide mix, 2.5 ml 1.5 M Tris pH=8.8, 0.1 ml 10% SDS, 0.01 ml 10% ammonium persulphate [APS], 0.001 ml tetramethylethylenediamine [TEMED]. For 3 ml stacking gel: 2.1 ml H_2O, 0.5 ml 30% acrylamide mix, 0.38 ml 1 M Tris pH=6.8, 0.03 ml 10% SDS, 0.01 ml 10% APS, 0.01 ml

TEMED). It was run at 100 V for 20 min and then at 120 V for ~1 h. These gels were used in Chapter 4.

- A NuPAGE 4-12% Bis-tris gradient gel (Invitrogen). It was run at 200 V for 50 min. These gels were used in Chapter 3 to be able to separate different proteins on one gel.

The proteins on the gel were then transferred onto a nitrocellulose membrane (Fisher Scientific) for 2 h at room temperature at 250 mA. The membranes were blocked in 5% milk in TBST (150 mM NaCl, 10 mM Tris pH=8, 0.05% Tween-20) for 1 h at room temperature and incubated with the appropriate dilution of the primary antibody (see Table 2-1) in 3% bovine serum albumin (BSA) (Sigma) in TBST overnight at 4°C. Next day the membranes were washed 3 x 10 min in TBST, incubated 1 h with the appropriate horseradish peroxidase (HRP)-conjugated secondary antibody (Amersham Biosciences) (see Table 2-2), and washed again 3 x 10 min in TBST. To detect the proteins, the membranes were incubated with the enhanced chemiluminescence (ECL) reagent (GE Healthcare) for 2 min.

Immunohistochemistry

Cerebella were removed from mice and fixed with 4% paraformaldehyde (PFA). Cerebellar sagittal sections of 10 µm were cut on a cryostat and mounted onto superfrost slides (VWR international). Slides were stored at -80°C until use. When staining with an antibody, slides were dried at room temperature and washed 3 x 5 min in phosphate buffered saline (PBS). They were then microwaved at 80 W for 15 min in pre-warmed antigen retrieval solution (1mM EDTA, 5 mM Tris pH=8 in PBS). Slides were left to cool down. Next the slides were blocked for 1 h at room temperature with 200 µl of 5% BSA (Sigma), 3% normal goat serum (Sigma), 0.5% Triton X-100 (Sigma) in PBS, with parafilm on top of the slide. Blocking solution was removed onto a tissue and a Liquid Blocker Super Pap pen was used to draw around each cerebellar section. Antibodies were diluted in the blocking buffer at an appropriate concentration (see Table 2-1) and 50 µl were pipetted directly onto each cerebellar

section. The primary antibodies were left on the section for 2 days at 4˚C in a humidified chamber. The slides were then washed 3 x 5 min in PBS. The secondary antibody was diluted appropriately in blocking buffer (see Table 2-2) and incubated on sections for 4 h at room temperature. The slides were then washed 3 x 5 min with PBS. The coverslip was mounted on the slide using the VECTASHIELD® Mounting medium with 4',6-diamidino-2-phenylindole (DAPI) (VECTOR laboratories). The slides were visualised under an Axioplan 200 fluorescent microscope using Axiovision 4.6 software.

Tissue Culture

A human neuroblastoma cell line SH-SY5Y and a human embryonic kidney cell line HEK293T were used in this thesis. Culture media Dulbecco's Modified Eagle Medium (DMEM) (for HEK293T) and DMEM-F12 (for SH-SY5Y) (Invitrogen) were supplemented with 10% foetal bovine serum (Sigma) and 50 units/ml penicillin with 50 µg/ml streptomycin (Gibco).

Cells were transfected when ~50% confluent with FuGENE® 6 (Roche) according to the manufacturer's instructions. Cells were lysed (for western blot or immunoprecipitation) or fixed (for immunocytochemistry) 24 h later.

In Chapter 4, cells were additionally treated with 1-oleoyl-2-acetyl-sn-glycerol (OAG) (Sigma) to imitate the effect of the *Mwk* mutation. For this, OAG was diluted in the appropriate media to the final concentration of 100 µM. Then, 24 h after the cells were transfected, the cells' media was changed either for fresh media (negative control) or for media containing 100 µM OAG for 5 min. After 5 min the media was again replaced with the fresh one. Cells were then either lysed (for western blot) or fixed (for immunocytochemistry).

Constructs

Constructs were made by inserting genes of interest into the pcDNA™3.1 Directional TOPO® (Invitrogen), 3xFLAG-CMVTM-7.1 (Sigma) or the pCMV-HA (Clontech) vectors, according to the manufacturer's instructions. Primers used for cloning are summarised in Table 2-3, Table 2-4 and Table 2-5. All constructs used in this thesis are summarised in Table 2-6.

For CaMKII, contactin 1, PI synthase, PLCδ3, Rab3a, SNAP25, syntaxin 1A and syntaxin 1B, the cDNA was amplified from a wild-type mouse cerebellum and cloned into a pcDNA^{TM}3.1 Directional TOPO® vector. The HA tag was then introduced into the vector by insertional mutagenesis using the QuickChange® Site-Directed Mutagenesis Kit (Stratagene) according to manufacturer's instructions. Synaptotagmin 1 was amplified from a wild-type mouse cerebellum and cloned into a pCMV-HA vector, which already contained an HA tag. Human CaMKIV was amplified from another construct containing a FLAG tag and inserted into the pCMV-HA vector. Rat Ip3r1 construct was kindly given to us by Professor GA Mignery (Loyola University Chicago) and contained no tags. The HA-NFAT1-GFP construct was obtained from Addgene. The human 3xFLAG-Trpc3 in the 3xFLAG-CMV^{TM}-7.1 vector was made by Dr Esther Becker and is routinely used in the lab. Trpc3 ΔC and ΔN were amplified from the 3xFLAG-Trpc3 vector and inserted into the 3xFLAG-CMV^{TM}-7.1 vector according to manufacturer's instructions.

All generated constructs were sequence verified by Beckman Coulter Genomics (COGENICS).

Table 2-3. Primers used for Immunoprecipitation constructs

Gene	Construct	Insertion	Location	Sequence

Gene		Sequence	Restriction Site	Insert Vector
CaMKII	F	5′ CACCATGGCCACCACGG 3′	-	pcDNA™3.1 Directional TOPO®
	R	5′ CTGCAGCGGGGCCACT 3′		
CaMKIV	F	5′ GAGACTCGAGGTATGCTCAAAGTCACGGTGCCC 3′	XhoI	pCMV-HA
	R	5′ GAGAGCGGCCGCTTAGTACTCTGGCAGGATCAC 3′	NotI	
Contactin 1	F	5′ CACCATGAAAATGCCATTGC 3′	-	pcDNA™3.1 Directional TOPO®
	R	5′ GAATTCCGAGTAGACAAGAAAGCC 3′		
IP3R1	F	5′ CACCATGTCTGACAAAATGTCGAGT 3′	-	pcDNA™3.1 Directional TOPO®
	R	5′ GGCCGGCTGCTGTGG 3′		
PI Synthase	F	5′ CACCATGCCAGAGGAAAATATCTTC 3′	-	pcDNA™3.1 Directional TOPO®
	R	5′ TTTCTTCTTGGCGCGGTC 3′		
PLCδ3	F	5′ CACCATGCTGTGCGGTG 3′	-	pcDNA™3.1 Directional TOPO®
	R	5′ AGAGTTCTGAATGCGGATGTG 3′		
RAB3A	F	5′ CACCATGGCTTCCGCCAC 3′	-	pcDNA™3.1 Directional TOPO®
	R	5′ GCAGGCACAATCCTGATGAGG 3′		
SNAP25	F	5′ CACCATGGCCGAAGACGC 3′	-	pcDNA™3.1 Directional TOPO®
	R	5′ ACCACTTCCCAGCATCTTTGTTG 3′		
Synaptotagmin 1	F	5′ GAGAGAATTCGCCACCATGGTGAGTGCCAGTCGTCC 3′	EcoRI	pCMV-HA
	R	5′ GAGAGCGGCCGCGCCACCTTACTTCTTGACAGCCAGCATGG 3′	NotI	
Syntaxin 1A	F	5′ CACCATGAAGGACCGAACCC 3′	-	pcDNA™3.1 Directional TOPO®
	R	5′ TCCAAAGATGCCCCCGAT 3′		
Syntaxin 1B	F	5′ CACCATGAAGGATCGGACTCAG 3′	-	pcDNA™3.1 Directional TOPO®
	R	5′ CAAGCCCAGTGTCCCCC 3′		

Table 2-4. Primers used for TRPC3 binding domain study constructs

Gene		Sequence	Restriction Site	Insert Vector
TRPC3 ΔN	F	5′ GAGAAAGCTTTGTCTCGTTGTGCTGGTCG 3′	HindIII	3xFLAG-CMV™-7.1
	R	5′ GAGATCTAGATCATTCACATCTCAGCATGCTG 3′	XbaI	
TRPC3 ΔC	F	5′ GAGAGAATTCAATGGAGGGAAGCCCATCCC 3′	EcoRI	3xFLAG-CMV™-7.1
	R	5′ GAGAGATATCTCAAAAGTTAACAATTCGCATGATG 3′	EcoRV	

PI Synthase	pcDNA™3.1 Directional TOPO®	HA tag	N-terminus	F 5′ CCCTTCACCATGGGATACCCTTACGACGTTCCTGATTACGCTCCAGAGGAAAATATC 3′ R 5′ GATATTTTCCTCTGGAGCGTAATCAGGAACGTCGTAAGGGTATCCCATGGTGAAGGG 3′
PLCδ3	pcDNA™3.1 Directional TOPO®	HA tag	N-terminus	F 5′ CCCTTCACCATGGGATACCCTTACGACGTTCCTGATTACGCTCTGTGCGGTGGCTGG 3′ R 5′ CCAGCCACCGCACAGAGCGTAATCAGGAACGTCGTAAGGGTATCCCATGGTGAAGGG 3′
RAB3A	pcDNA™3.1 Directional TOPO®	HA tag	N-terminus	F 5′ CCCTTCACCATGGGATACCCTTACGACGTTCCTGATTACGCTGCTTCCGCCACAGAC 3′ R 5′ GTCTGTGGCGGAAGCAGCGTAATCAGGAACGTCGTAAGGGTATCCCATGGTGAAGGG 3′
SNAP25	pcDNA™3.1 Directional TOPO®	HA tag	N-terminus	F 5′ CCCTTCACCATGGGATACCCTTACGACGTTCCTGATTACGCTGCCGAAGACGCAGAC 3′ R 5′ GTCTGCGTCTTCGGCAGCGTAATCAGGAACGTCGTAAGGGTATCCCATGGTGAAGGG 3′
Syntaxin 1A	pcDNA™3.1 Directional TOPO®	HA tag	N-terminus	F 5′ CCCTTCACCATGGGATACCCTTACGACGTTCCTGATTACGCTAAGGACCGAACCCAG 3′ R 5′ CTGGGTTCGGTCCTTAGCGTAATCAGGAACGTCGTAAGGGTATCCCATGGTGAAGGG 3′
Syntaxin 1B	pcDNA™3.1 Directional TOPO®	HA tag	N-terminus	F 5′ CCCTTCACCATGGGATACCCTTACGACGTTCCTGATTACGCTAAGGATCGGACTCAG 3′ R 5′ CTGAGTCCGATCCTTAGCGTAATCAGGAACGTCGTAAGGGTATCCCATGGTGAAGGG 3′

Table 2-5. Primers used for Site-directed mutagenesis

Table 2-6. Constructs used in this thesis

Vector	Source	Species	N- tag	Gene inserted	-C tag
3xFLAG-CMV™-7.1	Sigma (E7533)	h	3xFLAG	Trpc3	-
3xFLAG-CMV™-7.1	Sigma (E7533)	h	3xFLAG	Trpc3 ΔN	-
3xFLAG-CMV™-7.1	Sigma (E7533)	h	3xFLAG	Trpc3 ΔC	-
pEGFP	Addgene (11107)	m	HA	Nfat1 (=Nfatc2)	GFP
pCMVI-9	Provided by Prof GA Mignery	r	-	Ip3r1	-
pCMV-HA	Clontech (631604)	h	HA	Camk4	-
pCMV-HA	Clontech (631604)	m	HA	Synaptotagmin1	-
pcDNA™3.1 Directional TOPO®	Invitrogen (K4900-01)	m	HA	PI Synthase	V5
pcDNA™3.1 Directional TOPO®	Invitrogen (K4900-01)	m	HA	Plcδ3	V5
pcDNA™3.1 Directional TOPO®	Invitrogen (K4900-01)	m	HA	Rab3a	V5
pcDNA™3.1 Directional TOPO®	Invitrogen (K4900-01)	m	HA	Snap25	V5
pcDNA™3.1 Directional TOPO®	Invitrogen (K4900-01)	m	HA	Syntaxin1A	V5
pcDNA™3.1 Directional TOPO®	Invitrogen (K4900-01)	m	HA	Syntaxin1B	V5

Immunocytochemistry

Cells were grown in a 24-well plate with coverslips placed at the bottom of the wells. To fix the cells, the medium was removed and replaced with 4% PFA for 20 min. The cells were then washed twice with PBS (Sigma tablets dissolved in dH_2O). To permeabilise the cells, 0.4% Triton X-100 (Sigma) in PBS was added for 20 min. The solution was then removed and replaced with a blocking buffer (10% milk, 1% normal goat serum [Sigma] in PBS) for 1 h. The antibody was diluted to an appropriate dilution in 3% BSA (Sigma) in TBST (0.02% Tween in TBS [150 mM NaCl, 10 mM Tris pH=8]) (see Table 2-1). The coverslips were removed from the 24-well plate and placed in a dark humidified chamber and covered with the antibody dilution. The primary antibody was left on overnight at 4˚C. The next day the cells were washed three 3 x 5 min in PBS. Secondary antibody was diluted appropriately (see Table 2-2) and applied onto cells for 2 h at room temperature. The secondary antibody was then washed off with PBS 3 x 5 min. VECTASHIELD® Mounting medium with DAPI (VECTOR laboratories) was used to mount the cells onto the slides. The slides were visualised under an Axioplan 200 fluorescent microscope using Axiovision 4.6 software.

GST Pulldown from Brain for Mass Spectrometry Analysis

Four wild-type mice were sacrificed, their cerebella dissected out and kept on ice. One cerebellum per pulldown was used. Cerebellar protein extracts were prepared by 2 x 20 s sonication with 1 min rest on ice in 1 ml lysis buffer (1% 3[(3-cholamidopropyl)dimethylammonio]-propanesulfonic acid [CHAPS], 50 mM 4-(2-hydroxyethyl)-1-piperazineethanesulfonic acid [HEPES], 150 mM NaCl, 10% glycerol, 1.5 mM $MgCl_2$, 1mM ethylene glycol tetraacetic acid [EGTA], 100 mM NaF, 1 x Complete Protease Inhibitors [Roche]), followed by 20 min incubation on ice and 20 min centrifugation at 14,000 *g* at 4°C. The pulldown was performed with the following recombinant proteins: glutathione S-transferase (GST) (as a negative control), wild-type GST-S4/S5 linker (see Figure 1-9 for location of

the S4/S5 linker in the TRPC3 protein), phosphorylated wild-type GST-S4/S5 linker (in vitro protein kinase Cγ [PKCγ] kinase assay was carried out according to the manufacturer's protocol [Upstate Biotechnology]. Briefly, recombinant active PKCγ kinase [Millipore] was incubated with 50 µg recombinant wild-type GST-S4/S5 linker for 1 h at 30°C in 20 mM HEPES/NaOH pH=7.4, 0.1 mg/ml phosphatidylserine, 0.01 mg/ml diacylglycerol, 100 µM $CaCl_2$, and 100 µM adenosine-5'-triphosphate [ATP]) and *Mwk* GST-S4/S5 linker. The cerebellar lysates were pre-cleared with a mix of glutathione sepharose beads (GE healthcare) and GST by rotating for 1 h at 4°C and centrifuging for 2 min at 300 *g* at 4°C. The supernatants were incubated separately with 30 mg of different pulldown proteins and incubated for 2 h rotating at 4°C. The GST proteins were pulled down with glutathione sepharose beads by rotating for 1 h at 4°C and centrifuging for 2 min at 300 *g* at 4°C, and removing carefully with a syringe. GST constructs were briefly washed 5 times with lysis buffer. The NuPAGE LDS sample buffer (Invitrogen) was added to the pulled down proteins. The pulled down proteins were analysed by Invitrogen NuPAGE gel (1.5 mm, 10 well, 6-12%) and stained with Imperial Protein Stain (Pierce). The protein bands were cut out from the gel by clean razor blades into 1x1 mm pieces for a subsequent mass spectrometry analysis.

Immunoprecipitation from Brain for Mass Spectrometry Analysis

One cerebellum was used per one immunoprecipitation (IP) experiment for a subsequent mass spectrometry analysis. One cerebellum was lysed in either 1 ml CHAPS lysis buffer without calcium (1% CHAPS, 50 mM HEPES, 150 mM NaCl, 10% glycerol, 1.5 mM $MgCl_2$, 1 mM EGTA, 100 mM NaF, 1 mM Na_3Vo_4, 1 x Complete Protease Inhibitors [Roche]) or in 1 ml CHAPS lysis buffer containing calcium (1 mM EGTA was replaced by 2 mM $CaCl_2$), by sonicating 2 x 20 s with 1 min rest on ice. The lysed brains were incubated on ice for 10 min and then centrifuged for 20 min at 4˚C at maximum speed. The supernatant was collected. To the supernatant, 30 µl of protein G sepharose was added

and rotated for 1 hour at 4˚C to remove any unspecific binding. The sepharose beads were removed by centrifuging at 2,300 *g* for 2 min at 4˚C, the supernatant was collected. To the lysates, 2 µg of α TRPC3 antibody (Alomone) was added. The mixture was incubated for 3 h at 4˚C while rotating. After that 30 µl of protein G sepharose was added and incubated further for 1 h. The sepharose beads were then collected by centrifuging at 2,300 *g* for 2 min at 4˚C, the supernatant was removed. The beads were then briefly washed once in 1 ml CHAPS buffer, and centrifuged at 2,300 *g* for 2 min at 4˚C. The supernatant was carefully removed with a syringe after all washes. Then washed briefly in 20 mM Tris pH=7.5, and centrifuged at 2, 300 *g* for 2 min at 4˚C. To the beads 2x NuPAGE sample buffer (Invitrogen) was added and the mixture was boiled at 100˚C for 5 min and centrifuged for 1 min. The sample was loaded onto the NuPAGE 4-12% Bis-tris gradient gel (Invitrogen) and stained with Imperial Coomassie stain (Pierce).

LC-MS/MS Mass Spectrometry

The proteins in the gel bands were digested according to the tryptic digestion protocol described by Shevchenko and colleagues in the Nature Methods journal (Shevchenko et al 2006). Trypsin used in this protocol was from Promega.

Digested protein material was analysed by liquid chromatography using an Ultimate 3000 nano-HPLC system (Dionex, Sunnyvale, CA, USA) interfaced with a 3D high capacity ion trap mass spectrometer (AmaZon; Bruker Daltonics, Billerica, Massachusetts, USA). Raw liquid chromatography–mass spectrometry (LC-MS/MS) data were processed using DataAnalysis 3.4 (Bruker Daltonics) and Mascot software with the SwissProt database.

The LC-MS/MS mass spectrometry experiments were performed by Dr Frank Sobott and Dr Holger Kramer.

Immunoprecipitation from Brain for Western Blot Analysis

One cerebellum was used per three IP experiments for a subsequent analysis by western blot. One cerebellum was lysed in 1 ml nonyl phenoxypolyethoxylethanol (NP-40) lysis buffer (150 mM NaCl, 0.5% NP-40, 10 mM Tris pH=7.5, 1 mM EGTA, 100 mM NaF, 1 mM Na_3VO_4, 1 x Complete Protease Inhibitors [Roche]) by sonicating for 10 s. The lysed brains were incubated on ice for 10 min and then centrifuged for 20 min at 4˚C at maximum speed. The supernatant was collected and diluted in NP-40 buffer to make the total of 3 ml (1 ml per IP), and distributed to three separate tubes. As an input, 20 µl of this supernatant was used. To the supernatant, 30 µl of protein G sepharose was added, the mixture was left rotating for 1 hour at 4˚C to remove any unspecific binding. The sepharose beads were precipitated by centrifuging at 2,300 *g* for 2 min at 4˚C, the supernatant was collected (30 µl of this supernatant was saved and used as input). To the lysates, 1 µg of α TRPC3 antibody (Alomone) was added. The mixture was incubated for 1 h at 4˚C while rotating. After that 20 µl of protein G sepharose was added and incubated further for 1 h. The sepharose beads were then collected by centrifuging at 2,300 *g* for 2 min at 4˚C, the supernatant was removed. The beads were then washed briefly x 4 times in 1 ml NP-40 buffer, and centrifuged at 2,300 *g* for 2 min at 4˚C. The supernatant was carefully removed with a syringe after all washes. The last wash was in 1 ml of 20 mM Tris pH7.5, and centrifuged at 2,300 *g* for 2 min at 4˚C. The supernatant was removed. To the beads 2x NuPAGE sample buffer (Invitrogen) was added and the mixture was boiled at 100˚C for 5 min and centrifuged for 1 min. The sample was loaded onto the NuPAGE 4-12% Bis-tris gradient gel (Invitrogen) and a western blot analysis was performed.

Immunoprecipitation from Cells for Western Blot Analysis

24 h after cells were transfected with an appropriate construct (with a FLAG or HA tag) on a 12-well plate, cells were lysed in 1 ml NP-40 lysis buffer per well (150 mM NaCl, 0.5% NP-40, 10 mM Tris

pH=7.5, 1 mM EGTA, 100 mM NaF, 1 mM Na_3VO_4, 1 x Complete Protease Inhibitors [Roche]) by being scraped off. The lysed cells were incubated for 10 min on ice, and then centrifuged for 20 min at 4˚C at maximum speed. The supernatant was collected and 30 µl was kept as input. 10 µl of EZview™ Red ANTI-FLAG® M2 Affinity Gel (Sigma) beads were used to immunoprecipitate proteins with a FLAG tag; and 10 µl of EZview™ Red ANTI-HA® M2 Affinity Gel (Sigma) beads were used to immunoprecipitate proteins with an HA tag. The lysates with the beads were incubated for 2 h at 4˚C while rotating. The samples were then centrifuged for 30 s at 8,200 *g* at 4˚C and the supernatant was removed with a syringe. Then, the samples that had EZview™ Red ANTI-FLAG® beads, were briefly washed x 4 times in 0.5 ml NP-40 buffer and 1 x in 0.5 ml TBS with gently shaking the tube in-between washes and centrifuging for 30 s at 8,200 *g* at 4˚C. Each time the supernatant was carefully removed with a syringe. When EZview™ Red ANTI-HA beads were used, the samples were washed x 5 times in NP-40 buffer. To the beads 2x NuPAGE sample buffer (Invitrogen) was added and the mixture was boiled at 100˚C for 5 min and centrifuged for 1 min. The sample was loaded onto the NuPAGE 4-12% Bis-tris gradient gel (Invitrogen) and a western blot analysis was performed.

Laser-capture Microdissection RNase Inhibitor Method

The water used for laser-capture microdissection (LCM) was always nuclease-free (Invitrogen). ProtectRNA™ RNase inhibitor (Sigma) was added to all ethanol dilutions (50%, 75%, 95%). Sagittal 10 µm sections of the fresh frozen cerebella were cut on a cryostat and placed on PEN-membrane covered slides (Zeiss), which were pretreated with RNase Zap (Sigma), rinsed with nuclease-free water and left to dry in a tissue culture hood. After sectioning, the slides were fixed and hydrated in a series of 95%, 75%, 50% ice cold ethanol dilutions for 30 s each (containing RNase inhibitor), stained for ~1 min with 1% cresyl violet (Sigma) dissolved in water, washed in 50%, 75%, 95% ethanol dilutions for 30 s each (containing RNase inhibitor), dehydrated twice in 100% ethanol for 30 s and

twice in xylene (30 s and 5 min). The slides were left to air dry briefly before proceeding with the LCM. Purkinje cells were microdissected from the cerebellar sections using a P.A.L.M Micro Beam system in combination with Robo software (Carl Zeiss). Cerebellar sections were visualized under a light microscope and Purkinje cells were selected manually by a drawing tool. They were then automatically cut and catapulted into a tube cap containing 40 µl RLT lysis buffer (Qiagen) with β-mercaptoethanol (Sigma). For the microarray analysis, 1000 Purkinje cells were dissected; for the quantitative Reverse Transcription PCR (qRT-PCR) analysis, 300-500 cells were dissected. Immediately after LCM, the tubes were centrifuged to collect the cells from the cap to the bottom of the tube, and immediately frozen on dry ice and stored at -80°C until RNA extraction. The whole procedure, including slide preparation and LCM, was limited to approximately 1.5 hours in order to avoid unnecessary RNA degradation.

RNA Extraction

RNA was extracted using the RNeasy MICRO kit (Qiagen) according to the Fibrous Tissues protocol starting from point number 4 in 150 µl total volume. The RNA was eluted in 10µl of water. The RNA quality and integrity was assessed on a 2100 BioAnalyzer using the RNA 6000 Pico Assay (Agilent Technologies) by Sheena Lee.

Microarray

The microarray experiment was performed by Sheena Lee. Labelled ssDNA for hybridization was generated from 1 ng starting RNA as follows: 1 ng of RNA from each of 4 biological replicates was reverse transcribed and the cDNA was amplified using the Ovation Pico WTA system (NuGEN) according to manufacturer's instruction. One low input 0.1 ng control was processed together with the samples and no similar amplification was found ruling out any contamination. Amplified double-

stranded cDNA was transformed into single-stranded sense cDNA using the WT-Ovation™ Exon Module (NuGEN). Sense cDNA was fragmented and labelled with biotin using the Encore™ Biotin Module (NuGEN). Successful fragmentation was confirmed for all samples on the BioAnalyzer showing a peak sequence length of around 200 nucleotides. Fragmented and labelled single-stranded sense cDNA was hybridized to Affymetrix Mouse Gene 1.0 ST arrays at 45°C overnight. Arrays were washed and then stained using the GeneChip® Hybridization, Wash and Stain Kit (Affymetrix) on an Affymetrix GeneChip Fluidics Station 450. The microarrays were scanned on an Affymetrix GeneChip Scanner 3000.

For the microarray analysis, arrays were Robust Multichip Average (RMA) or Probe Logarithmic Intensity ERror (PLIER) normalised in GeneSpring GX 11 (Agilent) and differentially expressed genes were identified using an unpaired t-test or Welch t-test respectively, with a p-value cut off of ≤0.05 and a fold change difference between the *Mwk* and wild-type Purkinje cells of ≥ 1.5. Differentially expressed genes were hierarchically clustered. Over-representation statistics were calculated in GO-Elite (http://www.genmapp.org/go_elite/go_elite.html) to identify a minimal non-redundant set of Gene Ontology (GO) biological terms or pathways to describe the list of genes. Only ontologies with ≥3 genes changing and a permuted p-value ≤0.05 were selected. Gene interaction networks and canonical pathways were also analysed using the Ingenuity Pathways Analysis (Ingenuity® Systems, www.ingenuity.com).

qRT-PCR Primer Design and Validation

The primers were designed using the Primer Express 3.0 Programme (see Table 2-7 for list of primers). The following parameters were changed:

- Minimum primer % GC content: **40**
- Maximum primer % GC content: **60**
- Primer 3' GC clamp residues: **1**
- Minimum primer length: **18**
- Maximum primer length: **22**
- Maximum amplified region length: **≤250**

Whole cerebellar lysates were used for primer validation. mRNA was extracted from the whole cerebella using the RNeasy Mini Kit (Qiagen) according to manufacturer's instructions, and reverse transcribed using the Expand Reverse Transcriptase (Roche) with the Protector RNase Inhibitor (Roche). The following cDNA dilutions were then used in the qRT-PCR reaction for primer validation: 1/2, 1/5, 1/10, 1/20, 1/50, 1/100, 1/500, 1/1000. Original (not fast) SYBR® Green PCR Master Mix (Applied Biosystems) was used for the qRT-PCR reactions and the reaction was carried out on a 7500 Real-Time PCR Machine (Applied Biosystems). *Calbindin* gene was used as an endogenous control.

The qRT-PCR reaction:

cDNA	1 µl
10 µM Forward Primer	1 µl
10 µM Reverse Primer	1 µl
Nuclease-free water	7 µl
SYBR® Green Master Mix	10 µl
	Total = 20 µl

Each reaction was performed in triplicate on the same plate. For a reliable reaction, the amplification plot should show uniform expression of the three replicates. The Melt Curve plot should only have one peak, confirming the specificity of the primers. If these criteria were met, a graph "C_T vs. Log[cDNA]" was plotted, and primer efficiency was determined from its slope using the following formula: $E = (10^{-1/slope} - 1) \times 100\%$. The primers were considered efficient when efficiency was between 85%-105%.

Table 2-7. Primers for qRT-PCR

Gene		Sequence	Location in gene
Unc13c	F	5′ GGCTACCACACCCACCTACTG 3′	Exon 7
	R	5′ CCTCCGCACCGTGCTTAG 3′	Exon 8
Cntn3	F	5′ TGGAAGCCGATCTGAACTAGTG 3′	Exon 16
	R	5′ AAGCAACCACATACCCAAAACC 3′	Exon 17
Stk17b	F	5′ CGGGAGGACAAGGAGAACATC 3′	Exon 8
	R	5′ GGCAAGGAGTCATCGAATCG 3′	Exon 8
Nlk	F	5′ TCGCATCATCCGCAACAG 3′	Exon 1
	R	5′ CCAAAGGCTCCATATCCAATTG 3′	Exon 1
Tsg101	F	5′ GTTCTCCCGGCCTACTGTTTC 3′	Exon 5
	R	5′ GGTTGGGAGGGTATCCAGATG 3′	Exon 6
Hn1l	F	5′ GGAGCCCACACCTACAGTTGAC 3′	Exon 5
	R	5′ AGAAGGAGAGGCTGGATTTGC 3′	Exon 5
Zbtb20	F	5′ GCTACAGCGACATCGAAATCC 3′	Exon 14
	R	5′ GCACACCGCTGTACATGAAGTC 3′	Exon 14
Sv2c	F	5′ TGCATGTCTGTCAACGGATTC 3′	Exon 3
	R	5′ AGCAACCGACAGACGAGAAAG 3′	Exon 3
Ipo5	F	5′ GCGCAGTTTGGTGGAGATAAC 3′	Exon 23
	R	5′ AGCCTCTGGAGCCTGAATGAC 3′	Exon 24
Fbrs	F	5′ GGCCTCAGCTTCGAGTTTCTC 3′	Exon 11
	R	5′ TTACCCGCACAGACTCTTTGG 3′	Exon 11
Car2	F	5′ AAGATTGGACCTGCCTCACAAG 3′	Exon 4/5
	R	5′ ACGCTTCCCCTTTGTTTTAATG 3′	Exon 5
Opn3	F	5′ TCGAATGCTTCGCTGTGTTG 3′	Exon 2/3
	R	5′ CCATCAAAAAGCACATCTTTGC 3′	Exon 3
Bet1	F	5′ GCAGCTATGGGAACTATGGCTATG 3′	Exon 2
	R	5′ CCGTTACTTTGCTTCTCAGACTTTC 3′	Exon 2
Flt3	F	5′ TGCACCAAGCTGTTCACCATAG 3′	Exon 6
	R	5′ CCCCCACTTTCAGGAATAACTG 3′	Exon 7
Calbindin	F	5′ TGTGTGGGAAAGAGTTCAATAAGG 3′	Exon 9
	R	5′ TCCAGCTCATTTTCATCTATGTATCC 3′	Exon 10

qRT-PCR

To analyse the expression of genes of interest at different ages by qRT-PCR, reverse transcription reaction was performed using the SuperScript™ III First-Strand Synthesis System (Invitrogen), designed for small quantities of starting RNA, according to manufacturer's instructions. The RNA was pre-amplified using the TaqMan® PreAmp Master Mix Kit (Invitrogen) according to manufacturer's instructions. qRT-PCR reaction was performed using the original (not fast) SYBR® Green PCR Master Mix (Applied Biosystems) and a 7500 Fast Real-Time PCR Machine (Applied Biosystems).

Relative expression was calculated using the $\Delta\Delta C_T$ method:

- $\Delta C_T = C_T$(target) – C_T(endogenous control – calbindin) and
- $\Delta\Delta C_T = \Delta C_T$(*Mwk*) - ΔC_T(wild-type)

In situ hybridisation

RNase ZAP (Sigma) was used to clean surfaces and instruments. Glass bottles and magnetic fleas were baked at 250°C overnight. Water was diethylpyrocarbonate (DEPC)-treated.

The *in situ* probes were prepared using the pCR®4-TOPO® kit (Invitrogen). The primers are shown in Table 2-8 (For *Car2*, *Sv2c* and *Stk17b* primer sequences were the same as in the Allen Brain Atlas; for *Cntn3*, *Ipo5* and *Opn3* primers were designed by me):

Table 2-8. Primers for *in situ* hybridisation

Gene		Sequence	Insert Vector	Probe size (nt)
Car2	**F**	5′ ATTGTCAACAACGGCCAC 3′	pCR®4-TOPO®	840
	R	5′ CCGTGGCAGAGAAAAGATG 3′		
Cntn3	**F**	5′ ACAAGTCTGGACCATCGTTAC 3′	pCR®4-TOPO®	302
	R	5′ CGACTGTCTTCTTCAACAAATG 3′		
Ipo5	**F**	5′ CCAGAAGGAGCTGAGACTGC 3′	pCR®4-TOPO®	242
	R	5′ TAACCACGGGAAGGTACTGC 3′		
Opn3	**F**	5′ CGTGGACTGGAGATCCAAG 3′	pCR®4-TOPO®	294
	R	5′ GTGACCAGGTGTCCATAGCC 3′		
Sv2c	**F**	5′ TTCAGCCTACCAGTTCCACAG 3′	pCR®4-TOPO®	319
	R	5′ AATTCCGTACAGTTCGGTGC 3′		
Stk17b	**F**	5′ GCTAGGCTTCTGTTGGCTAGC 3′	pCR®4-TOPO®	973
	R	5′ GTTTTGGCGACGGAGTCTG 3′		

Expand High Fidelity polymerase (Roche) was used to amplify the probes from the DNA of a wild-type mouse cerebellum. The PCR product was then inserted into the pCR®4-TOPO® vector, according to the manufacturer's instructions. The probes were linearised by cutting the miniprep DNA with an

appropriate enzyme, depending on the direction of the insert (determined by sequencing): if the cDNA sequence was inserted in the forward direction, SpeI, PstI or PmeI restriction enzymes were used; if the cDNA sequence was inserted in the reverse direction, NotI restriction enzyme was used. The linearised vector was purified by gel purification (Qiagen). The *in vitro* transcription reaction was carried out for 1.5 h at 37˚C using either T3 RNA polymerase (for cDNA inserted in reverse direction) or T7 RNA polymerase (for cDNA inserted in forward direction) (Roche) as follows:

Linearised DNA (~1.5 µg)	10 µl
10X DIG RNA Labelling Mix (Roche)	2 µl
10X T3/T7 Polymerase Buffer	2 µl
Protector RNase Inhibitor (Roche)	1 µl
T3/T7 RNA Polymerase (Roche)	2 µl
H_2O	3 µl
	Total = 20 µl

The RNA *in situ* probes were purified using the mini Quick Spin RNA Columns (Roche) according to manufacturer's instructions and stored at -80˚C.

The 10 µm brain cryosections were prepared from fresh frozen brains and stored at -80°C. The slides were first thawed and fixed in 4% PFA in PBS for 10 min at room temperature and washed 3 x 3 min in PBS while shaking. The slides were then placed into the acetylation mix (5.69 ml triethanolamine, 780 µl HCl in 442 ml H_2O), while stirring with a magnetic flea. 1 ml of acetic anhydride was added dropwise over a 4 min period and left to stir for another 6 min. The slides were then washed 3 x 5 min in PBS. The slides were put on a rack in a chamber (so the bottom of the slide does not touch the bottom of the chamber). A line of vulcanised rubber (bike shops) was placed at each end of the slide to prevent liquid spreading, and 200 µl of hybridisation solution (50% Deionised Formamide, 200 µg/ml *E.Coli* tRNA [Sigma], 1X Denhardt's solution [Sigma], 100 mg/ml Dextran Sulphate, 35 mg/ml NaCl, 2.4 mg/ml SDS and 1 mM EDTA pH=8 in H_2O; heated to 60˚C to dissolve everything and cooled down) was pipetted directly onto the slides and incubated at room temperature for 1 h. After 1 h, the

slides were drained and the probe was added onto the sections: 1 µl probe in 200 µl hybridisation solution. Parafilm was put on top of the slides for an even distribution of the liquid. To the bottom of the chamber the following solution was added: 5X SSC (175 mg/ml NaCl, 88 mg/ml in H_2O) with 50% formamide. The chamber with the slides was then incubated overnight for 16-20 h at 60˚C. The next day the slides were removed and placed into 50 ml Falcon tubes containing 30 ml 5X SSC (pre-warmed in a 70˚C water bath) for 5 min at 70˚C. The parafilm was removed from the slides and placed into 0.2X SSC solution for 1 h in a 70˚C water bath with slight shaking. The slides were then washed in fresh 0.2X SSC solution for 5 min at room temperature. Then, the slides were incubated for 5 min at room temperature in B1 solution (150 mM NaCl, 100 mM Tris pH=7.6) after which the slides were drained from water and a Liquid Blocker Super Pap Pen was used to draw around the edges. The sections were blocked in 500 µl blocking solution (10 mg/ml blocking powder from digoxigenin (DIG) detection kit (Roche) in B1, stirred while heating and then cooled down) for 1 h at room temperature. The slides were again drained onto a tissue and 500 µl blocking buffer with anti-DIG antibody (Roche) (1:5000 dilution) was pipetted onto the slides. The slides were incubated in a chamber with water at 4˚C overnight. To detect the probes, the slides were washed 3 x 5 min in B1 and equilibrated for 5 min in B2 solution (100 mM NaCl, 100 mM Tris pH=9.5, 50 mM $MgCl_2$ in H_2O). The light-sensitive detection mixture (20 µl/ml nitro blue tetrazolium/5-bromo-4-chloro-3-indolyl phosphate [NBT/BCIP] solution [Roche] in B2) was pipetted directly onto slides and left in the dark at room temperature for 12-48 h depending on when the sections start developing the colour. Once the colour was visible, the slides were washed 2 x 5 min in PBS and mounted in 90% glycerol with glass coverslip, ready to be viewed under a light microscope.

Transcription factor binding sites

Sequence 1 Kb upstream of the genes of interest including 10 bp of the 5’ UTR was used for the Transcription Element Search System (TESS) analysis in order to identify potential transcription factor binding sites (http://www-bimas.cit.nih.gov/molbio/signal/).

CHAPTER 3. Identification of TRPC3 Interaction Partners

Introduction

The *Moonwalker* (*Mwk*) mouse is an animal model of cerebellar ataxia with motor and coordination defects and abnormal development of Purkinje cell dendrites. *Mwk* mice have a point mutation in a transient receptor potential canonical channel, type 3 (TRPC3), which is a non-selective ion channel permeable to Ca^{2+} and Na^{+} upon activation (Becker et al 2009). The *Mwk* point mutation in the *Trpc3* gene leads to the substitution of a polar threonine amino acid to a nonpolar alanine in the protein, which is located in the region between transmembrane domains four and five, and will be referred to as the "S4/S5 linker" (see Figure 1-9 for TRPC3 protein structure). The change of the amino acid alters TRPC3 channel gating by causing it to open more readily compared to the wild-type TRPC3. The mechanism of this gain-of-function mutation, however, remains to be elucidated.

The study of protein-protein interactions helps scientists to unravel the function and the mechanism of action of various proteins by elucidation of the functional protein complexes they take part in. TRPC3 interaction with different proteins is thought to be crucial for its proper function (Ambudkar & Ong 2007; Kiselyov et al 2005). There is a possibility that the *Mwk* mutation could alter binding affinity of some interaction partners/ regulators of TRPC3 due to the amino acid substitution. For instance, an *in vitro* kinase assay has shown that the *Mwk* mutation prevents phosphorylation of the S4/S5 linker by PKCγ, which is a mechanism of TRPC3 deactivation (Becker et al 2009; Venkatachalam et al 2003). Threonine in the S4/S5 linker that is replaced by alanine in the *Mwk* mutant protein is one of a few amino acids in the S4/S5 linker that can be phosphorylated, whereas an alanine residue

abolishes phosphorylation. The amino acid substitution could also cause a conformational change in the S4/S5 linker, altering the channel's properties. So, investigating the binding partners of the *Mwk* TRPC3 compared to the wild-type TRPC3 could shed light on why the channel is more active, and hence add to our understanding of abnormal development of Purkinje cells in the *Mwk* mice.

Therefore, we decided to investigate the cellular binding partners of both wild-type and *Mwk* TRPC3 channels. There are two widely used techniques that are used to identify protein interaction partners: Yeast Two Hybrid (Y2H) system and immunoprecipitation (IP) combined with mass spectrometry. Y2H screens a protein of interest against a library of proteins. However, the Y2H system depends on the solubility of the protein, therefore membrane proteins cannot be used in the original Y2H method. While this limitation was overcome in the split-ubiquitin version of the Y2H approach (Stagljar et al 1998), the methodology still requires expression of proteins in yeast, which does not support many post-translational modifications that are important for mammalian proteins. Therefore this technique was not chosen to investigate TRPC3 interaction partners. Tandem mass spectrometry is a powerful method for protein identification, based on their mass-to-charge ratio in combination with database searches. We decided to perform an IP experiment from cerebellar lysates with subsequent tandem mass spectrometry analysis in order to identify binding partners of wild-type and *Mwk* TRPC3 channels.

A number of proteins that interact with TRPC3 have already been identified and described in the literature (Table 3-1). The interaction sites of the known binding partners on the TRPC3 protein are displayed in Figure 3-1. It is evident from the figure that the known interactions occur either at the N-terminus or the C-terminus of the protein. However, no interactions are currently known to bind to the central region of the TRPC3 protein. It is therefore of particular interest to investigate whether any of the TRPC3 interaction partners bind the channel at the cytoplasmic linkers because their

binding affinity could be changed by the presence of the *Mwk* mutation in the S4/S5 linker. Also, when investigating wild-type TRPC3 binding partners, only one study so far has used an unbiased approach where all TRPC3 interactions were investigated by IP and mass spectrometry (Lockwich et al 2008). Lockwich and colleagues used crude membrane extracts from whole rat brains to perform the IP. Our study was designed not only to elucidate the differences between binding partners of wild-type and *Mwk* TRPC3, but would allow the identification of all protein interaction partners of TRPC3 in the mouse cerebellum.

Table 3-1. Interaction partners of the TRPC3 protein.

Sources: http://www.trpchannel.org, Ambudkar & Ong 2007

Aqp-2	Junctophilin-2	Plcγ2	Trpm4
Bkca	Mg29	Pmca	Trpp1
Calmodulin	Mxa	Rack1	Vamp2
Calreticulin	Ncx1	Rnf24	Wnk4
Cav1.2	Nkaα1	Ryr	Asnap
Caveolin-1	Orai1	Ryr2	
Epo-r	Orai2	Serca2	
Ezrin	Orai3	Snap23	
Fkbp12	Pde3a	Src	
Glut-4	Pka	Syntaxin3	
Gαq/11	Pkcβ	Trkb	
Homer-1	Pkg1	Trpc1	
Ip3r1	Plcβ1	Trpc4	
Ip3r2	Plcβ2	Trpc5	
Ip3r3	Plcβ3	Trpc6	
Junctate	Plcγ1	Trpc7	

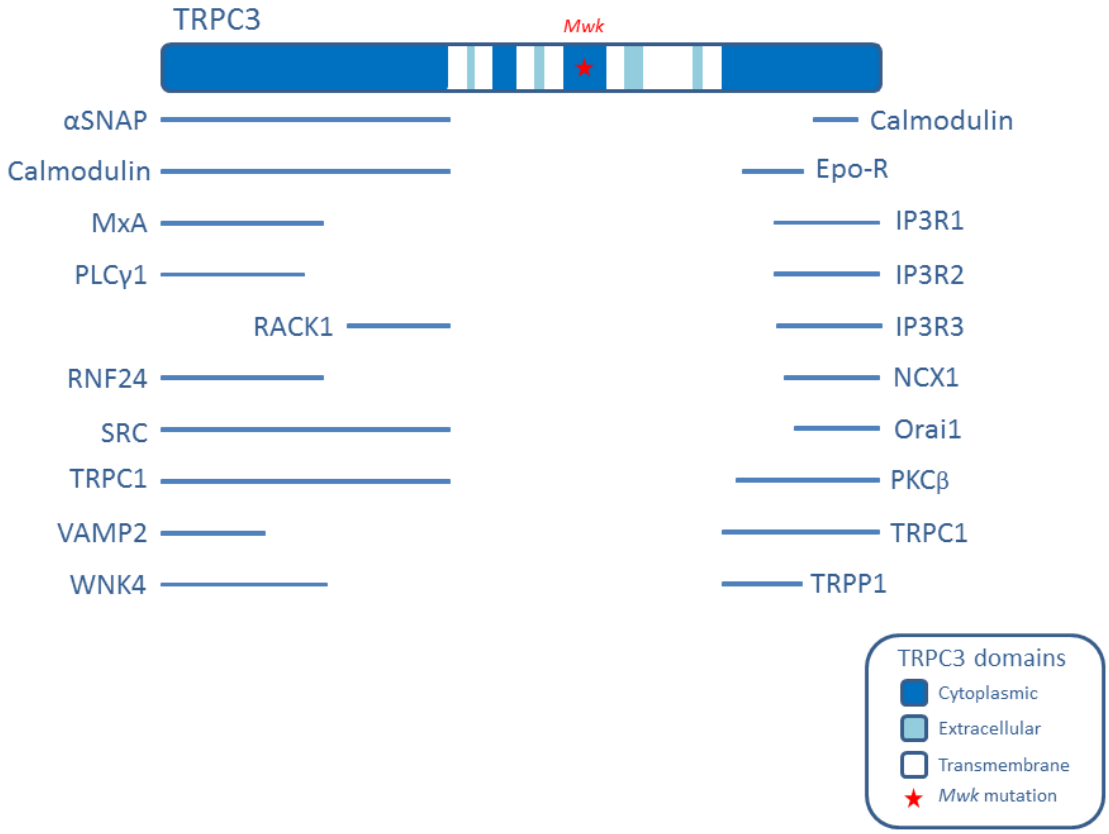

Figure 3-1. Binding sites of interaction partners on the TRPC3 protein. Schematic diagram of putative protein structure of the TRPC3 protein and the approximate location of binding of its known protein interaction partners. The data was retrieved from the TRIP database (http://www.trpchannel.org).

TRPC3 is located at the plasma membrane, where it can allow positively charged extracellular ions to enter the cell once the channel is activated by the mechanisms described in the main introduction (Cayouette & Boulay 2007). Furthermore, TRPC3 ion channels can also be found in small intracellular vesicles near the Endoplasmic Reticulum (ER) (Eder et al 2007). The channels that are located in these vesicles are inactive and upon activation they are translocated to the plasma membrane and fused with it through a VAMP-2 dependent mechanism, allowing the channel to be permeable to extracellular cations (Kim et al 2006; Singh et al 2004). The exact mechanism by which the wild-type TRPC3 is translocated into the plasma membrane is not completely understood, but it is believed that the binding partners of TRPC3 are important mediators of that process (Cayouette & Boulay 2007; Singh et al 2004).

One of the well-known interaction partners of TRPC3 is the inositol 1,4,5-triphosphate receptor (IP_3R) (Kiselyov et al 1998). The IP_3 receptors are a family of calcium channels located at the ER and they function by releasing calcium from internal stores upon activation by mGluR1 signalling (Mikoshiba 2011b). Particularly interesting for our study is the IP_3R1, because it is the major isoform in the central nervous system and is enriched in the Purkinje cells of the cerebellum (Furuichi et al 1993). But more importantly, a mutation in IP_3R1 or its deletion causes SCA15, and abnormal function of IP_3R1 has been associated with SCA2, SCA3, and possibly SCA1 (Bezprozvanny 2011; Chen et al 2008; Knight et al 2003; Liu et al 2009; van de Leemput et al 2007; Yamazaki et al 2011). Moreover, knockout of IP_3R1 in mice causes abnormal arborisation of Purkinje cell dendrites in the cerebellum (Hisatsune et al 2006). Double knock-out mice of IP_3R2 and IP_3R3 do not display ataxia (Futatsugi et al 2005).

In our experiment, IP_3R1 can, first of all, be used as a positive control to confirm that the experiment produces reliable results. Furthermore, it would be interesting to investigate whether the *Mwk* mutation changes the binding affinity of IP_3R1 to TRPC3.

Calmodulin, a prominent Ca^{2+} sensor, is another known interaction partner of TRPC3 and it binds to the same region of the TRPC3 protein as IP_3R1, which is called the Calmodulin/IP_3R binding (CIRB) domain (Tang et al 2001). Calmodulin is thought to be tethered to TRPC3 in its resting state, which prevents TRPC3 from spontaneous activation. Depletion of calcium internal stores through IP_3R1 activation leads IP_3R1 to displace calmodulin through binding to the CIRB region, which causes TRPC3 translocation to the plasma membrane and its activation. With increasing concentration of intracellular calcium, calmodulin again competes for binding to the CIRB region of TRPC3, hence, inactivating the channel (Tang et al 2001; Zhang et al 2001). The CIRB domain of TRPC3 has also been implicated in channel translocation to the plasma membrane independent of IP_3R1 or calmodulin binding (Wedel et al 2003). A proposed mechanism of TRPC3 translocation to and from the plasma membrane upon its activation is through interaction with the scaffolding protein Homer1 (Kim et al 2006). Interestingly, Homer 1 was shown to control the dendritic morphology of Purkinje cells via calcium release from intracellular stores (Tanaka et al 2006a).

This body of evidence demonstrates that protein-protein interactions between TRPC3 and its binding partners are essential for the proper cellular function of the channel. Any significant alterations could cause the cells to function abnormally and might contribute to the dendritic phenotype of the *Mwk* mice.

Results

GST Pulldown from wild-type mouse cerebella

In order to investigate whether the *Mwk* mutation alters affinity of protein binding partners to the TRPC3 protein, we decided to perform a pulldown experiment, using only the S4/S5 region of TRPC3 (Figure 1-9) which harbours the *Mwk* mutation.

The wild-type and the *Mwk* S4/S5 regions of the TRPC3 protein were subcloned and fused to glutathione S-transferase (GST) and the recombinant proteins were then expressed and purified from *E. coli* (these proteins were already available in the lab). As well as comparing interaction partners of wild-type and *Mwk* S4/S5 linkers, a phosphorylated wild-type S4/S5 linker was also included in the pulldown experiment, because it could have different binding partners to the non-phosphorylated form of the S4/S5 linker. Also, it was shown that the threonine-to-alanine amino acid substitution in the S4/S5 linker of the protein results in its inability to be phosphorylated by PKCγ, therefore it could lack phospho-dependent interactions. For this, the wild-type GST-fused S4/S5 linker was phosphorylated by PKCγ using an *in vitro* kinase assay. GST protein without a linker was used as a negative control. The recombinant proteins used in the pulldown experiment are summarised in Figure 3-2.

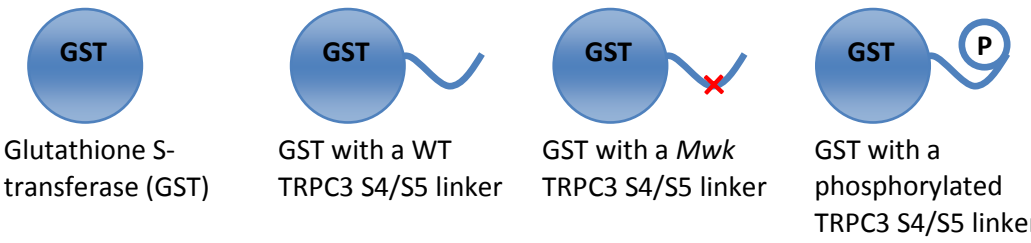

Figure 3-2. A schematic diagram of the recombinant proteins used in the cerebellar pulldown experiment to investigate whether the *Mwk* mutation alters interaction partners of TRPC3. The following GST-fusion proteins were used for the pulldown experiment: GST protein (used as a negative control), wild-type TRPC3 GST-S4/S5 linker, *Mwk* TRPC3 GST-S4/S5 linker and PKCγ phosphorylated wild-type TRPC3 GST-S4/S5 linker.

Whole wild-type cerebellar lysates were used to identify the interaction partners of the TRPC3 S4/S5 linkers. To pre-clear the cerebellar lysates, we used GST proteins and precipitated them together with unspecific binders using glutathione beads. The pre-cleared cerebellar lysates were then incubated with either GST proteins only (as a negative control), with the wild-type TRPC3 GST-S4/S5 linker, with the *Mwk* TRPC3 GST-S4/S5 linker, or the phosphorylated wild-type TRPC3 GST-S4/S5 linker. Glutathione beads were used to pull down GST proteins, which were then run on an SDS-PAGE gradient gel and stained with a Coomassie stain (Figure 3-3). The GST-fusion proteins were visible on the gel and are marked with an asterisk in the figure (*). The intensity of the GST-fusion protein bands allowed us to judge the amount of the starting recombinant proteins used to pull down their interaction partners. For this experiment, there was slightly less input of *Mwk* TRPC3 GST-S4/S5 linker, compared to other proteins. Taking into consideration this pulldown coomassie-stained gel, and also gels from other experiments performed previously, we selected four bands that showed differences in staining pattern between the different GST-fused S4/S5 linkers. The sizes of these proteins were approximately 230 kD, 75 kD, 70 kD and 60 kD, and they are marked with an arrow in the figure. The protein bands were cut out from each lane, cut into smaller pieces (approximately 1x1 mm), digested by trypsin, and analysed by LC-MS/MS mass spectrometry. The mass spectrometry was performed by Dr Frank Sobott and Dr Holger Kramer.

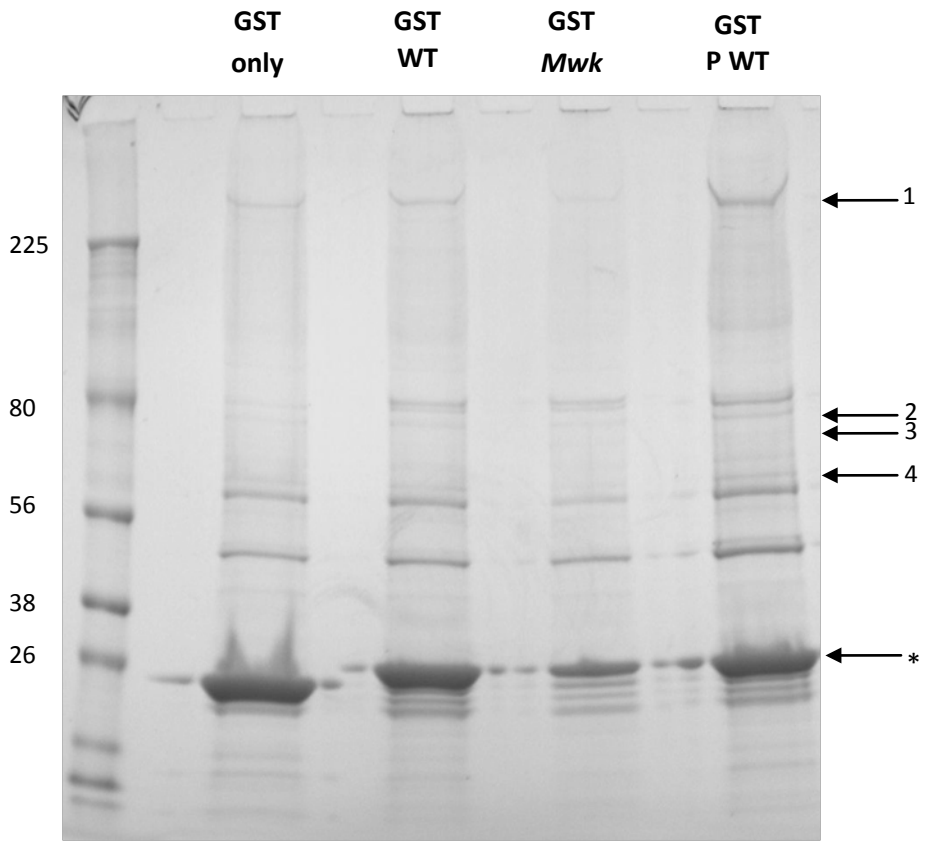

Figure 3-3. A NuPage gradient gel showing the results of a GST pulldown experiment. Proteins pulled down from wild type (WT) mouse whole cerebellar lysates with GST only, WT TRPC3 GST-S4/S5 linker, *Mwk* TRPC3 GST-S4/S5 linker, or phosphorylated (P) WT TRPC3 GST-S4/S5 linker. The proteins were run on a gradient NuPage gel (4-12%) and stained with an Imperial stain. Bands that were considered the most interesting from several pulldown experiments are marked with an arrow, and they were cut out from all four lanes, digested with trypsin and analysed by mass spectrometry. * These bands correspond to GST proteins. GST only protein in the first lane is smaller than the other recombinant proteins due to the lack of the GST-fused TRPC3 S4/S5 linker. n=3

The results of the tandem mass spectrometry experiment are shown in Table 3-2. Proteins that were also identified in the negative control GST lane are shown in grey and were not considered as true binding partners to the TRPC3 S4/S5 linker region. The first protein band corresponded to a protein called spectrin, which is a very common protein to emerge from the mass spectrometry experiments (Dr Frank Sobott, personal communication), and is most likely not specific to the S4/S5 linker. The second band showed a caskin 2 protein, which binds to both wild-type and *Mwk* S4/S5 linker, but not to the phosphorylated wild-type linker. From the same band, a protein called ELKS was identified as binding to the *Mwk* S4/S5 linker only. And a 78 kD glucose regulating protein was found binding to the phosphorylated wild-type S4/S5 linker. One of the proteins

identified from the third band was serum albumin, which is a common protein to be identified in a mass spectrometry experiment and it is not likely to be a genuine binding partner of TRPC3. In the third band syntaxin-binding protein 1 and V-type proton ATPase were found binding to the wild-type and phosphorylated wild-type S4/S5 linkers, but not to the *Mwk* linker. And a neurofilament light polypeptide bound only to the phosphorylated wild-type S4/S5 linker. The fourth protein band revealed ATP synthase α and protein disulphide-isomerase A3 binding to the phosphorylated wild-type S4/S5 linker. And puryvate kinase isozymes M1/M2 bound to both wild-type and phosphorylated wild-type S4/S5 linkers, but not to the *Mwk* linker.

So far, only the N- and the C-termini of TRPC3 have been implicated in interactions with other proteins. However, our results indicate that a number of proteins also can bind to and interact with the cytoplasmic S4/S5 region of TRPC3. Also, the tandem mass spectrometry experiments suggest differences between the binding partners of the wild-type S4/S5 linker, phosphorylated wild-type S4/S5 linker and the *Mwk* S4/S5 linker.

Table 3-2. Mass spectrometry results of the GST pulldown experiment. Proteins of the mouse cerebellum that bind to the GST protein (negative control), wild-type TRPC3 GST-S4/S5 linker, *Mwk* TRPC3 GST-S4/S5 linker and PKCγ phosphorylated wild-type TRPC3 GST-S4/S5 linker. Proteins identified in the negative control are shown in grey. The lane numbers correspond to different protein bands shown in Figure 3-3.

	GST only	GST – S4/S5 WT	GST – S4/S5 *Mwk*	GST – S4/S5 WT P
1	-	Spectrin α chain	Spectrin α chain	Spectrin α chain Spectrin β chain
2	Heat shock 71 kDa Stress-70 protein	Heat shock cognate 71kDa Heat shock 70 kDa Heat shock 70 kDa protein 1B Caskin-2 Stress-70 protein	Stress-70 protein Heat shock cognate 71 kDa ELKS/RAB6-interactin/CAST family member 1 Caskin-2	78 kDa glucose-regulated protein Heat shock cognate 71 kDa Heat shock 70 kDa Heat shock 70 kDa protein 1B Stress-70 protein
3	-	Dihydropyrimidinase-related protein 2 (DRP-2) Serum albumin Syntaxin-binding protein 1 V-type proton ATPase catalytic subunit A (V-ATPase subunit A)	-	Dihydropyrimidinase-related protein 2 (DRP-2) Neurofilament light polypeptide (NF-L) Serum albumin Syntaxin-binding protein 1 V-type proton ATPase catalytic subunit A (V-ATPase subunit A)
4	α Internexin Dihydropyrimidinase-related protein 2 (DRP-2)	α Internexin Dihydropyrimidinase-related protein 2 (DRP-2) Pyruvate kinase isozymes M1/M2	Dihydropyrimidinase-related protein 2 (DRP-2)	α Internexin ATP synthase α Dihydropyrimidinase-related protein 2 (DRP-2) Protein disulphide-isomerase A3 Pyruvate kinase isozymes M1/M2

Immunoprecipitation from wild-type and *Mwk* cerebella

In order to investigate, whether the proteins that have been identified in the GST pulldown were also precipitated by the whole TRPC3 protein, as well as to identify other TRPC3 interaction partners, we performed an immunoprecipitation (IP) experiment using α TRPC3 antibody to retrieve protein complexes from wild-type and *Mwk* whole cerebellar lysates. The cerebellar lysates were pre-cleared with protein-G sepharose beads, incubated with α TRPC3 antibody or α GFP antibody as a negative control, and precipitated with protein-G sepharose. We chose α GFP antibody for a negative control as it is also a polyclonal rabbit antibody, as is the α TRPC3 antibody that we used in the IP experiments. As we have reasons to believe that there is increased calcium influx into Purkinje cells of *Mwk* mice, it was important to investigate whether presence of calcium (2 mM $CaCl_2$) in the IP buffer affected the binding of proteins to TRPC3. Precipitated proteins were run on an SDS-PAGE gradient gel and stained with a coomassie stain (see Figure 3-4). The results show that there are differences between the affinities of TRPC3 binding partners when using the lysis buffer without calcium [A] and with calcium [B], which is evident from changes in the intensity of many bands when calcium is present in the buffer. There were a lot more proteins on the IP gel, compared to the GST pulldown, which is to be expected as the whole TRPC3 protein has a lot more potential interaction domains than the small S4/S5 region. In addition to that, the intact integral membrane TRPC3 protein is likely to exhibit a wider range of specific and non-specific membrane associated binders than a soluble protein construct. Endogenous wild-type and *Mwk* TRPC3 together with their binding partners were immunoprecipitated from wild-type and *Mwk* cerebellar lysates respectively. Due to the presence of a large number of protein bands, it is difficult to spot obvious differences between wild-type and *Mwk* binding partners. Also, the negative control lane shows many proteins that are also present in the TRPC3 IPs which highlights the challenges of IP experiments of integral membrane proteins. Therefore, whole lanes were excised and used for the subsequent tandem mass

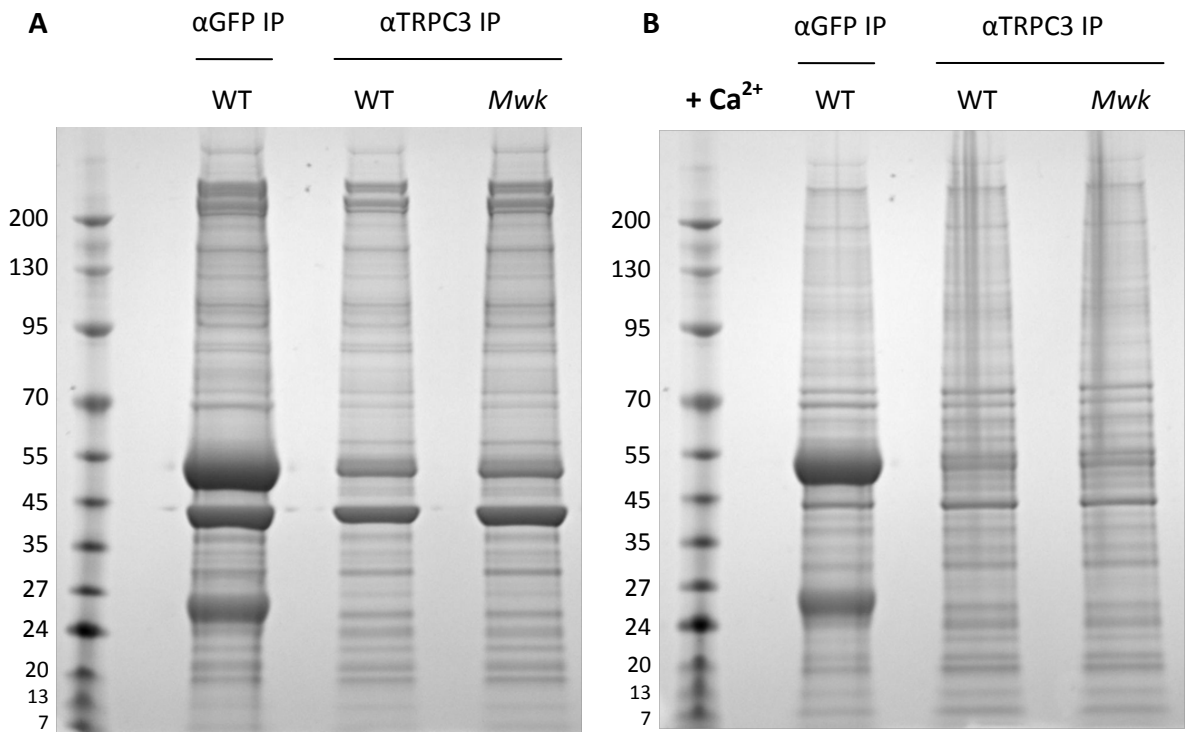

Figure 3-4. TRPC3 immunoprecipitation experiment from wild-type and *Mwk* mouse cerebella. Proteins precipitated from mouse whole cerebellar lysates with α GFP antibody as a negative control and α TRPC3 antibody without calcium in the lysis buffer (A) and with calcium in the lysis buffer (B). Samples were run on a gradient NuPage gel (4-12%) and stained with an Imperial stain. Whole lanes were cut out, digested with trypsin and analysed by mass spectrometry. n=2

spectrometry analysis. Each lane was first cut into eight segments (approximately 1x1 cm), which were processed by in-gel trypsin digestion individually in order to maximise the performance of the tandem mass spectrometry analysis. After the proteins were identified by database searches of the tandem mass spectrometry data, the results from each segment of the same lane were pooled together. The IP experiment was performed twice, the results of both experiments were combined and are shown in full in the Appendix A. Note that protein hits that were also identified in the negative control lane were removed from the TRPC3 IP results. Also, the following proteins were removed from the list as they are common contaminants in tandem mass spectrometry-based proteomics experiments: actin, actin-related proteins, ribosomal proteins, heat-shock proteins, histones, immunoglobulins, keratin, myelin, myosin and tubulin.

IP_3R1 was also found in the negative control lane of the IP experiment (binding to the GFP antibody); however, as it is a known binding partner of TRPC3, it was not removed from the results and was found to be associated with both wild-type and *Mwk* TRPC3 with and without calcium in the buffer.

The GST pulldown experiment had identified ELKS, caskin-2, syntaxin-binding protein, neurofilament proteins, pyruvate kinase isozyme M1/M2 and protein disulphide isomerase A3 (Table 3-2); however, none of these proteins were observed in the TRPC3 IP experiment.

V-type proton ATPase did not bind the *Mwk* S4/S5 linker whereas it was found to bind the wild-type and phosphorylated wild-type linker, as evident from the GST pulldown experiment. IP tandem mass spectrometry results, however, show that the V-type proton ATPase binds both wild-type and *Mwk* TRPC3 in the absence and presence of calcium, as well as being present in the negative control in the presence of calcium. Hence, the *Mwk* mutation most likely does not prevent binding of V-type proton ATPase to TRPC3, although it may still affect the strength of binding.

Based on the known functions of the proteins and their preference of binding wild-type or *Mwk* TRPC3, I selected 12 proteins for further studies, which are summarised in Table 3-3. These include CaMKIV and CaMKIIβ, which bind to *Mwk* TRPC3 with and without added calcium in buffer, respectively. PI synthase, binding to wild-type TRPC3 without calcium, *Mwk* TRPC3 with and without calcium, but not to the wild-type TRPC3 in the presence of calcium. Contactin 1, was only found to bind to the mutant *Mwk* TRPC3. PLCδ3 and syntaxin 1B were both identified to only bind wild-type TRPC3 in the presence of calcium. I also included syntaxin 1A in further validation experiments as it was previously found to interact with TRPC3 (Lockwich et al 2008). RAB3A binds wild-type TRPC3 without calcium and Mwk TRPC3 with and without calcium in the buffer, and does not bind TRPC3

Table 3-3. A list of interesting TRPC3 binding partners identified by IP and mass spectrometry from cerebellar lysates.

NAME	SHORT	GENE	WT	WT + Ca^{2+}	*Mwk*	*Mwk* + Ca^{2+}
Calcium/Calmodulin-dependent protein kinase type II subunit β	CaMKIIβ	Camk2b	-	-	-	√
Calcium/Calmodulin-dependent protein kinase type IV	CaMKIV	Camk4	-	-	√	-
Phosphatidylinositol synthase	PI synthase	Cdipt	√	-	√	√
Contactin 1		Cntn1	-	-	√	-
Inositol 1,4,5-trisphosphate receptor 1*	IP_3R1	Itpr1	√	√	√	√
Nuclear factor of activated T-cells 1**	NFAT1	Nfat1	-	-	-	-
Phospholipase C delta 3	PLC δ3	Plcd3	-	√	-	-
RAB3A		Rab3a	√	√	-	√
Synaptosomal-associated protein 25	SNAP25	Snap25	-	√	-	√
Syntaxin 1A		Stx1A	-	-	-	-
Syntaxin 1B		Stx1B	-	√	-	-
Synaptotagmin 1		Syt1	-	-	-	√

*IP_3R1 was present in the negative control, but because it is a known binding partner of TRPC3 we did not remove it from the results.

**NFAT1 was not identified in the mass spectrometry experiments, however, TRPC3 is known to activate NFAT-dependent transcription in muscle cells, and it would be interesting to investigate whether the two proteins interact.

with calcium in the buffer. SNAP25 binds to both wild-type and *Mwk* TRPC3 in the presence of calcium. And synaptotagmin 1 was found to bind to the mutant *Mwk* TRPC3 in the presence of calcium. In the subsequent validation experiments I also studied interaction with NFAT1, even though it was not identified in our tandem mass spectrometry experiments, because TRPC3 signalling has been shown to activate NFAT-regulated transcription in the heart (Poteser et al 2011). IP_3R1 was used as a positive control in the following validation experiments.

Constructs for co-immunoprecipitation experiments

To confirm whether the proteins of interest, selected from the tandem mass spectrometry experiments, can bind TRPC3 *in vitro*, we decided to express FLAG-tagged TRPC3 together with HA-tagged potential interaction partners in HEK293T cells. This cell line was chosen because it is known to be easily transfected with plasmid vectors.

The list of constructs used in this chapter can be found in Chapter 2. For PI synthase, PLCδ3, Rab3a, SNAP25, syntaxin 1A and syntaxin 1B, the cDNA was amplified from a wild-type mouse cerebellum and cloned into a pcDNA^{TM}3.1 Directional TOPO® vector. The HA tag was then introduced into the vector by insertional mutagenesis. Synaptotagmin 1 was amplified from a wild-type mouse cerebellum and cloned into a pCMV-HA vector, which already had an HA tag. Human CaMKIV was amplified from another construct containing a FLAG tag and inserted into the pCMV-HA vector. Rat Ip3r1 construct was kindly given to us by Professor GA Mignery (Loyola University Chicago) and contained no tags. The HA-NFAT1-GFP construct was obtained from Addgene. The human 3xFLAG-Trpc3 in the 3xFLAG-CMV^{TM}-7.1 vector was made by Dr Esther Becker and is routinely used in the lab. Western blots in Figure 3-5 show successful over-expression of the recombinant proteins of interest in HEK293T cells. Two constructs showed no protein expression in the cells or their expression was too low to be detected by immunoblotting, even though the cloning worked well and the correct sequence was inserted in frame as confirmed by DNA sequencing. These constructs were HA-PLCδ3 and HA-Synaptotagmin 1. For a

further two proteins of interest from Table 3-3, CaMKIIβ and Contactin 1, I was unable to amplify their genes from the mouse cerebellum or subclone them into a vector. These proteins were not analysed further.

Immunoprecipitation from HEK293T cells, co-transfected with 3xFLAG-TRPC3 and HA-tagged proteins of interest

Co-IP experiments were performed in HEK293T cells, in order to confirm the binding of proteins of interest to wild-type TRPC3. Unfortunately, transfecting any type of cells with *Mwk* TRPC3 results in cell death and therefore it was impossible to use *Mwk* TRPC3 in tissue culture experiments. HEK293T cells were co-transfected with 3xFLAG-tagged TRPC3 and HA-tagged protein of interest, lysed and incubated with EZview α FLAG beads. The beads bound 3xFLAG-TRPC3 and are expected to precipitate all proteins that bind to TRPC3 with sufficient affinity. These were then run on an SDS-PAGE gradient gel and probed with an α HA antibody to detect the HA-tagged protein of interest. Figure 3-6 [A-H] shows western blot analyses of the IP experiments run on a gradient gel, where the membranes were first probed for the protein of interest and then re-probed for FLAG to confirm the presence of 3xFLAG-TRPC3 in the IP samples. All IP experiments have good levels of 3xFLAG-TRPC3 expression. The first two lanes show the input of cells transfected with the protein of interest and empty 3xFLAG vector (negative control) and cells transfected with the protein of interest and 3xFLAG-TRPC3. The results of the IP experiment with an empty FLAG vector (negative control) are shown in lane 3, and the results of the 3xFLAG-TRPC3 IP are shown in lane 4.

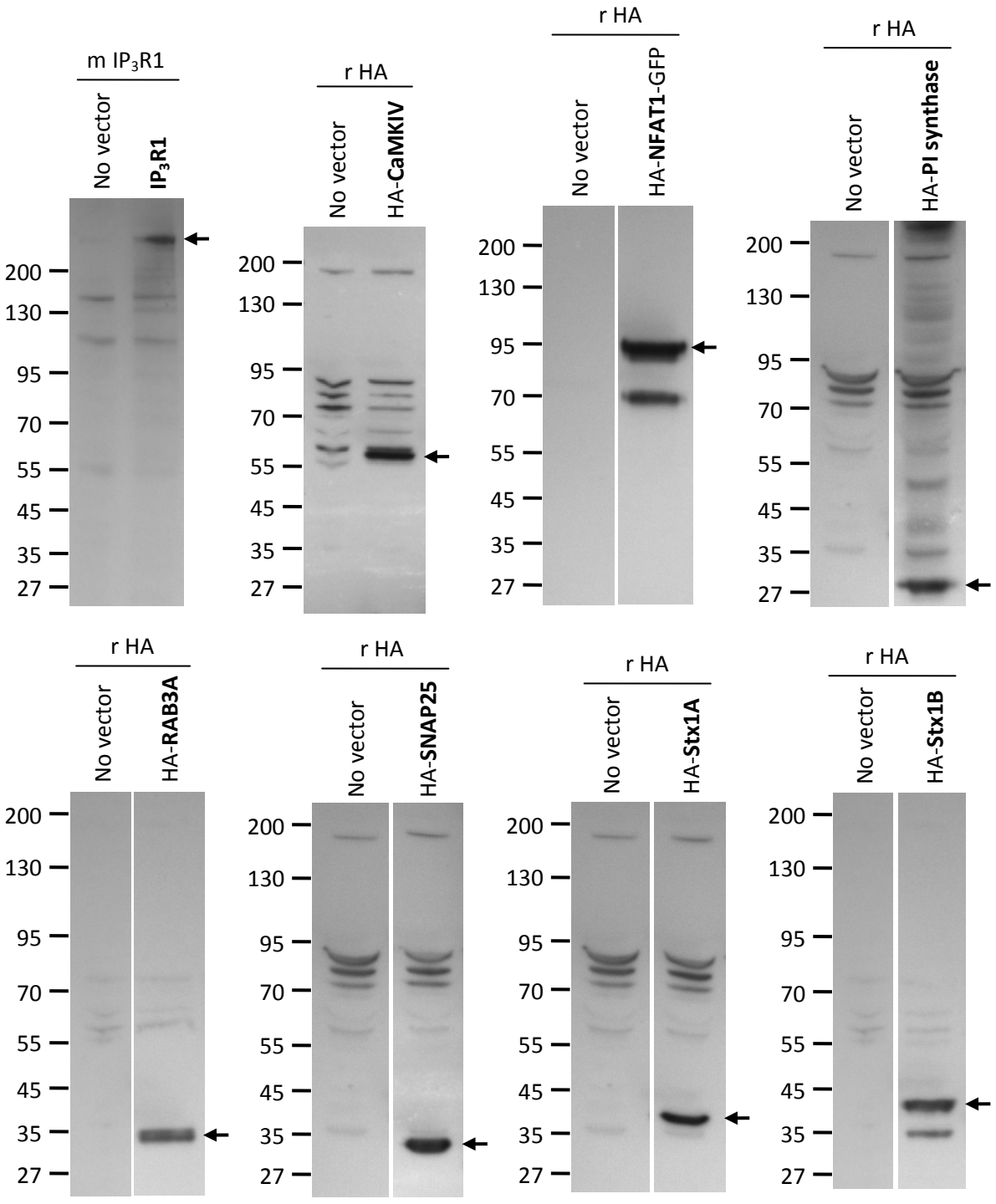

Figure 3-5. Expression of our proteins of interest in HEK293T cells. Western blots showing expression of potential TRPC3 binding partners compared to non-transfected cells. IP_3R1 vector was kindly given by Prof Gregory Mignery. All other constructs were subcloned from mouse cerebellum, except for CaMKIV which was subcloned from another vector. Arrows indicate the HA-tagged proteins of interest. n=2

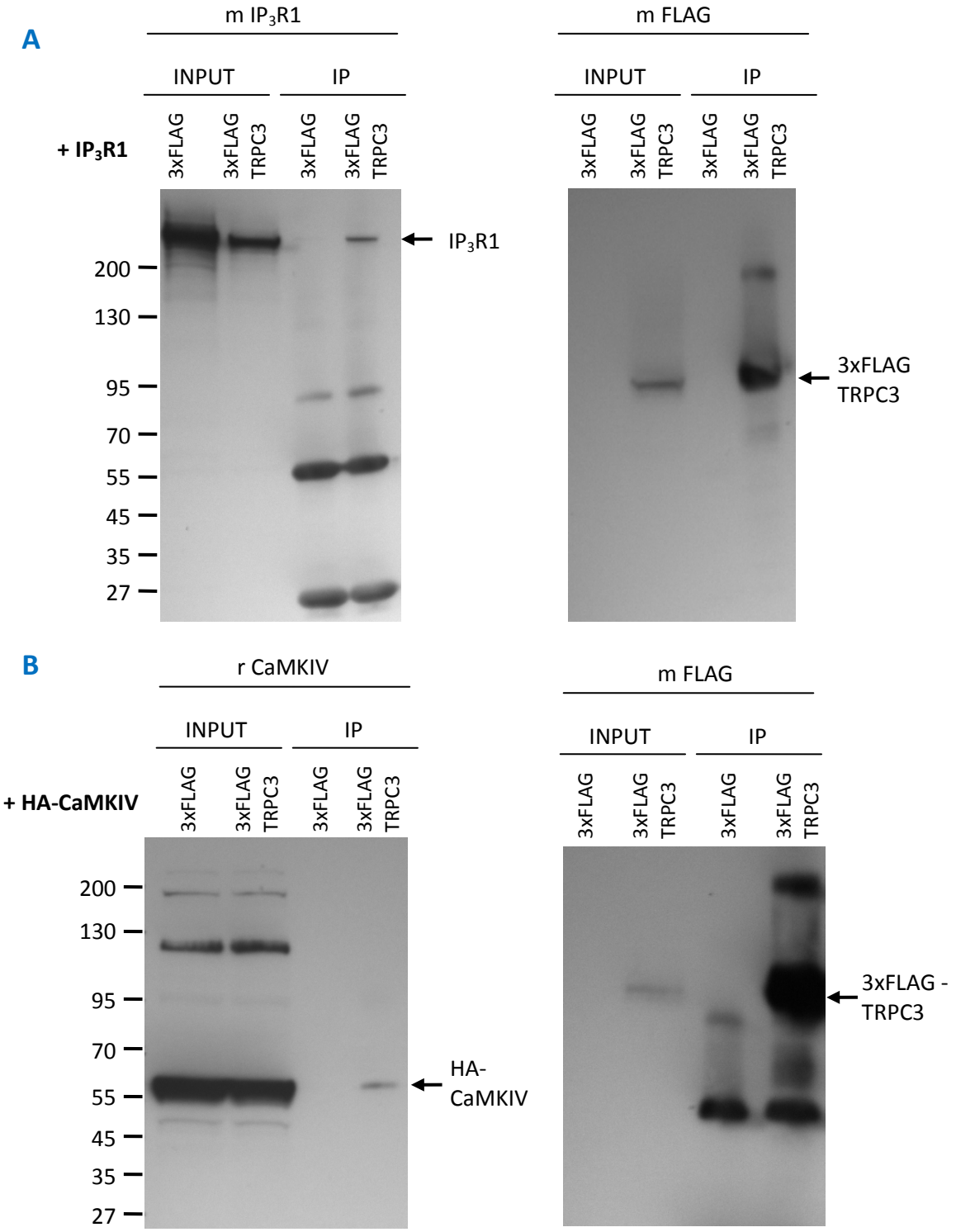

Figure 3-6 (A, B). Immunoprecipitation experiments using EZview α FLAG beads, precipitating FLAG-TRPC3 and its potential binding partners from transfected HEK293T cells. HEK293T cells were co-transfected with FLAG-TRPC3 and a potential binding partner constructs. They were then lysed and incubated with EZview α FLAG beads in order to pull down FLAG-TRPC3 together with its binding partners. The precipitated proteins were run on a gradient NuPAGE gel and probed for an appropriate antibody to detect the presence of potential binding partners. IP_3R1 (A) and HA-CaMKIV (B) both bind FLAG-TRPC3, and do not bind the negative control empty FLAG. Membranes were then re-probed using α FLAG antibody to confirm FLAG-TRPC3 expression. n=2

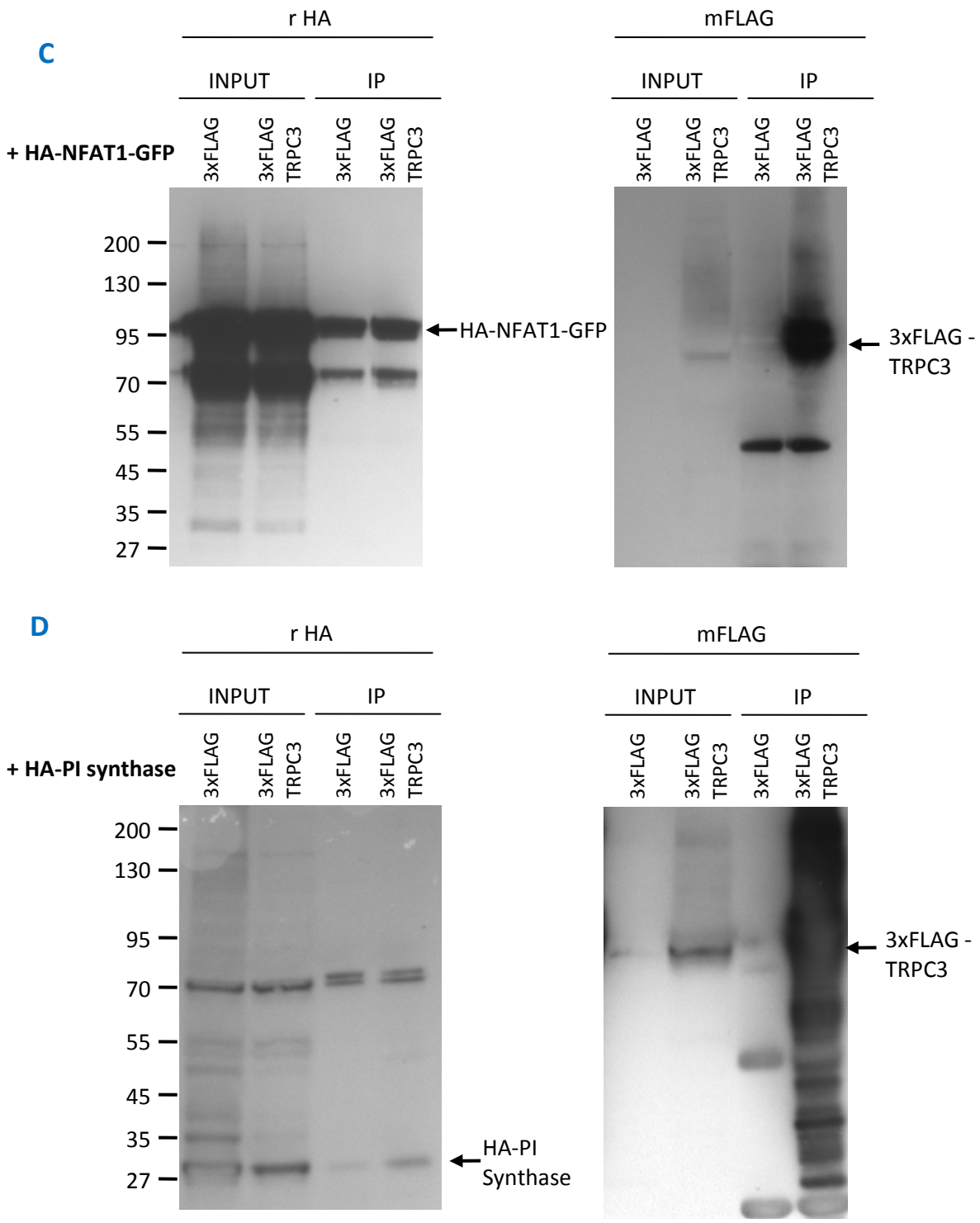

Figure 3-6 (C, D). Immunoprecipitation experiments using EZview α FLAG beads, precipitating FLAG-TRPC3 and its potential binding partners from transfected HEK293T cells. HA-NFAT1-GFP (C) and HA-PI synthase (D) bind both the negative control empty FLAG and FLAG-TRPC3, although the interaction between HA-PI synthase and empty FLAG is minimal. Membranes were then re-probed using α FLAG antibody to confirm FLAG-TRPC3 expression. n=2

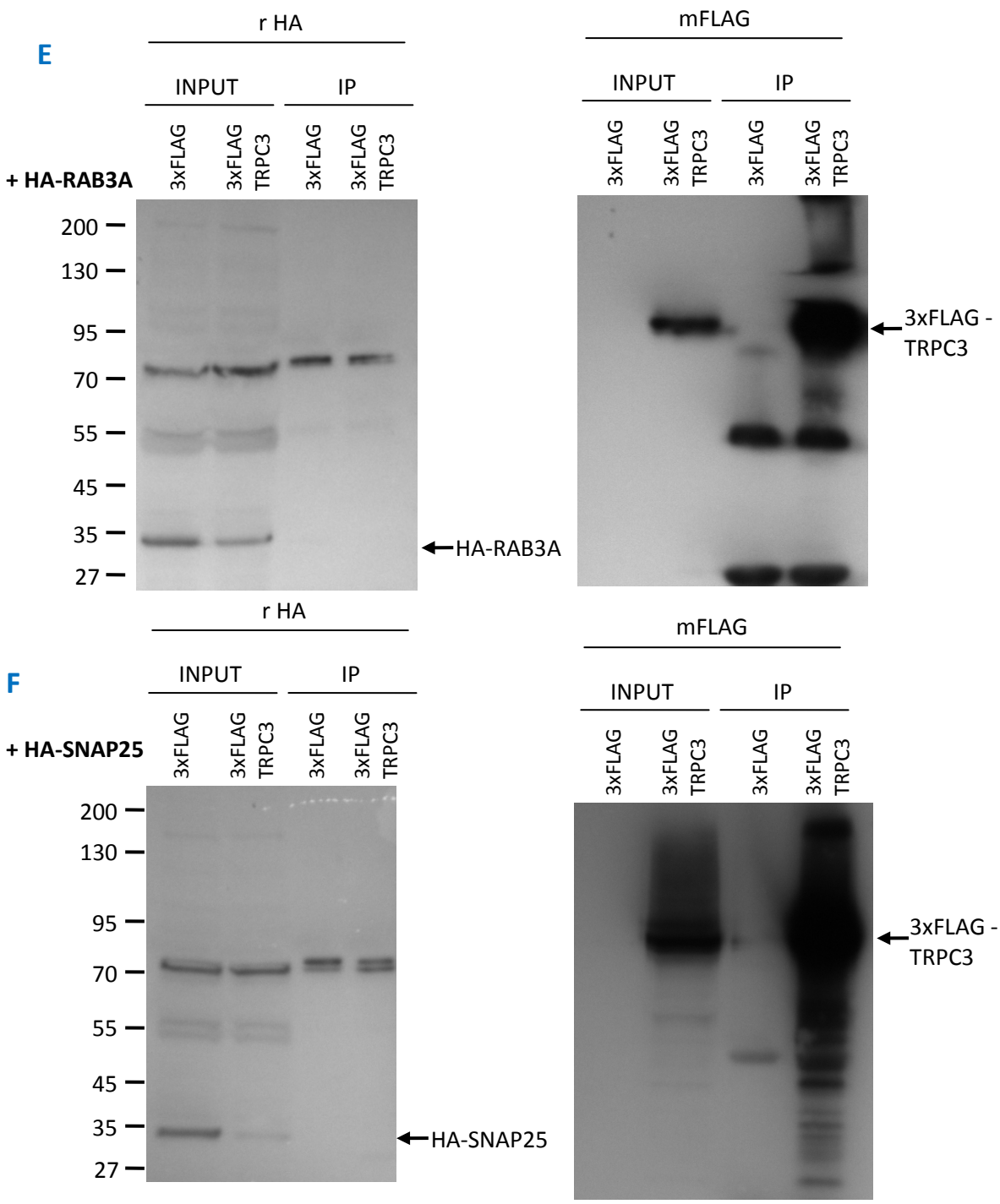

Figure 3-6 (E, F). Immunoprecipitation using EZview α FLAG beads, precipitating FLAG-TRPC3 and its potential binding partners from transfected HEK293T cells. HA-RAB3A (E) and HA-SNAP25 (F) do not bind FLAG-TRPC3. Membranes were re-probed using α FLAG antibody to confirm FLAG-TRPC3 expression. n=2

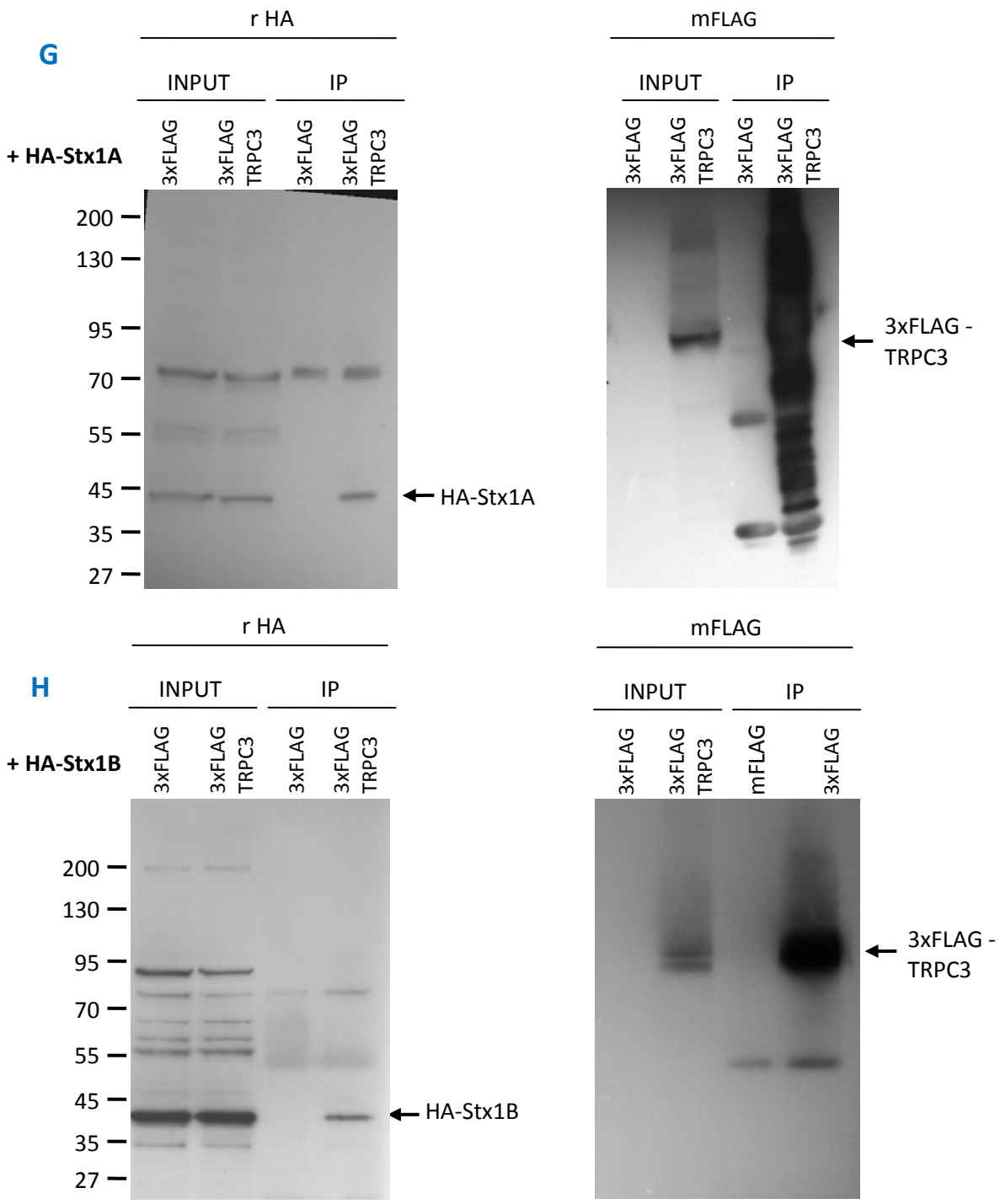

Figure 3-6 (G, H). Immunoprecipitation using EZview α FLAG beads, precipitating FLAG-TRPC3 and its potential binding partners from transfected HEK293T cells. HA-Stx1A (G) and HA-Stx1B (H) both bind FLAG-TRPC3 and not the negative control FLAG. Membranes were re-probed using α FLAG antibody to confirm FLAG-TRPC3 expression. n=2

The IP experiments in HEK293T cells show that IP_3R1 specifically binds to 3xFLAG-TRPC3 and does not bind the negative control 3xFLAG (Figure 3-6[A]). As IP_3R1 is a known binding partner of TRPC3, this indicates that the IP experiments in HEK293T cells work reliably.

We confirmed a novel binding partner of TRPC3 – CaMKIV, which was identified in the previous tandem mass spectrometry experiments. As shown in Figure 3-6[B], HA-CaMKIV was precipitated by 3xFLAG-TRPC3, and was not present in the negative control lane, even though it was expressed well in both samples. This demonstrates that CaMKIV specifically binds TRPC3.

Binding of NFAT1 to TRPC3 could not be determined, since HA-NFAT1-GFP was also present in the negative control, binding to 3xFLAG (see Figure 3-6[C]).

Binding of PI synthase to 3xFLAG-TRPC3 is shown in Figure 3-6[D]. Even though weak binding of PI synthase is observed in the negative control 3xFLAG, PI synthase shows stronger binding to 3xFLAG-TRPC3 which indicates that the interaction with TRPC3 is likely to be specific.

Interaction of proteins RAB3A and SNAP-25 with 3xFLAG-TRPC3 could not be confirmed *in vitro* (see Figure 3-6[E, F]), even though they were identified in the tandem mass spectrometry experiment. This probably means that these proteins were precipitated in a large complex and did not bind TRPC3 directly. Potentially neuronal specific proteins were required for them to be precipitated successfully by TRPC3 in HEK293T cells.

IP experiment showed that both syntaxin 1A and syntaxin 1B bind TRPC3, without binding the negative control 3xFLAG (Figure 3-6[G, H]). Syntaxin 1A has been previously shown to bind TRPC3 in a mass spectrometry study (although has not been confirmed by another technique) (Lockwich et al 2008), whereas, syntaxin 1B is a novel binding partner.

To perform the reverse experiment and to investigate whether the HA-tagged proteins of interest that were precipitated by 3xFLAG-TRPC3 could also precipitate the target protein (3xFLAG-TRPC3), EZview α HA beads were used. Transfection of the cells with 3xFLAG-TRPC3 and an empty

HA vector was used as a negative control, and showed that HA alone does not bind 3xFLAG-TRPC3 (Figure 3-7[A]). The western blot membrane was first probed for FLAG to observe whether 3xFLAG-TRPC3 was immunoprecipitated by the HA tagged protein of interest. The membrane was then re-probed for HA to confirm that the HA-tagged protein of interest was present. All HA-tagged proteins of interest were expressed and immunoprecipitated successfully in the IP experiments (Figure 3-7[A-E]). We confirmed that HA-tagged CaMKIV, PI synthase, syntaxin 1A and syntaxin 1B all bind and immunoprecipitate 3xFLAG-TRPC3 (Figure 3-7[B-E]). These results are in line with the results obtained by α FLAG IP.

Immunoprecipitation from wild-type and *Mwk* mouse cerebella using α TRPC3 antibody

To further investigate the interactions between TRPC3 and some of its binding partners, we performed an α TRPC3 IP from cerebellar lysates of wild-type and *Mwk* cerebella. For a negative control, α HA antibody was used to precipitate proteins from the wild-type cerebellum, which is another polyclonal rabbit antibody, like the α TRPC3 antibody. The results of the IP experiments were analysed by SDS-PAGE on gradient gels and probed for IP_3R1 and CaMKIV by immunoblotting with specific antibodies.

The results shown in Figure 3-8 demonstrate that IP_3R1 is immunoprecipitated by both wild-type and *Mwk* TRPC3, and it is not precipitated by the negative control α HA antibody. The immunoblot shows that there is slightly less IP_3R1 precipitated with the *Mwk* TRPC3, compared to the wild-type TRPC3. This is a very interesting result, suggesting that the interaction between IP_3R1 and the *Mwk* TRPC3 could be affected by the mutation. However, repeat experiments could not confirm that result and

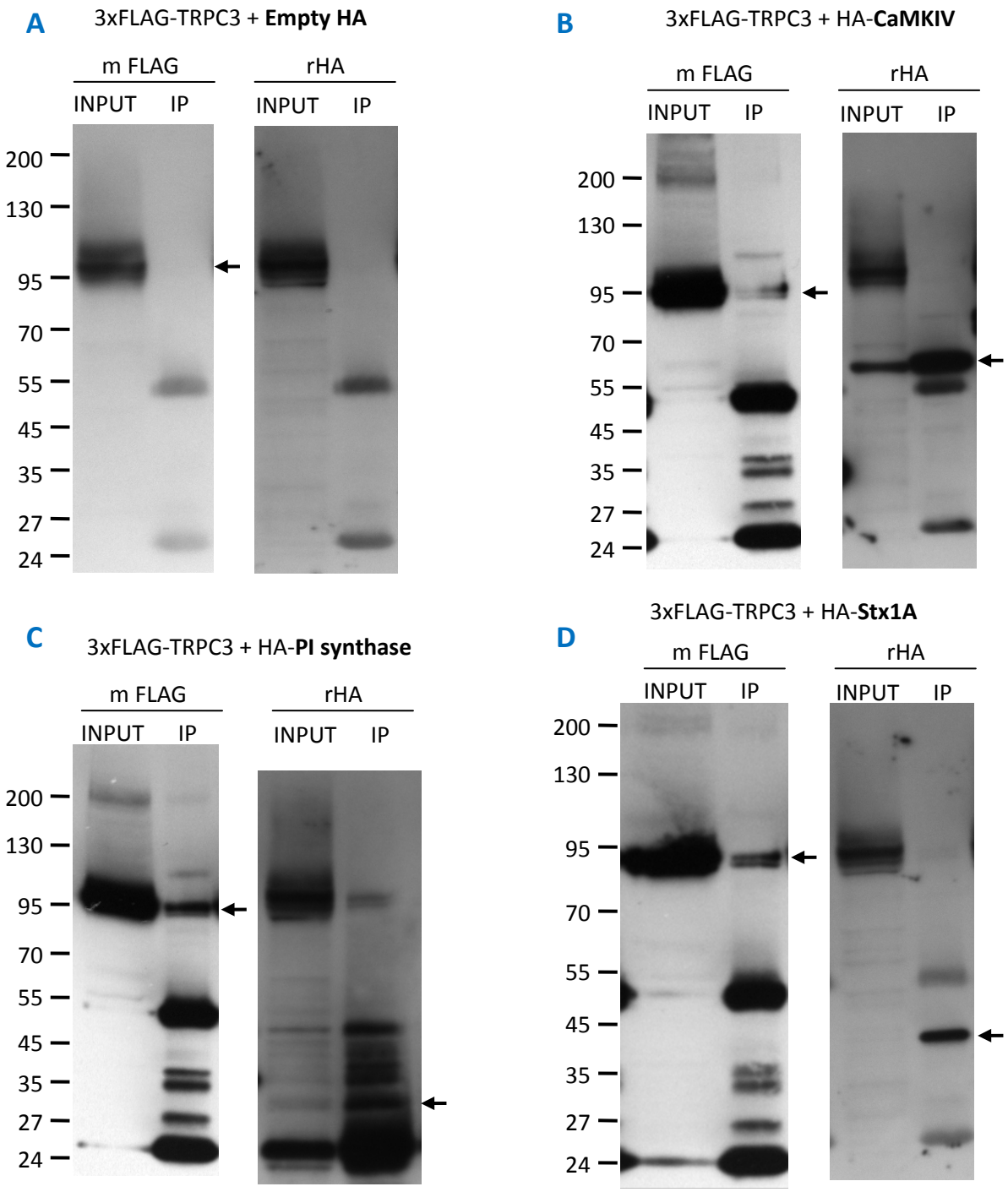

.

Figure 3-7 (A-D). Immunoprecipitation using EZview α HA beads to detect pulldown of TRPC3 by potential binding partners. HEK293T cells co-transfected with 3xFLAG-TRPC3 and Empty HA vector (A) or HA-CaMKIV (B) or HA-PI synthase (C) or HA-Stx1A (D) constructs. HA tagged proteins were immunoprecipitated by EZview α HA beads (Sigma) and the gel was probed for α FLAG antibody to detect TRPC3. Negative control empty HA shows no pulldown of TRPC3. HA-CaMKIV, HA-PI Synthase and HA-Stx1A show TRPC3 pulldown. All membranes were re-probed for HA to detect pulled down proteins of interest. n=2

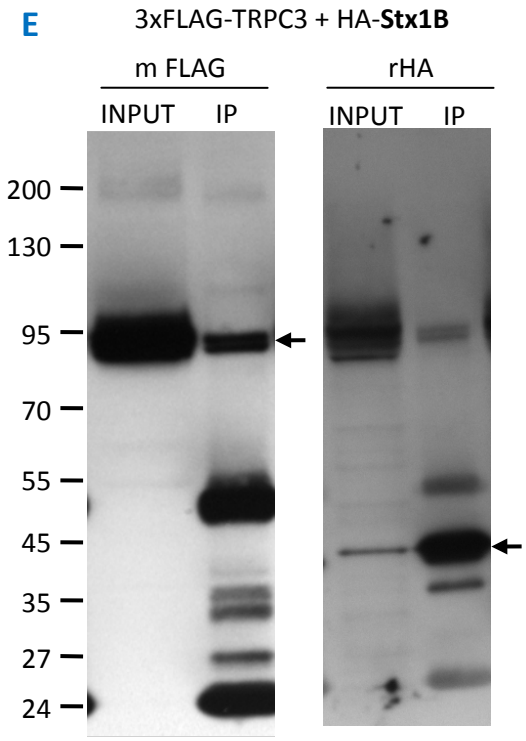

Figure 3-7 (E). Immunoprecipitation using EZview α HA beads to detect pulldown of TRPC3 by potential binding partners. HEK293T cells co-transfected with 3xFLAG-TRPC3 and HA-Stx1B (E). HA tagged proteins were immunoprecipitated by EZview α HA beads (Sigma) and the gel was probed for α FLAG antibody to detect TRPC3. HA-Stx1B shows that TRPC3 is pulled down. The membrane was re-probed for HA to detect pulled down HA-Stx1B. n=2

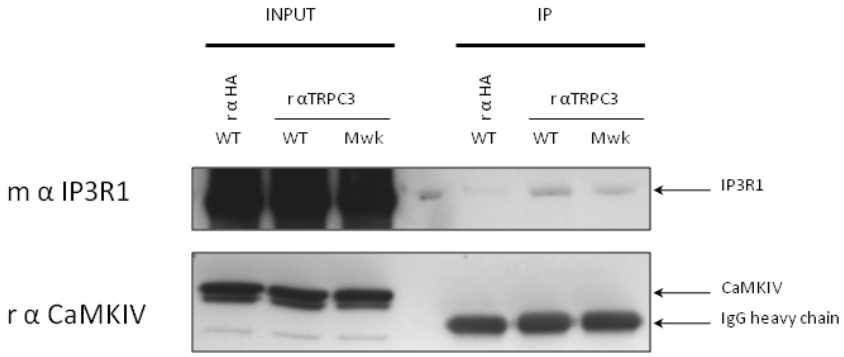

Figure 3-8. Immunoprecipitation of TRPC3 protein from mouse cerebellum. WT and Mwk cerebellar lysates were used to precipitate TRPC3 with its binding partners by α TRPC3 antibody. A rabbit α HA antibody was used as a negative control. As seen from the western blot, both IP_3R1 and CaMKIV are present in the cerebellar lysates. IP_3R1 is not pulled down by the negative control α HA antibody, whereas it is precipitated by both WT and *Mwk* TRPC3 proteins. CaMKIV is not precipitated by the negative control HA or TRPC3.

showed either the same amount of IP_3R1 being precipitated, or showed a very unclear blot from which nothing can be concluded.

CaMKIV was not precipitated by either wild-type or *Mwk* TRPC3, or by the negative control. This could be because the conditions of the IP were too stringent to recognise the interaction between these proteins and more optimisation is required.

Other interaction partners were not investigated *in vivo* because we did not have the appropriate antibodies to detect them.

Immunocytochemistry to observe localisation of proteins of interest

In order to further investigate the localisation pattern of TRPC3 interaction partners in HEK293T cells, immunocytochemistry (ICC) experiments were performed by co-transfecting the cells with 3xFLAG-TRPC3 and the HA-tagged proteins of interest. The proteins of interest were visualised by labelling the fixed and permeabilised cells on coverslips with appropriate antibodies.

3xFLAG-TRPC3 proteins expressed in HEK293T cells can be observed throughout the cytoplasm and concentrated in intracellular vesicles, located near the ER (Figure 3-9[A-E]). A small proportion of FLAG-TRPC3 can also be observed at the plasma membrane.

IP_3R1, the known binding partner of TRPC3, showed localisation around the nuclear rim in the cells and a somewhat similar pattern of expression to 3xFLAG-TRPC3 (Figure 3-9[A]). In case of IP_3R1, as the protein did not have an HA tag, mouse α IP_3R1 antibody was used to detect IP_3R1. Therefore, mouse α FLAG antibody could not be used to detect 3xFLAG-TRPC3 as done in all other experiments, and a rabbit α TRPC3 antibody was used. Both antibodies did not produce good quality of staining and it is difficult to observe, whether they are located in the same regions.

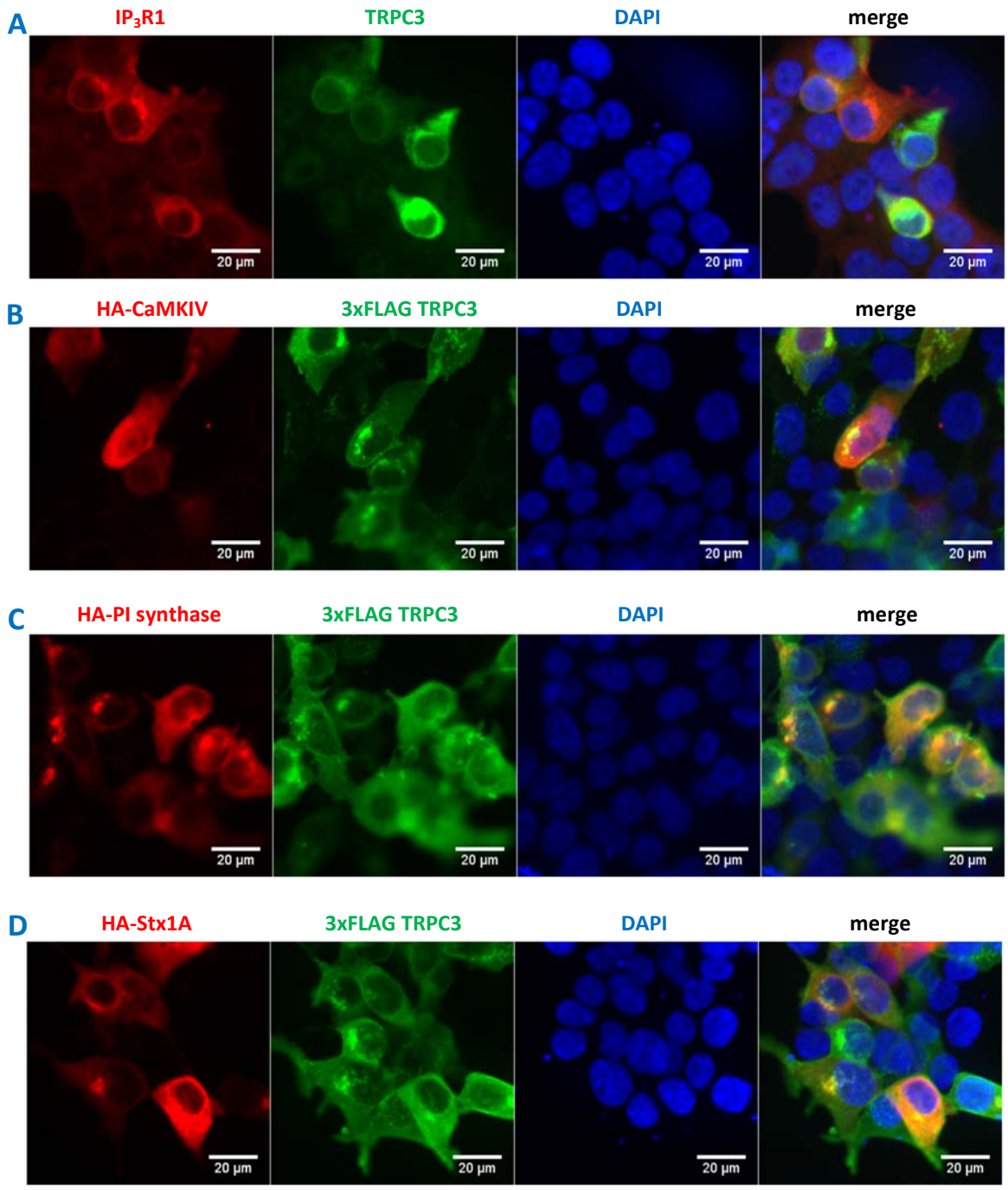

Figure 3-9 (A-D). Immunocytochemistry displaying localisation of FLAG-TRPC3 and its potential interaction partners in HEK293T cells. Cells were cotransfected with FLAG-TRPC3 and a potential interaction partner. The cells were then fixed, permeabilised and stained with appropriate antibodies. IP_3R1 (A) expression looks similar to that of FLAG-TRPC3. HA-CaMKIV (B) shows a more uniform expression troughout the cell than FLAG-TRPC3. HA-PI synthase (C) is expressed in cytoplasmic clusters precisely where FLAG-TRPC3 is expressed. HA-Stx1A (D) expression localisation is similar to that of FLAG-TRPC3. n=2

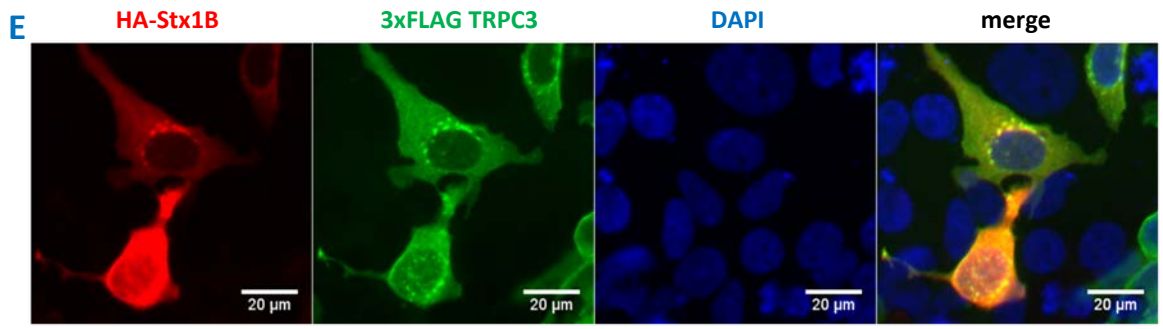

Figure 3-9 (E). Immunocytochemistry displaying localisation of FLAG-TRPC3 and its potential interaction partners in HEK293T cells. HA-Stx1B (E) expression shows very striking resemblence to the expression of FLAG-TRPC3. n=2

Expression of HA-CaMKIV is spread out fairly evenly throughout the cytoplasm and is also present in the nucleus to some extent (Figure 3-9[B]). HA-CaMKIV does not show the same pattern of subcellular localisation as 3xFLAG-TRPC3, which might mean that it is not part of the 3xFLAG-TRPC3 complex in a resting cell, and their interaction could occur during a specific process.

ICC experiments show very precise co-localisation of HA-PI synthase with 3xFLAG-TRPC3 (Figure 3-9 [C]), which demonstrates that the interaction between PI synthase with TRPC3 is indeed present in HEK293T cells, even though HA-PI synthase also bound weakly to the negative control 3xFLAG in the IP experiments.

There is also considerable overlap in the expression of HA-Syntaxin 1A and 3xFLAG-TRPC3 (Figure 3-9[D]), which provides additional evidence that they are genuine interaction partners. HA-Syntaxin 1B shows even more striking similarities in the expression pattern with 3xFLAG-TRPC3 (Figure 3-9[E]).

Limitation of visualising by immunocytochemistry whether the two over-expressed proteins of interest are co-localised is that it can be difficult to find cells that express both proteins if the transfection levels are not high enough. In our experiments, approximately 50% of cells were transfected with FLAG-TRPC3, and different rates of expression were observed for other proteins of interest, which were less than that of FLAG-TRPC3.

Constructs of TRPC3 without N- or C-terminus

Interaction between TRPC3 and its binding partners could occur at different domains of the ion channel. So far, all interactions have been demonstrated either at the N- or at the C-termini. However, that does not rule out the possibility that some interactions occur at the cytoplasmic linker domains between the transmembrane regions. These interactions would be particularly interesting for us as they could include interactions with the S4/S5 linker of the TRPC3 protein,

which is the site where the *Mwk* mutation lies. Therefore, the *Mwk* mutation could cause alterations in binding affinity of TRPC3 interaction partners that are mediated by the S4/S5 linker.

In order to investigate which part of the TRPC3 ion channel interacts with the binding partners, the following constructs were made: 3xFLAG-TRPC3 without the C terminus (3xFLAG-TRPC3 ΔC), and 3xFLAG-TRPC3 without the N terminus (3xFLAG-TRPC3 ΔN). The schematic diagrams of the 3xFLAG-TRPC3 protein and the 3xFLAG-TRPC3 proteins without the C- and N-termini are shown in Figure 3-10[A]. All constructs carry a 3xFLAG-tag at their N-terminus. We chose to use such different TRPC3 domains in order to determine whether the interaction partner binds to the C-terminus (no interaction with 3xFLAG-TRPC3 ΔC), to the N-terminus (no interaction with 3xFLAG-TRPC3 ΔN); or indeed binds to both, or binds to the cytoplasmic linkers between the transmembrane domains of TRPC3 (interacts with both 3xFLAG-TRPC3 ΔC and 3xFLAG-TRPC3 ΔN). But first, it was essential to investigate whether the new TRPC3 constructs are expressed in the HEK293T cells. ICC results shown in Figure 3-10[B] demonstrate that both 3xFLAG-TRPC3 ΔC and 3xFLAG-TRPC3 ΔN are expressed at similar levels to the 3xFLAG-TRPC3 in the HEK293T cells. Interestingly, the pattern of expression of the 3xFLAG-TRPC3 ΔN was very similar to that of the whole TRPC3 protein, i.e. the expression was evident in the cytoplasm, but intracellular compartments were found close to the ER at one side of the nucleus. In contrast, 3xFLAG-TRPC3 ΔC expression was more uniform throughout the cytoplasm and less punctate. This suggests that the C-terminus could be responsible for the recruitment of TRPC3 to the cytoplasmic vesicles. Western blot probing for FLAG confirmed expression of 3xFLAG-TRPC3 ΔC and 3xFLAG-TRPC3 ΔN in the cells compared to the full-length 3xFLAG-TRPC3, however the results show more expression of 3xFLAG-TRPC3 ΔC, rather than 3xFLAG-TRPC3 ΔN (Figure 3-10[C]). The full-length 3xFLAG-TRPC3 runs at ~100 kD, whereas 3xFLAG-TRPC3 ΔN runs at ~50 kD, and 3xFLAG-TRPC3 ΔC at ~80 kD.

So, the different domains of TRPC3 were expressed well in the HEK293T cells and could therefore be used in the IP experiments to investigate which part of the TRPC3 ion channel binds its interaction partners.

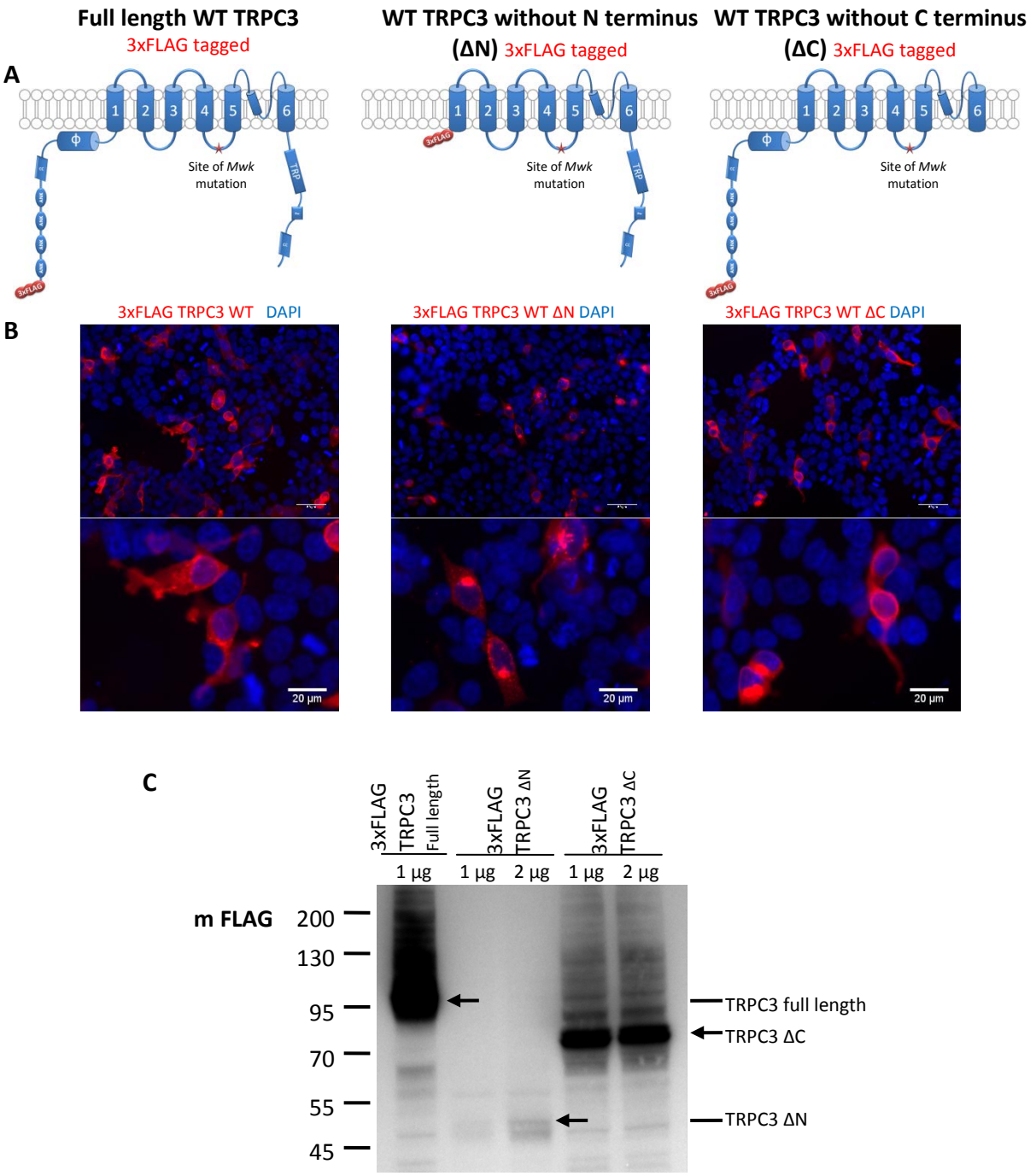

Figure 3-10. TRPC3 domain study. A – schematic diagram showing the wild-type (WT) full length 3xFLAG TRPC3 and the cloned 3xFLAG TRPC3 without the N terminus (ΔN) and without the C terminus (ΔC). **B** – Immunocytochemistry showing expression of WT full length TRPC3, TRPC3 ΔN and TRPC3 ΔC stained with α FLAG antibody (Sigma). Scale bar = 50 µm (top picture) and 20 µm (bottom picture). **C** – Western blot showing expression of WT full length TRPC3, TRPC3 ΔN and TRPC3 ΔC stained with α FLAG antibody (Sigma). n=2

Immunoprecipitation from HEK293T cells using 3xFLAG-TRPC3 ΔC and 3xFLAG-TRPC3 ΔN

The IP experiments to identify the region of TRPC3 that its interaction partners bind to were carried out by co-transfecting cells with HA-tagged protein of interest (the only protein without an HA tag was IP_3R1) and either 3xFLAG-TRPC3 ΔC or 3xFLAG-TRPC3 ΔN.

IP_3R1 is known to bind TRPC3 at its C-terminus; however, our results demonstrated that 3xFLAG-TRPC3 ΔN, as well as 3xFLAG-TRPC3 ΔC, both bind IP_3R1, with more binding evident with 3xFLAG-TRPC3 ΔN (Figure 3-11[A]). Therefore, it is possible that IP_3R1 also binds to either the N-terminus or to one of the cytoplasmic linkers of TRPC3. The western blot results show binding of 3xFLAG-TRPC3 ΔC to IP_3R1 with a lower affinity than to 3xFLAG-TRPC3 ΔN, but there was also less 3xFLAG-TRPC3 ΔC in the input. This result suggests a new TRPC3 binding site for IP_3R1 binding.

The novel TRPC3 interaction partner CaMKIV is shown to bind both TRPC3 domain proteins (Figure 3-11[B]). It is, therefore, possible that CaMKIV binds one of the cytoplasmic regions of the TRPC3 protein between the transmembrane domains. However, the binding with 3xFLAG-TRPC3 ΔC is a lot stronger, suggesting that N terminus could be required for more efficient binding.

PI synthase also binds both 3xFLAG-TRPC3 ΔC and 3xFLAG-TRPC3 ΔN (Figure 3-11[C]), although to a slightly lesser extent 3xFLAG-TRPC3 ΔC.

Syntaxin 1A and syntaxin 1B both bind 3xFLAG-TRPC3 ΔC, as well as 3xFLAG-TRPC3 ΔN (Figure 3-11[D,E]). Affinity to 3xFLAG-TRPC3 ΔN is stronger for both proteins, which indicates that the C-terminus is required for a better binding efficiency.

Experiments using different domains of TRPC3, first of all, confirmed the results obtained from TRPC3 IP experiments, and they also showed us which part of TRPC3 is essential for the binding to occur.

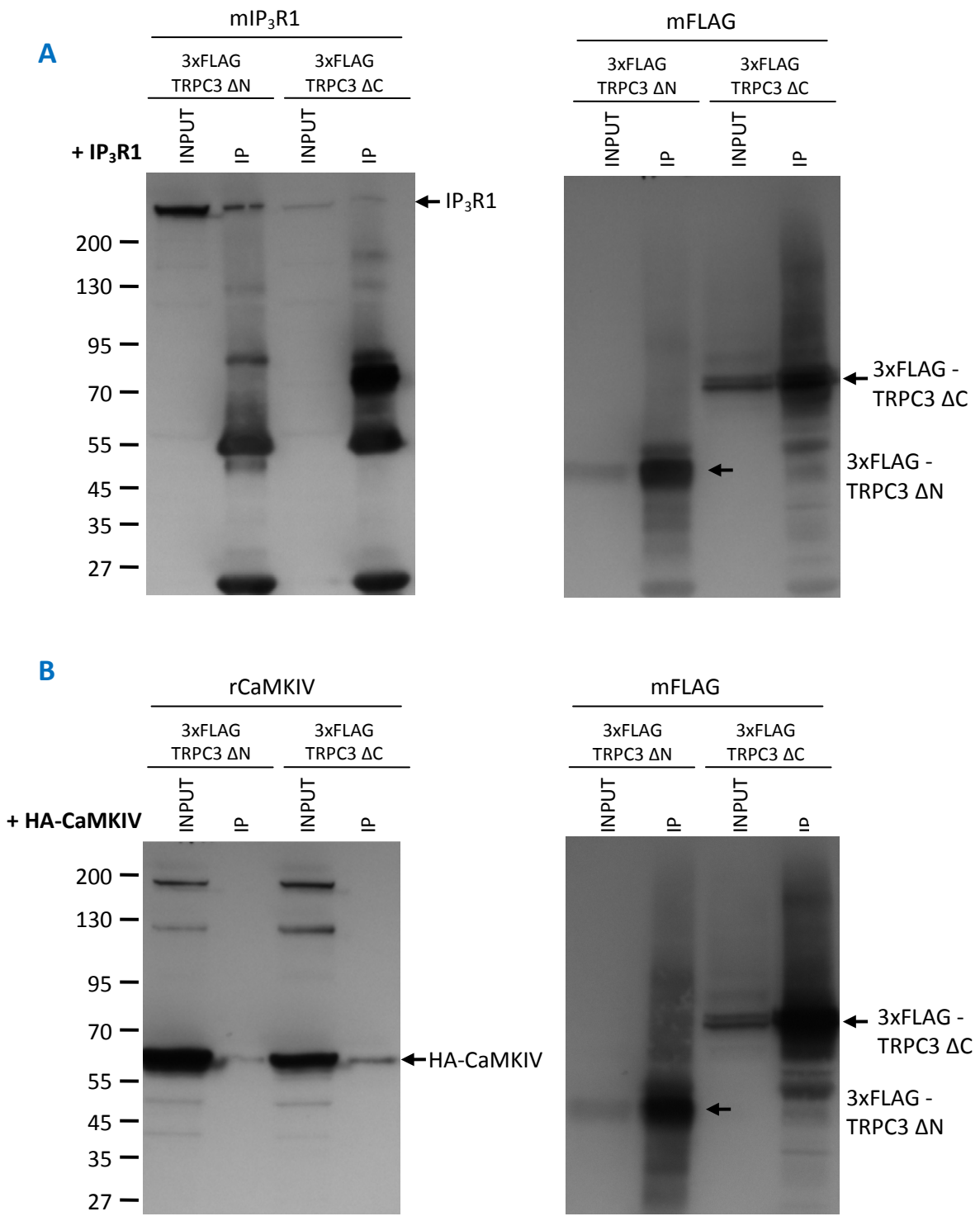

Figure 3-11 (A, B). Immunoprecipitation using EZview α FLAG beads, precipitating FLAG-TRPC3 ΔN/ ΔC and its potential binding partners from transfected HEK293T cells. HEK293T cells were co-transfected with FLAG-TRPC3 ΔN/ ΔC and a potential binding partner construct. They were then lysed and incubated with EZview α FLAG beads in order to pull down FLAG-TRPC3 ΔN/ ΔC together with its binding partners. The precipitated proteins were run on a gradient NuPAGE gel and probed for an appropriate antibody to detect the presence of potential binding partners. IP_3R1 (A) bound to both FLAG-TRPC3 ΔN and ΔC proteins, with higher affinity binding to FLAG-TRPC3 ΔN. HA-CaMKIV (B) also bound both FLAG-TRPC3 ΔN and ΔC proteins, with higher affinity binding to FLAG-TRPC3 ΔC. Membranes were re-probed using α FLAG antibody to confirm FLAG-TRPC3 ΔN and ΔC expression. n=2

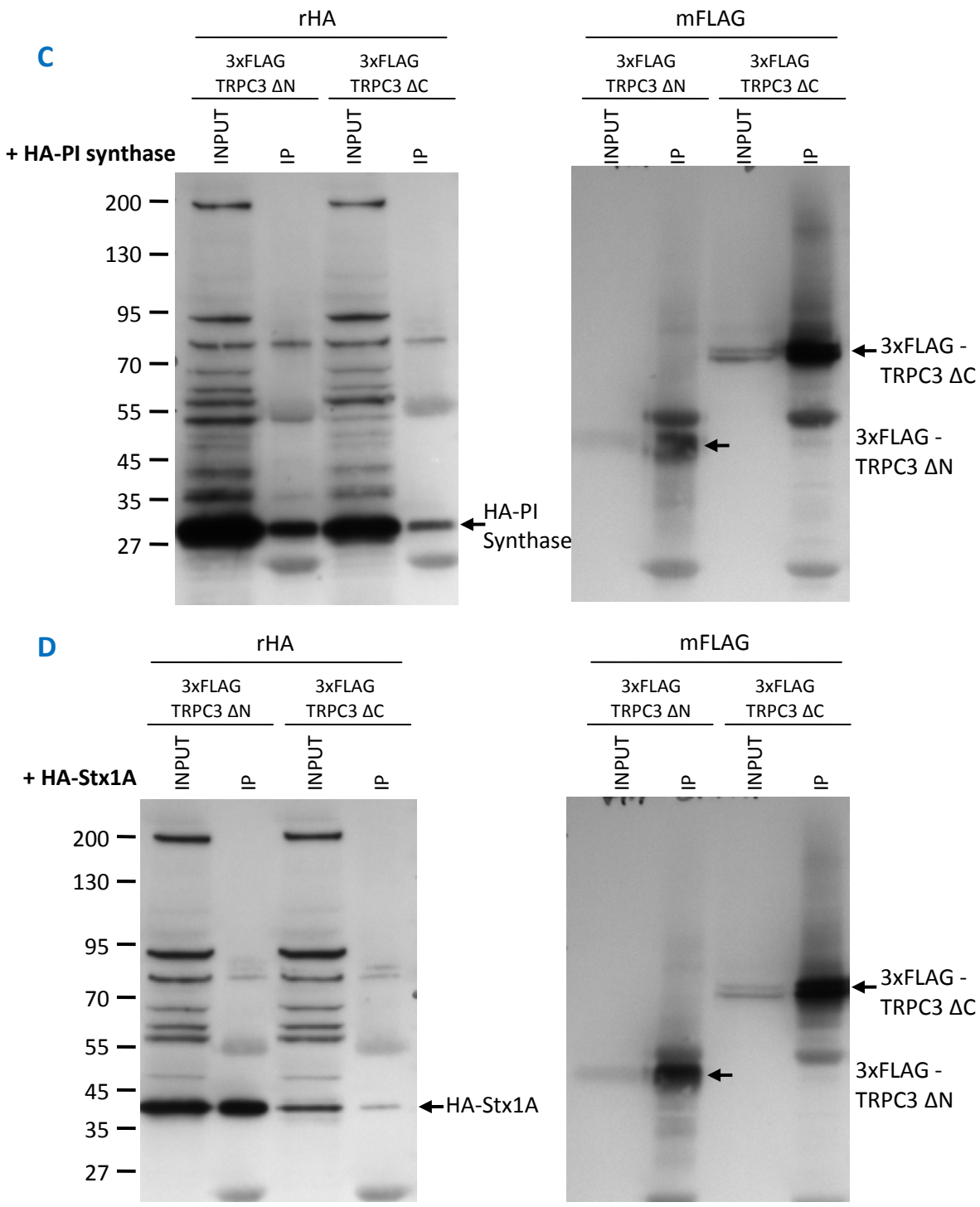

Figure 3-11 (C, D). Immunoprecipitation using EZview α FLAG beads, precipitating FLAG-TRPC3 ΔN/ ΔC and its potential binding partners from transfected HEK293T cells. HA-PI synthase (C) and HA-Stx1A (D) bound both FLAG-TRPC3 ΔN and ΔC proteins. Membranes were re-probed using α FLAG antibody to confirm FLAG-TRPC3 ΔN and ΔC expression. n=2

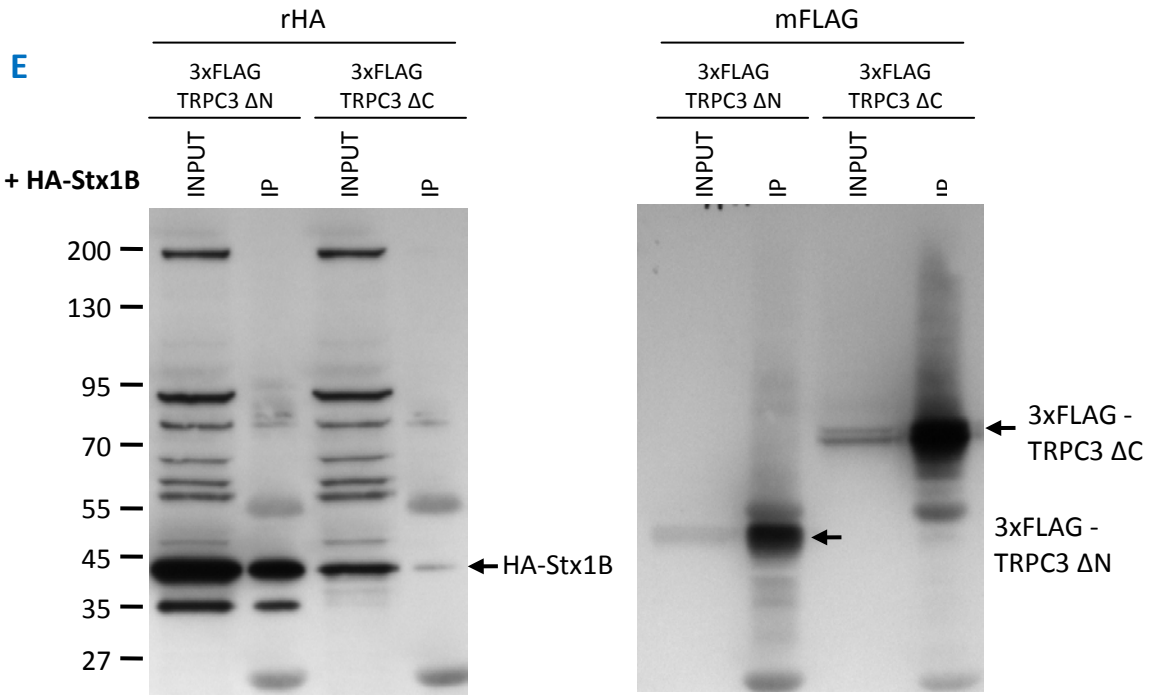

Figure 3-11 (E). Immunoprecipitation using EZview α FLAG beads, precipitating FLAG-TRPC3 ΔN/ ΔC and its potential binding partners from transfected HEK293T cells. HA-Stx1B (E) binds both FLAG-TRPC3 ΔN and ΔC proteins. Membranes were re-probed using α FLAG antibody to confirm FLAG-TRPC3 ΔN and ΔC expression. n=2

Summary

We have identified a number of TRPC3 interaction partners by IP and mass spectrometry. We were able to confirm the interaction between TRPC3 and IP_3R1, CaMKIV, PI synthase, syntaxin 1A and syntaxin 1B. Interactions occur when either the whole N-terminus or the whole C-terminus are absent from the TRPC3 protein, which indicates that their interaction could occur at the cytoplasmic linkers of the protein, one of which is the site of the *Mwk* mutation.

Discussion

Since it has been proposed that interaction between TRPC3 and other proteins are important for the channel's proper function (Kiselyov et al 2005), we investigated the interaction partners of TRPC3 by IP and mass spectrometry. We confirmed some of the identified interactions with the wild-type TRPC3 *in vitro*. We also speculated that the *Mwk* mutation could cause changes in the affinity of TRPC3 to some binding partners, which could be the reason behind alterations in channel gating. Indeed, mass spectrometry identified some differences between the binding partners of wild-type and *Mwk* TRPC3 proteins, however, these still need to be confirmed. Discussed below are the proteins that were identified by mass spectrometry and confirmed to bind to the wild-type TRPC3 *in vitro*.

TRPC3 Regulators

- **IP_3R1**

Our results confirmed the binding of IP_3R1 to TRPC3, which is a previously known interaction (Kiselyov et al 1998). We also found that IP_3R1 not only binds to the C-terminus of TRPC3 as previously reported (Boulay et al 1999; Kiselyov et al 1999), but also binds either to the N-terminus of TRPC3, or to its intracellular loops. In order to discover this, our experiments minimally disrupted the structure of the TRPC3 protein, as the whole N- or C-termini were removed but the transmembrane domain together with the other terminus remained the same. This indicates that IP_3R1 binding to another part of the TRPC3 is real. Also, there is a possibility that the *Mwk* TRPC3 does not bind to IP_3R1 as strongly as the wild-type TRPC3, which could lead to alterations in the *Mwk* TRPC3 activation mechanism that involves IP_3R1 binding (Zhang et al 2001).

- **PI synthase**

HA-tagged PI synthase was found to interact with 3xFLAG-TRPC3, as well as with the negative control 3xFLAG, but with a much lower affinity, hence the interaction between PI synthase and TRPC3 most likely does take place. In the initial IP and mass spectrometry experiments, PI synthase was precipitated with wild-type TRPC3, as well as *Mwk* TRPC3. In the presence of calcium, however, the wild-type TRPC3 did not bind PI synthase, whereas the *Mwk* TRPC3 still could interact with the protein.

PI synthase is an essential membrane-bound enzyme that is mainly located in the ER (Antonsson 1997). Expression of PI synthase has been confirmed in the Purkinje cells and granule cells of the rat cerebellum (Saito et al 1998). The enzyme catalyses the following reaction:

CDP-diacylglycerol + *myo*-inositol → phosphatidylinositol (PIP) + CMP

Cleavage of the phosphorylated form of phosphatidylinositol – PIP_2 – by PLC generates IP_3 and DAG, which are both involved in TRPC3 activation (Berridge 1993; Hofmann et al 1999). Moreover, PIP_2 binding to TRPC3 is important for the channel to be able to remain at the plasma membrane (Soboloff et al 2007). This indicates that PI synthase could be involved in TRPC3 activity, and any changes in their interaction might be responsible for changes in TRPC3 activity that we observe in *Mwk* mice.

- **PLCδ3**

PLCδ3 is a Ca^{2+}-dependent protein involved in the phosphoinositide turnover (Pawelczyk & Matecki 1999), hence it is possible that PLCδ3 is also involved in the regulation of TRPC3. The mass spectrometry experiment identified PLCδ3 binding to the wild-type TRPC3 protein with Ca^{2+} in the buffer, and not to the *Mwk* TRPC3. Interestingly, PLCδ3 knockdown inhibits neurite formation of cerebellar granule cells (Kouchi et al 2011). The possible reduction in binding affinity to the *Mwk* protein could cause changes in TRPC3 activity.

Our data suggests that there could be changes in the binding affinity of some regulatory proteins to the *Mwk* TRPC3, which potentially could be responsible for the gain-of-function of the protein.

CaM Kinases

CaMKII and CaMKIV are multi-functional kinases that are activated in response to increasing intracellular Ca^{2+} (Ohmstede et al 1989; Yamauchi 2005). Calmodulin – a calcium sensor – forms calcium-calmodulin complexes that activate different CaM kinases, including CaMKII and CaMKIV (Ghosh & Greenberg 1995). Since TRPC3 is a non-selective cation channel, permeable to Ca^{2+}, it could regulate the CaM kinase cascade. Indeed, TRPC3 has been implicated in CaM kinase-dependent gene transcription regulation in muscle cells (Morales et al 2007). Our experiments implicated CaMKIV, and possibly CaMKIIβ, in binding to TRPC3.

- **CaMKIV**

CaMKIV is a member of the Ca^{2+}/calmodulin-protein dependent kinase cascade and is one of the major kinases implicated in neuronal calcium signalling, by phosphorylating a number of proteins, such as CREB, which leads to the initiation of gene transcription in the cells (Anderson & Kane 1998; Wayman et al 2008). Binding of calmodulin to CaMKIV in the presence of Ca^{2+} allows CaMKIV phosphorylation by CaMKK, as well as allowing auto-phosphorylation, which activates the kinase (Park & Soderling 1995).

A novel interaction between TRPC3 and CaMKIV has been identified by our IP experiments. The IP showed that 3xFLAG-TRPC3 precipitated HA-CaMKIV, and the negative control 3xFLAG did not. The initial IP and mass spectrometry experiments did not identify CaMKIV being bound to wild-type TRPC3, but found CaMKIV precipitated with the *Mwk* TRPC3. This could mean that the interaction between CaMKIV and *Mwk* TRPC3 is stronger than between CaMKIV and wild-type TRPC3. To investigate this, the IP from the mouse cerebella followed by a western blot using α CaMKIV antibody needs to be optimised further, as currently it shows no interaction between

wild-type or *Mwk* TRPC3 and CaMKIV. The IP conditions could be too harsh to preserve the interaction. Also, CaMKIV size is very similar to that of the immunoglobulin heavy chain, therefore, unless it is a very clear blot, it can be indistinguishable whether the band is the heavy chain of the antibody or it is indeed CaMKIV.

When investigating which part of the TRPC3 protein binds CaMKIV, it was evident that the N-terminus of TRPC3 is preferential for the interaction. However, there was also a weaker interaction between CaMKIV and TRPC3 without the N terminus. Therefore there is a possibility that CaMKIV could interact with the middle portion of the protein, as well as with N- and C-termini.

The interaction between TRPC3 and CaMKIV is very interesting for our study, as it could provide a mechanism by which TRPC3 could regulate Purkinje cell development. However, it cannot be concluded from the IP experiments, whether the interaction is direct. This needs to be tested in a cell-free system. From what is known about CaMKIV and TRPC3, one could speculate that their interaction could occur via calmodulin, because calmodulin is a known binding partner of TRPC3 and CaMKIV in the presence of calcium (Ghosh & Greenberg 1995; Tang et al 2001). Interaction between TRPC3 and calmodulin occurs at the N-terminus of the TRPC3 protein. Our studies have shown that interaction between CaMKIV and TRPC3 is stronger in the presence of N-terminus. So this interaction could be mediated through calmodulin. However, it is also possible that the interaction between CaMKIV and the C-terminus or the middle portion of TRPC3 could be calmodulin-independent, as calmodulin is not known to bind TRPC3 at its C terminus. Moreover, it could be speculated from our results that TRPC3, together with calmodulin and CaMKIV, could form a complex of proteins at the membrane surface, which might be important for the function of all the proteins involved.

- **CaMKIIβ**

CaMKII is another major kinase responsible for gene transcription, with CaMKIIβ being a cerebellar specific isoform (Sun et al 1994; Wayman et al 2008). Our mass spectrometry results revealed that CaMKIIβ was precipitated with *Mwk* TRPC3 in the presence of calcium. Unfortunately, I was unable to clone the CaMKIIβ gene into a vector, so no follow-up binding studies have been performed. However, a recent study that has looked at the binding of the β isoform of CaMKII to the members of the TRPC family discovered that only TRPC5 can form complexes with CaMKIIβ (Puram et al 2011). Perhaps, CaMKIIβ binds to TRPC3 indirectly.

If CaMKII and CaMKIV are regulated by TRPC3 via direct interaction or through a cascade of events, it is possible that the mechanism of their usual function is altered in *Mwk* Purkinje cells. Therefore it would be interesting to investigate the levels of activity of these proteins in Purkinje cells of *Mwk* mice and compare them to the normal levels of wild-type mice (see the next Chapter). This could give us an indication of which mechanisms could be altered in *Mwk* mice and perhaps lead to the disease.

Synaptic Vesicle Proteins

The main function of the synaptic vesicle proteins is the release of neurotransmitter at the pre-synaptic membrane (Sudhof 1995; 2004). Therefore, the interaction between TRPC3 and the synaptic vesicle proteins likely occurs at the terminal of the Purkinje cell axon.

TRPC3 is known to interact with VAMP-2 vesicular SNARE protein (Singh et al 2004) and we have identified additional vesicle proteins that bind TRPC3 or that are part of the TRPC3 complex.

- **Syntaxin 1A/1B**

Syntaxins 1A and 1B are nervous system specific synaptic vesicle proteins, involved in the docking and fusion of synaptic vesicles with the plasma membrane, and they have also been suggested to

have a role in general membrane trafficking (Bennett et al 1992; Bennett et al 1993). Syntaxin 1A and syntaxin 1B interact with synaptotagmin, syntaxin-binding protein 1, N-type and P/Q-type calcium channels, sodium and potassium channels, and IP_3R1 (Liu et al 2004; Perez-Branguli et al 2002; Sheng et al 1998; Tanaka et al 2011; Xu et al 2005; Yang et al 2000). Interestingly, they are thought to regulate calcium entry into the cells via interaction with the calcium channels (Leung et al 2003). Syntaxin 1A favours the inactivated state of the channels, either by direct inhibition or inhibiting the translocation of the channel to the plasma membrane (Leung et al 2003). This suggests that any changes in binding of syntaxin 1A to TRPC3 could alter its gating. Syntaxin 1B has been proposed to be involved in synaptic plasticity and long-term potentiation (Helme-Guizon et al 1998; Hicks et al 1997; Salin et al 2002). In the cerebellum, syntaxin 1 proteins are located on the plasma membrane and in synaptic vesicles at the pre-synaptic terminals along the dendrites of Purkinje cells, as well as along the plasma membrane, ER and the nuclear envelope of the granule cells (Koh et al 1993; Sheng et al 1998). Both syntaxin 1A and 1B are expressed very strongly in the granule cells. Purkinje cell layer mainly contains syntaxin 1B, although syntaxin 1A is also present (RuizMontasell et al 1996).

Our mass spectrometry results identified syntaxin 1B as a binding partner of the *Mwk* TRPC3, but not of the wild-type TRPC3. However, co-IP experiments using HEK293T cells showed very strong interaction between wild-type 3xFLAG-TRPC3 and HA-Stx1B. Also, even though it did not come up in our study, previously it has been found that syntaxin 1A binds to TRPC3 (Lockwich et al 2008), and we were also able to confirm that *in vitro*.

Both syntaxin 1A and 1B bind to TRPC3 without the N and without the C termini, although their preference is to bind TRPC3 without the C-terminus. This indicates that the interaction could occur in the middle region of the TRPC3 protein and that the *Mwk* mutation could potentially change that.

- **SNAP25**

SNAP25 is a member of the target SNARE protein, which involved in the vesicle fusion, and it interacts with syntaxin 1A (Wagner & Tamm 2001; Wang & Tang 2006).

In our tissue culture experiments, there was no interaction between the HA-tagged SNAP25 and the 3xFLAG-TRPC3. Interestingly, mass spectrometry identified interactions between wild-type and *Mwk* TRPC3 only when calcium was present in the lysis buffer. Therefore, it is still possible that an interaction between SNAP25 and TRPC3 is initiated in the presence of calcium. However, it is also possible that SNAP25 was pulled down in a complex of proteins bound to syntaxin 1A, rather than binding to TRPC3 directly.

- **RAB3A**

RAB3A is a member of the Rab family of proteins, which are involved in directing the membrane traffic (Nuoffer & Balch 1994; Simons & Zerial 1993; Sudhof 1995). RAB3A is involved in exocytosis by regulating the late step of vesicle fusion. However, RAB3A is thought to mediate exocytosis of neurotransmitter vesicles, hence it is thought to be expressed in the axons at the pre-synaptic cleft. Nothing is known about the function of RAB3A in the dendrites.

Mass spectrometry results showed that RAB3A bound to wild-type TRPC3 with and without calcium, and also to the *Mwk* TRPC3 but only in the presence of calcium in the buffer. However, follow-up experiments in cells did not confirm interaction between wild-type TRPC3 and RAB3A. It is still possible that RAB3A is part of a complex of proteins that includes TRPC3, and that it could not be precipitated by TRPC3 in HEK293T cells because neuronal-specific proteins could be required for their interaction.

- **Synaptotagmin 1**

Synaptotagmin 1 is a sensor for vesicular Ca^{2+} levels and a trigger of fast vesicle exocytosis (Sudhof 2004). Our mass spectrometry experiments revealed that synaptotagmin 1 bound to wild-type TRPC3 in the buffer without calcium, but it was also present in the negative control. In the buffer containing calcium, synaptotagmin 1 bound *Mwk* TRPC3, but not wild-type TRPC3. I could not prepare a synaptotagmin 1 construct, hence no follow-up experiments were performed with this protein. However, another study in the rat validated the interaction between the wild-type TRPC3 protein and synaptotagmin 1 by western blot (Lockwich et al 2008), and it is likely that the same interaction occurs in mice. Function of synaptotagmin 1 suggests that it could be involved in the translocation of TRPC3 to the plasma membrane.

Our data suggests that many synaptic vesicle proteins could be present in or near the intracellular vesicles that contain TRPC3, in order for the TRPC3-containing vesicles to be able to translocate to fuse with the plasma membrane upon TRPC3 activation.

Other Proteins

- **NFAT1**

NFAT-mediated transcription has been shown to be regulated by TRPC3 channel signalling in the heart and muscle, with a probable exception of NFAT1 (Bush et al 2006; Kar et al 2011; Poteser et al 2011). It was interesting to investigate whether the two proteins actually interact with each other. In our study, no NFAT proteins were present in the mass spectrometry results and unfortunately, the HA-NFAT1-GFP protein expressed in HEK293T cells bound the negative control 3xFLAG, as well as the 3xFLAG-TRPC3. Therefore, it is not possible to say from our results whether the two proteins actually interact. It is, however, well-known that TRPC3 activates NFAT signalling via calcineurin, which dephosphorylates the NFAT proteins and facilitates their translocation to the nucleus where they initiate transcription (Crabtree & Schreiber 2009). Therefore, it is

probably unlikely that there is a direct interaction between TRPC3 and the NFAT proteins. Perhaps the more appropriate experiment would be to investigate the level of phosphorylation of NFAT proteins in *Mwk* cerebella. Furthermore, their expression could be visualised by immunohistochemistry to reveal their localisation in wild-type cerebellum, and compare it to the expression in the *Mwk* cerebellum, as their translocation to the nucleus indicates activation. Interestingly, calcineurin was identified in our mass spectrometry experiment, binding to the wild-type TRPC3 in the presence of calcium, and not to the *Mwk* TRPC3.

- **Contactin 1**

Contactin 1 is the immunoglobulin superfamily member cell adhesion molecule (Gennarini et al 1989). In our mass spectrometry study we identified contactin 1 as a potential interactor of the *Mwk*, but not the wild-type TRPC3 protein. I have not been able to clone the contactin 1 gene, so no further experiments were done with this protein. Interestingly, contactin 1 has been implicated in neurite extension *in vitro* (Gennarini et al 1991). Moreover, its absence in mice causes cerebellar ataxia with defects in axon and dendrite development (Berglund et al 1999; Davisson et al 2011). And other members of the contactin family have also been implicated in the development of granule cells of the cerebellum (Baeriswyl & Stoeckli 2008; Bizzoca et al 2003; Coluccia et al 2004; Stoeckli 2010; Stottmann & Rivas 1998; Wang et al 2011). Perhaps the potential interaction of contactin 1 with the *Mwk* TRPC3 somehow is involved in the developmental abnormalities of Purkinje cells in *Mwk* mice.

Limitations

The tandem mass spectrometry technique sometimes cannot identify all proteins in the sample when it contains a large number of peptides, which makes it hard to compare two sets of samples (for example, the wild-type and the *Mwk* samples in our case). To make the identification process easier, two-dimensional gel electrophoresis is often used prior to tandem mass spectrometry in order to separate proteins by their mass, as well as by their isoelectric point. Computer software

can be used to compare two gels and find any differences, which can then be identified by tandem mass spectrometry. Another possibility is to use quantitative mass spectrometry, which allows comparing the levels of precipitated proteins in two different samples (Bantscheff et al 2007). When confirming interactions of two proteins *in vitro*, the most accurate way is to use endogenous proteins. However, this technique depends on the availability of a good antibody, which is often not possible, and therefore leads to the use of over-expressed proteins. For a more accurate approach to visualise co-localisation of two proteins, confocal images should be used.

Summary

We were able to identify interaction partners of the wild-type TRPC3 protein using the IP experiment from a mouse cerebellum, followed by mass spectrometry. We identified several proteins that could potentially be involved in TRPC3 regulation, like PI synthase and PLCδ3. Also, CaM kinase signalling cascade member CaMKIV, and possibly CaMKII, likely interact with TRPC3, suggesting that TRPC3 could be involved in their regulation as it has a role in Ca^{2+} influx, required for their activation. Another category of proteins that interact with TRPC3 are the synaptic vesicle proteins: syntaxin 1A, syntaxin 1B and possibly synaptotagmin 1. SNAP25 and RAB3A that were identified in the mass spectrometry experiment, but did not bind TRPC3 in vitro, could still be part of a complex of proteins that bind TRPC3. These proteins are probably required for the fusion of intracellular vesicles containing TRPC3 with the plasma membrane for the channel's activation.

If the *Mwk* mutation causes changes to the affinity of binding of any of these proteins, potential consequences could cause changes in TRPC3 activation, which might explain the increased activity of the protein. There could also be an altered vesicle trafficking mechanism in the *Mwk* mice, for example, TRPC3 could translocate to the plasma membrane without any activation signals or with less stimulation than would be required for the wild-type TRPC3 activation. In case of CaMKIV, TRPC3 binding might be required for its activation, and any changes in the binding affinity could potentially alter CaM kinase signalling in Purkinje cells.

Figure 3-12 displays known interaction partners of TRPC3 and adds proteins that we identified in this study.

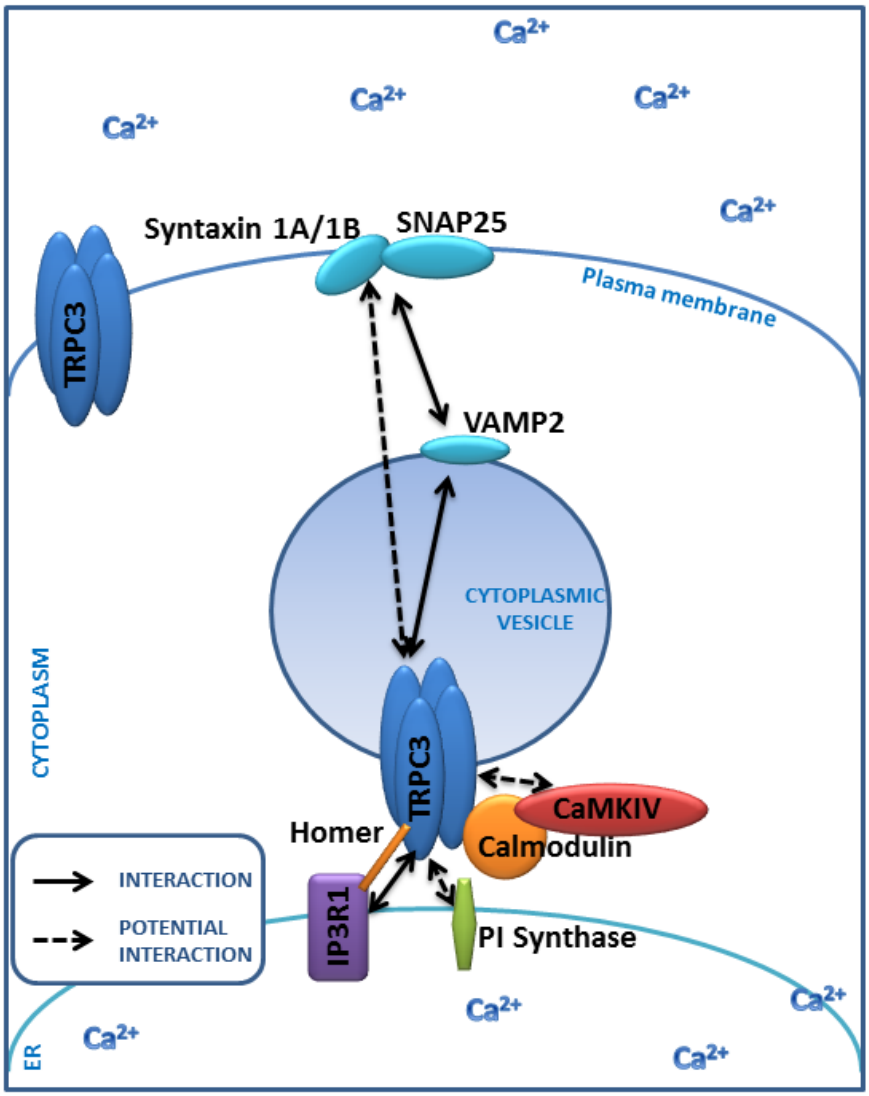

Figure 3-12. Interaction of TRPC3 with other proteins. TRPC3 is located on the plasma membrane as well as in cytoplasmic vesicles near the Endoplasmic Reticulum. In its inactive state, TRPC3 is bound by calmodulin. A scaffolding protein Homer is connecting TRPC3 with IP_3R1 at the Endoplasmic Reticulum. Activation of IP_3R1 and depletion of internal calcium stores causes IP_3R1 to displace calmodulin by binding to the same region of TRPC3. This causes TRPC3 translocation to the plasma membrane and its activation. TRPC3 has also been previously shown to interact with a SNARE protein VAMP2, which is in turn known to interact with syntaxin 1A/1B and SNAP25 upon vesicle fusion. Our results demonstrated that TRPC3 binds syntaxin 1A and 1B, but not SNAP25, which could indicate that their interaction is direct and not mediated through VAMP2, because if the interaction was via VAMP2, then SNAP25 would have likely been precipitated with TRPC3 in the IP experiment. Our results demonstrated that TRPC3 interacts with CaMKIV. We do not know whether their interaction is direct, or occurs via calmodulin, but they could also be part of the complex of proteins bound to TRPC3. We have also identified an interaction with PI synthase which is located at the ER and could be involved in TRPC3 regulation.

CHAPTER 4. Calcium Signalling Pathways in Moonwalker mice

Introduction

The *Moonwalker* (*Mwk*) mice have been generated by ENU-mutagenesis and have a point mutation in the transient receptor potential canonical channel, type 3 (TRPC3), which causes abnormal development of Purkinje cell dendrites and ataxia in the mice (Becker et al 2009). Abnormalities in Purkinje cell dendrites can be observed at two weeks of age *in vitro* and at three weeks of age *in vivo,* with ataxia being noticeable around three weeks of age. Normally, Purkinje cells have a single primary dendrite which becomes extensively branched during dendritic development (Kapfhammer 2004). The dendrites of *Mwk* Purkinje cells appear shorter and less branched in culture, whereas in the mouse cerebellum the dendritic tree has fewer terminal branches. The mechanism that leads to dendritic abnormalities has not been established.

TRPC3 is a channel permeable to positively charged ions, thus it allows Ca^{2+} and Na^{+} to enter the cells upon its activation (Li et al 1999; Zhu et al 1996). The *Mwk* mice have a more active TRPC3 channel, so we speculate that it allows more calcium to enter neurons when comparing to wild-type mice. There are several possible ways by which active TRPC3 could lead to the increase of Ca^{2+} in *Mwk* Purkinje cells. Firstly, Ca^{2+} could enter the cells through the activated TRPC3 channel; thereby TRPC3 would directly cause Ca^{2+} increase. Also, TRPC3 could cause an indirect increase of Ca^{2+} by allowing Na^{+} ions to enter the cells, which in turn would activate voltage-gated calcium channels (VGCC) that would lead to Ca^{2+} influx into the cells (Waterman 2000). Because the P/Q-type VGCC accounts for approximately 90% of the total voltage-gated calcium influx (Usowicz et al 1992), over-activation of this channel could lead to a significant increase in intracellular Ca^{2+} in *Mwk* Purkinje cells (Poteser et al 2011). A recent study actually has evidence that major calcium

influx into Purkinje cells via the mGluR1 activation cascade is facilitated by P/Q-type and T-type VGCCs (Gugger et al 2012), so it is likely that increased calcium levels in *Mwk* Purkinje cells are caused by *Mwk* TRPC3 activating other calcium channels. Another possibility is that TRPC3 could cause the release of Ca^{2+} from intracellular stores via inositol-1,4,5-triphosphate receptor 1 (IP_3R1) through a so-called Ca^{2+}-induced Ca^{2+} release (Berridge 1998). Any changes in interaction between the *Mwk* TRPC3 and IP_3R1 could potentially affect this type of Ca^{2+} release (see Chapter 3).

Ca^{2+} is an essential second messenger in neuronal cells (Tai et al 2009). It plays a crucial role in the nervous system, being responsible for neuronal proliferation and survival, synaptic transmission and plasticity, dendritic development, learning and memory through controlling gene expression and neurotransmitter release (Berridge 1995; 1998; Ginty 1997; Greer & Greenberg 2008; Lynch et al 1983; Malenka et al 1988; Mellstrom & Naranjo 2001; Tai et al 2008; Wojda et al 2008; Zieg et al 2008).

Ca^{2+} homeostasis inside the cell is maintained by different processes which are summarised in Figure 4-1. Ca^{2+} levels are very low inside the resting cells (~100 nM) compared to the extracellular Ca^{2+} (~2 mM), which allows for a rapid response to the intracellular Ca^{2+} concentration increase (Clapham 1995; Greer & Greenberg 2008). Calcium can enter the cells from the extracellular space through the plasma membrane calcium channels: VGCCs, N-methyl-D-aspartic (NMDA) receptors, α-amino-3-hydroxy-5-methyl-4-isoxazolepropionic acid (AMPA) receptors and TRPC channels. Calcium is also stored inside the intracellular stores, such as the Endoplasmic Reticulum (ER), and can be released into the cytoplasm through ER receptors IP_3R and ryanodine (RyR) upon their activation. Resting intracellular calcium levels can be restored by removing Ca^{2+} from the cell into the extracellular space via Ca^{2+} pumps: Na^+/Ca^{2+} exchangers (NCX) and plasma membrane calcium ATPases (PMCA); or into the ER via the smooth endoplasmic

reticulum calcium ATPase (SERCA) Ca^{2+} pumps, which also restores levels of Ca^{2+} in the intracellular stores (Berridge 1998; Clapham 1995; Clapham 2007).

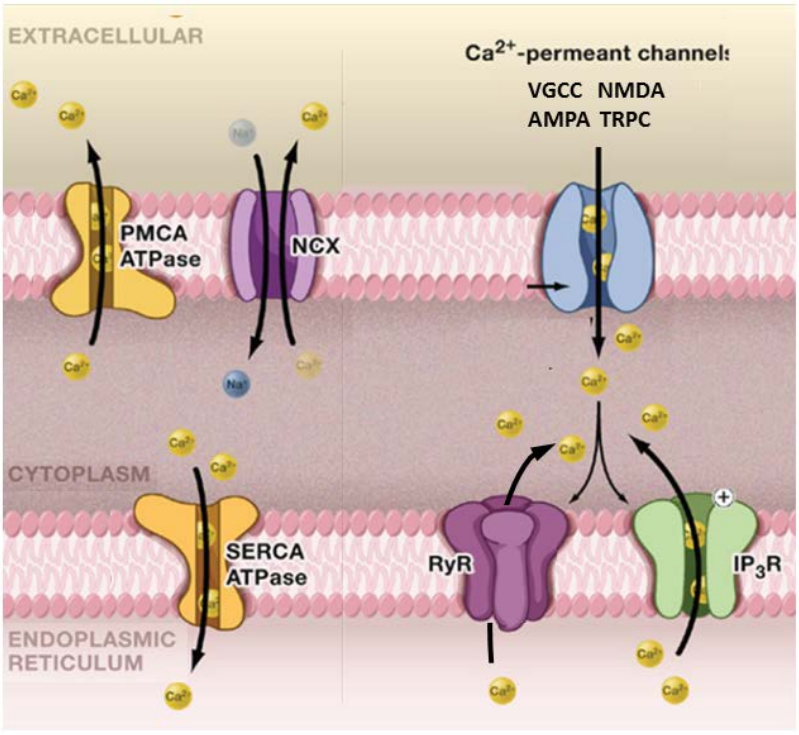

Figure 4-1. Calcium homeostasis. Ca^{2+} homeostasis inside a cell is maintained by many different channels. Ca^{2+} can enter the cells from the extracellular space through voltage-gated Ca^{2+} channels (VGCCs), N-methyl-D-aspartic (NMDA) receptors, α-amino-3-hydroxy-5-methyl-4-isoxazolepropionic acid (AMPA) receptors and transient receptor potential canonical (TRPC) channels. Ca^{2+} levels are restored to the resting state levels by plasma membrane calcium ATPases (PMCA) and Na^{+}/Ca^{2+} exchangers (NCX). Ca^{2+} can also enter the cell from the intracellular stores (e.g. Endoplasmic Reticulum). This is achieved by inositol-1,4,5-triphosphate receptors (IP_3R) and Ryanodine receptors (RyR). Intracellular Ca^{2+} store levels are replenished by the smooth endoplasmic reticulum calcium ATPase (SERCA) Ca^{2+} pumps. Adapted with permission from Clapham 2007.

In Purkinje cells, calcium plays a very important role: for example, Ca^{2+} is responsible for the initiation of long-term depression (LTD), which is crucial for the proper development of Purkinje cells and motor learning (Hartmann & Konnerth 2005; Konnerth et al 1992), but most importantly it plays a role in their dendritic growth (Schilling et al 1991). Calcium can enter the Purkinje neurons via the AMPA receptors, although they have a low permeability to Ca^{2+}. AMPA receptors can also trigger Ca^{2+} influx by causing depolarisation, which is necessary for the VGCCs to open

and let Ca^{2+} ions enter the cell. The most abundant VGCC in Purkinje cells is the P/Q-type. Purkinje cells have also been shown to have NMDA receptors, which has been unknown before (Piochon et al 2007). Another mechanism of Ca^{2+} entry in Purkinje cells is via activation of the mGluR1 receptor (Hartmann & Konnerth 2009). Interestingly, activation of mGluR1 was shown to inhibit dendritic growth of Purkinje cells (Sirzen-Zelenskaya et al 2006). So, the mechanism of mGluR1 activation is as follows: glutamate activates mGluR1, which activates the $G\alpha_q$ receptor, that activates PLCβ. PLCβ cleaves phosphatidylinositol 4,5-bisphosphate (PIP_2) to produce inositol 1,4,5-trisphosphate (IP_3) and diacylglycerol (DAG) (Berridge 1993). IP_3 then activates the intracellular Ca^{2+} store receptors IP_3R that release Ca^{2+} from stores (Mikoshiba 2011a). IP_3R1 expression levels are the highest in Purkinje cells of the cerebellum (Marchenko & Thomas 2006). DAG, on the other hand, activates TRPC channels, which allows them to open and let positive ions (including Ca^{2+}) to enter the cell from the extracellular space (Hofmann et al 1999).

Changes in Ca^{2+} concentration lead to various responses, such as initiation of transcription and cell cycle progression (Clapham 1995; Greer & Greenberg 2008; Negulescu et al 1994). Consequences of abnormally high Ca^{2+} levels and alterations in calcium signalling pathways differ, causing a range of responses from neuronal dysfunction to cell death and apoptosis (Choi 1988; Clapham 1995). One of the causes of cell death is caused by calcium overload through the mitochondria (mitochondria are also intracellular Ca^{2+} stores), which activates caspases leading to cell death (Buchholz et al 2007). Also, disturbances in calcium homeostasis have been implicated in neurological diseases, such as spinocerebellar ataxias (SCAs), Alzheimer's, Parkinson's, Huntington's and amyotrophic lateral sclerosis (ALS) (Bezprozvanny 2009; Wojda et al 2008).

We wanted to confirm that the *Mwk* mutation causes increased calcium influx into the cells and to investigate the pathways that likely become altered as a consequence. The most accurate way of doing this would be to use cell cultures transfected with WT and *Mwk* TRPC3 constructs, and compare the calcium influx into the cells by calcium imaging. Unfortunately, these experiments

could not be performed as TRPC3 with the *Mwk* mutation is toxic to the cells and causes their death, possibly through Ca^{2+} overload. Therefore, instead, we decided to investigate whether there are any abnormalities in activity of some key calcium signalling proteins *in vivo*.

Downstream molecular events conveying Ca^{2+} signals are complex and mostly involve phosphorylation cascades (Greer & Greenberg 2008). Some of the key neuronal calcium signalling pathways are demonstrated in Figure 4-2. These include the calcium/calmodulin-dependent protein (CaM) kinase signalling cascade, the mitogen-activated protein (MAP) kinase signalling cascade and the nuclear factor of activated T-cells (NFAT) signalling cascade (Greer & Greenberg 2008; Zieg et al 2008).

The CaM kinase cascade is demonstrated in Figure 4-2 in blue. When calmodulin is activated by Ca^{2+}, it activates CaMKK, which can then phosphorylate CaMKII and CaMKIV (Soderling 1999; Soderling & Stull 2001; Wayman et al 2008; Wayman et al 2011). Activation of these kinases leads to gene expression as they phosphorylate transcription factors, such as the cyclic-AMP response element binding protein (CREB). CREB can be phosphorylated at several serine residues: serine-129, serine-133, serine-142, and serine-143 (Kornhauser et al 2002). However, only phosphorylation at serine-133 appears to be essential for CREB-dependent transcription. Phosphorylation of CREB at serine-142 and serine-143, without serine-133, inhibits its interaction with the CREB-binding protein (CBP) and disrupts transcription of its target genes (Sun et al 1994). Activation of gene transcription by CREB, phosphorylated by CaMKIV, is involved in the formation of long-term plasticity of Purkinje cells (Marchenko & Thomas 2006). What is interesting, TRPC family member TRPC6 promotes the development of the dendrites of the hippocampal neurons via the influx of Ca^{2+} and the CaMKIV and CREB pathway (Tai et al 2008). It has been also shown that CaMKII and CREB could be regulated by TRPC3 and that TRPC3 has been implicated in CaM kinase-dependent gene transcription regulation in muscle cells (Jia et al 2007; Morales et al 2007). Furthermore, in Chapter 3 I have shown that CaMKIV, and maybe CaMKII, interact with the

wild-type TRPC3 protein, and it is possible that the interaction is disrupted in *Mwk* mice. This suggests that the CaM kinase signalling cascade is a very likely pathway that could be deregulated in the Purkinje cells of the cerebellum.

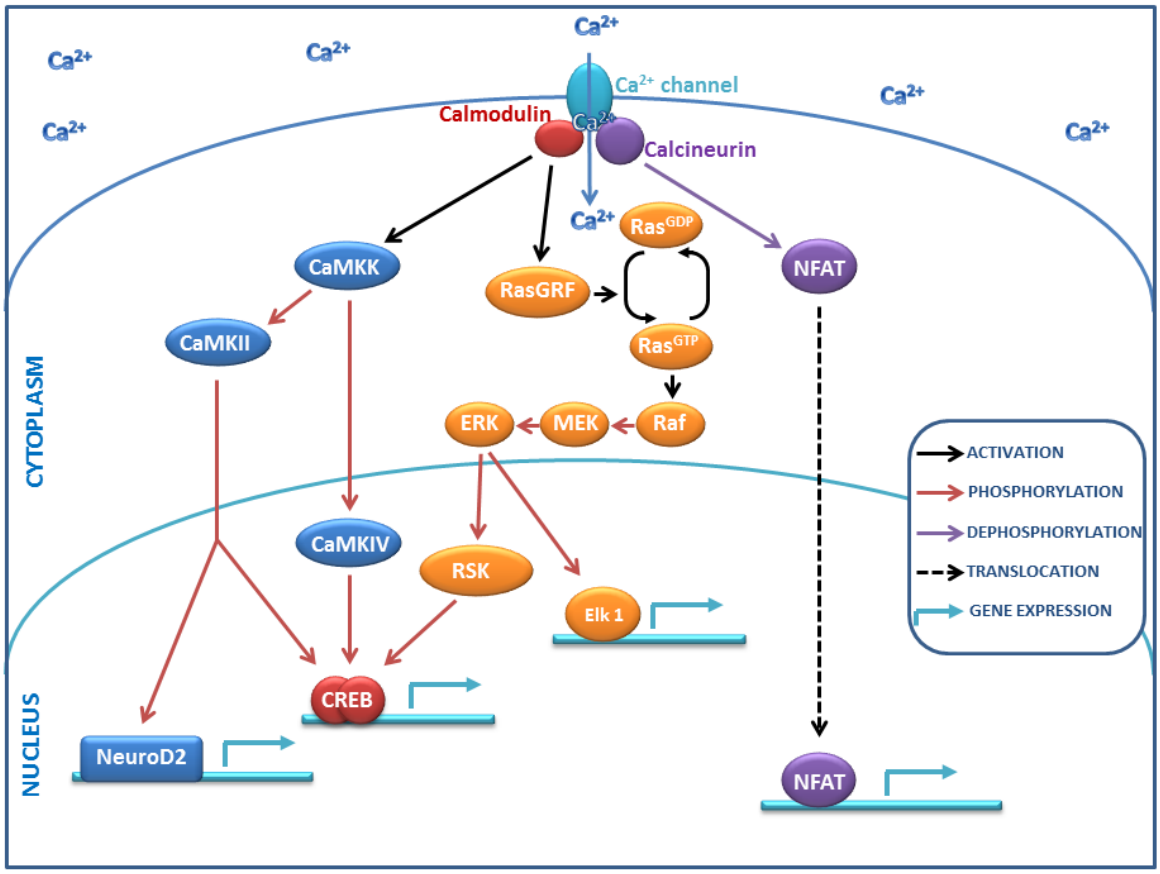

Figure 4-2. Calcium signalling in neurons. The complex signalling events that occur upon calcium entry into the neurons and include the CaM kinase signalling cascade (blue), the MAP kinase signalling cascade (orange) and the NFAT signalling cascade (purple). Abbreviations: **CaMK**, calcium/calmodulin-dependent protein kinase; **CaMKK**, calcium/calmodulin-dependent protein kinase kinase; **CREB**, cyclic AMP response element-binding protein; **Elk1**, ETS-like transcription factor; **ERK**, extracellular signal-regulated kinases; **MEK**, MAPK/ERK kinase; **NeuroD2**, neurogenic differentiation 2; **NFAT**, nuclear factor of activated T cells; **Raf**, ras-activated factor; **RasGRF**, ras protein-specific guanine nucleotide-releasing factor; **RSK**, ribosomal s6 kinase.

The MAP kinase signalling cascade is demonstrated in Figure 4-2 in orange. Briefly, Ca^{2+} that enters the cell activates calmodulin, which as well as activating the CaM kinase signalling cascade, also activates RasGRF (Ras protein-specific guanine nucleotide-releasing factor), which converts Ras^{GDP} to Ras^{GTP}. The activated form Ras^{GTP} is able to associate with Raf (Ras-activated factor),

which can now phosphorylate the MAPK/ERK kinase (MEK), that can then phosphorylate and activate ERK. Phosphorylated ERK can either directly phosphorylate transcription factors, such as Elk 1; or it can activate transcription factors indirectly through phosphorylation of other proteins, such as RSK, that phosphorylate CREB (Johnson & Lapadat 2002; Robinson & Cobb 1997). Blocking ERK along with CaMKII in the granule cells of the cerebellum diminishes the protective effect that TRPC3 has on granule cells during their development (Jia et al 2007). Hence, it is possible that TRPC3 could also regulate the activity of the MAP kinase signalling pathway.

The NFAT signalling cascade is demonstrated in Figure 4-2 in purple. The NFAT pathway is activated by a calcium dependent phosphatase calcineurin, which de-phosphorylates NFAT transcription factors (NFATc1-c4), causing them to translocate to the nucleus and regulate gene transcription (Crabtree & Olson 2002; Nguyen & Di Giovanni 2008). TRPC3 has been shown to regulate NFAT-dependent gene transcription in the heart and muscle (Bush et al 2006; Rosenberg et al 2004). Moreover, recent studies demonstrated that the *Mwk* mutation in the TRPC3 channel causes NFAT-dependent transcription silencing in tissue culture experiments (Poteser et al 2011). Therefore, since the calcineurin-NFAT pathway is already known to be regulated by TRPC3, it would be curious to investigate whether the *Mwk* mutation causes any changes to it.

Any changes in Ca^{2+} signalling could be the cause of abnormal development and function of *Mwk* Purkinje cells. Therefore, for our study we decided to investigate whether these calcium signalling pathways are altered in *Mwk* mice compared to their wild-type littermates.

Results

Gain-of-function *Mwk* mutation in the TRPC3 channel likely leads to increased Ca^{2+} levels in Purkinje cells. Alterations in calcium homeostasis could lead to many complications, including neuronal dysfunction. Because the *Mwk* TRPC3 protein is toxic to different types of cells in tissue culture, experiments to measure and compare Ca^{2+} concentrations inside cells containing wild-type and *Mwk* TRPC3 cannot be performed. With changes in calcium concentration inside a cell, it is logical to assume that calcium signalling pathways become deregulated. A way to investigate activity of some proteins is to measure their phosphorylation levels, or to look at their localisation inside a cell.

Analysis of phosphorylation levels of key calcium signalling proteins by Western blot

We investigated the levels of phosphorylation of some key calcium signalling molecules: CaMKII, CaMKIV, CREB, ERK and NFAT. Phosphorylation of CaMKII, CaMKIV, CREB and ERK leads to their activation, whereas phosphorylation of NFAT leads to its deactivation.

For the western blot experiments, cerebella of wild-type and *Mwk* littermates were lysed and their total protein concentration was measured, in order for the same amount of protein to be loaded onto a gel for a direct comparison of calcium signalling protein levels. When observing the phosphorylation levels, we compared them to the whole protein levels in order to confirm precise loading and make an accurate judgement.

A range of ages was used from P15 to P46 to observe whether there are any early changes that could cause the *Mwk* phenotype or any later changes that could occur as a consequence of abnormal neuronal function. Each age represents one litter with both wild-type and *Mwk* pups.

When looking at levels of phosphorylated CaMKII (P-CaMKII), no changes were evident until the age of P46, where P-CaMKII levels were increased in three *Mwk* mice compared to one wild-type

littermate (Figure 4-3). At P20 and P22 one *Mwk* sample in each age showed less protein, however it could be due to the fact that it was the last lane on a gel, and sometimes it can be a slightly inaccurate representation of the blot. At P42 one wild-type sample showed less phosphorylation levels than all the other samples. Therefore, it is possible that the levels of CaMKII phosphorylation start changing slightly earlier than P46, however more experiments need to be performed in order to conclude that.

Interestingly, levels of phosphorylated CaMKIV showed a potentially subtle decrease at P21 (Figure 4-4). The decrease in activation of CaMKIV was slightly more evident at P22, P25 and P46. This is an exciting result as P21 is the time-point at which dendritic abnormalities are evident in the *Mwk* mice and it also is the onset of their ataxic behaviour, which means that CaMKIV could possibly be part of the pathway which directly causes these abnormalities. This result is encouraging, but needs more replicates to be confirmed.

A transcription factor CREB can be phosphorylated at several sites and we were interested in its phosphorylation at the serine-133 residue because it can be phosphorylated by CaMKII, CaMKIV and ERK (indirectly). CREB phosphorylation at Serine-133 was indeed up-regulated in *Mwk* mice from P21 (Figure 4-5). The up-regulation of the phosphorylation was present to an extent throughout the ages, but was most evident at P42.

The occurrence of ERK phosphorylation is more erratic when compared to other calcium signalling proteins, with its expression varying among wild-type and *Mwk* samples throughout all ages (Figure 4-6). However, a clear increase in phosphorylation of ERK was evident from P42 and remained high at P46.

None of the NFAT antibodies worked for the western blot experiments, therefore we were unable to determine whether there are any changes in the NFAT phosphorylation state in *Mwk* mice.

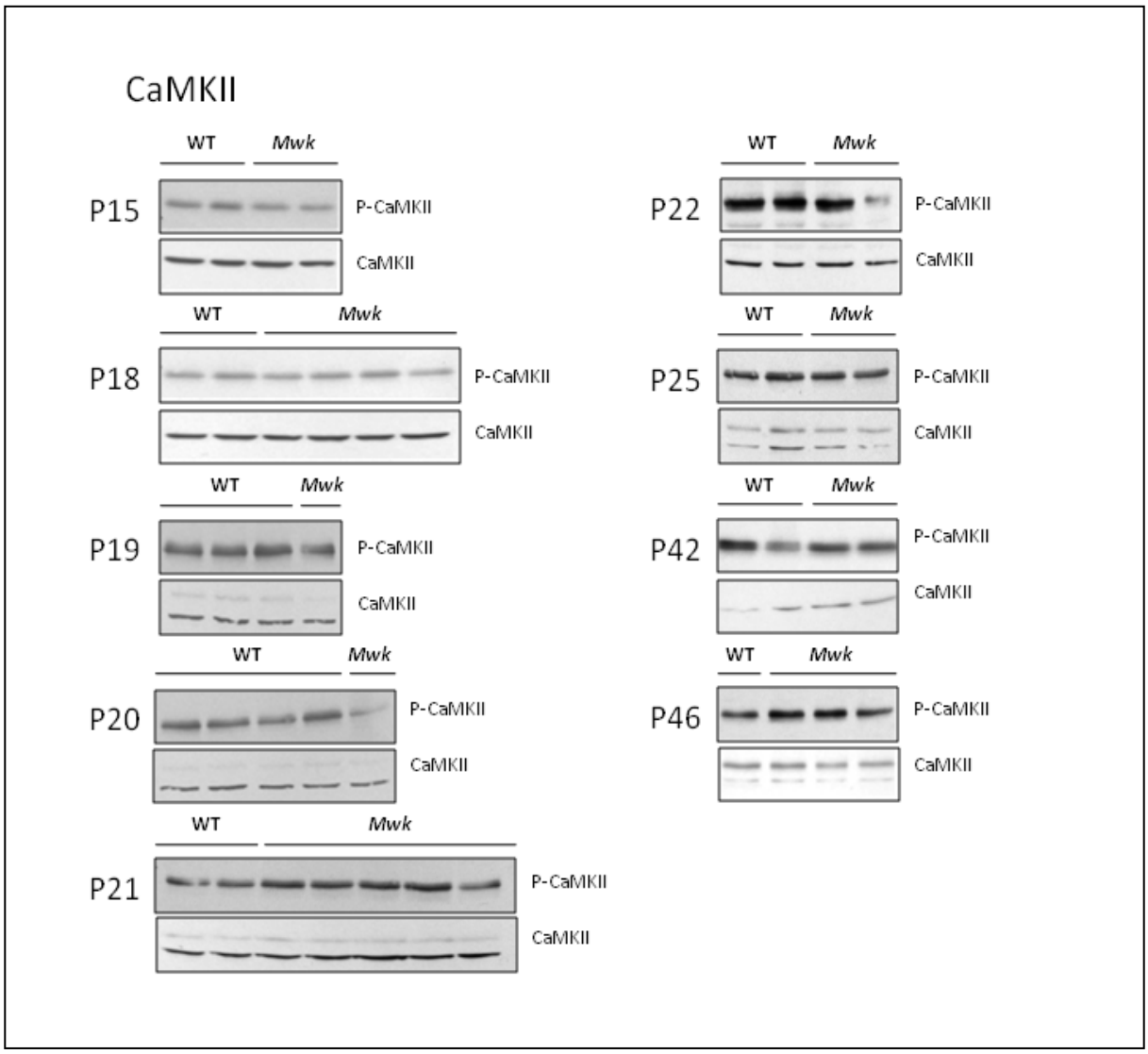

Figure 4-3. Activity of calcium/calmodulin-dependent protein kinase type II (CaMKII) in *Mwk* mice cerebellar lysates compared to wild-type (WT) littermates. Different ages were tested: P15, P18, P19, P20, P21, P22, P25, P42 and P46. P-CaMKII protein levels represent active form of CaMKII. Equal loading is shown with total CaMKII levels. Activity of CaMKII starts increasing in *Mwk* mice compared to wild-type mice at P46.

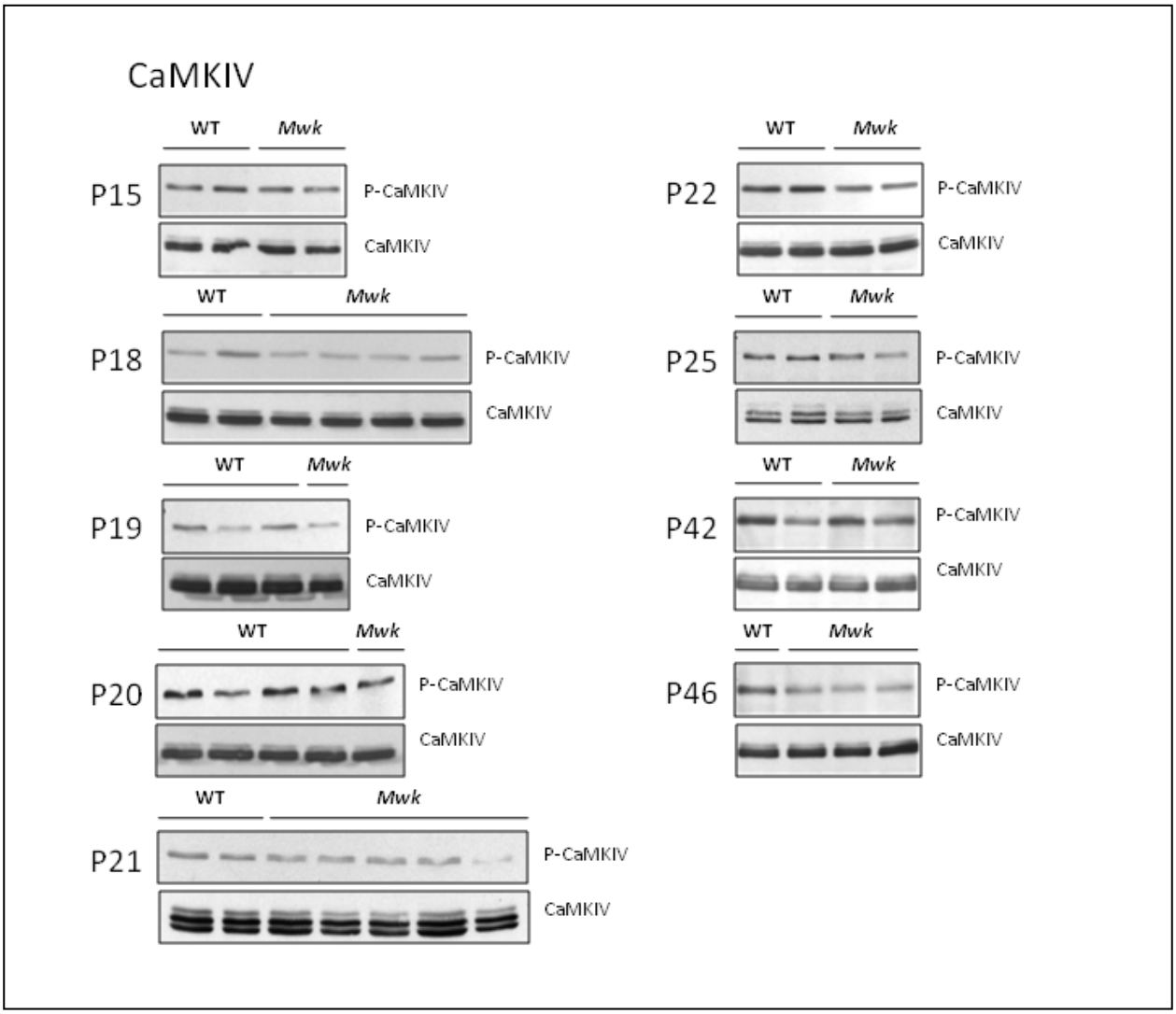

Figure 4-4. Activity of calcium/calmodulin-dependent protein kinase type IV (CaMKIV) in *Mwk* mice cerebellar lysates compared to wild-type (WT) littermates. Different ages were tested: P15, P18, P19, P20, P21, P22, P25, P42 and P46. P-CaMKIV protein levels represent active form of CaMKIV. Equal loading is shown with total CaMKIV levels. Activity of CaMKIV starts decreasing in *Mwk* mice compared to wild-type mice at P21.

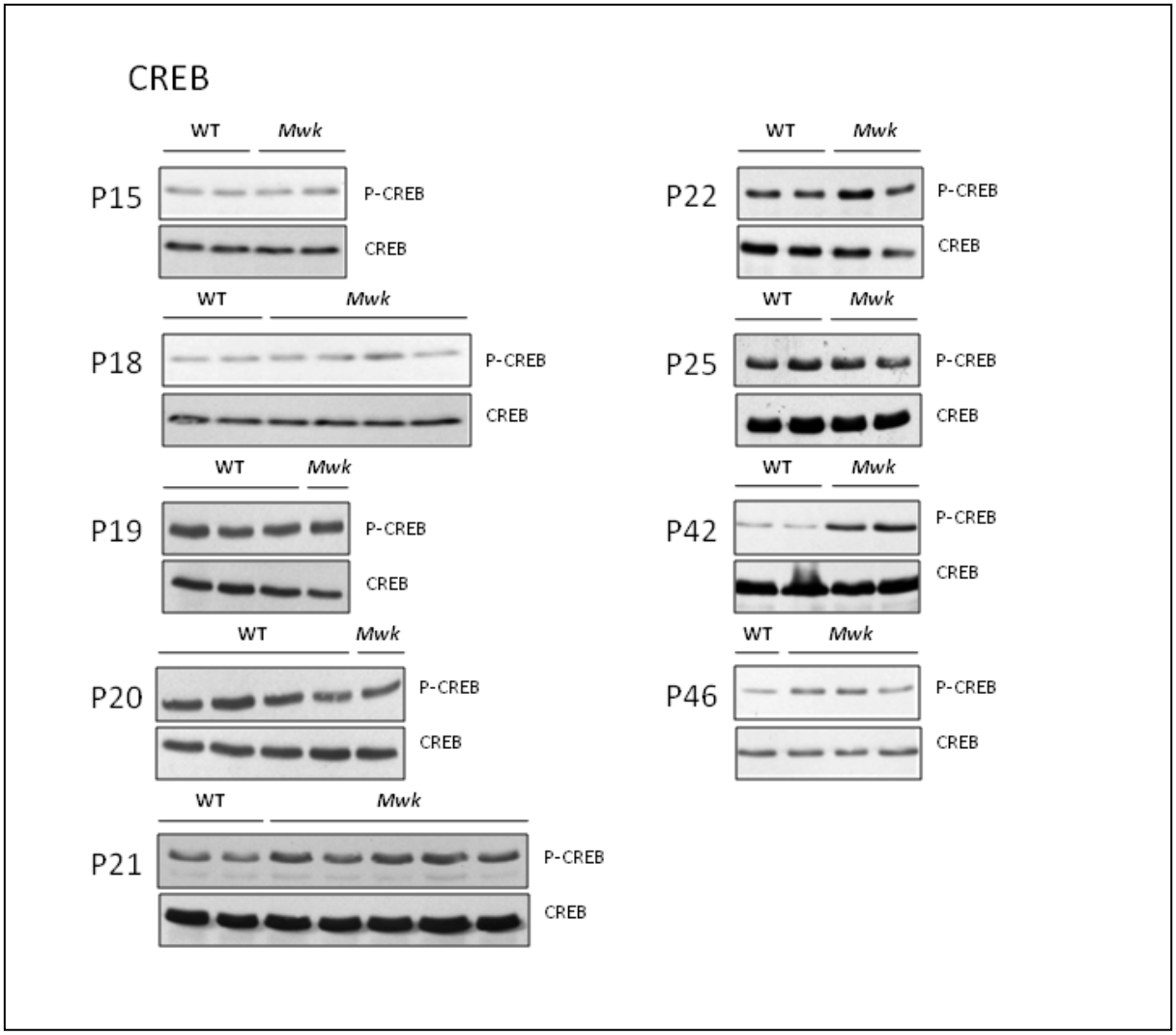

Figure 4-5. Activity of cyclic-AMP response element binding protein (CREB) in *Mwk* mice cerebellar lysates compared to wild-type (WT) littermates. Different ages were tested: P15, P18, P19, P20, P21, P22, P25, P42 and P46. P-CREB protein levels represent active form of CREB. Equal loading is shown with total CREB levels. Activity of CREB starts increasing in *Mwk* mice compared to wild-type mice at P21, and is very pronounced after P42.

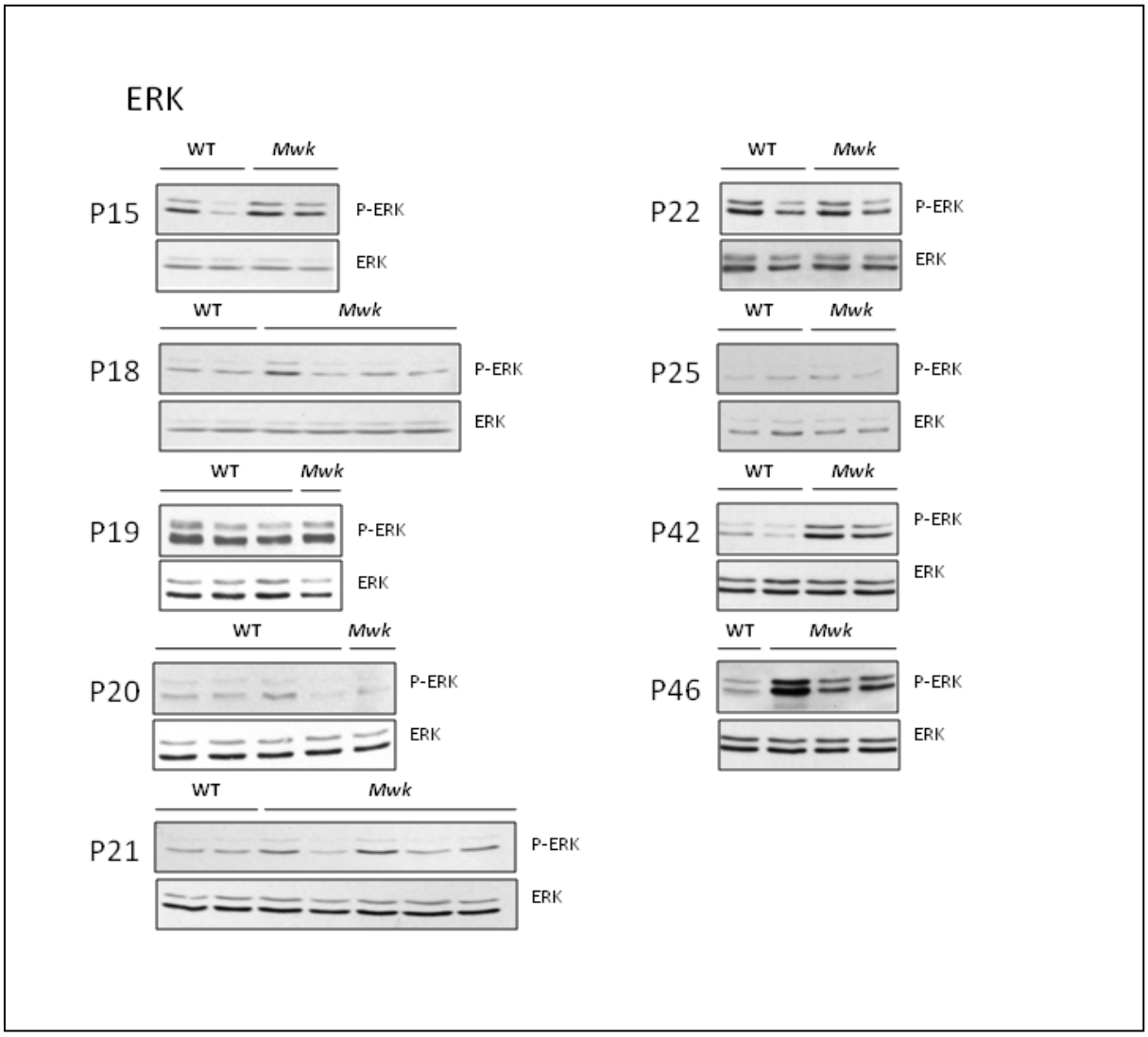

Figure 4-6. Activity of extracellular signal regulated kinase (ERK) in *Mwk* mice cerebellar lysates compared to wild-type (WT) littermates. Different ages were tested: P15, P18, P19, P20, P21, P22, P25, P42 and P46. P-ERK protein levels represent active form of ERK. Equal loading is shown with total ERK levels. Top band represents ERK1, and bottom band represents ERK2. Activity of ERK1/2 starts increasing in *Mwk* mice compared to wild-type mice at P42.

Localisation of calcium signalling proteins in the cerebellum

TRPC3 protein is highly enriched in the Purkinje cells and, to our knowledge, the *Mwk* mutation only causes abnormal development of Purkinje cells of the cerebellum. Because whole cerebellar lysates were used to investigate phosphorylation levels of CaMKII, CaMKIV, CREB and ERK, it was important to observe which cell types in the cerebellum express these proteins.

Immunohistochemistry (IHC) experiments demonstrated that the phosphorylated form of CaMKIV was only expressed in the Purkinje cells of the cerebellum in the perikaryon and also the dendrites, but not in the nucleus (Figure 4-7). This means that the decreased levels in P-CaMKIV, which we observed in *Mwk* mice by western blot, reflect the changes in Purkinje cells, rather than the whole cerebellum. The localisation of P-CaMKIV is the same in wild-type and *Mwk* mice and does not change at different ages (P18, P20 or P46).

Phosphorylated CREB, on the other hand, was expressed in Purkinje cells, as well as in granule cells (Figure 4-8). Therefore the increase in P-CREB levels in *Mwk* mice that we detected by western blot could occur in Purkinje cells and granule cells. Interestingly, CREB was expressed in the perikaryon, and the nucleus. Nuclear expression presumably indicates that CREB is regulating transcription. However, preliminary experiments showed no differences in the percentage of cells expressed in the perikaryon vs. nucleus between wild-type and *Mwk* cerebella (data not shown).

Only NFATc3 out of NFATc1-NFATc4 could be detected in the IHC experiments. NFATc3 was expressed only in the cytoplasm of the Purkinje cells (cell body and dendrites), and not in the nucleus (Figure 4-9). No change was observed between expression localisation in the wild-type and *Mwk* samples. However, the activity of other NFAT members could still be altered in *Mwk* Purkinje cells.

The antibodies for P-CaMKII and P-ERK did not stain the cryosections.

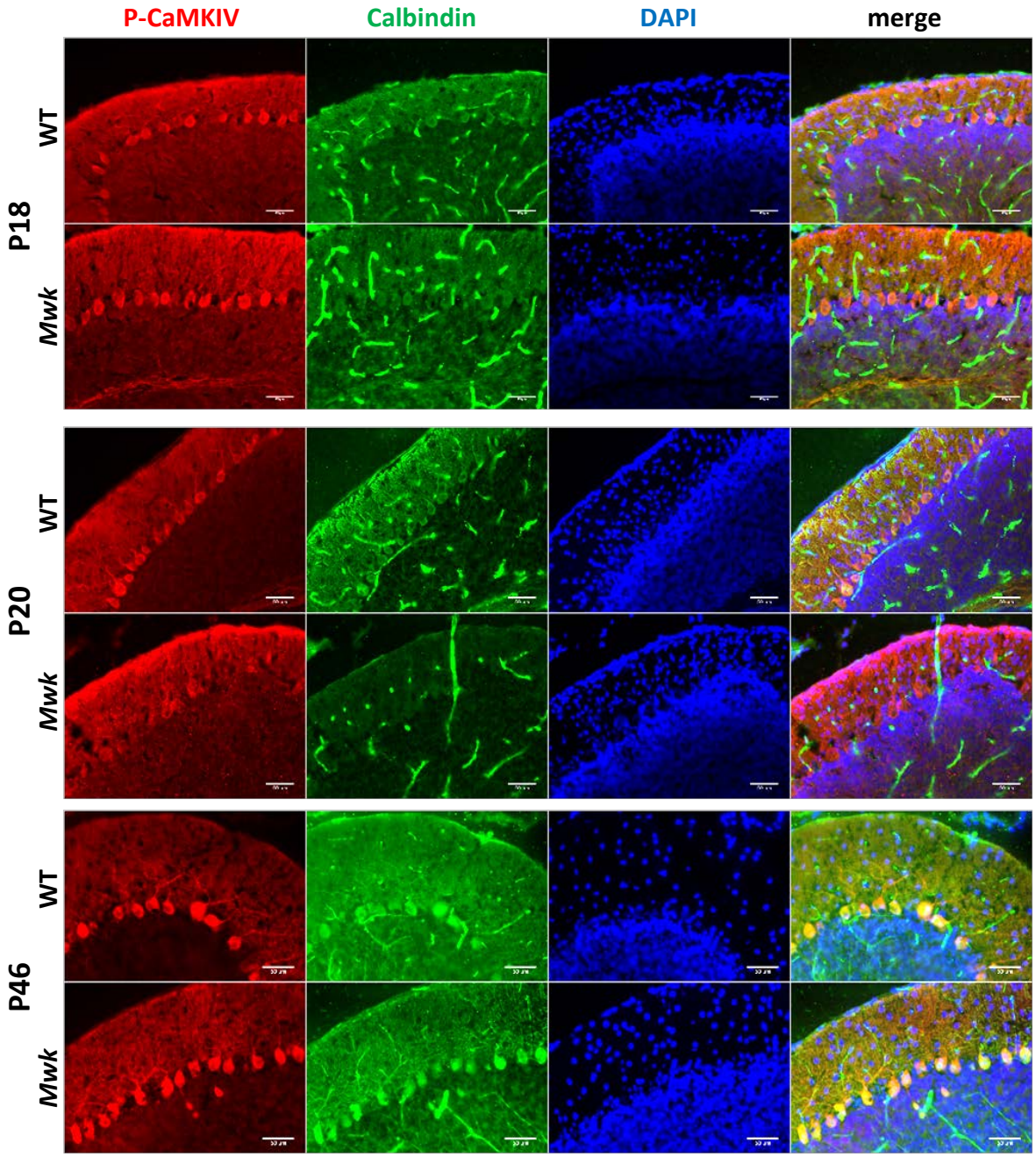

Figure 4-7. Expression patterns of P-CaMKIV in the cerebellum of wild-type (WT) and *Mwk* mice are the same. Immunohistochemistry results showing expression of P-CaMKIV in the perikaryon and dendrites of Purkinje cells of the cerebellum in both wild-type and *Mwk* mice at ages P18, P20 and P46 stained with anti-P-CaMKIV and anti-calbindin antibodies. Scale bar = 50 µm. n=2

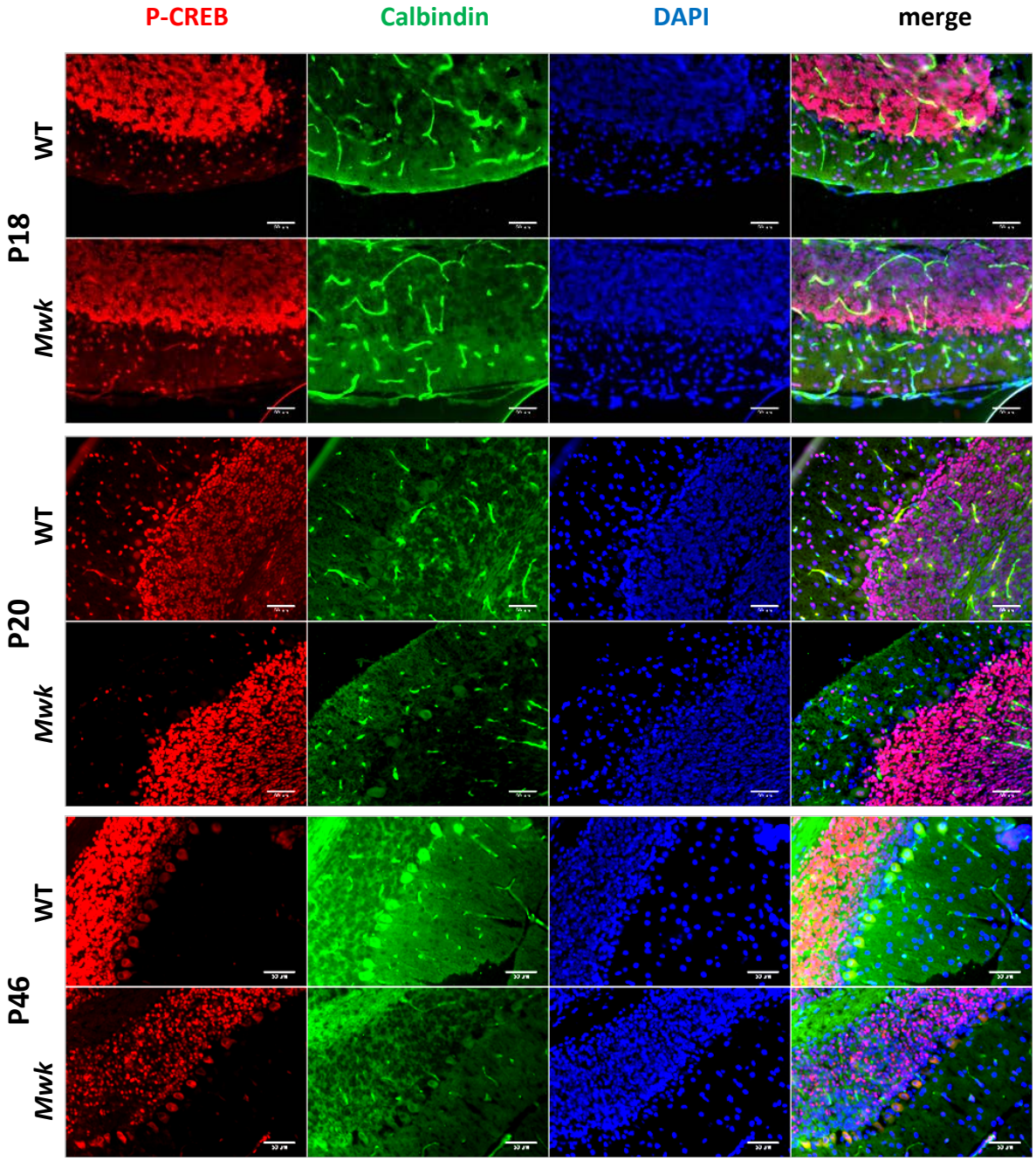

Figure 4-8. Expression patterns of P-CREB in the cerebellum of wild-type (WT) and *Mwk* mice are the same. Immunohistochemistry results showing expression of P-CBER in both the granule cells and in the perikaryon and nucleus of Purkinje cells of the cerebellum in wild-type and *Mwk* mice at ages P18, P20 and P46 stained with anti-P-CREB and anti-calbindin antibodies. Scale bar = 50 µm. n=2

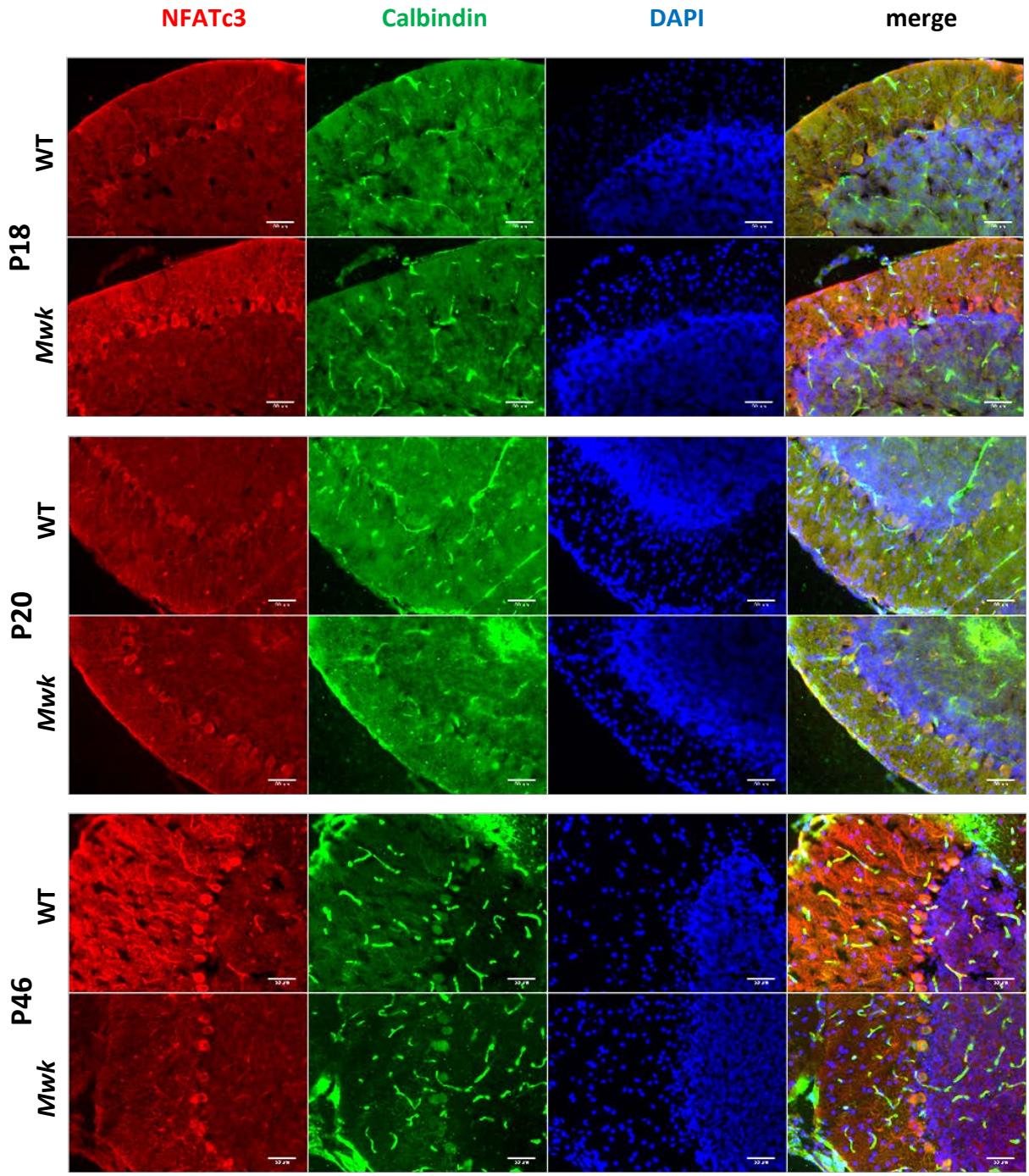

Figure 4-9. Expression patterns of NFATc3 in the cerebellum of wild-type (WT) and *Mwk* mice are the same. Immunohistochemistry results showing expression of NFATc3 in the perikaryon and dendrites of the Purkinje cells in the cerebellum in both wild-type and *Mwk* mice at ages P18, P20 and P46 stained with anti-NFATc3 and anti-Calbindin antibodies. Scale bar = 50 µm. n=2

Levels of phosphorylation of Stathmin – a CaMKIV target

Because we observed a potential down-regulation in CaMKIV phosphorylation as early as P21, we decided to investigate further whether CaMKIV could affect abnormal development of Purkinje cells. CaMKIV can influence transcription of the cell as well as its structural development. One of the targets of CaMKIV in the cytoplasm is stathmin – which destabilises microtubule proteins when in its un-phosphorylated state and is known to regulate Purkinje cell dendritic growth (Belmont et al 1996; Gradin et al 1997; Ohkawa et al 2007). Phosphorylation of stathmin by CaMKIV causes inactivation of stathmin and hence leads to more stable microtubules. To check whether decreased levels of CaMKIV phosphorylation in the *Mwk* Purkinje cells have influenced phosphorylation of stathmin, western blot of cerebellar lysates was probed for P-stathmin and stathmin (Figure 4-10). The results showed that there were no changes between the levels of phosphorylation of stathmin in *Mwk* mice compared to their wild-type littermates throughout the tested ages.

Phosphorylation of calcium signalling proteins in response to OAG in SH-SY5Y cells

To confirm changes in Ca^{2+} signalling cascades *in vivo* and to verify whether there is an up- or down-regulation of CREB, we used a neuroblastoma SH-SY5Y cell line transfected with a 3xFLAG-TRPC3 construct. As mentioned earlier, *Mwk* TRPC3 is toxic to the cells and thus it is not possible to use it in tissue culture experiments. However, diacylglycerol (DAG) is a known activator of TRPC3 and thus could be used to imitate the effect of the gain-of-function *Mwk* mutation as it would activate TRPC3 and thus allow more calcium to flow into the cells. For the tissue culture experiments we used a DAG analogue 1-oleoyl-2-acetyl-sn-glycerol (OAG).

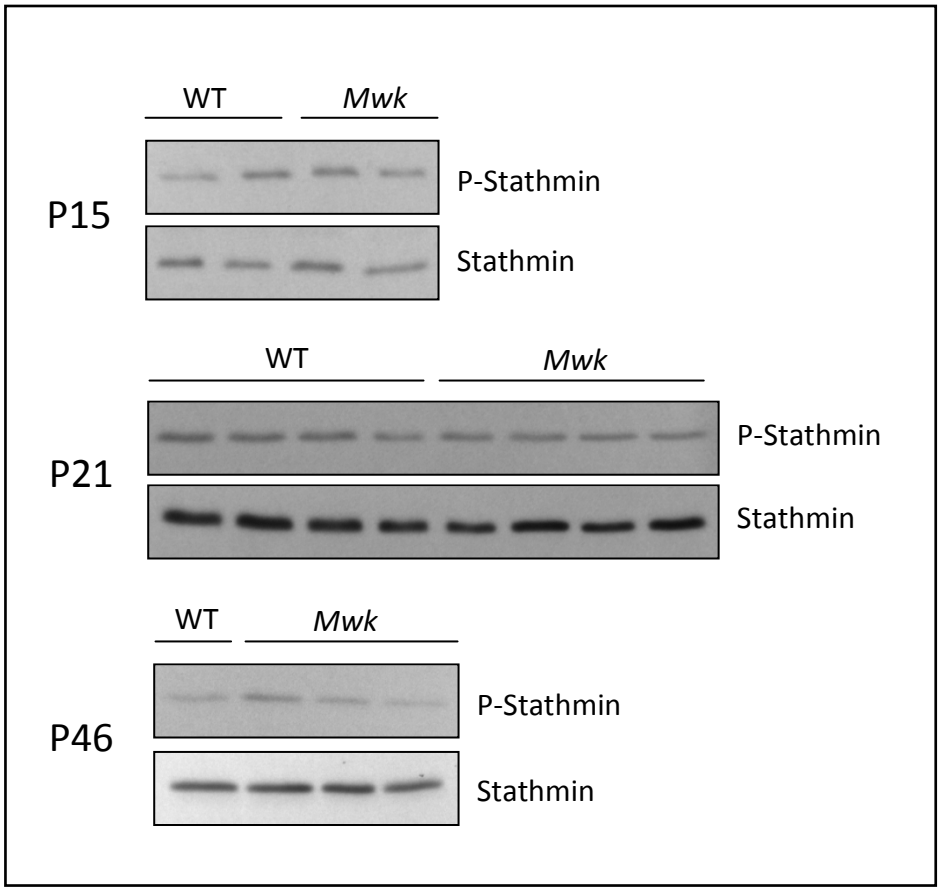

Figure 4-10. Stathmin phosphorylation levels are not altered in *Mwk* cerebella. Activity of stathmin in *Mwk* mice cerebella lysates compared to wild-type (WT) littermates at different ages (P15, P21 and P46). P-stathmin protein levels represent active form of stathmin. Equal loading is shown with total stathmin levels. n=2

Cells to which 100 µM and 200 µM OAG was added to for 5 minutes were compared to cells without the addition of OAG to investigate by western blot whether the addition of OAG alters the amount of phosphorylation of CaMKII, CaMKIV, CREB and ERK. Also, 3xFLAG-TRPC3 transfected cells were compared with non-transfected cells to make sure that if any changes were observed, they were only present in the 3xFLAG-TRPC3 transfected cells. As shown in Figure 4-11, the only changes detected after OAG addition were with P-ERK, but P-ERK levels increase in both transfected and un-transfected cells. Phosphorylation of other proteins was unaffected with the addition of OAG.

Localisation of calcium signalling proteins in SH-SY5Y cells in response to OAG

Location of proteins is important for their function. For instance, CREB can be found in the cytoplasm and the nucleus, but it can only influence transcription when it is in the nucleus. So we examined whether localisation of P-CAMKII, P-CaMKIV, P-CREB, P-ERK, NFATc3 and NFAT1 (=NFATc2) changes with the addition of OAG by immunocytochemistry (ICC). Cells were transfected with 3xFLAG-TRPC3 and either treated with 100 µM OAG or not (Figure 4-12[A-F]). However, CaMKII, CaMKIV and CREB were already present in the nucleus in the un-stimulated state and they remained in the nucleus after the addition of OAG. Keeping the cells in a serum-free media did not change the location of these proteins either (data not shown). P-ERK, NFATc3 and HA-NFAT1-GFP were expressed in the cytoplasm, and stimulation with OAG did not cause their translocation to the nucleus. Perhaps the addition of OAG did not imitate the effect of the *Mwk* mutation in TRPC3 on cells.

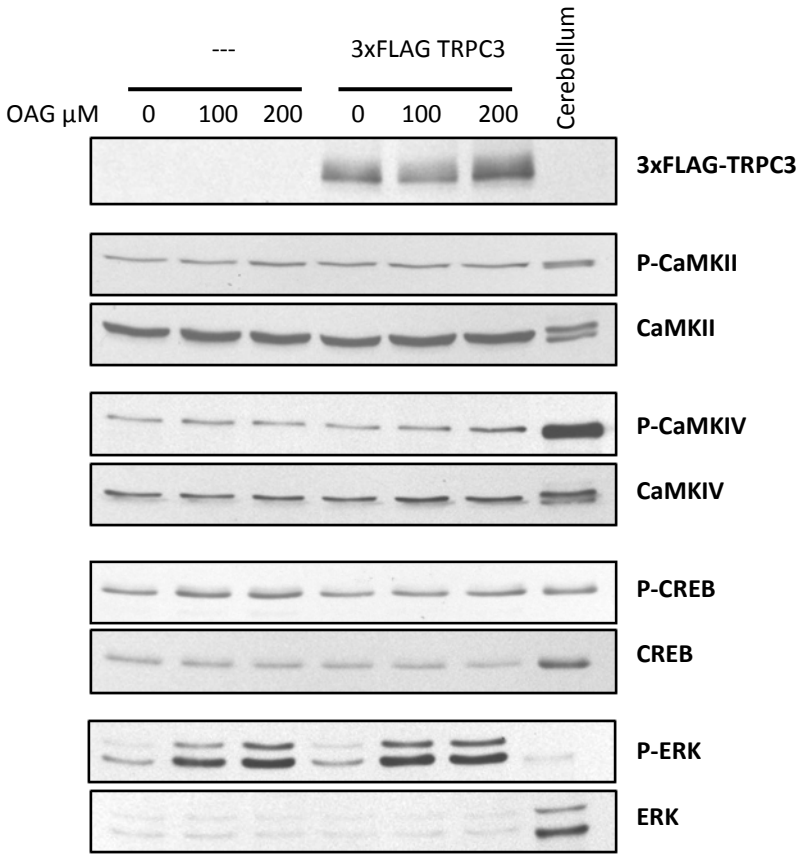

Figure 4-11. Levels of phosphorylation of key calcium signalling proteins do not change in SH-SY5Y cells after stimulation with OAG. Western blot showing the responses of P-CaMKII, P-CaMKIV, P-CREB and P-ERK in 3xFLAG-TRPC3 transfected SH-SY5Y cells after administration of 0, 100 and 200 µM OAG for 5 min which stimulates the opening of the TRPC3 channel, compared to the non-transfected cells. Total protein levels are shown with CaMKII, CaMKIV, CREB and ERK respectively. n=3

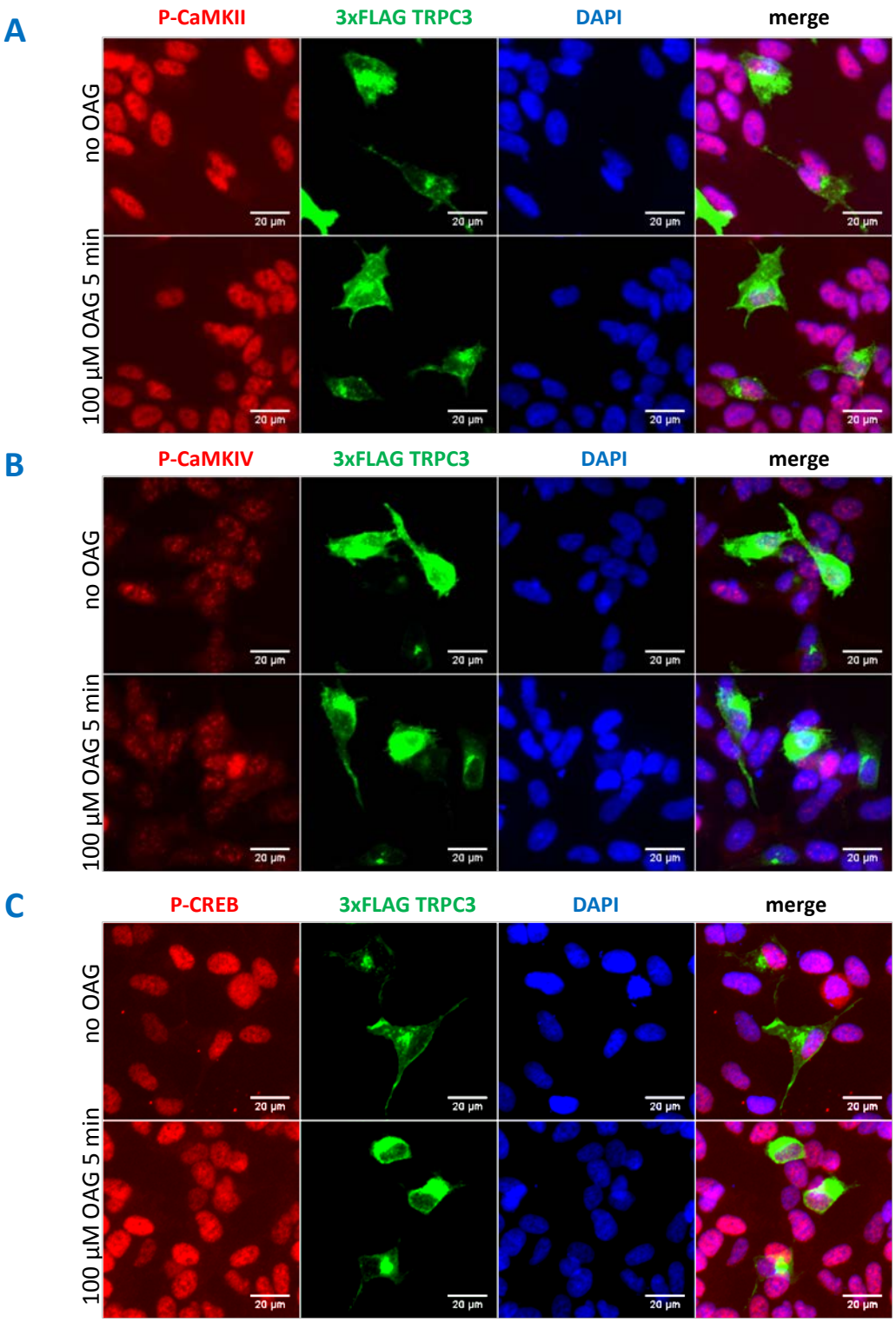

Figure 4-12 (A-C). Response of P-CaMKII, P-CaMKIV and P-CREB in SH-SY5Y cells to the addition of 100 µM OAG for 5 min. Immunocytochemistry showing the expression patterns of active forms of CaMKII (A), CaMKIV (B) and CREB (C) in 3xFLAG-TRPC3 transfected SH-SY5Y cells remained the same after the addition of 100 µM OAG for 5 minutes which should stimulate the opening of the TRPC3 channel. Cells were stained with anti-P-CaMKII, anti-P-CaMKIV and anti-P-CREB antibodies respectively and anti-FLAG antibody. Scale bar = 20 µm. n=2

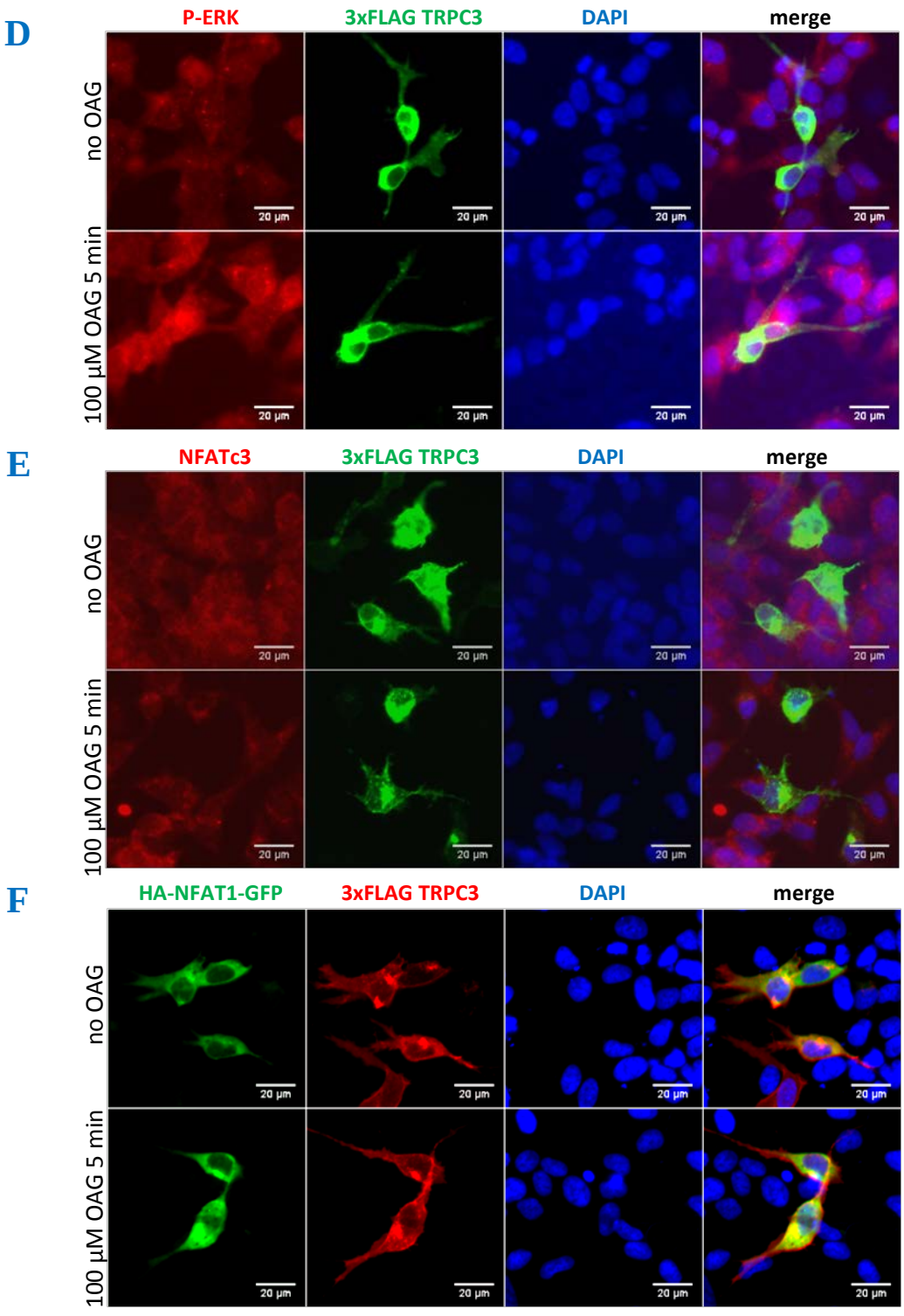

Figure 4-12 (D-F). Response of P-ERK, NFATc3 and HA-NFAT1-GFP in SH-SY5Y cells to the addition of 100 µM OAG for 5 min. Immunocytochemistry showing the expression patterns of an active form of ERK (D), NFATc3 (E) and HA-NFAT1-GFP (F) in 3xFLAG-TRPC3 transfected SH-SY5Y cells remained the same after the addition of 100 µM OAG for 5 minutes which should stimulate the opening of the TRPC3 channel. Cells were stained with anti-P-ERK and anti-NFATc3 antibodies respectively and anti-FLAG antibody. Scale bar = 20 µm.

Summary

Several Ca^{2+} signalling pathways are deregulated in the *Mwk* cerebella, indicating that there are changes in Ca^{2+} levels inside Purkinje cells of the cerebellum. These include the CaMK and ERK signalling pathways. CaMKIV phosphorylation is potentially down-regulated in *Mwk* Purkinje cells during the onset of ataxia and dendritic abnormalities. CREB phosphorylation is up-regulated at the same time, although it is not clear whether this actually happens in Purkinje cells. CaMKII and ERK phosphorylation is up-regulated at a later stage in Purkinje cell development, so these kinases might not be responsible for the *Mwk* phenotype.

Discussion

A point mutation in a TRPC3 ion channel leads to abnormal development of Purkinje cell dendrites and ataxia in *Mwk* mice. Previous findings have shown that the *Mwk* TRPC3 is activated at lower concentrations of (S)-3,5-dihydroxyphenylglycine (DHPG) – an agonist of mGluR1– when the wild-type TRPC3 remains inactive (Becker et al 2009). This suggests that more Ca^{2+} could flow into the Purkinje cells of the *Mwk* mice, which would likely cause changes to the homeostasis of Ca^{2+} signalling cascades. In this chapter we investigated changes to phosphorylation of some of the key Ca^{2+} signalling proteins in order to elucidate the mechanism by which *Mwk* TRPC3 ion channel could cause abnormal Purkinje cell development. We have, indeed, confirmed that Ca^{2+} signalling is deregulated in the cerebella of *Mwk* mice, which confirms changes in Ca^{2+} homeostasis.

CaM kinase signalling cascade

Many responses to increased intracellular calcium levels in the nervous system are mediated by CaM kinase signalling, which is demonstrated in Figure 4-1 (Wayman et al 2008). When Ca^{2+} enters the cell, it binds to a calcium sensing molecule calmodulin which undergoes a conformational change to become activated (Hoeflich & Ikura 2002; Soderling 1999). This Ca^{2+}/calmodulin complex is then able to activate calcium/calmodulin-dependent protein kinase kinase (CaMKK). CaMKK phosphorylates several types of CaM kinases, including CaMKII and CaMKIV, which are autoinhibited in the absence of Ca^{2+}. Phosphorylation of CaMKII and CaMKIV by CaMKII and their autophosphorylation is required for their full activation (Soderling & Stull 2001). Both these kinases are multifunctional, meaning that they control a wide range of substrates (Wayman et al 2011). Some of the downstream phosphorylation targets of CaMKII and CaMKIV are the same, such as a transcription factor CREB, while some are distinct. Both CaMKII

and CaMKIV are ubiquitously expressed, but are especially abundant in the brain (Wayman et al 2008). They have a very similar structure, but CaMKII has a unique C-terminal domain (Soderling & Stull 2001).

In our study we investigated whether the phosphorylation levels of CaMKIV, CaMKII and CREB were altered in the *Mwk* mice. We have, indeed, found by western blot analysis that all three proteins show changes to their phosphorylation levels in whole cerebellar lysates: CaMKIV phosphorylation is reduced in *Mwk* cerebella starting from P21; CREB phosphorylation is increased from P21; and CaMKII phosphorylation is increased starting from P46. Immunohistochemistry revealed that P-CaMKIV expression is restricted to the Purkinje cells of the cerebellum and is absent from granule cells, hence the reduction of P-CaMKIV we observe by western blot likely occurs in the Purkinje cells. P-CREB, however, is present in both Purkinje cells and the granule cells; therefore because whole cerebellar lysates were investigated, we cannot conclude that CREB phosphorylation is indeed altered in Purkinje cells.

- **CaMKIV & CREB**

CaMKIV is a multifunctional serine-threonine kinase that is activated in response to increasing intracellular calcium levels, it has a key role in neuronal calcium signalling, and is essential for the development of the cerebellum (Ho et al 2000; Ribar et al 2000). Downstream targets of CaMKIV include transcription factors, such as CREB and MEF2 (Blaeser et al 2000; Redmond et al 2002); as well as other proteins, including CBP (Chawla et al 1998), cytoskeletal proteins and their regulators, such as the microtubule regulating protein stathmin (Gradin et al 1997).

CaMKIV is expressed in the granule cells of the rat cerebellum, as well as more weakly in Purkinje cells of the cerebellum (Ohmstede et al 1989; Ribar et al 2000). Our studies could not confirm that by IHC as the α CaMKIV antibody did not stain the cerebellar cryosections. Although, surprisingly, we revealed that in the cerebellum the phosphorylated active form of CaMKIV is only

expressed in the Purkinje cells, and is absent from all other cell types, including the granule cells. So the function of CaMKIV might be particularly important for the Purkinje cells of the cerebellum.

Within the cell, CaMKIV is known to be located in the cytoplasm and in the nucleus (Jensen et al 1991; Soderling & Stull 2001). This indicates that CaMKIV could potentially have two distinct functions: in the nucleus, CaMKIV could regulate transcription by phosphorylating transcription factors, such as CREB; whereas in the cytoplasm CaMKIV could be responsible for stabilising the dendritic structure or neurite outgrowth via phosphorylating stathmin. Our data demonstrated that the phosphorylated form of CaMKIV is only present in the cytoplasm of Purkinje cells, but is absent from the nucleus. It is still, however, possible that CaMKIV can influence gene expression by phosphorylating transcription factors in the cytoplasm and causing them to translocate to the nucleus. For example, our experiments have shown that P-CREB is expressed in both the perikaryon and the nucleus. Phosphorylation of CREB by CaMKIV is important for Purkinje cell development, since it is implicated in the LTP formation (Marchenko & Thomas 2006).

Since there is a reduction in CaMKIV phosphorylation levels and an increase in CREB phosphorylation in the cerebellum, this raises the question whether the CREB-dependent transcription regulated by CaMKIV is actually altered in the Purkinje cells of *Mwk* mice. Because phosphorylation levels were measured from whole cerebellar lysates and CREB is expressed in Purkinje cells and granule cells, we cannot conclude that CREB phosphorylation is altered in the Purkinje cells of the cerebellum. In fact, it is even possible that CREB phosphorylation is decreased in Purkinje cells, and could be masked by an increase in P-CREB in granule cells. This theory can be supported by the fact that CREB phosphorylation is significantly reduced in the brains of CaMKIV knockout mice (Ho et al 2000).

In addition to CREB-dependent transcription, cytoplasmic CaMKIV can activate transcription via other signalling cascades, like the MAP-kinase cascade (Soderling 1999). So it is still very likely

that the reduced phosphorylation of CaMKIV in *Mwk* mice could influence Purkinje cell transcription.

In the cytoplasm, CaMKIV is known to phosphorylate stathmin, which is a microtubule destabilising protein (Belmont et al 1996). Phosphorylation of stathmin by CaMKIV deactivates the protein and hence promotes microtubule assembly (Gradin et al 1997). Interestingly, stathmin has been shown to negatively regulate the development of Purkinje cell dendrites (Ohkawa et al 2007). Our data, however, demonstrated that there is no difference in the phosphorylation levels of stathmin throughout the different ages of *Mwk* mice. Hence, there is no reason to believe that stathmin function is abnormal in the *Mwk* mice, or that abnormalities of Purkinje cell dendrites are caused by stathmin malfunction.

It is interesting that we observe a reduction of CaMKIV phosphorylation in *Mwk* mice, as we were expecting an increase in activity of Ca^{2+} signalling molecules with increased intracellular Ca^{2+}. Also, transgenic mice over-expressing TRPC6 have an up-regulation in CaMKIV and CREB phosphorylation, which led to a more complicated dendritic structure of hippocampal neurons (Tai et al 2008). However, other factors could cause the inhibition of CaMKIV phosphorylation. For example, we identified CaMKIV to bind TRPC3 in the mass spectrometry experiment and confirmed the interaction by co-IP experiments (see Chapter 3). The interaction between CaMKIV and TRPC3 could be important for CaMKIV activation, and it is possible that TRPC3 harbouring a *Mwk* mutation causes a reduced phosphorylation of the CaMKIV kinase.

CaMKIV knockout mice display motor coordination abnormalities, altered cerebellar function with reduced number and immature development of Purkinje cells, and impaired LTD of Purkinje cells (Ahn et al 1999; Ho et al 2000; Ribar et al 2000). A reduction in CaMKIV activity has also been implicated in the inhibition of neurite outgrowth, and CaMKIV overexpression was shown to promote dendritic growth (Redmond et al 2002; Takemura et al 2009). Other studies have demonstrated that CaMKIV is critical for dendrite complexity as it is implicated in branching and

elongation of cortical neuron dendrites, but not in the formation of the primary dendrite (Nagendran & Hardy 2011). This is very similar to what we observe in the dendritic trees of *Mwk* Purkinje cells: the primary dendrite formation is not affected, whereas the dendritic branching *in vivo* is reduced and organotypic slice cultures develop smaller and less branched dendrites (Becker et al 2009). This suggests that reduction in CaMKIV activity might be responsible for the developmental abnormalities in *Mwk* Purkinje cells, as well as the onset of cerebellar ataxia.

- **CaMKII**

CaMKII is another serine/threonine kinase that is activated in response to increasing intracellular Ca^{2+} levels. CaMKII is especially abundant in the brain (Soderling & Stull 2001). In the cerebellum, CaMKII β is the predominant isoform and its expression increases significantly during cerebellar development (Burgin et al 1990; Erondu & Kennedy 1985). CaMKII has many important roles in the nervous system, including learning and memory; calcium-dependent dendritic growth; and gene expression, through phosphorylation of transcription factors, such as CREB (Tanaka 2009; Yamauchi 2005). We have identified CaMKII as a potential interaction partner of TRPC3 by mass spectrometry, however, we have not yet confirmed it by co-IP experiments (see Chapter 3).

Our studies have demonstrated that the phosphorylation levels of CaMKII do indeed change in the *Mwk* cerebella, however, the change occurs much later compared to the onset of Purkinje cell abnormalities. This is why CaMKII signalling most likely is not involved in the *Mwk* pathogenesis.

MAP kinase signalling cascade

MAP kinases, or ERK kinases, are a family of protein serine/threonine kinases that are activated in response to their phosphorylation by MEK (Ortiz et al 1995). MAP kinase signalling cascade is demonstrated in Figure 4-1. Briefly, Ca^{2+} that enters the cell through a calcium channel activates calmodulin. As well as activating the CaM kinase signalling cascade, calmodulin also activates the MAP kinase signalling cascade. Activated calmodulin causes RasGRF to convert an inactive Ras^{GDP}

to an active form Ras^{GTP}. Ras^{GTP} is able to associate with Raf, which phosphorylates MEK, that then phosphorylates ERK. Phosphorylated ERK can either directly phosphorylate transcription factors, such as Elk 1; or it can activate transcription factors indirectly through phosphorylation of other proteins, such as RSK, that phosphorylate a transcription factor CREB (Johnson & Lapadat 2002; Robinson & Cobb 1997).

MAPK signalling is important in the regulation of many physiological responses, such as cell proliferation, survival and apoptosis (Kolch 2000; Wan et al 1996). ERKs are distributed throughout the organism, but are mostly expressed in the central nervous system where they are involved in learning and memory (Boulton et al 1991; Johnson & Lapadat 2002; Ortiz et al 1995). MAP kinase signalling activation increases the formation of primary dendrites as well as dendritic branching (Ha & Redmond 2008).

Our study demonstrated that ERK phosphorylation increases from the age of P42. Therefore, the MAP kinase signalling cascade is most likely not involved in the initiation of Purkinje cell developmental abnormalities in *Mwk* mice.

NFAT signalling cascade

NFAT signalling cascade is demonstrated in Figure 4-1. Calcineurin – a calcium dependent protein phosphatase – activates NFAT transcription factors (NFATc1-c4) by dephosphorylating them and causing their translocation from the cytoplasm into the nucleus (Crabtree & Olson 2002; Nguyen & Di Giovanni 2008).

TRPC3 is known to activate the calcineurin/NFAT signalling that leads to gene transcription in heart and muscle cells (Bush et al 2006; Rosenberg et al 2004). But most importantly, recent tissue culture experiments revealed that the TRPC3 harbouring a *Mwk* mutation causes silencing of the NFAT-dependent transcription (Poteser et al 2011). Therefore, even though we were unable to demonstrate any changes in NFAT phosphorylation levels or location because of the

antibody limitations, it is still possible that the NFAT signalling cascade is responsible for the abnormal development of Purkinje cells in *Mwk* mice.

Limitations

In our work we wanted to compare phosphorylation levels of different Ca^{2+} signalling kinases among littermates, because littermates have less variability and thus makes the study more reliable. However, it is difficult to find litters with the required number and ratio of wild-type and *Mwk* mice. Therefore, in the future it would be better to age- and genotype-match mice from different litters in order to compare a sufficient number of mice ($n \geq 3$). Also, for a more accurate analysis, it would be important to quantify western blots in order to make an accurate conclusion.

Summary

Our study indicates that there are changes in the phosphorylation levels of some of the key Ca^{2+} signalling proteins, involved in the CaMK and MAPK signalling cascades. This suggests that Ca^{2+} homeostasis in *Mwk* cerebella is altered, with a likely increase in Ca^{2+} concentration due to the gain-of-function nature of the mutation. We revealed a probable early-onset Purkinje cell-specific reduction in CaMKIV phosphorylation, i.e. activity, which could be responsible for reduced dendritic branching of Purkinje cells in *Mwk* mice. Phosphorylation of CREB was increased at an early age in whole cerebellar lysates, so it is not known in which cells this change occurs. Phosphorylation levels of ERK and CaMKII were also increased, but much later in development, indicating that these signalling cascades are probably not responsible for the *Mwk* phenotype.

Ca^{2+} signalling cascades are important controls of gene transcription in neuronal cells (Clapham 2007; Greer & Greenberg 2008). Therefore, due to changes in activity of Ca^{2+} signalling cascades in *Mwk* mice, we propose that they also have alterations in gene expression in Purkinje cells of the cerebellum. Changes in gene transcription levels are common in neurological diseases and studying the changes helps elucidate the mechanism of disease pathogenesis (Bitoun et al 2009;

Crespo-Barreto et al 2010; Li et al 2010b). Microarrays that investigate the changes between wild-type and disease samples most commonly use lysates of the whole tissue, e.g. the cerebellum. But since we are only interested in the gene expression inside Purkinje cells, as this is where we observe developmental abnormalities and where TRPC3 is most highly expressed, we decided to isolate Purkinje cells from the rest of the cerebellum by laser-capture microdissection, which is described in the next chapter.

CHAPTER 5. Laser-Capture Microdissection Method Optimisation

Introduction

The *Moonwalker* (*Mwk*) mice have a mutation in the transient receptor potential canonical channel, type 3 (TRPC3), which is highly enriched in the Purkinje cells of the cerebellum, and causes their abnormal development in *Mwk* mice (Becker et al 2009). Our studies have shown alterations in activity of major players in the Ca^{2+} signalling cascades in the *Mwk* mice, which likely lead to changes in gene expression (see Chapter 4). To investigate the potential gene changes caused by the *Mwk* mutation, we decided to perform a microarray analysis.

Despite the cerebellum constituting only 10% of the brain, it contains 80% of the total neurons, which primarily consist of two types: granule neurons, which are the major neuronal cell type of the cerebellum and the brain, and Purkinje neurons, comprising less than 1% of cerebellar neurons (Goldowitz & Hamre 1998). The cerebellum also contains basket, stellate and Golgi cells. For the microarray experiment, it was crucial to separate Purkinje cells from other cell types in the cerebellum, such as the granule cells, due to the high expression of TRPC3 in these cells (Hartmann et al 2008), and the fact that the *Mwk* mutation only causes abnormalities in the Purkinje cells of the cerebellum.

There are two main methods used to separate specific cell types from a mixed population: fluorescence activated cell sorting (FACS) and laser-capture microdissection (LCM). FACS is a system of sorting fluorescently labelled cells from a heterogeneous suspension. Cells are passed through a focused laser beam and fluorescent cells are detected and are separated from the rest of the suspension (Parks & Herzenberg 1984). This method is limited by the requirement of a fluorescent signal, either by the expression of a fluorescently-labelled fusion protein, such as a

green fluorescent protein (GFP), in the desired cell type, or by using a fluorescently-labelled antibody, specific for the protein of interest. Unless working with an animal line that specifically expresses a cell-specific fluorescent marker, the former is not possible. In addition, work previously done in our laboratory to enrich for GFP-expressing Purkinje cells from the cerebellum has shown this approach to be problematic. Labelling cells for the presence of a protein of interest using antibodies is limited by the availability of specific, high affinity antibodies. LCM, on the other hand, has been extensively used by our group for a very similar project with great success (Bitoun et al 2009), therefore, we decided to use LCM in order to isolate Purkinje cells from the rest of the cerebellum. LCM is a technique that enables isolation of pure subpopulation of cells identifiable by optical microscopy from heterogeneous tissues to avoid contamination with other cell types. Cells isolated by LCM are used to analyse cell specific gene expression. Also, LCM has been used to identify different cell types within a population of cells on the basis of their gene expression patterns (Kamme et al 2003). LCM has even been used for proteomic analysis (Banks et al 1999).

The LCM technique was first developed and described in 1995 at the National Institute of Health (EmmertBuck et al 1996). It was proposed as a fast and reliable method with a much higher throughput in cell collection, and an improved alternative to other cell isolation techniques, such as destruction of unwanted tissue by UV radiation, while protecting the area of interest (Shibata et al 1992); and microdissection with manual tools, such as a needle or an ultrafine pipette tip to scrape off the area of interest (Going & Lamb 1996; Zhuang et al 1995). Those methods required very skilled operators, were very time-consuming, labour-intensive and not always reliable (EmmertBuck et al 1996; Simone et al 1998). The system proposed by Emmert-Buck et al used a thin layer of transparent film placed on top of the tissue, the slide with the tissue was directly visualised using a microscope and the cells were selectively adhered to the film using a pulse from an infra-red laser (EmmertBuck et al 1996). In 1996 it was made into a commercial instrument in collaboration with Arcturus Engineering Inc. (Bonner et al 1997).

An improved method described in 1998 by Schutze and Lahr allowed isolation of cells of any shape and size and used the laser to cut, as well as catapult, the cells into a tube cap, something they called LPC, or laser pressure catapulting (Schutze & Lahr 1998). Our current LCM protocol is based on this method. Figure 5-1 demonstrates a typical set-up of the LCM machine.

Figure 5-1. A set-up of a typical LCM machine. The image of the section under the microscope is visualised on the computer under a 40X magnification. The cells of interest are manually selected using a drawing tool. The laser, located underneath the slide, cuts out the selected cells and catapults them into a cap of an Eppendorf tube located right above the section.

The success of reliably purifying specific cell types lies on the ability of the user to recognise them under the microscope. Lack of a coverslip makes it more difficult to differentiate between cells as they show reduced cellular detail (Fend et al 1999; Goldsworthy et al 1999; Simone et al 1998). Many cells can be identified with a simple Nissl stain; however, some cell types do not have an easily distinguishable architecture compared to their neighbours. In the cerebellum, Purkinje cells are much bigger in size compared to their neighbouring granule cells and their location is easily identified as they are located just outside the very densely stained granule cell layer. Figure 5-2[A] shows a section of the cerebellum stained with cresyl violet, where Purkinje cells (PC) are identified as large nuclei compared to the small dense granule cells (GC). The Purkinje cells are selected manually (Figure 5-2[B]), and laser-capture microdissected into a tube, leaving empty space on the slide (Figure 5-2[C]). It is also possible to rapidly stain cryosections with an antibody

before performing LCM, which, depending on the antibody, would lead to a more obvious staining of the desired cell type (Fend et al 1999). This method should be kept in mind if the staining of the cerebellum by Nissl stain does not produce a section with easily identifiable cells.

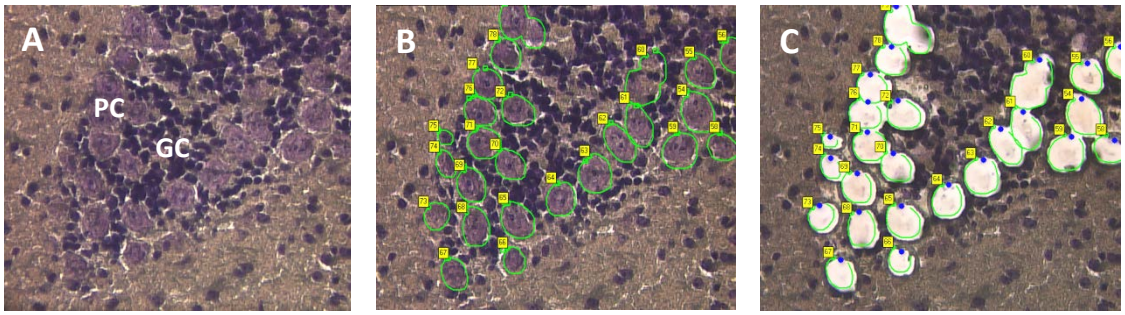

Figure 5-2. Section of the cerebellum stained with cresyl violet and used for laser-capture microdissection. A – section of the cerebellum stained with cresyl violet under 40X magnification. Purkinje cells (PC) and granule cells (GC) can be clearly distinguished. B – Purkinje cells are identified and are selected using a drawing tool. C – the selected cells are cut by the laser and catapulted into a tube, leaving empty space on the slide. These images were kindly provided by Dr Emmanuelle Bitoun.

It is widely known that successful microarray and qRT-PCR experiments depend on good RNA quality (Bustin 2002; Fleige & Pfaffl 2006). Poor RNA quality can make the downstream applications inaccurate. Previously it was very difficult to check the RNA quality of valuable samples due to their limited availability. It has now become possible due to the development of a method of capillary gel electrophoresis, which uses very small quantities of the sample and is sensitive enough to detect picograms of RNA (Perez-Novo et al 2005). RNA quality is represented as an RNA Integrity Number (RIN). RIN ranges from 1 to 10, where 1 is poor RNA quality and 10 is intact RNA.

RIN number is determined from the shape of the curve in the electropherogram (Fleige & Pfaffl 2006). An example of an electropherogram of a very good quality RNA sample is shown in Figure 5-3, where 18S and 28S ribosomal RNA peaks are clearly visible and there is no baseline noise. For high quality RNA it is thought that 28S RNA peak area should be twice the size of the 18S RNA peak area, however, in practise this ratio is hard to achieve (Fleige & Pfaffl 2006). In our

experiments, the quality and RNA integrity was assessed on an Agilent BioAnalyzer, using the RNA 6000 Pico Assay.

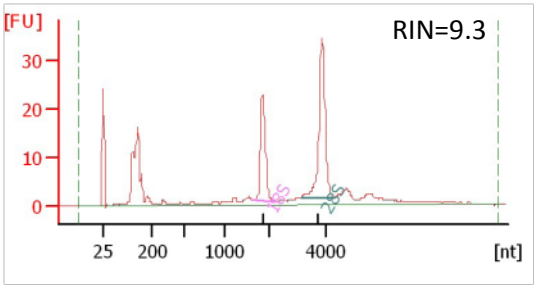

Figure 5-3. Example of an electropherogram showing very good quality RNA, with RIN = 9.3. The 18S and 28S ribosomal RNA peaks are distinctly visible and there is no baseline noise. This electropherogram was provided by Sheena Lee.

When comparing two different sets of samples (in our case wild-type vs. *Mwk*), it is very important to do everything concurrently: the samples need to be collected at a similar time, within the same length of time, also they need to be analysed at the same time. RNase-free conditions are extremely important when collecting RNA. Unfortunately RNA is not protected from degradation even at low temperatures and it is very sensitive to degradation during the processes of tissue handling and storage (Holland et al 2003; Perez-Novo et al 2005). It was therefore imperative to ensure the highest possible quality of isolated RNA was prepared for the microarray analysis.

This chapter describes different methods that were tested in order to maximise the quality of the RNA of the laser-capture microdissected Purkinje cells.

Results

Standard Method

In our group, the LCM technique was optimised by Dr Emmanuelle Bitoun, and it was used for a microarray study of Purkinje cell gene expression of an ataxic mouse model (Bitoun et al 2009). Although the microarray data was validated for these studies (confirmed by qRT-PCR), the RNA quality was poor (RIN≈3, data not shown). For reliable microarray results, RNA quality is very important and, therefore our goal was to optimise the LCM method to obtain high quality RNA from microdissected Purkinje cells. Figure 5-4 shows a schematic diagram of the tissue preparation method for LCM, used by Bitoun et al 2009, and which was the starting point for optimisation and referred to herein as the "**Standard Method**". Briefly, a 10 µm section of freshly frozen cerebellum was cut on a cryostat and placed on a special membrane coated slide. It was then fixed and hydrated in a series of ethanol dilutions (95%, 75%, 50% ethanol), stained with 1% cresyl violet (dissolved in water), washed in a series of ethanol dilutions (50%, 75%, 95% ethanol), dehydrated twice in 100% ethanol and twice in xylene. The slide was left to air dry briefly before proceeding with LCM. During LCM, the cerebellar sections were visualised through a microscope, Purkinje cells were identified by drawing around them using the Robo software (Carl Zeiss), and the cells were subsequently cut using the P.A.L.M Micro Beam system and catapulted into a tube cap containing RLT lysis buffer (QIAGEN). The whole procedure, including slide preparation and LCM, was limited to approximately 1.5 hours in order to avoid unnecessary RNA degradation.

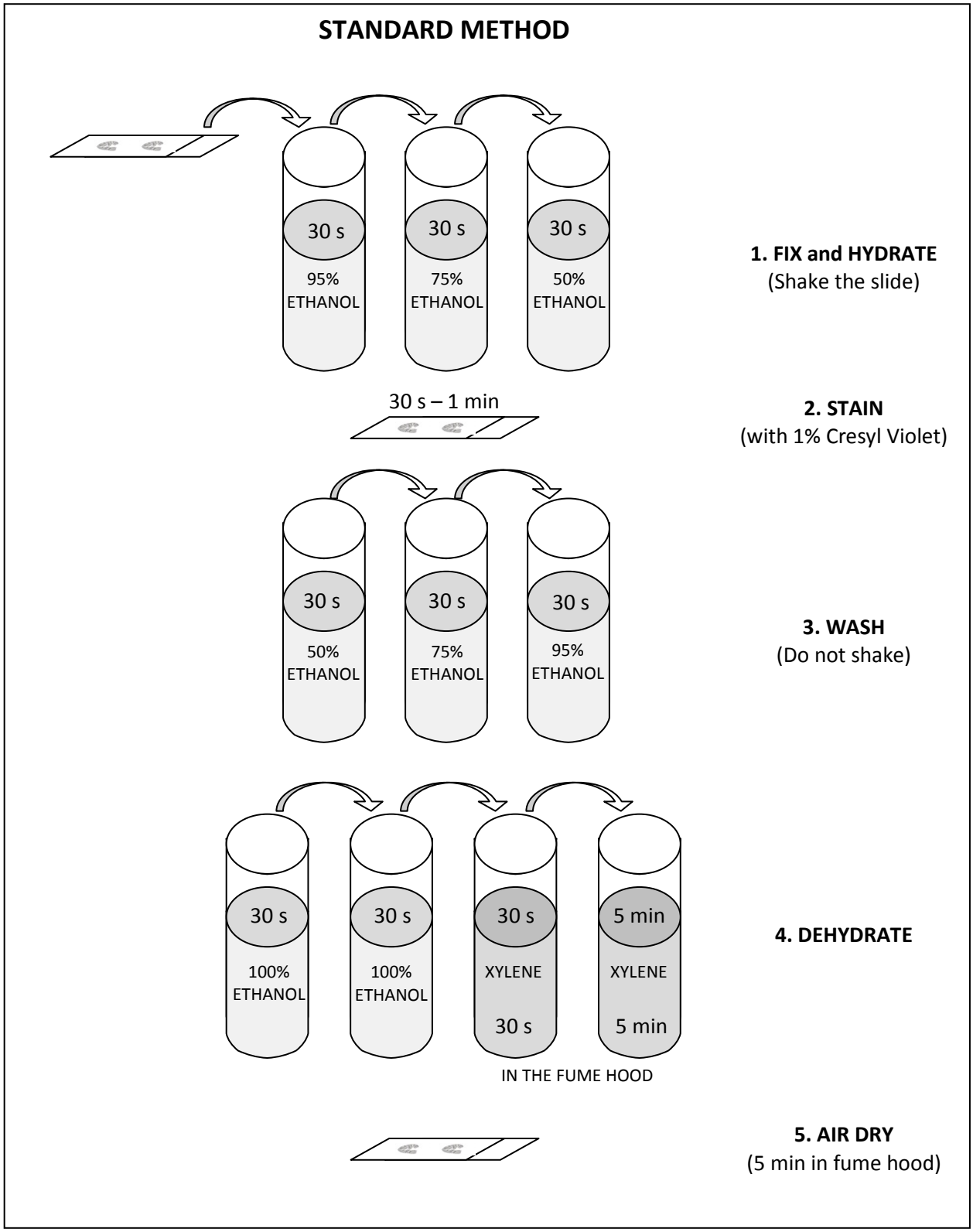

Figure 5-4. Standard Method of slide preparation for LCM (Bitoun *et al* 2009). This method has been used previously in our group producing good microarray data, however the RNA quality was poor.

RNA quality was determined at each step of the procedure to investigate when the degeneration was greatest. The controls that were used during optimisation are summarised in Table 5-1. First of all, the RNA quality of the starting material (freshly frozen cerebellum) had to be tested. This was done by placing a 10 µm cerebellar section on a slide, immediately lysing it in RLT lysis buffer and storing at -80°C until further analysis. This control was labelled **C1**. Second control was to test for the slide preparation procedure and for the time spent at room temperature: the section was prepared and stained exactly the same way as it would be for LCM, and it was left at room temperature for as long as the microdissection would take place (in total 1.5 hours), it was then lysed in RLT lysis buffer. This control was labelled **C2**. The last control was to check RNA quality of the section post-LCM, in other words, the section was lysed in RLT lysis buffer once Purkinje cells have been microdissected from it. This is an important control because it is possible that a small amount of RNA from Purkinje cells is more prone to degradation than the whole section. This control was labelled **C3**. The sample (microdissected Purkinje cells catapulted into a tube cap containing RLT lysis buffer) was labelled **S**. For the purposes of LCM optimisation, 500 Purkinje cells were collected for RNA quality analysis.

Table 5-1. A table explaining controls that were used during optimisation of the LCM technique.

Abbreviation	Description
C1	Control for the quality of the fresh frozen section: the section is cut on the cryostat, followed by immediate lysis of the section.
C2	Control for the slide preparation procedure and time spent at room temperature: the section is prepared exactly the same way as it would be for the LCM and stays at room temperature for as long as the LCM process would take, but it is not subject to microdissection.
C3	Control for the microdissection procedure: a post-LCM section from which Purkinje cells were microdissected is lysed.
S	Sample of Purkinje cells which have been microdissected from C3.

When using the Standard Method for LCM, the quality of the starting material (fresh frozen cerebellum) was very good: RIN (C1) = 7.7 (see Figure 5-5). The preparation of the tissue (fixing, staining, washing, dehydration) and the time spent at room temperature did not affect the quality of the RNA, it remained very high: RIN (C2) = 8.2. When looking at the quality of the RNA of the section post-LCM, a significant difference was noticeable: the RNA became degraded with RIN (C3) = 3.8. The poor quality of RNA was also noticeable from the profile of the electropherogram: a lot of baseline noise was observable and the 18S and 28S rRNA peaks were less distinguishable. It was not, therefore, surprising that the RNA of the microdissected Purkinje cells was severely degraded: RIN (S) = 2.5, where the rRNA peaks were barely visible. The fact that not only the microdissected cells, but also the whole section from which those cells were dissected, had degraded RNA means that a large number of cells (C3) are as susceptible to RNA degradation as individual cells (S) during LCM. Also, to rule out RNA degradation as a consequence of light or heat exposure from the microscope, we tried switching the microscope lamp off during laser cutting and room temperature was maintained with an air conditioner. The RNA quality of the

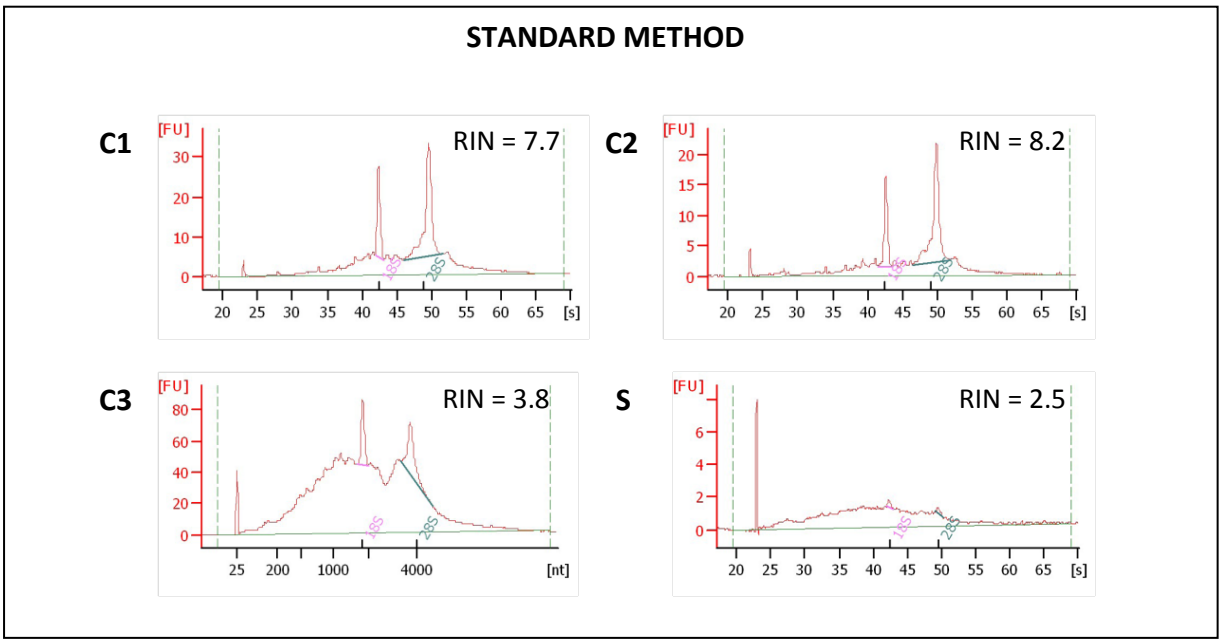

Figure 5-5. RNA quality of the sample (S) is poor when using the Standard Method of slide preparation for LCM. RNA quality of the tissue is very good (C1) and it does not change after the slide preparation procedure (C2). The standard method shows degradation of RNA during LCM (C3 & S).

samples (S) or the C3 control was unaffected by these changes and remained poor (data not shown).

It is important to note, that the RNA quality of dissected cells was reduced when adding a communal lab stock of β-mercaptoethanol to the RLT lysis buffer. This signifies the importance of separating reagents used for LCM from all other use, because RNase-free conditions are essential for RNA work.

RNase inhibitors are widely used when handling RNA. Therefore we decided to include an RNase inhibitor in the RLT lysis buffer, while using the Standard Method of tissue preparation. This way the catapulted microdissected cells can be kept in RNase-free conditions while performing LCM and during sample storage. RNA integrity of samples with (+) and without (-) RNase inhibitor in the lysis buffer are compared in Figure 5-6. Both methods had a good starting material: RIN (C1+) = 8, RIN (C1-) = 7.2. A C2 control was not performed, as from the Standard Method results it was concluded that C2 RNA samples are not affected by degradation. Post-LCM controls showed a significant degree of RNA degradation, independent of whether the RNase inhibitor was added to the lysis buffer or not: RIN (C3+) = 3.1, RIN (C3-) = 2.9. Consequently, RNA of the microdissected samples was of very poor quality: RIN (S+) = 2.5, RIN (S-) = 2.5. This result indicates that RNA in the microdissected cells could be degraded prior to microdissection, perhaps during sample preparation.

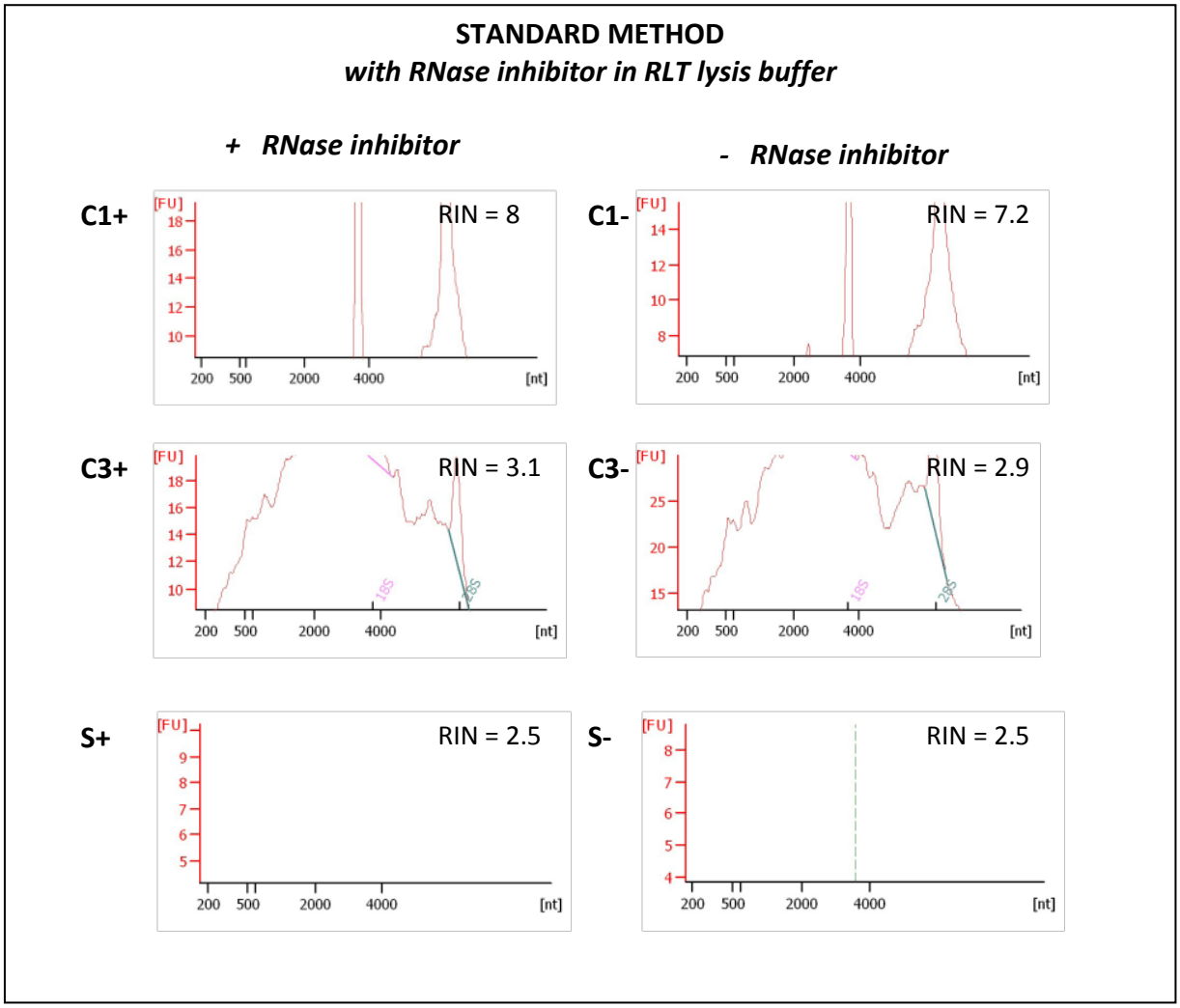

Figure 5-6. Addition of the RNase inhibitor to the RLT lysis buffer when using the Standard Method of section preparation does not improve the quality of the RNA. RNA quality of the starting tissue (C1+ & C1-) is very good. Degradation of RNA during LCM occurs even in the presence of the RNase inhibitor in the lysis buffer (C3+, C3- & S+, S-). The electropherograms show a zoomed rRNA graph which cannot be changed.

Low Water Method

Clement-Ziza et al published a paper describing an alternative staining method which uses less water in the section preparation procedure (Clement-Ziza et al 2008), because it is believed that water causes endogenous RNase activity (Fend et al 1999). This "**Low Water Method**" was assessed by us on Purkinje cell microdissection. Compared to the Standard method, the Low Water Method, as shown in Figure 5-7, uses only 95% ethanol dilution when fixing, hydrating and washing the tissue section. Also, 1% cresyl violet is dissolved in 75% ethanol rather than in water, which reduced the solubility of the dye. RNA quality of the starting material, and of the section which had undergone LCM preparation, were very high: RIN (C1) = 8.1, RIN (C2) = 7.9 (see Figure 5-8). Preparation of samples using the Low Water Method reduced RNA degradation of the post-LCM sections: RIN (C3) = 6.3. However, it is still lower than RNA quality of the starting material and the stained tissue (C1 & C2) which indicates that the Low Water Method does not fully protect the sample from endogenous RNA activation. The RNA quality of the sample was noticeably less than that of C3, but it showed a considerable improvement compared to the standard method: RIN (S) = 4.6. It is clear from the results that this method still needs improvement and that perhaps small amount of water in the 95% ethanol still influences endogenous RNases.

Changing the section preparation procedure had a very positive effect on the quality of the RNA. Therefore, a successful LCM is greatly dependant on the tissue processing method. To further improve sample preparation, we assessed a commercially available staining kit (LCM Staining Kit – Ambion). However, the provided cresyl violet stain completely failed to stain the cerebellum and no further analysis could be done.

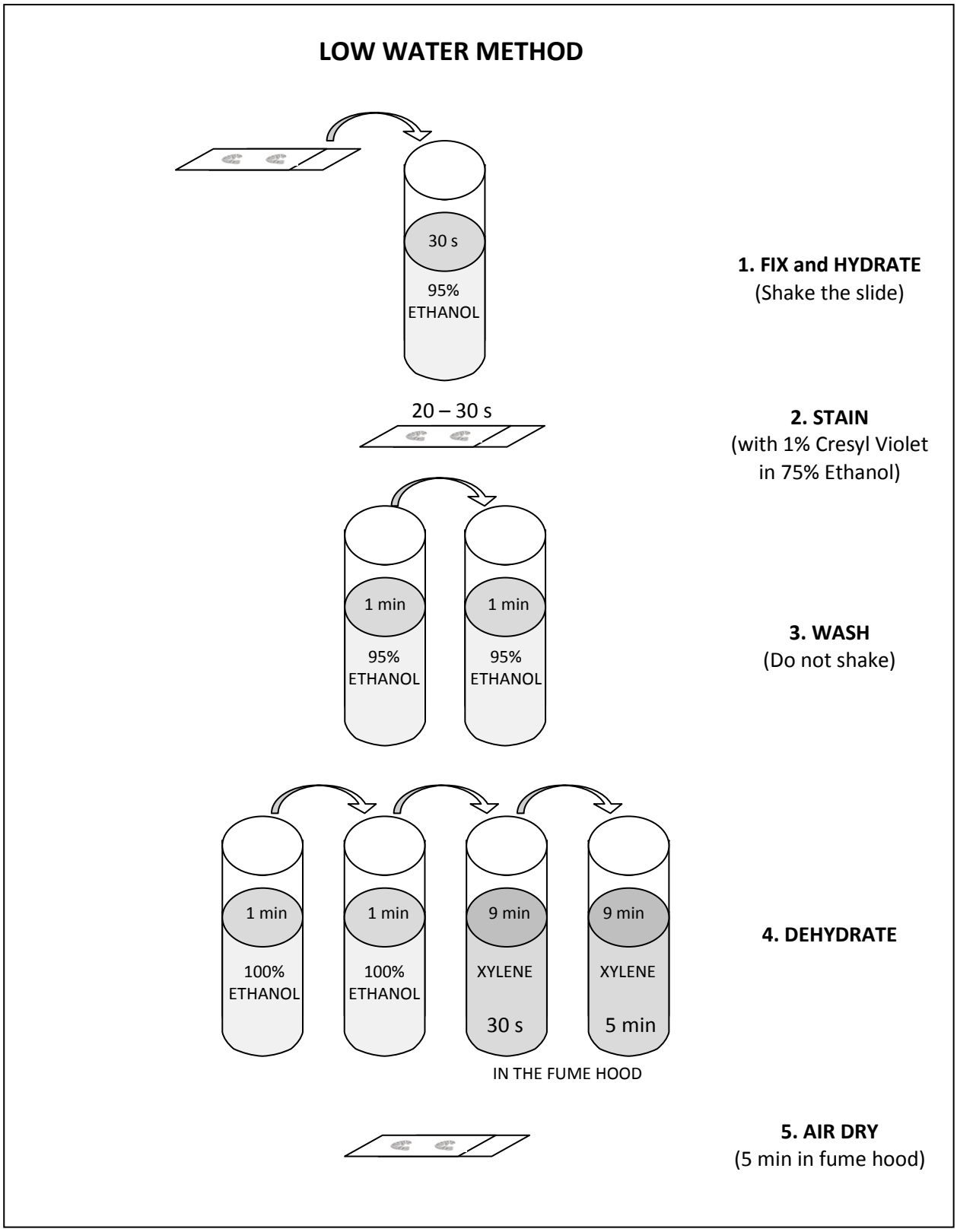

Figure 5-7. Low Water Method for slide preparation for LCM (Clement-Ziza *et al* 2008). This method minimises the use of water in the fixation, hydration, staining and washing steps to avoid activation of endogenous RNases in the sample.

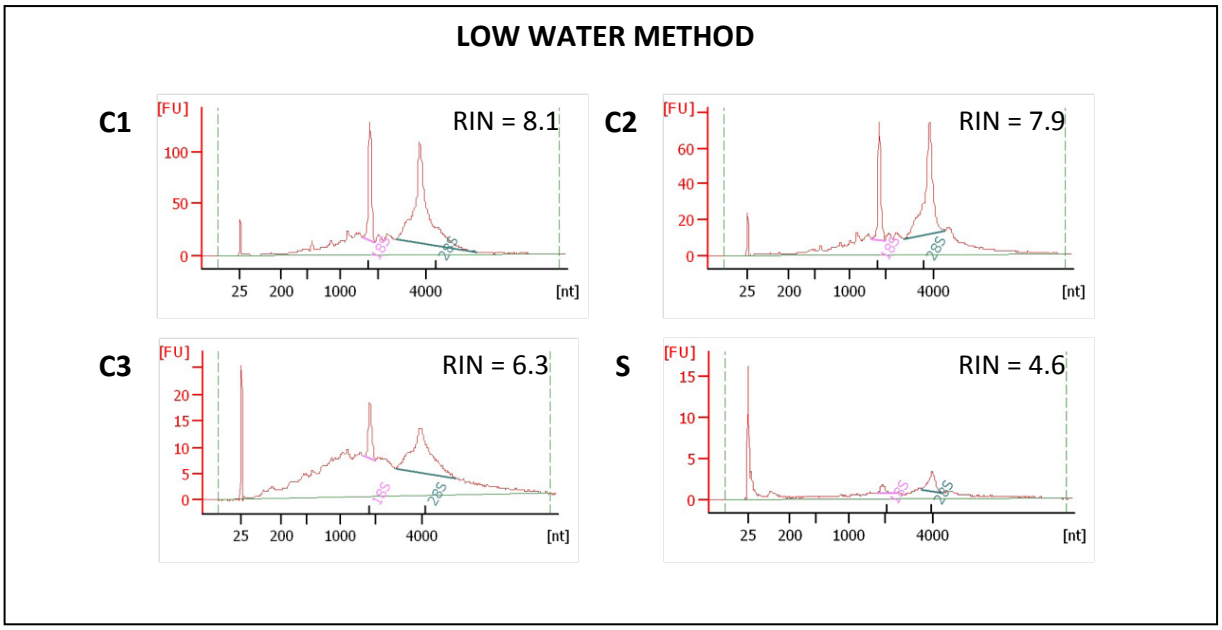

Figure 5-8. RNA quality of the sample is satisfactory when using the Low Water Method of slide preparation for LCM. RNA quality of the tissue is very good (C1) and it stays high after the slide preparation procedure (C2). There is a slight decrease is RNA quality after the tissue has been subjected to LCM (C3). The RNA quality of microdissected cells (S) is lower than that of C3, but is of satisfactory quality for the microarray experiment.

RNase Inhibitor Method

Although addition of the RNase inhibitor to the lysis buffer did not protect the samples from RNA degradation, it is possible that it would be beneficial to add RNase inhibitor to solutions involved in tissue preparation prior to LCM, since this seems to be very important for improving RNA integrity. However, the use of an RNase inhibitor during section processing is impractical due to the high costs of the inhibitors and the large volumes of fixing, hydrating and washing solutions. One affordable RNase inhibitor is available (Sigma), however its red/brown colour interfered with the cresyl violet staining of the cerebellum when added to all solutions involved in section preparation for LCM (data collected by Dr Emmanuelle Bitoun during Standard Method optimisation). But I hypothesised that the RNase inhibitor only needs to be added to the solutions containing water, because water is thought to activate RNases in the samples. Figure 5-9 shows a schematic diagram of the "**RNase Inhibitor Method**". The coloured Sigma RNase inhibitor is only added to 50%, 75% and 95% ethanol dilutions, but not to 100% Ethanol or Xylene. Initially, RNase inhibitor was also added to the 1% cresyl violet stain, but occasionally this prevented staining of the cerebellar sections due to cresyl violet aggregation in the stain. Ever since this was discovered, the RNase inhibitor was not added to the stain, which did not affect the quality of the sample RNA (data not shown). An additional 100% ethanol washing step could be added if removal of excess stain is required. Figure 5-10 shows that the starting material (cerebellum) was of very high RNA quality: RIN (C1) = 8.1. Tissue preparation method did not affect the RNA: RIN (C2) = 8.5. When adding the RNase inhibitor to ethanol dilutions, post-LCM section had a very slight decrease in quality, while still remaining very high: RIN (C3) = 7.5. The microdissected sample quality was also unaffected: RIN (S) = 7.6. This method proved to be the most effective, with RNA integrity of microdissected cells being very high, and only slightly decreasing compared to the initial RNA integrity of the cerebellar section.

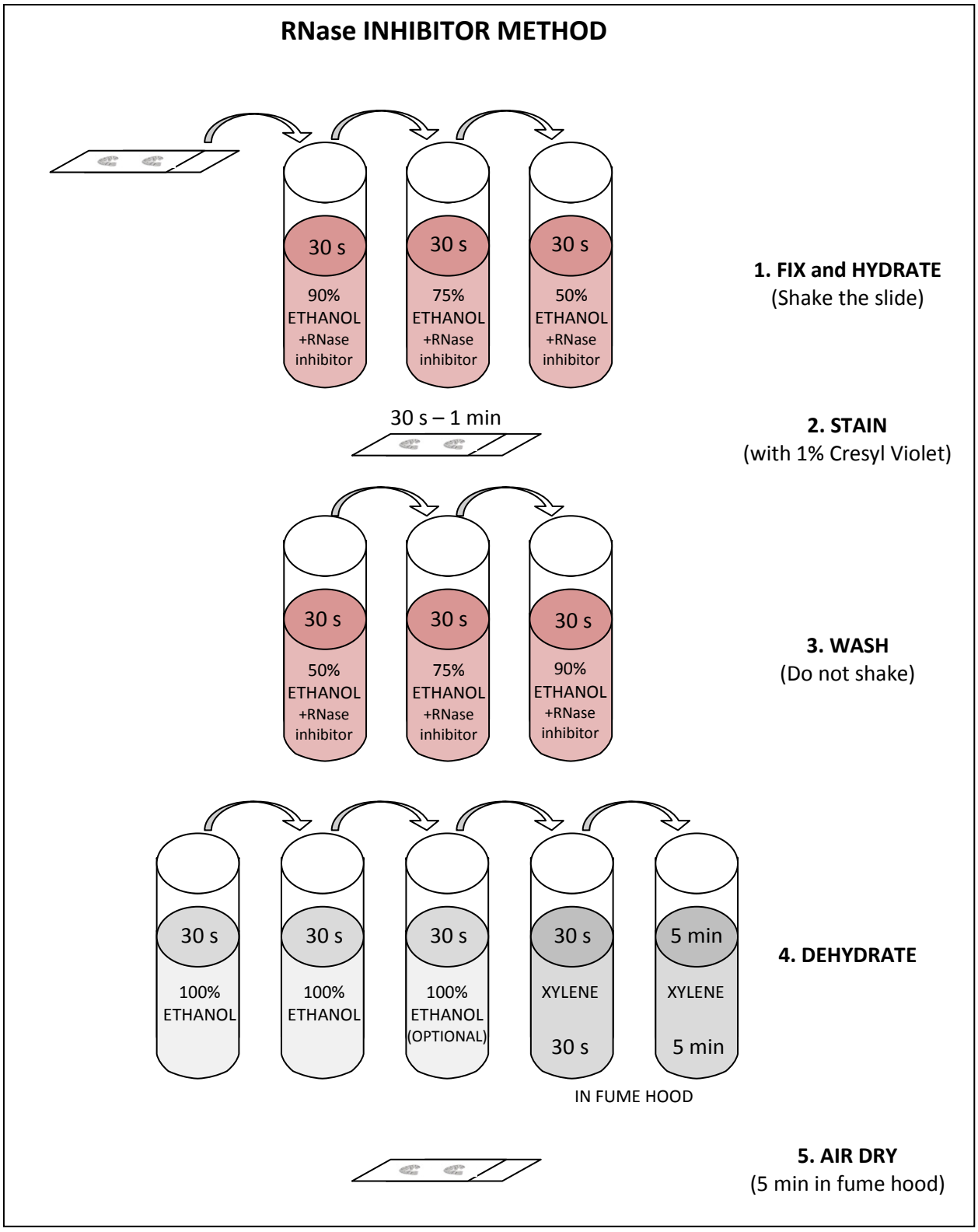

Figure 5-9. RNase Inhibitor Method for slide preparation for LCM. In this method RNase inhibitor (Sigma, red in colour) is added to 50%, 75% and 90% ethanol dilutions to avoid activation of endogenous RNases in the sample due to the presence of water.

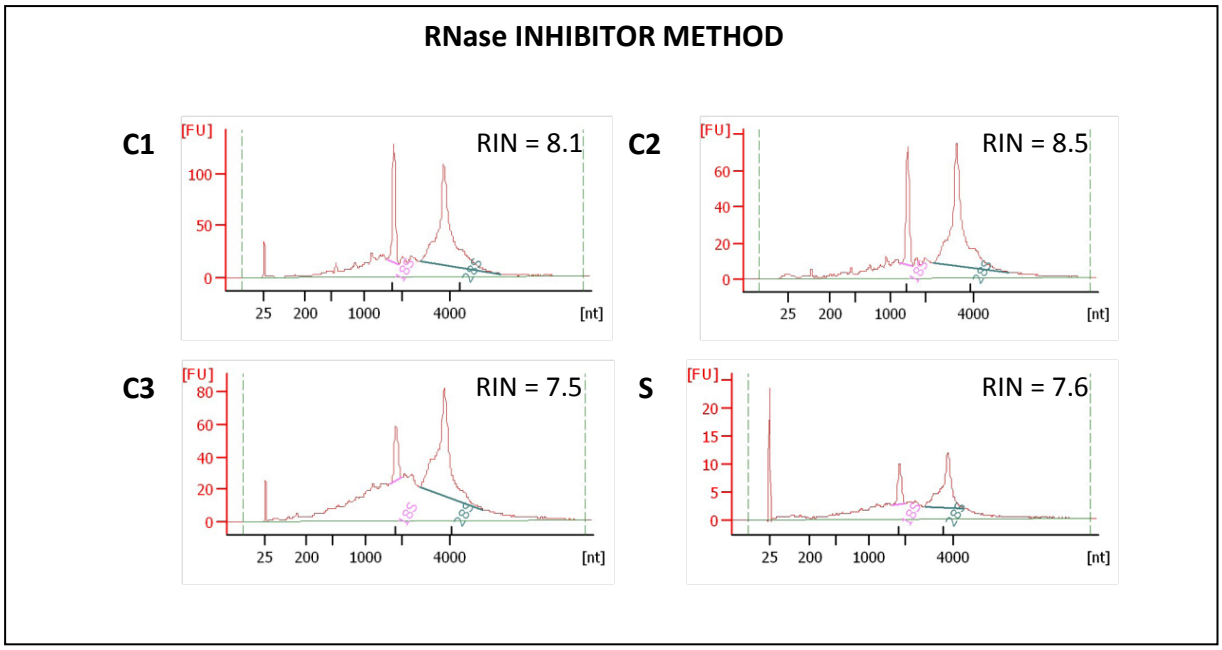

Figure 5-10. RNA quality of the sample is high when using the RNase Inhibitor Method for slide preparation for LCM. RNA quality of the tissue is very good (C1) and it stays high after the slide preparation procedure (C2). The RNA quality of the tissue practically does not change after microdissection (C3) and RNA quality of laser-captured Purkinje cells (S) remains high. Addition of RNase inhibitor to water containing ethanol dilutions stops activation of endogenous RNases in the sample. Sample S contains 500 microdissected Purkinje cells.

To investigate whether the RNA quality of the sample could be improved by combining the Low Water Method with the RNase Inhibitor Method, the two protocols were combined. However, staining of the cerebellar sections was too intense due to the presence of the coloured RNase inhibitor and the lack of destaining steps, and Purkinje cells could not be distinguished from other cell types (data not shown).

The above optimisation procedures resulted in the isolation of high quality of RNA. Therefore, to isolate Purkinje cell RNA for the microarray analysis, as well as for further validation by qRT-PCR, the RNase Inhibitor Method was selected. Table 5-2 displays RIN numbers and electropherograms of the samples used in the microarray experiment, with the lowest RIN = 6.2. Occasionally the BioAnalyzer failed to determine the RIN number. Therefore, their electropherograms were compared to those of samples with high RIN numbers to assess the quality. Electropherograms of samples used in the microarray experiments were all similar.

Table 5-2. Laser-capture microdissected Purkinje cells (P18) for the microarray. Two litters of mice were sacrificed at P18 (M17 & M18). Two wild-type (WT) and two *Mwk* mice were chosen from each litter and each genotype had a male and a female. RNA Integrity Number of the samples for the microarray experiment was above 6.2. For some samples the BioAnalyzer did not determine the RIN number, however, the electropherogram showed a similar 18S/28S pattern to the other samples.

Sample	Sex	Litter	RIN	Electropherogram
WT1	F	M17	6.9	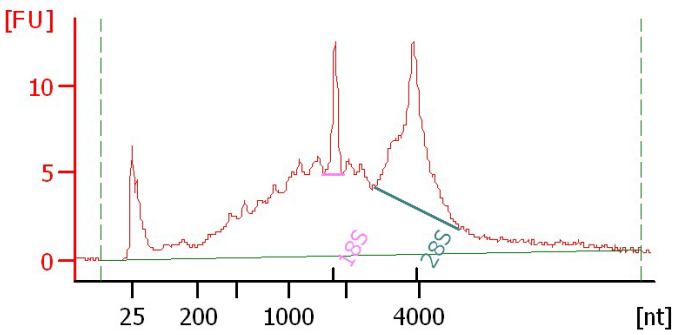
WT2	M	M17	6.6	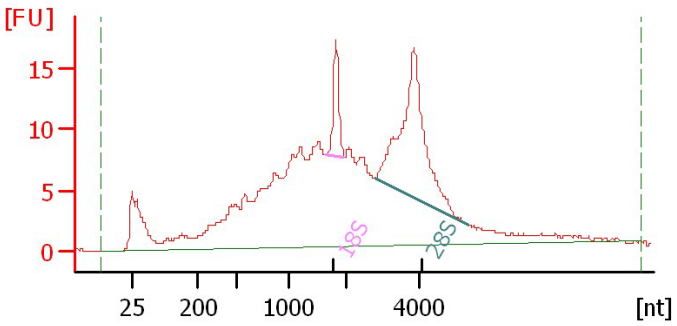
WT3	F	M18	7.5	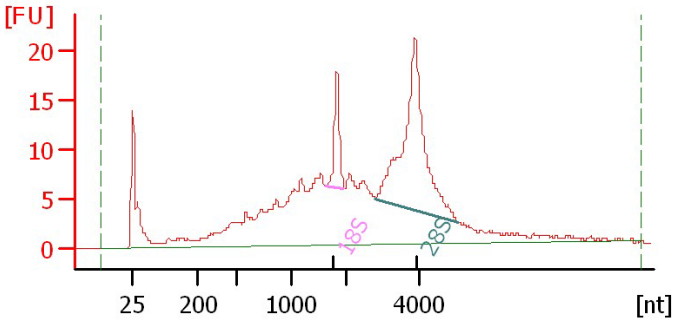
WT4	M	M18	6.9	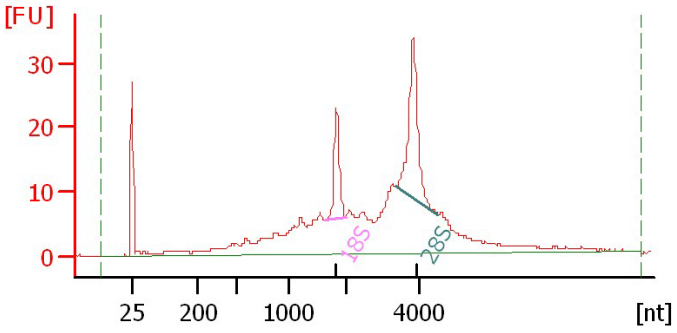

Sample	Sex	Litter	RIN	Electropherogram
Mwk1	F	M17	-	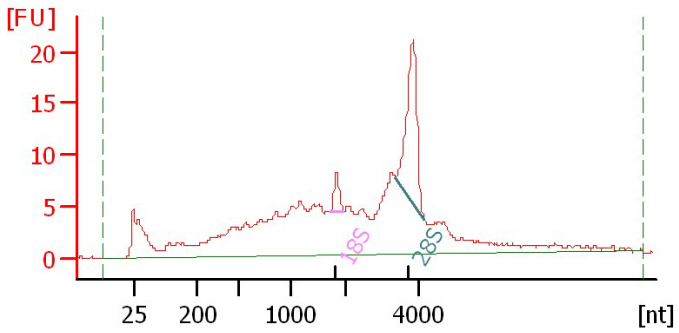
Mwk2	M	M17	-	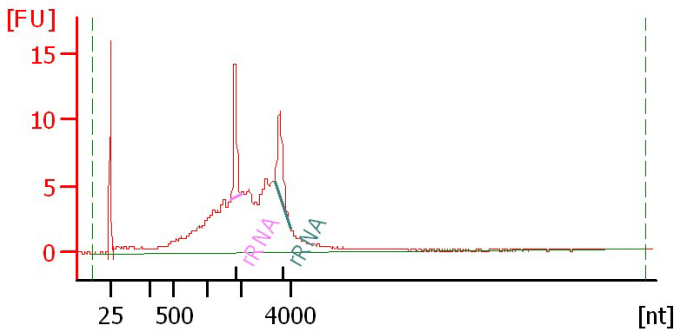
Mwk3	F	M18	-	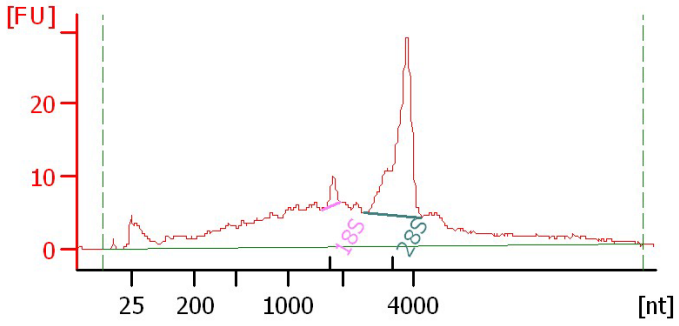
Mwk4	M	M18	6.2	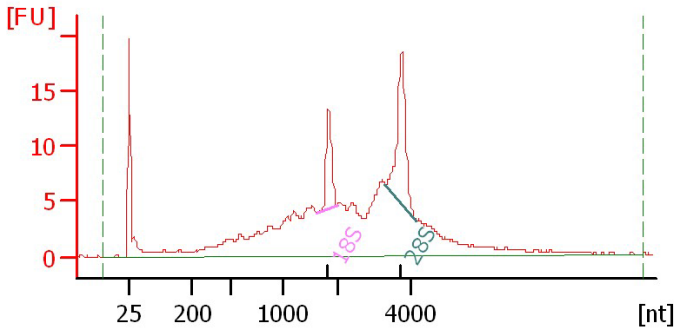

Discussion

Ca^{2+} signalling cascades are affected in the cerebella of *Mwk* mice, with reduced or increased activation of some of its key members (see Chapter 4). Ca^{2+} signalling plays an important role in initiation of cell transcription (Greer & Greenberg 2008), and changes in activity of key Ca^{2+} signalling proteins in *Mwk* mice would therefore likely lead to abnormalities in gene expression. For our study it was important to use LCM in order to isolate Purkinje cells of the cerebellum, because the *Mwk* mutation only affects the development of these cells in the cerebellum. Any other cell type in the sample would invalidate the changes caused by the *Mwk* mutation.

Reliable gene expression studies are dependent upon good quality RNA samples, because RNA of poor quality could compromise the accuracy of the results. Extracting RNA from whole tissues does not pose a problem for the RNA quality if standard RNase-free conditions are fulfilled. However, if the LCM technique is involved to isolate a specific cell population, the RNA of the microdissected cells is often degraded (Clement-Ziza et al 2008).

We have optimised a method of LCM that yields RNA of good quality, which can be used for further analysis by microarray or qRT-PCR. High RNA Integrity Numbers (RIN) were attained by adding RNase inhibitor to all water containing ethanol dilutions, which prevented the activation of endogenous RNases in the sample by water. This method gives consistent and reliable results, with RIN numbers averaging ~7.

It is, however, important to note that LCM together with the downstream experiments have to be performed quickly, as sample storage time can reduce RNA quality and compromise further analysis results.

One paper, which has been discovered during the course of this study, also uses the RNase inhibitor in the tissue preparation solutions, which results in good quality RNA after LCM (Kube et

al 2007). But they report that RNA quality declines due to the staining procedure, whereas we found that the staining of the tissues alone does not affect the quality of the RNA. Also, they report that they included the RNase inhibitor in all staining solutions. Previous studies in our group by Dr Emmanuelle Bitoun showed that adding the coloured RNase inhibitor to all solutions alters the staining of the tissue and makes it impossible to distinguish Purkinje cells from other cell types in the cerebellum. Optimisation of the LCM protocol in this chapter demonstrates that staining is improved when the RNase inhibitor is only added to water containing ethanol dilutions, and not to the 100% ethanol or xylene. Moreover, Kube et al did not use the RIN number to assess RNA quality, which is currently a standard method for measuring RNA quality, as they found the RIN numbers to vary significantly (Kube et al 2007). They developed their own method for determining RNA quality by measuring the ratio between an amplified 3' and 5' regions of the gene, where a higher number indicates more degradation, as there is less amplification of the 5' end. In our study, however, we found that the RIN numbers were consistent and therefore are a reliable tool for determining RNA quality.

Summary

To summarise, we have achieved an easy and reliable LCM protocol, which produces good quality RNA from laser-capture microdissected cells, averaging RIN~7. This is achieved when an RNase inhibitor is added to all water containing ethanol dilutions that are used during the tissue staining process. The RNA integrity values measured by the BioAnalyzer are consistent.

CHAPTER 6. Microarray Analysis of Purkinje Cell Gene Expression in *Moonwalker* Mice

Introduction

The *Moonwalker* (*Mwk*) mouse is a mouse model of cerebellar ataxia, with a point mutation in the transient receptor potential canonical channel, type 3 (TRPC3). TRPC3 channel is enriched in the Purkinje cells of the cerebellum, which show growth and differentiation abnormalities from 3 weeks of age in *Mwk* mice (Becker et al 2009). Because TRPC3 channel is permeable to positively charged ions upon activation and the *Mwk* mutation causes it to be more sensitive to stimulation, we believe that there is an increased Ca^{2+} influx into the Purkinje cells of the *Mwk* mice. Moreover, in Chapter 4 I demonstrated alterations in activity levels of key Ca^{2+} signalling proteins, which confirms changes in Ca^{2+} homeostasis in *Mwk* cerebella.

Ca^{2+} influx into a cell sets off a cascade of events that regulate gene expression, controlling various aspects of neuronal development, such as dendritogenesis and neuronal survival (Berridge 1998; Clapham 2007; Greer & Greenberg 2008; Zieg et al 2008). For instance, one of the pathways activated by calcium in neurons is the Ca^{2+}/calmodulin (CaM) kinase signalling pathway, and calcium-induced dendritic growth is inhibited by CaMK inhibitors (Redmond et al 2002). CaMKII and CaMKIV are known to phosphorylate transcription factors, such as CREB, which leads to Ca^{2+}-dependent activation of genes important for dendrite formation, synaptic plasticity and function (Lonze & Ginty 2002). Deletion of the *Camk4* gene in mice causes cerebellar ataxia, impaired CREB-dependent gene expression, and leads to decreased number of Purkinje cells and their immature morphological characteristics (Ho et al 2000; Ribar et al 2000). Our studies have demonstrated that CaMKIV, CaMKII and CREB are all deregulated in the cerebella of *Mwk* mice

(Chapter 4). Another pathway regulated by Ca^{2+} is the calcineurin-NFAT signalling pathway, which has been shown to be regulated by TRPC3: the up-regulation of TRPC3 expression leads to the activation of the calcineurin-NFAT signalling pathway and stimulates the NFAT-dependent gene transcription in cardiac myocytes (Bush et al 2006; Nakayama et al 2006). Moreover, the *Mwk* mutation has been shown to lead to silencing of the NFAT-dependent gene transcription in a cardiac muscle cell line (Poteser et al 2011). This information lead us to hypothesise that there are transcriptional changes in Purkinje cells of the *Mwk* mice due to abnormal Ca^{2+} signalling.

To test the involvement of transcriptional dysregulation in the abnormal development and malfunction of Purkinje cells induced by the *Mwk* TRPC3 channel, we decided to perform a microarray experiment, which permits analysis of several thousand genes in a single sample. Purkinje cells were separated from other cell types in the cerebellum by laser-capture microdissection (LCM), as described in Chapter 5.

Other studies investigating mutations that lead to cerebellar ataxia and abnormal Purkinje cell development have also used a microarray approach in combination with LCM in order to elucidate the mechanisms of abnormal neuronal development. For example, a microarray analysis was performed on the Purkinje cells of a *robotic* mouse model of cerebellar ataxia, which has a missense mutation in the *Af4* transcription factor gene (Isaacs et al 2003). The experiment revealed down-regulation of the *Igf-1* gene and reported that AF4 is a negative transcriptional regulator of the IGF-1 signalling pathway, and its deregulation leads to Purkinje cell death (Bitoun et al 2009). Microarray studies on the *Purkinje cell degeneration* mouse model of cerebellar ataxia, that has a mutation in the *Nna1* gene and displays abnormal development of Purkinje cell dendrites, revealed an increase in *Lox* gene expression in Purkinje cells, which leads to abnormal dendritic development of Purkinje cells via inhibition of the NF-κB signalling pathway and microtubule stability (Li et al 2010a).

For a microarray analysis it is important to choose the right time point at which to analyse the gene expression changes. When choosing the time point for our microarray experiment to compare wild-type and *Mwk* samples, we took into consideration the time frame of the dendritic development, the beginning of abnormal development of Purkinje cell dendrites and the onset of cerebellar ataxia in *Mwk* mice. In the mouse, dendritogenesis of Purkinje cells occurs during the first postnatal month, when the dendrites extend into the molecular layer, branch and form synapses with parallel and climbing fibers (Kapfhammer 2004). The rapid growth and branching of the dendritic tree occurs between the second and fourth weeks after birth (see Figure 1-3 in Chapter 1). Expression of TRPC3 is developmentally regulated as it starts increasing from birth, peaks around three weeks of age, and remains constant thereafter (see Figure 1-11 in Chapter 1). The onset of ataxia in *Mwk* mice is around three weeks of age. At the same time we also see less elaborate dendritic arbors of Purkinje cells *in vivo* (Becker et al 2009). In organotypic slice cultures, however, the effect is more pronounced and a significant reduction in size and complexity of *Mwk* Purkinje cell dendrites is visible already at two weeks. Taking all this information into consideration, we decided to choose P18 as the time-point for the microarray experiment, because this is when Purkinje cell dendrites are in their rapid stage of development, and it is just prior to the changes in the dendritic tree and the onset of ataxia in *Mwk* mice. This way, any gene changes at this time point would reflect causative changes, rather than changes that result from abnormal development.

Results

Analysis of gene expression changes in Purkinje cells of *Mwk* mice compared to wild-type mice.

For the microarray experiment, four wild-type and four *Mwk* mice were sacrificed at the age of P18, which was just prior to the onset of dendritic abnormalities and ataxia in the *Mwk* mice. A total of 1,000 Purkinje cells were collected by LCM from each sample as described in Chapter 5. The microarray was performed on an Affymetrix Mouse Gene 1.0 ST array by Sheena Lee.

The microarray results were analysed by RMA (Robust Multichip Average) and PLIER (Probe Logarithmic Intensity ERror) probe set algorithms (for both gene lists see Appendix B). It has been reported, that detection of differential expression is better achieved by PLIER rather than RMA, and PLIER has a better estimation of fold changes (Mieczkowski et al 2010). Also, it has been shown that PLIER is the best algorithm for avoiding false positive results with poorly performing probe sets (Seo & Hoffman 2006). Some groups evaluate results using at least two different algorithms (Konradi 2005). Comparing different results can help identify genes of actual importance, since data processing can give variable results (Shedden et al 2005). Taking this information into consideration, I decided to use a combined list of genes that come up in both RMA and PLIER algorithms, in order to choose interesting hits for further studies (see Table 6-1). To analyse the data using Ingenuity Pathway analysis and Gene Ontology (GO) analysis, I decided to use the PLIER list, because the combined list would have an insufficient amount of genes for an accurate analysis. A detection threshold of a 1.5 fold change expression score and a cut-off p value of 0.05 ($p \leq 0.05$) were used.

Table 6-1. Combined PLIER and RMA Algorithm Microarray results comparing Purkinje cell gene expression between wild-type (WT) and *Mwk* mice at the age of P18. Sorted by PLIER fold change.

Transcripts Cluster ID	Regulation	PLIER p-value	PLIER Fold Change	PLIER WT Signal	PLIER Mwk Signal	RMA p-value	RMA Fold Change	RMA WT Signal	RMA Mwk Signal	Gene Symbol
10594963	down	0.0011	10.6	260	23	1.5E-04	8.2	232	26	Unc13c
10424411	down	0.0459	5.9	758	185	1.4E-02	3.3	582	188	Tsg101
10417359	up	0.0433	5.9	87	360	6.1E-03	2.3	63	147	Hn1l
10435769	up	0.0265	5.6	88	405	3.1E-02	1.9	113	219	Zbtb20
10360454	up	0.0242	5.1	748	3068	1.4E-03	3.7	157	569	Opn3
10557644	up	0.0144	4.5	153	699	4.0E-02	2.3	164	401	Fbrs
10411274	up	0.0104	4.4	229	910	1.6E-03	3.4	169	567	Sv2c
10542959	up	0.0312	4.2	86	298	1.4E-02	1.9	81	159	Bet1
10535780	down	0.0017	4.0	471	122	1.5E-02	1.5	149	97	Flt3
10477006	up	0.0248	3.9	56	252	1.0E-02	2.2	33	80	Nsfl1c
10454912	up	0.0213	3.6	93	307	5.7E-04	1.6	73	119	Ankhd1
10417070	up	0.0001	3.2	452	1469	7.0E-04	2.5	312	798	Ipo5
10452213	up	0.0050	3.2	122	377	5.1E-03	2.0	74	145	Gtf2f1
10470788	up	0.0276	2.9	127	331	3.6E-02	1.6	110	174	Odf2
10400710	up	0.0138	2.8	81	216	6.5E-03	1.8	54	97	Gm71
10542857	down	0.0462	2.8	2117	845	3.0E-02	2.0	648	343	Mlstd1
10493758	down	0.0236	2.5	796	312	2.4E-02	2.0	399	185	Gatad2b
10546736	up	0.0064	2.2	105	238	3.7E-03	1.6	77	125	Cntn3
10369877	down	0.0347	2.2	896	428	2.3E-02	1.8	694	397	Ube2d1
10487267	down	0.0179	2.2	1321	616	3.4E-02	2.1	1061	509	Polr2l
10401028	down	0.0265	2.2	478	210	3.8E-02	1.7	127	72	Sgpp1
10417689	down	0.0436	2.2	1094	541	2.3E-02	2.2	996	486	Psmd6
10543904	down	0.0337	2.1	1004	497	3.9E-04	1.6	305	191	Cnot4
10523893	down	0.0454	2.1	1810	839	2.3E-02	1.9	942	474	Rpl5
10563643	down	0.0250	2.1	619	296	8.7E-03	1.9	282	148	Tsg101
10435075	up	0.0426	2.1	352	676	1.8E-02	2.1	116	237	Tfrc
10514985	up	0.0475	2.0	216	406	5.8E-03	1.8	65	115	Zyg11b
10441422	down	0.0287	2.0	1610	825	3.7E-02	1.7	868	527	Zdhhc14

10474915	down	0.0097	2.0	1220	630	1.4E-02	1.7	811	484	Gchfr
10425158	down	0.0183	1.9	577	314	1.9E-02	1.8	282	164	Pdxp
10556113	up	0.0393	1.8	838	1497	4.9E-03	1.7	70	120	Rbm3
10478647	down	0.0289	1.8	673	392	1.8E-03	1.8	226	127	Slc12a5
10358454	up	0.0154	1.7	739	1256	7.7E-03	1.6	202	325	Rbm3
10424370	up	0.0033	1.7	671	1125	1.6E-03	1.5	112	171	Trib1
10388884	down	0.0412	1.7	1467	904	4.8E-03	1.7	963	569	Nlk
10446656	up	0.0394	1.7	259	448	2.2E-02	1.6	164	263	Lpin2
10577544	down	0.0437	1.7	777	478	3.6E-02	1.5	486	312	Polb
10544523	up	0.0244	1.6	72	120	3.1E-02	1.6	37	62	Rny1
10569886	down	0.0370	1.6	1233	761	2.2E-02	1.6	694	434	Trappc5
10569200	down	0.0363	1.6	2094	1288	3.0E-02	1.5	1151	741	Polr2l
10455588	down	0.0177	1.6	3875	2518	4.9E-03	1.6	3321	2132	Hspe1
10602166	down	0.0463	1.5	464	308	3.1E-02	1.6	181	112	Nxt2
10526792	up	0.0032	1.5	382	574	2.8E-02	1.6	184	306	Rik
10354588	down	0.0014	1.5	3649	2419	2.3E-03	1.7	1842	1106	Stk17b

There was an approximately 1:1 ratio between up- and down-regulated genes in the microarray data for both RMA and PLIER algorithms (see Figure 6-1). Hierarchical clustering of the statistically significant microarray gene changes is shown in Figure 6-2, where visible differences are observed between wild-type and *Mwk* samples (genes that did not show any change were omitted). The microarray data analysis did not demonstrate any obvious differences between male and female samples, or between the two different litters.

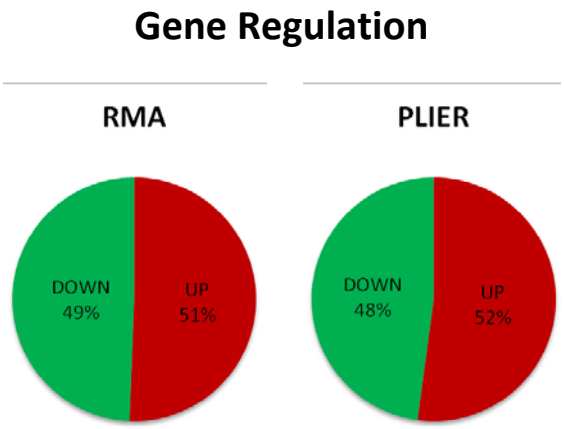

Figure 6-1. Pie charts showing percentage of genes up- and down-regulated in the wild-type vs. *Mwk* microarray experiment using RMA and PLIER algorithms.

To investigate which pathways were deregulated in the *Mwk* Purkinje cells, we performed an Ingenuity System Pathway Analysis. Ingenuity's Canonical Pathways that emerged using the PLIER algorithm are shown in Figure 6-3. Ca^{2+} signalling is a proof of concept pathway to have arisen, as we hypothesise that the *Mwk* mice have increased Ca^{2+} influx in Purkinje cells. Sphingolipid metabolism is interesting, because sphingolipids have been implicated in the development of Purkinje cell dendritic arbors (Furuya et al 1995). Clathrin-mediated endocytosis suggests that vesicle transport could be altered in *Mwk* mice (Slepnev & De Camilli 2000).

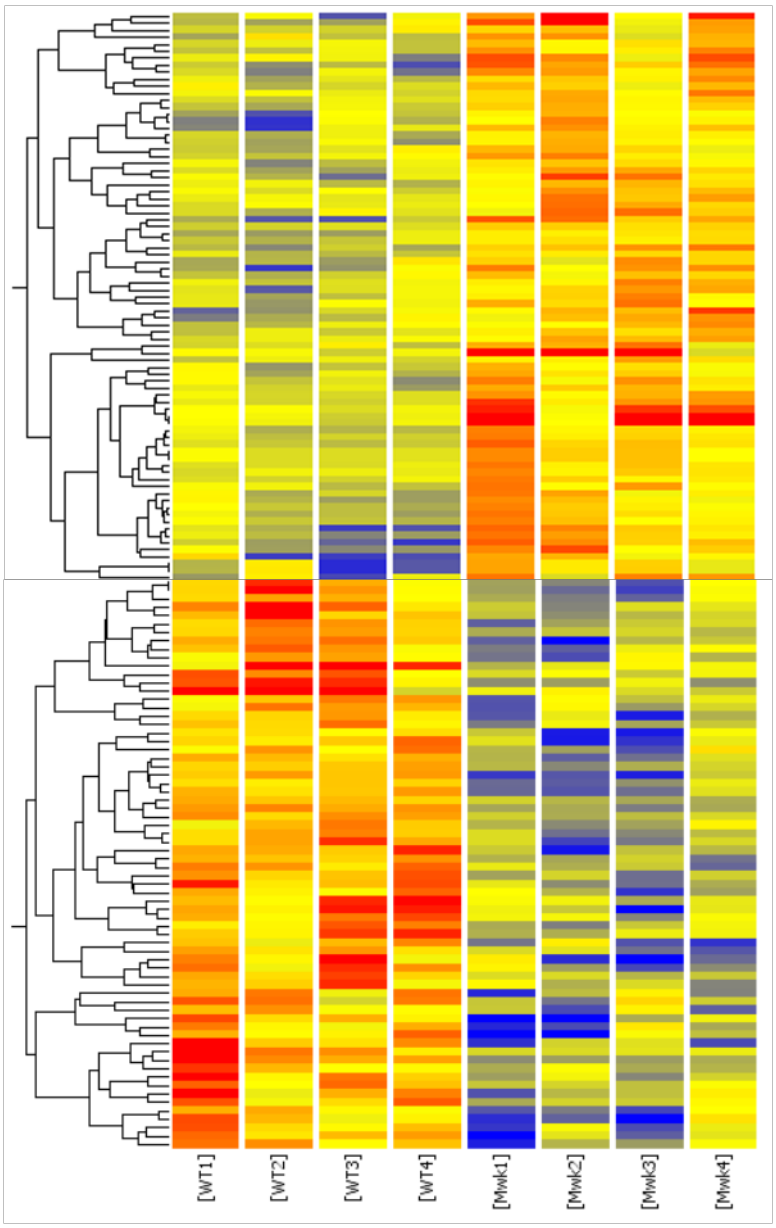

Figure 6-2. Hierarchical clustering of the microarray data. Statistically significant changes ($p \leq 0.05$) with a 1.5 fold change or above are represented in this figure, with clear differences between wild-type (WT) and *Moonwalker* (*Mwk*) samples. Each row represents a different sample (WT 1-4, *Mwk* 1-4) and each row represents a gene.

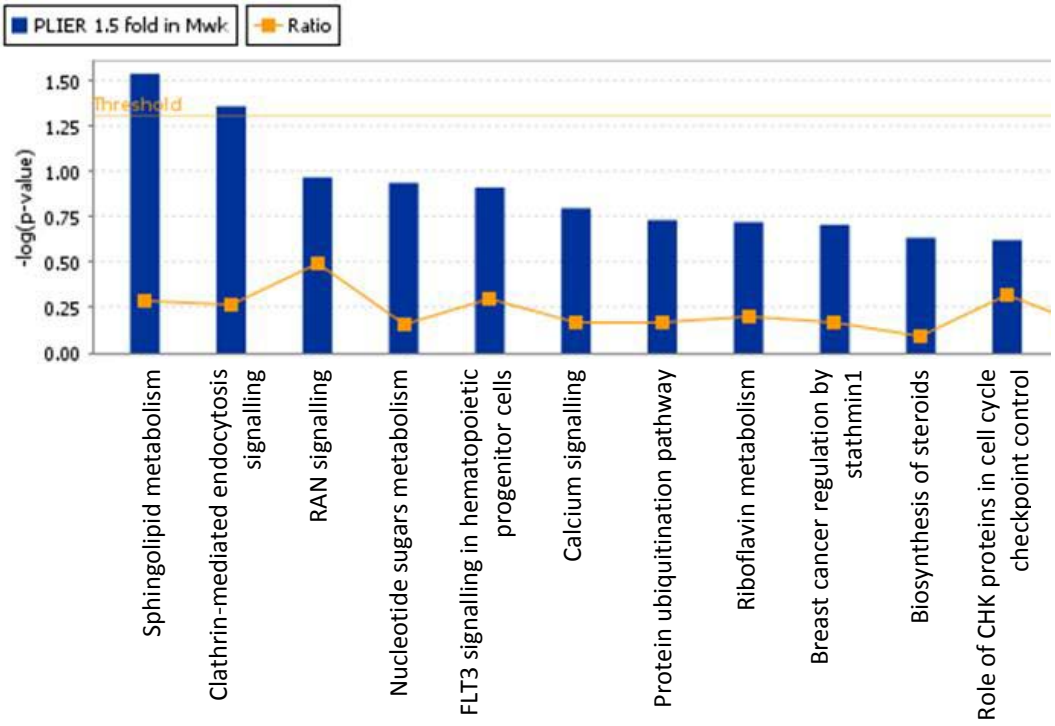

Figure 6-3. Ingenuity Canonical Pathways. The Canonical Pathways that are involved in the analysis of *Mwk* vs. wild-type Purkinje cells are displayed along the x-axis. The y-axis displays the -log of p-value which is calculated by Fisher's exact test right-tailed. The graph displaying the various pathways that are altered in the Purkinje cells of *Mwk* mice is presented from largest to smallest p-value. Threshold line represents the p-value of 0.05. Ratio, which is represented by orange points, is calculated as follows: the number of genes in a given pathway that meet the cutoff criteria of 1.5 fold, divided by total number of genes that make up that pathway.

Ingenuity's Top Biological Functions that were related to the *Mwk* mouse, gathered by the PLIER algorithm, are summarised in Table 6-2. In the "Disease and Disorders" biological function, several categories came up, including "Developmental Disorder". In "Molecular and Cellular Functions" categories such as "Cell-To-Cell Signalling & Interaction", "Cellular Assembly and Organisation" and "Gene Expression" were present. "Physiological System Development and Functions" showed "Nervous System Development and Function", "Embryonic Development and Behaviour" as top categories. These categories suggest that the results obtained in the microarray experiment are describing a neurological developmental disorder, such as cerebellar ataxia.

It was impossible to obtain molecular pathways that were significantly altered in *Mwk* mice using the GO Analysis with a 1.5 fold change cut-off.

A combined gene list from both RMA and PLIER algorithms is shown in Table 6-1. The list comprises of 44 different genes, of which 48% are up-regulated, and 52% are down-regulated. Even though gene changes found in the microarray experiments were statistically significant, many genes demonstrated a substantial degree of variation among the four wild-type or the four *Mwk* samples. Therefore, in order to select the genes for further analysis, I looked at the individual signals for each wild-type and *Mwk* sample for every gene in the combined gene list. The variation among samples could be due to the prolonged storage of mRNA before the microarray analysis, which could cause some degree of RNA degradation. Genes that showed a lot of variation were discarded from further investigation. Genes shown in Figure 6-4 demonstrated the highest degree of conservation between all wild-type and all *Mwk* samples and therefore were chosen to be analysed further. They are summarised in Table 6-3. All genes, except carbonic anhydrase 2 (*Car2*) were present in both algorithm lists. *Car2* was only present in the RMA list, because in the PLIER list *Car2* expression change was not considered significant because the p value was too high. It was chosen for further analysis as it was down-regulated in a SCA7 mouse

model (Chou et al 2010), and its family member Car8 was found deregulated in ataxia mouse models SCA1 and *staggerer* (Crespo-Barreto et al 2010; Gold et al 2003).

Table 6-2. Ingenuity Top Biological Functions using a PLIER algorithm of microarray hits at a cut-off of 1.5 fold change.

Biological Functions	Category	Molecules	p-value
Diseases and Disorders	Antimicrobial Response	HSPE1	0.0088
	Cardiovascular Disease	ASAH1, CASQ2, CLIP1, CMIP, CNTN3, DARS, FLT3, GABRG2, GFRA2, GRIK2, LPIN2, LYRM4, P2RY12, RPS6KA5, SCN9A, SETX, SPATA5, TPM1, TRIM44, ZNF706	0.0088-0.0348
	Dermatological Diseases and Conditions	FLT3, SCN9A, SNAP29	0.0088-0.0175
	Developmental Disorder	BBS4, CASQ2, TPM1	0.0088-0.0302
	Organismal Injury and Abnormalities	FLT3, LRP8, ZBTB20	0.00652-0.0175
Molecular and Cellular Functions	Cell-To-Cell Signalling and Interaction	GABRG2, GRIK2, SLC12A5, SNAP29, STXBP1, SV2C, UNC13C	0.000678-0.0348
	Cellular Assembly and Organization	AP1G1, BBS4, BET1, CASQ2, CLIP1, DNAJB6, KIF1C, NSFL1C, OSBPL1A, RPL5, SCP2, SLC12A5, SNAP29, STXBP1, TPM1, TSG101	0.00634-0.0479
	Small Molecule Biochemistry	ASAH1, CTSD, DARS, FAR2, HSPE1, POLB, SLC11A2, SCP2, SGPP1	0.000455-0.0433
	Gene Expression	CCNC, DVL3, GTF2F1, GTF2F1, ETV5, POLB	0.00401-0.0433
	Lipid Metabolism	ASAH1, FAR2, SCP2, SGPP1	0.00401-0.0433
Physiological System Development and Functions	Nervous System Development and Function	BBS4, DNAJB6, EN2, GABRG2, GRIK2, GFRA2, KCNAB1, LRP8, POLB, RPS6KA5, SLC12A5, SNAP29, STXBP1, SV2C, UNC13C	0.000678-0.0433
	Connective Tissue Development and Function	NLK, TSG101	0.0088-0.0262
	Digestive System Development and Function	GFRA2	0.0088
	Embryonic Development	CLIP1, DNAJB6, GATAD2A, GOPC, HSPE1, LRP8	0.0088-0.04330.
	Behaviour	CHD7, GABRG2, GFRA2, GRIK2, KCNAB1, LRP8, RPS6KA5, SLC11A2, UNC13C	0.00208-0.0447

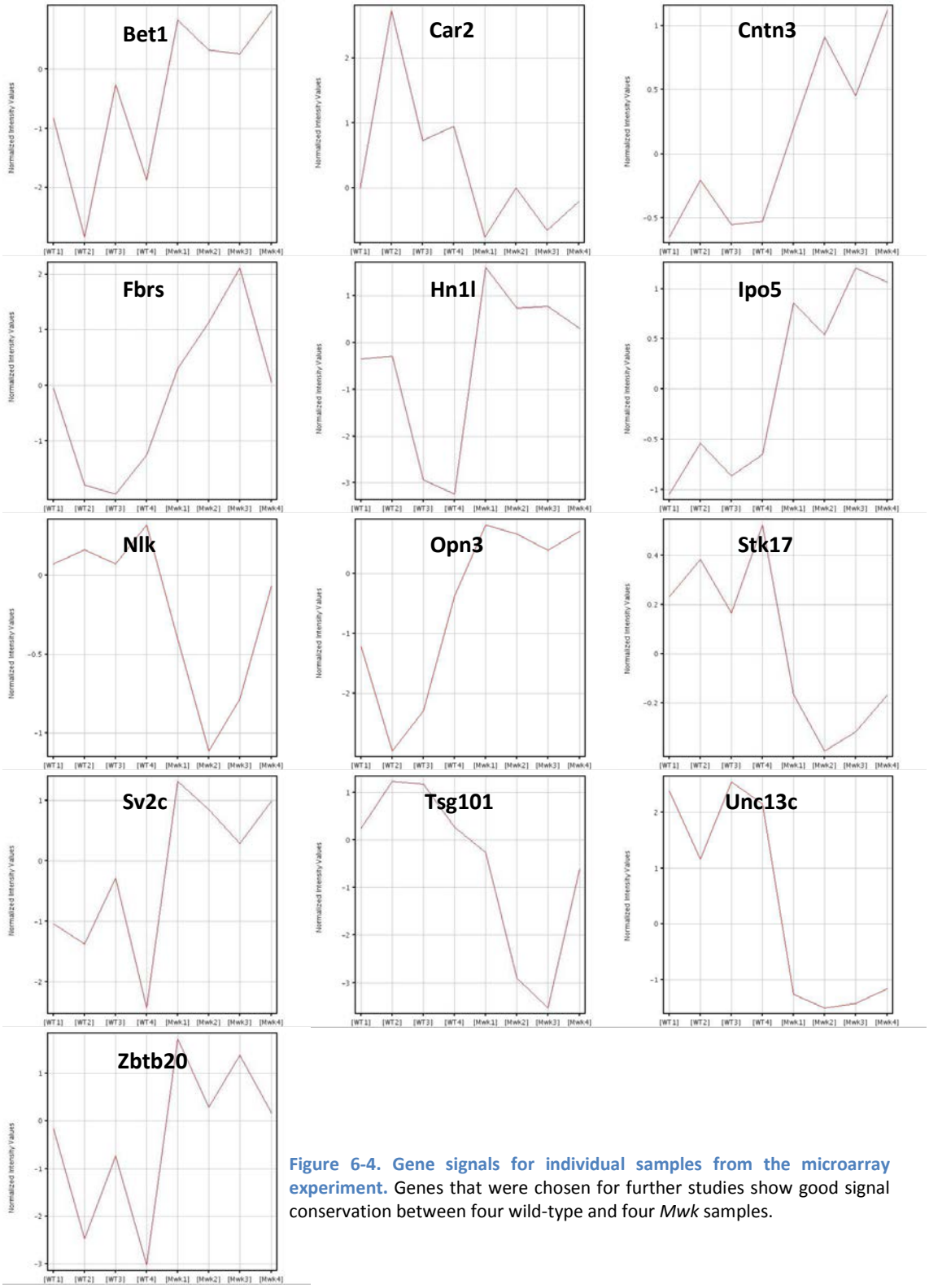

Figure 6-4. Gene signals for individual samples from the microarray experiment. Genes that were chosen for further studies show good signal conservation between four wild-type and four *Mwk* samples.

Table 6-3. Genes that have significant differences between wild-type and *Mwk* expression levels that were chosen for further studies. This is a combined list of RMA and PLIER algorithms.

Gene	Protein	Regulation	PLIER Fold Change	RMA Fold Change
Unc13c	Munc13-3	down	10.6	8.2
Tsg101	Tumor susceptibility gene 101	down	5.9	3.3
Hn1l	Hematological and neurological expressed 1-like	up	5.9	2.3
Zbtb20	Zinc finger and BTB domain containing 20	up	5.6	1.9
Opn3	Opsin 3	up	5.1	3.7
Fbrs	Fibrosin	up	4.5	2.3
Sv2c	Synaptic vesicle glycoprotein 2c	up	4.4	3.4
Bet1	Blocked early in transport 1 homolog	up	4.2	1.9
Flt3	FMS-like tyrosine kinase 3	down	4.0	1.5
Ipo5	Importin 5	up	3.2	2.5
Car2	Carbonic anhydrase 2	down	-	2.4
Cntn3	Contactin 3	up	2.2	1.6
Nlk	Nemo-like kinase	down	1.7	1.7
Stk17b	Serine-threonine kinase 17b, apoptosis-inducing	down	1.5	1.7

Microarray results can be confirmed by further laboratory analyses, such as qRT-PCR, northern blot and *in situ* hybridisation (Chuaqui et al 2002). We first performed the qRT-PCR experiment, which is the only quantitative technique for analysing levels of expression change. We then investigated the expression of the genes of interest by *in situ* hybridisation to determine in which cells of the cerebellum they are expressed.

qRT-PCR primer validation

It is necessary to validate microarray results using an independent method, such as qRT-PCR, which was done for all the genes chosen for our further studies (see Table 6-3). Primers for the following genes were designed: *Bet1, Car2, Cntn3, Fbrs, Flt3, Hn1l, Ipo5, Nlk, Opn3, Stk17b, Sv2c, Tsg101, Unc13c* and *Zbtb20* using the Primer Express 3.0 software. *Calbindin* primer was provided by Dr Esther Becker and was used as an internal control for qRT-PCR. *Calbindin* is a very common control used for Purkinje cell studies as it is specific for these cells in the cerebellum. No changes in calbindin protein levels were found in *Mwk* mice compared to wild-type littermates (Dr Esther Becker, personal communication). The microarray data confirmed no significant changes in gene expression level of *Calbindin* in *Mwk* mice (see Figure 6-5). Calbindin was, therefore, a good internal control to normalise the qRT-PCR results.

When possible, primers were designed to span an intron region in order to avoid genomic DNA

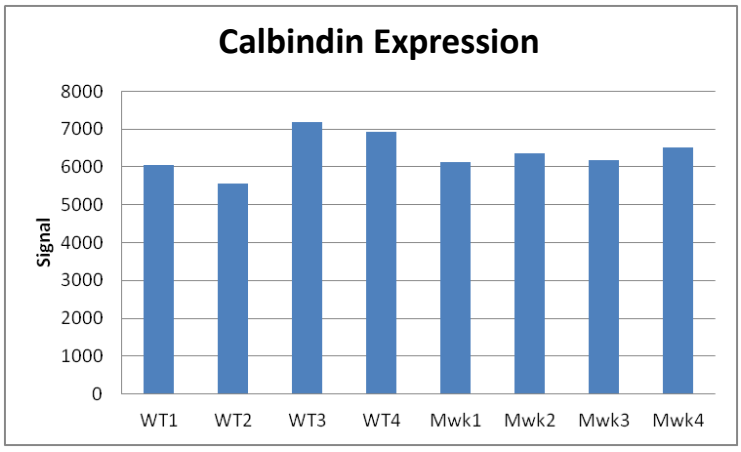

Figure 6-5 Calbindin expression is equal in wild-type (WT) and *Mwk* Purkinje cells. Data from the microarray experiment using the PLIER algorithm.

amplification. However, for some genes this could not be achieved and primers that anneal to the same exon and, hence, amplify a region in the same exon, were chosen. During the process of mRNA extraction the samples were DNase I treated to degrade any genomic DNA in the sample. Also, mRNA (from which the cDNA was reverse transcribed) was included in the qRT-PCR reaction as a negative control, which controlled for the presence of genomic DNA in the mRNA sample: no amplification was observed. Hence, there was no genomic DNA amplification.

Whole cerebellar lysates were used for primer validation. Figure 6-6 shows Amplification Plots, Melt Curves, and "C_T vs. log[cDNA]" linear regression plots for all gene primers. Primer specificity can be confirmed from the Melt Curve: there should only be one Melt Curve peak which represents a number of products that were amplified in the reaction. All designed primers produced one melt curve, therefore they were all specific. A range of cDNA concentrations from whole cerebellar lysates was used to test primer efficiency. The linear regression plot shows a relationship between the number of cycles (C_T) and the cDNA concentration, from which the slope is determined for the following analysis of primer efficiency. The efficiency (E) of the primer was calculated using the following formula:

$$E = (10^{-1/slope} - 1) \times 100\%$$

All primers had an efficiency of 85% – 105%, which was considered suitable for the qRT-PCR experiments.

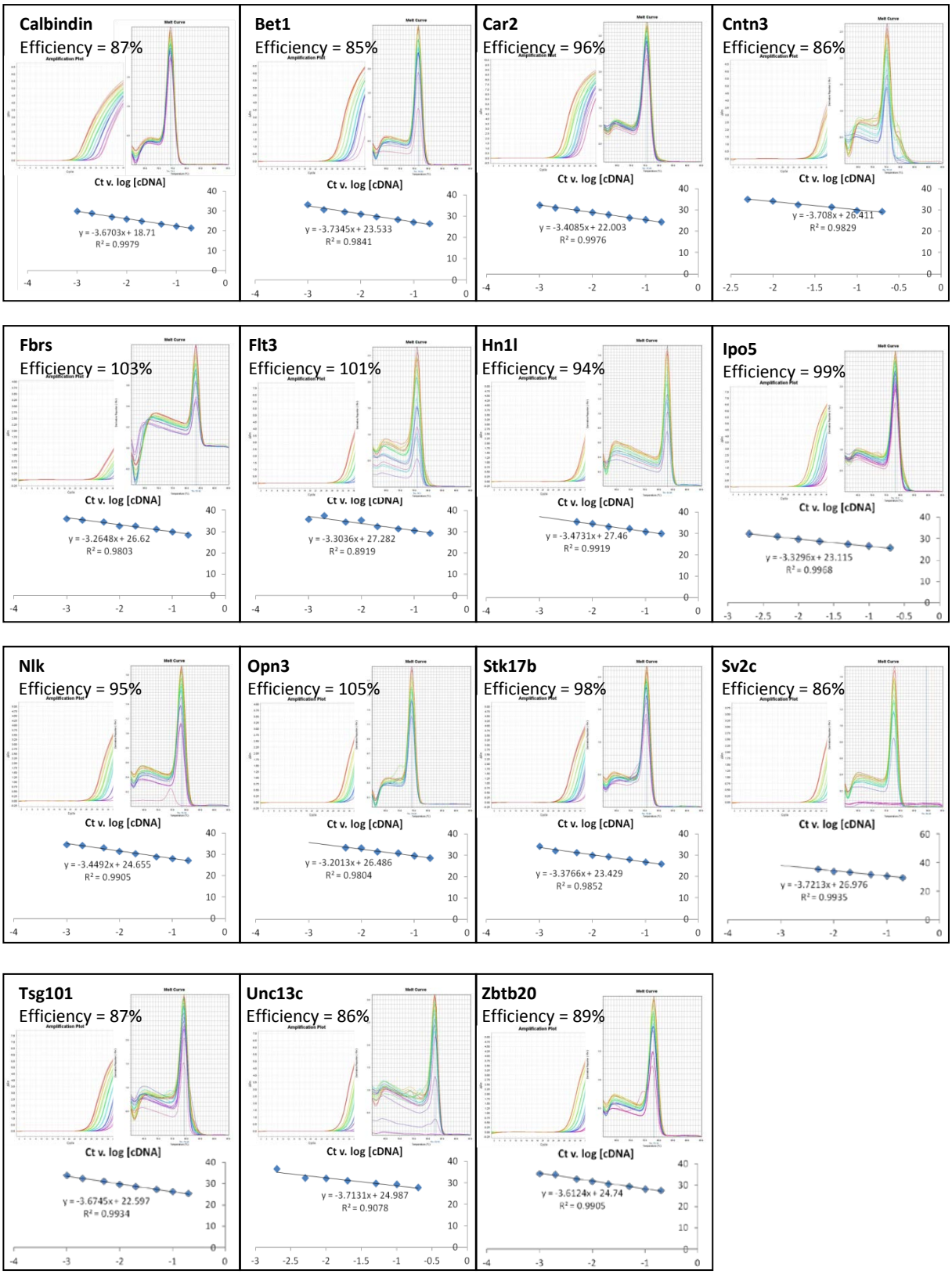

Figure 6-6. qRT-PCR primer validation. For each primer, the figure shows an Amplification Plot, a Melt Curve and a "C_T vs. log[cDNA]" plot which determines primer efficiency. All primers were efficient.

Optimisation of qRT-PCR for laser-capture microdissected cells

Primer efficiency was validated using the whole cerebellar lysates rather than the microdissected Purkinje cells. The qRT-PCR validation needed to be performed on the laser-capture microdissected Purkinje cells. Figure 6-7 shows that time spent handling the laser-capture microdissected samples played a crucial role in performing a good and reliable qRT-PCR reaction. The amplification plot of 200 cells which were microdissected and mRNA extracted and reverse transcribed in a few days showed a very good amplification plot and low C_T values even when the sample was diluted 10 times. However, when 500 cells were collected and stored at -80°C for

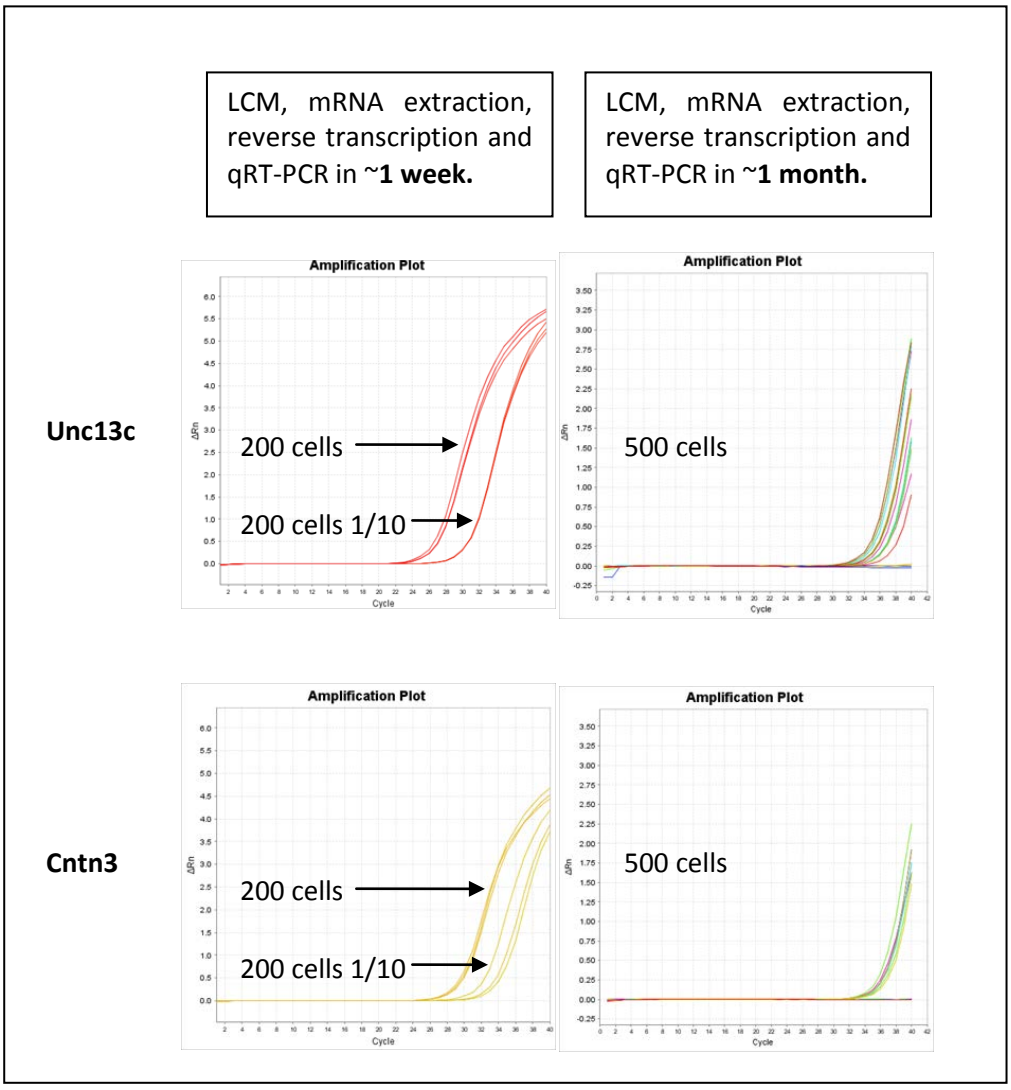

Figure 6-7. qRT-PCR reaction depends on the time spent between LCM and the qRT-PCR reaction. Amplification plots for *Unc13c* and *Cntn3* genes show that 200 cells and 200 cells diluted 10 times can produce good results if the qRT-PCR reaction is performed within 1 week. If the process takes longer, the qRT-PCR reaction fails even if more microdissected cells are used.

more than a month before the mRNA was extracted, the amplification plot showed very little amplification with very high, variable and hence unreliable C_T values. This finding signified the importance of working fast with laser-capture microdissected cells. Unfortunately, this was discovered after the microarray experiment was performed, where the cells were collected within approximately a 2 week period after which the mRNA was extracted and kept at -80°C for another few weeks. For the qRT-PCR experiments, the whole process was finished in 3-4 days.

It was essential to choose an appropriate reverse transcriptase enzyme, because most available enzymes cannot efficiently reverse transcribe small starting amounts of mRNA. Initially, we used the SensiScript reverse transcriptase (QIAGEN), because it had been used in the qRT-PCR experiment for laser-capture microdissected cells in another study in our lab (Bitoun et al 2009). However, when using laser-capture microdissected cells in our experiment, SensiScript produced multiple Melt Curve peaks for all genes. Reverse transcriptase reaction using SensiScript enzyme took place at 37°C for 1 hour, and perhaps this temperature was too low for the specificity of the enzyme. Also, G/C – rich and secondary structure-rich templates can cause the enzyme to stop the reaction, dissociate from the mRNA or skip parts of the mRNA (Bustin 2002). These could be the reasons behind the multiple Melt Curve peaks that were observed. Consequently there was a need for a different reverse transcriptase enzyme. SuperScript III enzyme (Invitrogen) was therefore tested against SensiScript (Figure 6-8). SuperScript III is a much better choice of enzyme to make the cDNA from laser capture microdissected cells as it only produced a single Melt Curve peak, meaning that it is specific and suitable for reverse transcribing low amounts of starting material. Therefore, SuperScript III was used for the qRT-PCR validation of microarray data.

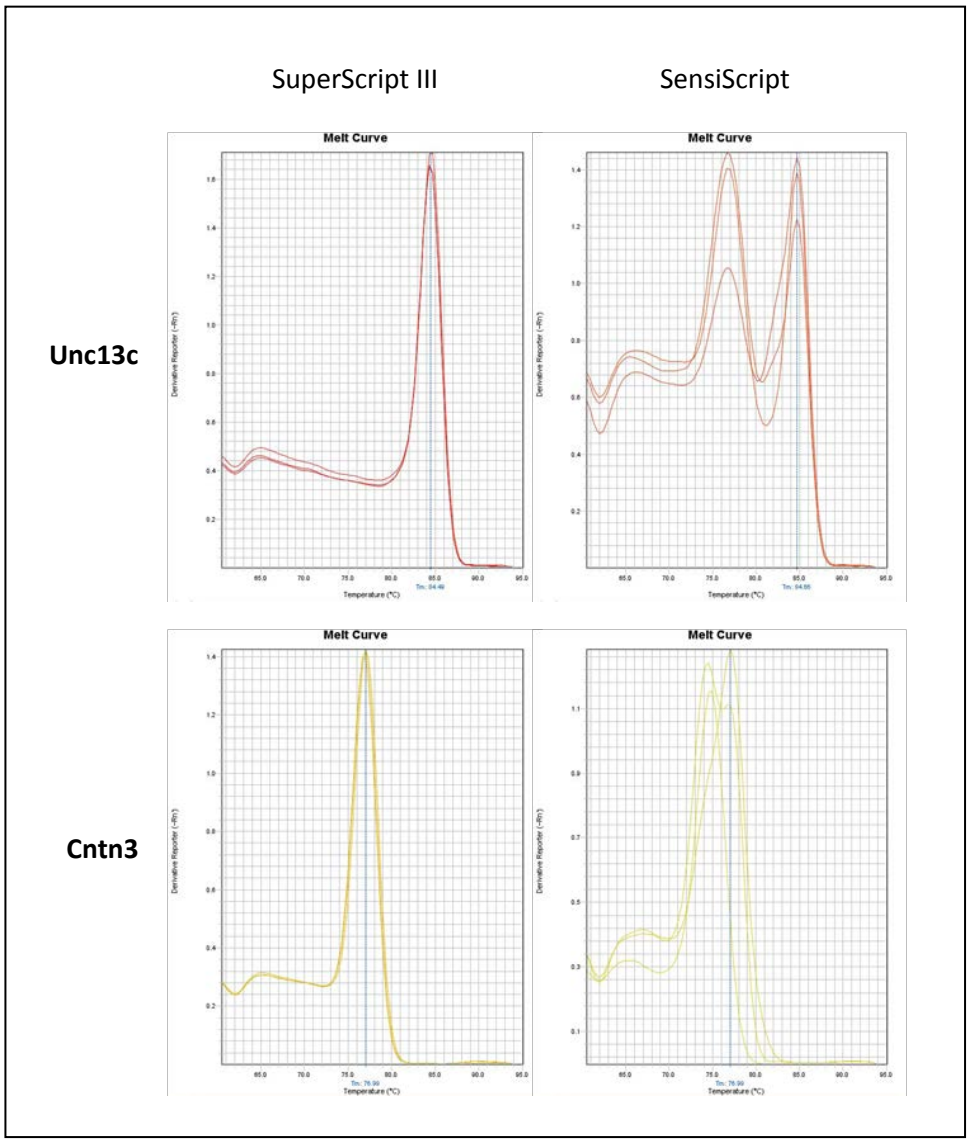

Figure 6-8. Differences in qRT-PCR Melt Curves when cDNA is made using different reverse transcriptases. As shown by the example of genes *Unc13c* and *Cntn3*, SensiScript reverse transcriptase produces multiple melt curves which means that multiple different products are being amplified. When using the SuperScript III reverse transcriptase, there is one melt curve, meaning that there is only one specific amplified product.

For a very few genes it was possible to achieve low C_T values for qRT-PCR, probably due to their high expression in the Purkinje cells. However, for most genes, even when producing a single melt curve peak, the C_Ts for the laser-capture microdissected cells were very inconsistent and too high for a reliable analysis. It was, therefore, important to amplify the cDNA prior to the qRT-PCR experiment. A TaqMan PreAmp Master Mix Kit (Applied Biosystems) is designed to amplify low quantities of cDNA for further analysis by qRT-PCR. The equal rate of pre-amplification was validated by performing qRT-PCR reaction on a range of cDNA concentrations: cDNA from 600 microdissected Purkinje cells, cDNA from 600 cells diluted two times, and cDNA from 600 cells diluted four times. The results of a linear regression correlation between the relative number of cells (600 cells = 1; 600 cells diluted two times = ½; 600 cells diluted four times = ¼) and C_Ts are displayed in Figure 6-9. Signal correlation (R^2) determined from the plots is shown for every gene. Pre-amplification R^2 for all genes was more than 0.95, which showed that all C_T values were very close to the linear regression, because $R^2 = 1$ indicates a perfect fit and the closer the value is to 1, the better the correlation. These results confirmed equal rate of amplification of cDNA for all primers when using the TaqMan PreAmp Master Mix Kit, which was therefore used in the subsequent qRT-PCR experiments.

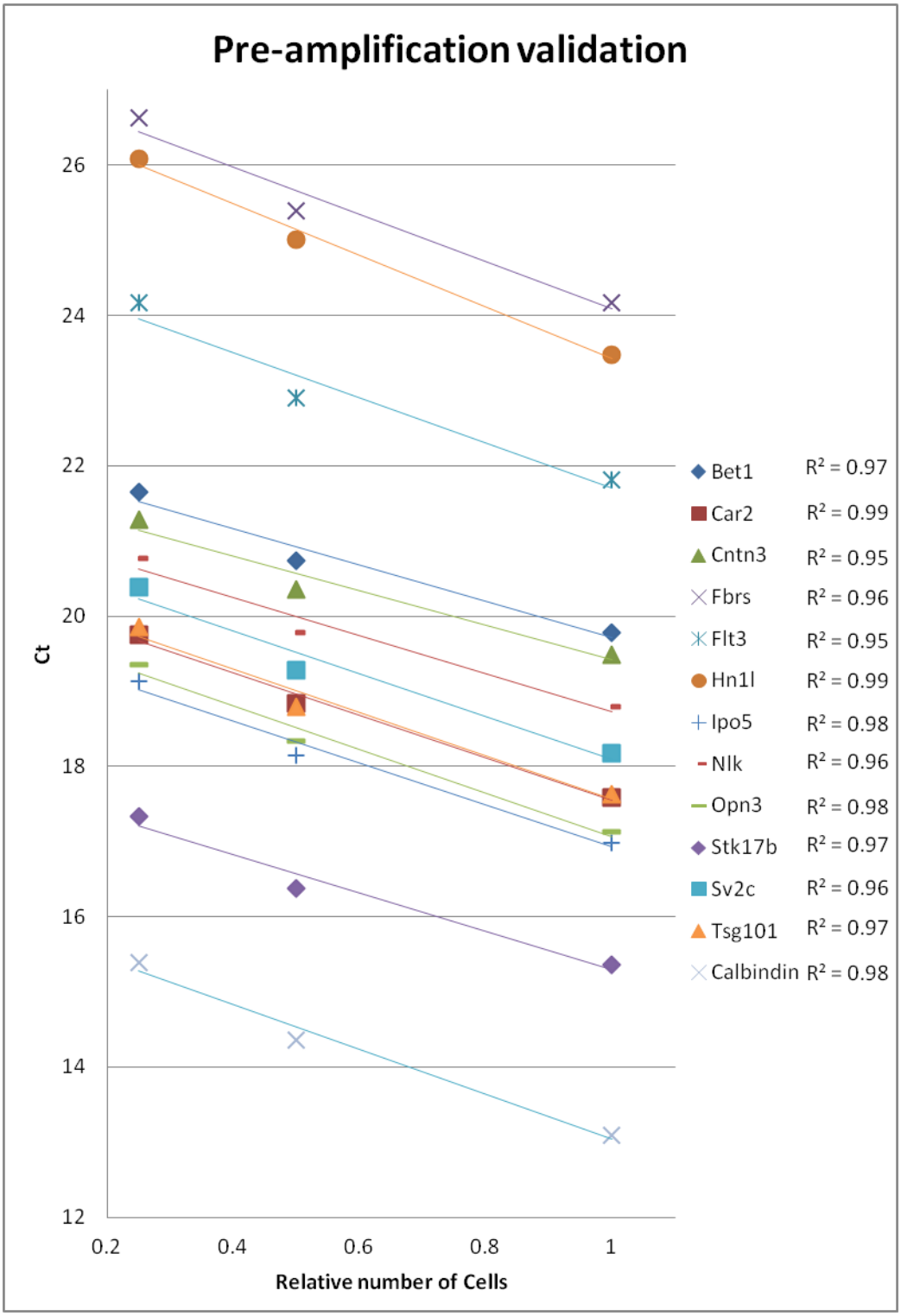

Figure 6-9. cDNA pre-amplification validation. Pre-amplification reaction was performed using 600 microdissected Purkinje cells (=1), 600 cells diluted ½ (=½), and 600 cells diluted ¼ (=¼). The plot shows a linear relationship between three different dilutions for each gene. R^2 is shown for each gene and shows that the rate of pre-amplification is uniform for all genes.

Verification of the selected gene set by qRT-PCR

As in the microarray experiment, four wild-type and four *Mwk* mice at the age of P18 were sacrificed for the qRT-PCR validation experiments. For each sample, 300-500 Purkinje cells were collected by LCM (equal amount for all samples of the same age, and collected from all lobes of the cerebellum). The cDNA was pre-amplified prior to the qRT-PCR analysis, which was a crucial step for the qRT-PCR to work. Because it is difficult to determine the concentration of samples with very small amounts of cDNA, every qRT-PCR had to include an invariable endogenous control to correct for sample variations. We therefore used *Calbindin* as an internal control, as it showed no significant variation between wild-type and *Mwk* samples in the microarray experiment (Figure 6-5).

Gene expression changes could not be confirmed by qRT-PCR for the following genes: *Bet1, Fbrs, Flt3, Hn1l, Nlk, Tsg101, Unc13c* and *Zbtb20* (Figure 6-10). I speculate that qRT-PCR and microarray experiments had different results due to the long-term mRNA storage before the microarray experiment. Some genes, for example *Bet1* and *Unc13c*, showed some degree of change in the qRT-PCR experiment, however, it was not statistically significant. It is likely that they could show significant changes at later time-points as a consequence to other changes that occur in the Purkinje cells.

The other six genes from Table 6-3 were confirmed by qRT-PCR as significantly changing in *Mwk* Purkinje cells at P18. These genes were: carbonic anhydrase 2 (*Car2*), contactin 3 (*Cntn3*), importin 5 (*Ipo5*), opsin 3 (*Opn3*), serine-threonine kinase 17b (*Stk17b*) and synaptic vesicle glycoprotein 2c (*Sv2c*). The results of the qRT-PCR experiment are shown in Figure 6-11. This figure also displays a time-course, including ages P11, P14 and P18. Table 6-4 quantifies these changes.

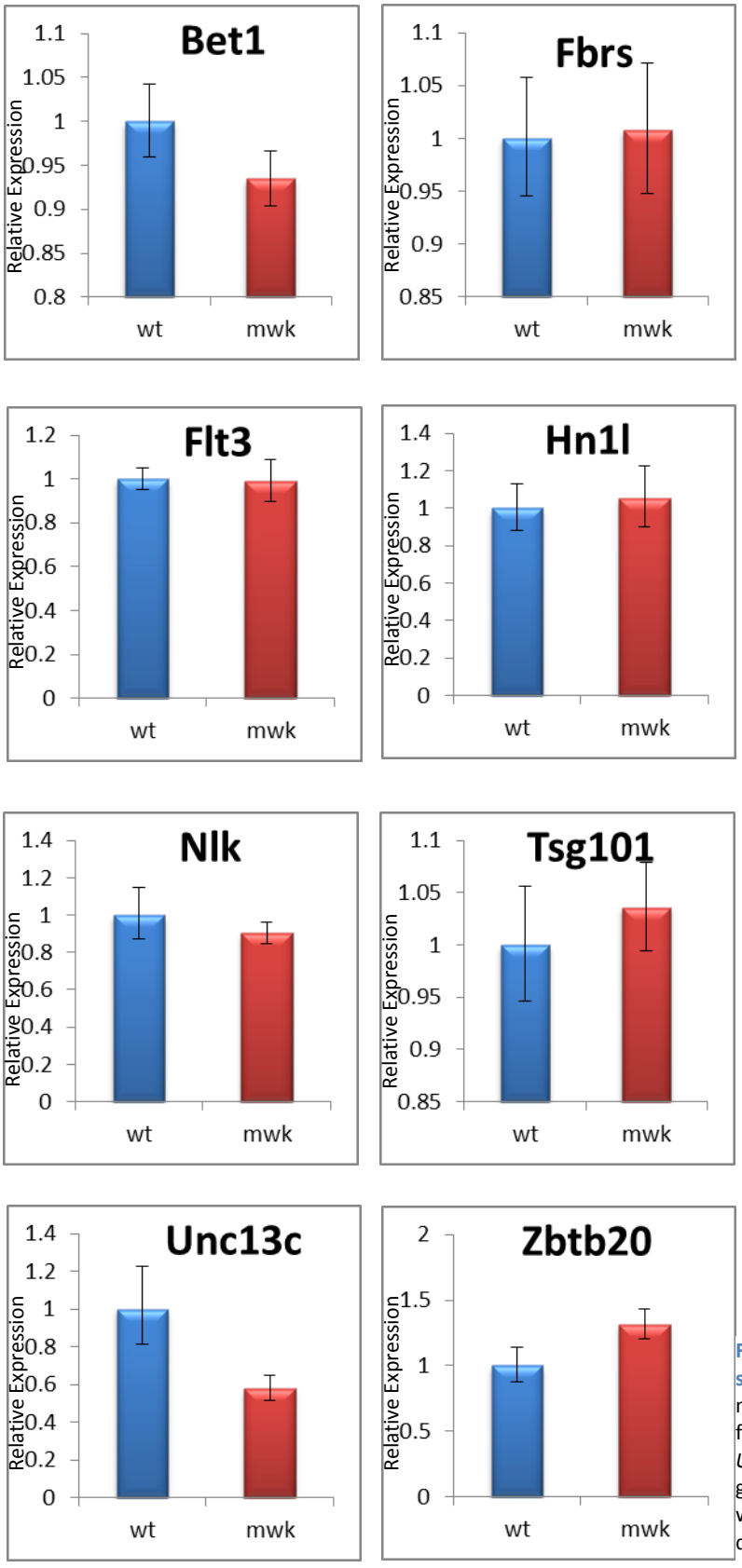

Figure 6-10. Genes that do not show a significant change at P18 by qRT-PCR. The microarray results could not be confirmed for *Bet1, Fbrs, Flt3, Hn1l, Nlk, Tsg101, Unc13c* and *Zbtb20*. Therefore these genes will not be investigated further. The wild-type values were set to 1 to demonstrate relative expression.

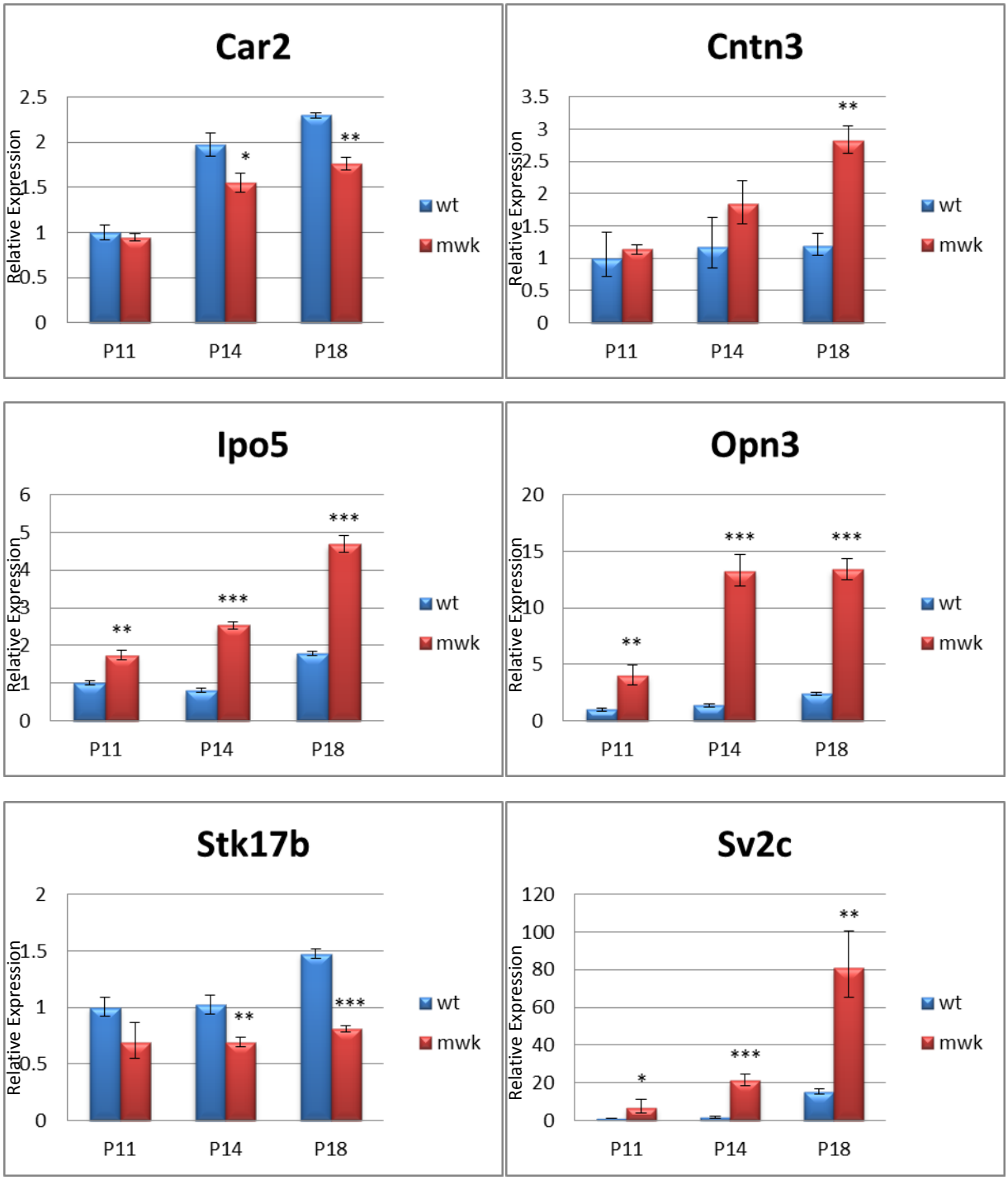

Figure 6-11. A time-course of gene expression changes for *Car2, Cntn3, Ipo5, Opn3, Stk17b* and *Sv2c*. These genes showed significant changes in gene expression levels between wild-type (wt) and *Mwk* Purkinje cells at P18, confirming the microarray results. Their expression was also investigated at earlier time points (P11 and P14), where *Ipo5, Opn3* and *Sv2c* show significant changes from P11; and *Car2* and *Stk17b* demonstrated changes from P14. $p<0.05$ *, $p<0.01$**, $p<0.001$***. Relative expression of gene was shown, where the wild-type expression at P11 was set to 1.

Table 6-4. Summary of gene expression fold changes at different time points for genes that have been confirmed by qRT-PCR.

Protein	Gene	qRT-PCR P11	qRT-PCR P14	qRT-PCR P18	MICROARRAY P18
Carbonic anhydrase 2	Car2	---	↓1.3	↓1.3	--- (PLIER) ↓2.4 (RMA)
Contactin 3	Cntn3	---	---	↑2.4	↑2.2 (PLIER) ↑1.6 (RMA)
Importin 5	Ipo5	↑1.7	↑3.1	↑2.6	↑3.2 (PLIER) ↑2.5 (RMA)
Opsin 3	Opn3	↑3.9	↑9.8	↑5.6	↑5.1 (PLIER) ↑3.7 (RMA)
Serine-threonine kinase 17b	Stk17b	---	↓1.5	↓1.8	↓1.5 (PLIER) ↓1.7 (RMA)
Synaptic vesicle glycoprotein 2c	Sv2c	↑6.5	↑12.1	↑5.3	↑4.4 (PLIER) ↑3.4 (RMA)

For *Cntn3*, qRT-PCR at P18 showed a 2.4 fold up-regulation, which was consistent with a 2.2 fold up-regulation in microarray (PLIER). This gene did not show any significant changes at earlier time-points. *Car2* was down-regulated at P18 by 1.3 fold in the qRT-PCR, which was less than in the microarray (2.4 fold down-regulation, RMA). *Car2* was also down-regulated by 1.3 fold at P14; and was unchanged at P11. At P18 *Stk17b* was 1.8 fold down-regulated, consistent with the microarray result (1.7 fold down-regulation, RMA); and showed a 1.5 fold down-regulation at P14, remaining unaffected at P11. *Ipo5*, *Opn3* and *Sv2c* showed significant changes in *Mwk* Purkinje neurons for all three time-points. *Ipo5* was up-regulated 2.6 fold at P18 (consistent with 2.5 fold up-regulation, RMA), 3.1 fold up-regulation at P14 and 1.7 fold up-regulation at P11. *Opn3* was up-regulated at P18 by 5.6 fold (5.1 fold up-regulation, PLIER), 9.8 fold up-regulation at P14 and 3.9 fold up-regulation at P11. *Sv2c* was up-regulated 5.3 fold at P18 (4.4 fold up-regulation, PLIER), 12.1 fold up-regulation at P14 and 6.5 fold up-regulation at P11.

In situ hybridisation showing expression of the chosen gene set in the cerebellum

To investigate *Car2, Cntn3, Ipo5, Opn3, Stk17b* and *Sv2c* gene expression in the cerebellum, *in situ* hybridisation experiments were performed. A time course shown in Figure 6-12 (ages P7, P15, P22 and Adult) demonstrates expression of all six genes in the Purkinje cells of the cerebellum of wild-type mice. Only *Car2* was also expressed in another cell type and since it is known to be expressed in oligodendrocytes, we assumed that oligodendrocytes were also showing *Car2* expression in our *in situ* hybridisation experiments. To investigate whether the gene expression in the *Mwk* cerebella was altered compared to wild-type cerebella, an *in situ* hybridisation was performed on P18 littermates (Figures 6-13 and 6-14). It is interesting to note that the intensity of expression varied, and was related to the changes we saw in the microarray and qRT-PCR: for *Car2* and *Stk17b*, the *in situ* hybridisation analysis demonstrated a decrease in mRNA expression in *Mwk* samples, and for *Cntn3, Ipo5, Opn3* and *Sv2c*, it demonstrated a slight increase in expression.

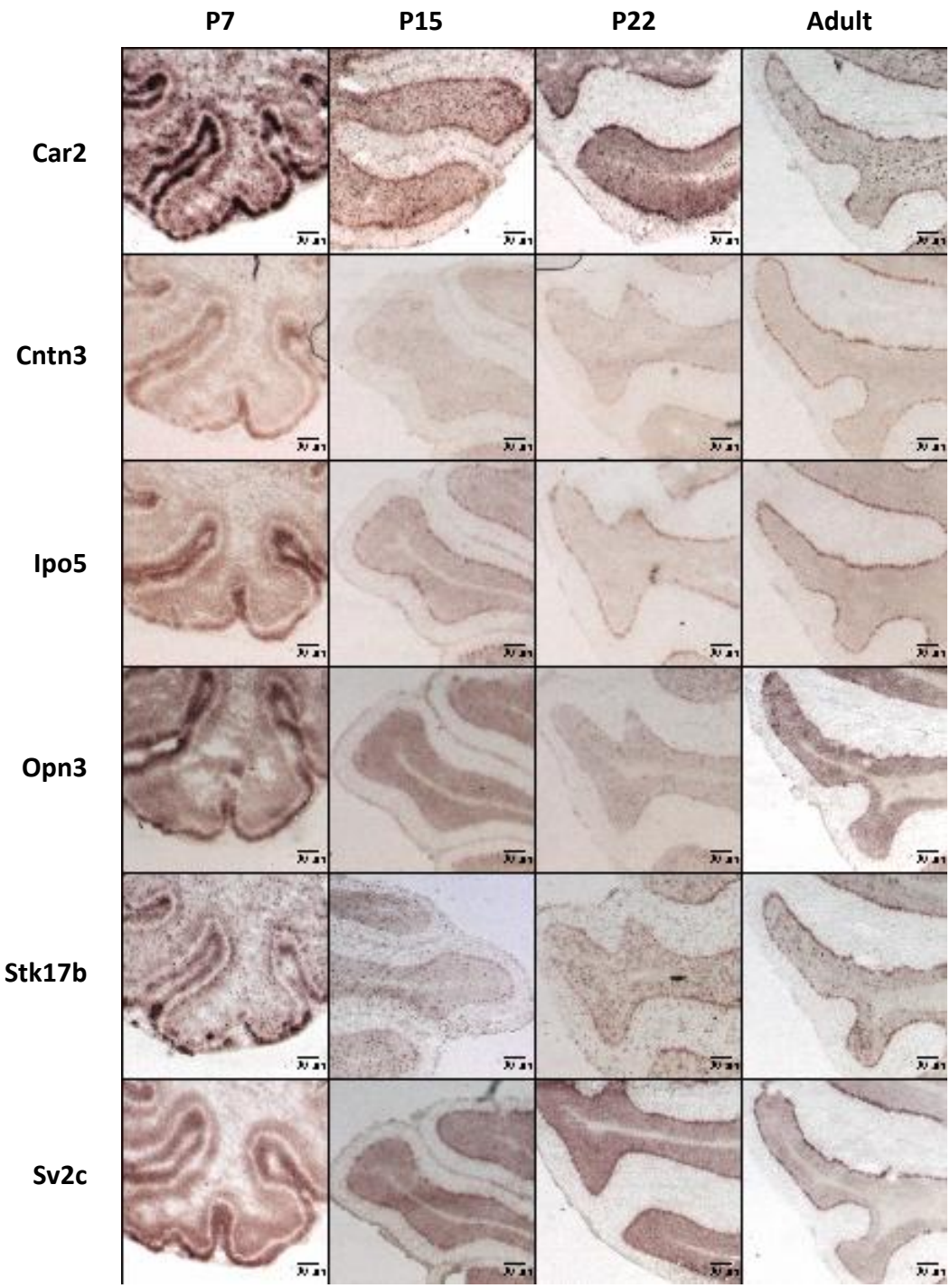

Figure 6-12. *In situ* hybridization looking at gene expression at different time points in wild-type mice. These genes show expression in the Purkinje cell layer of the cerebellum. Scale bar = 100 µm. The cerebellar cryosections were kindly provided by Dr Esther Becker and Elizabeth Zhang. n=2

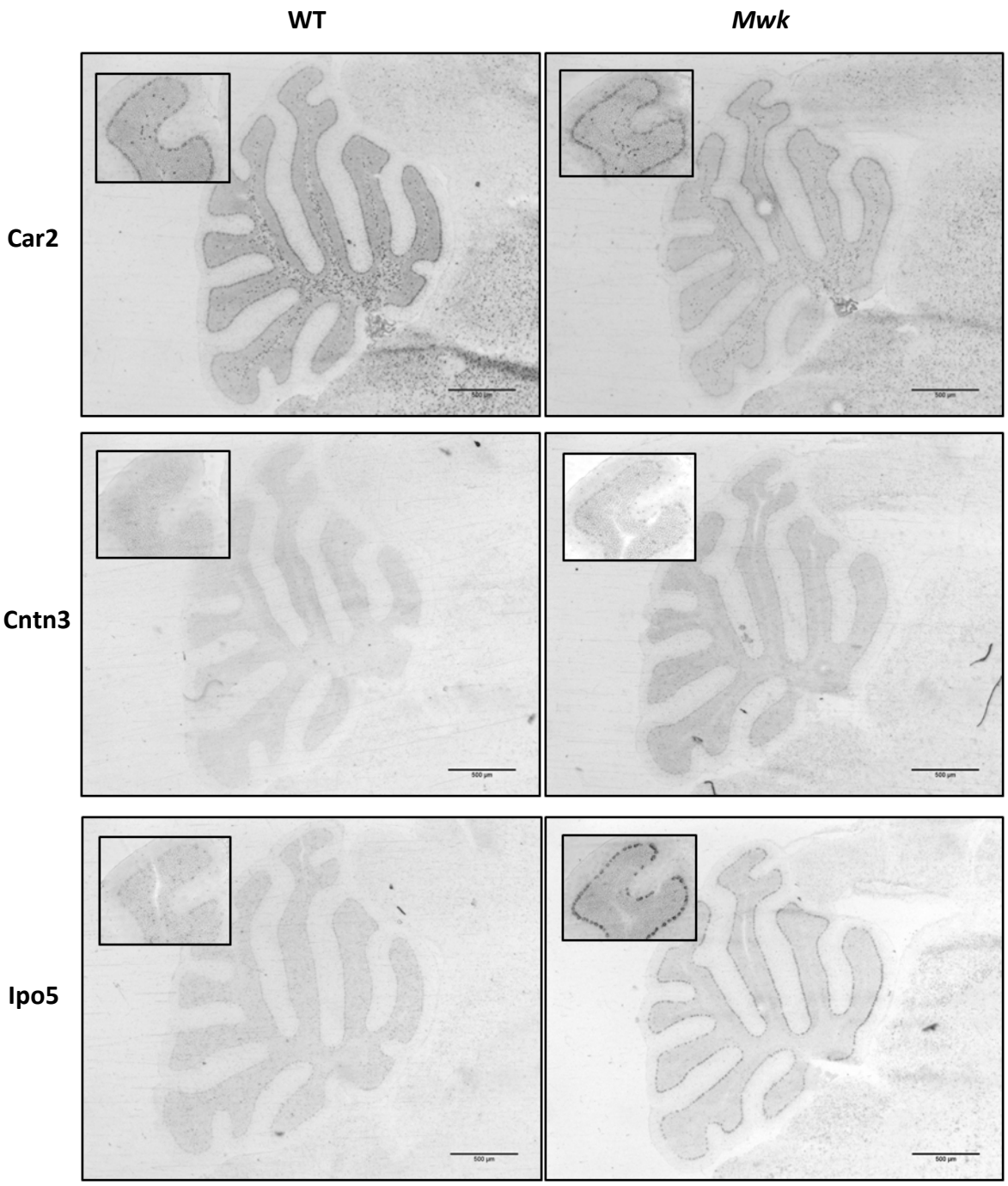

Figure 6-13. Comparing *Car2*, *Cntn3* and *Ipo5* gene expression patterns between wild-type (WT) and *Mwk* cerebella by *in situ* hybridization at P18. These genes are expressed in the Purkinje cells of the cerebellum in both wild-type and *Mwk* mice. *Car2* is also expressed in the oligodendrocytes. Scale bar = 500 µm. n=2

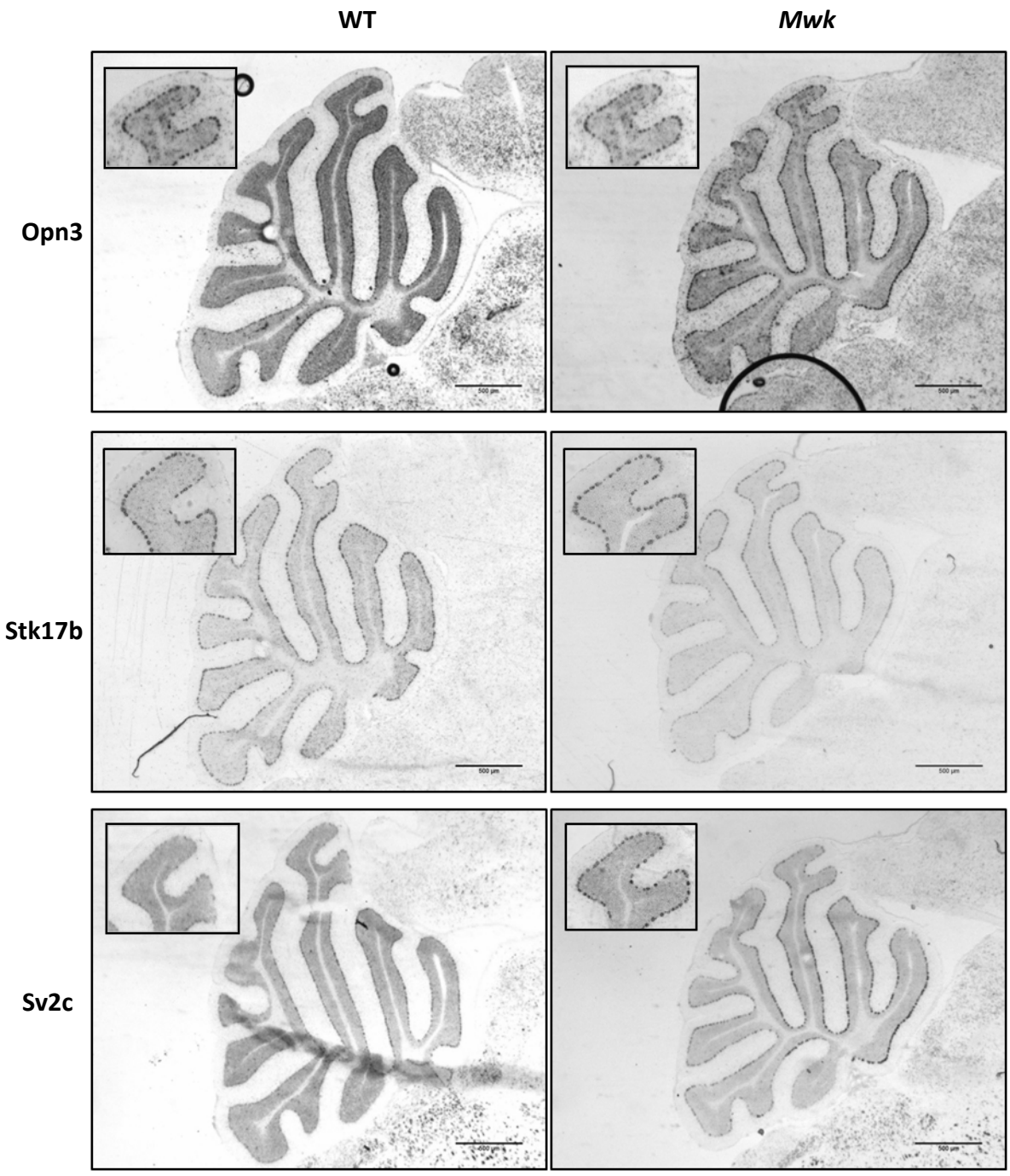

Figure 6-14. Comparing *Opn3*, *Stk17b* and *Sv2c* gene expression patterns between wild-type (WT) and *Mwk* cerebella by *in situ* hybridization at P18. These genes are expressed exclusively in the Purkinje cells of the cerebellum in both wild-type and *Mwk* mice. Scale bar = 500 µm. n=2

Immunohistochemistry comparing localisation of Stk17b in wild-type vs. *Mwk* cerebella

To investigate the Stk17b protein expression pattern in the cerebellum, immunohistochemistry was performed with an α Stk17b antibody on P20 cerebellar cryosections (see Figure 6-15). The results revealed that in the cerebellum, Stk17b was expressed in Purkinje cells and another cell type in the molecular layer (basket cells or stellate cells), as well as weakly in granule cells. The expression was evident in the perikaryon of Purkinje cells (including weak expression in the primary dendrites), and in many cells also in the nucleus. However, there was no difference between the expression pattern of Stk17b in the cerebella of wild-type and *Mwk* mice.

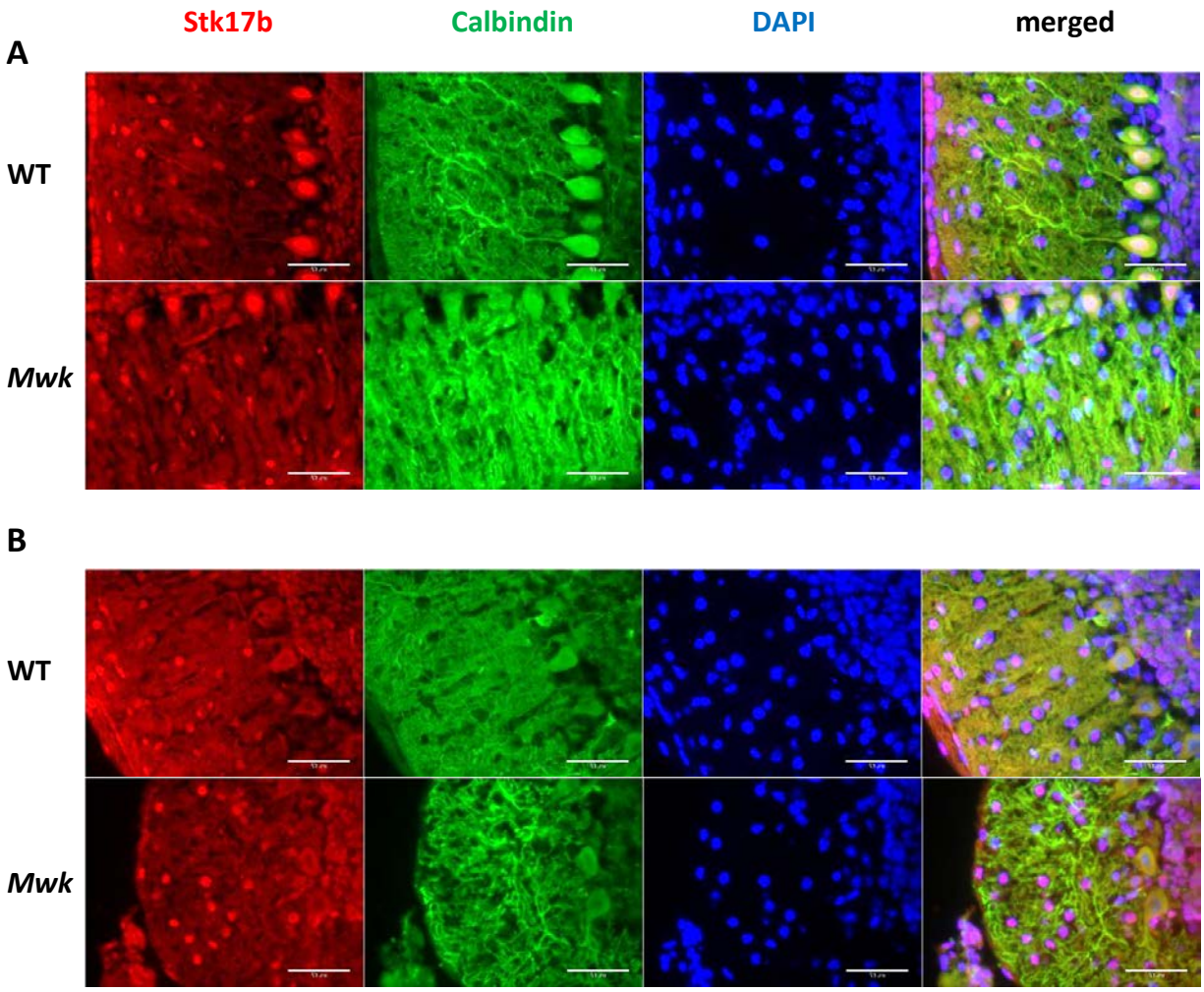

Figure 6-15. Expression of Stk17b protein by immunohistochemistry shows no difference between wild-type (WT) and *Mwk* cerebella at P20. Stk17b is strongly expressed in the nucleus (A) or in the cytoplasm (B) of Purkinje cells of the cerebellum in both wild-type and *Mwk* mice. Some expression is also evident in the granule cells, as well as in the cells of the molecular cell layer (basket cells or stellate cells). Scale bar = 50 µm. n=2

Analysis of potential transcription factor binding sites of genes identified in the microarray experiment

A Transcription Element Search System (TESS) was used to identify whether the six confirmed genes have any common transcription factor binding sites that could regulate their expression (http://www-bimas.cit.nih.gov/molbio/signal/). Also, we wanted to investigate whether any of the genes have potential NFAT transcription factor binding sites, as the calcineurin/NFAT signalling pathway is of interest to us and we could not study it due to the lack of good NFAT antibodies (Chapter 4). Sequence 1 Kb upstream of the gene of interest including 10 bp of the 5' UTR was used for the analysis. Table 6-5 shows common transcription factor binding sites among *Car2, Cntn3, Ipo5, Opn2, Stk17b* and *Sv2c.* Transcription factor binding sites unique to each gene are shown in Table 6-6.

There was a substantial amount of overlap between genes that change at P11 and P14. However, since genes that change at P11 were all up-regulated and genes changing at P14 were down-regulated, it likely means that changes in expression of these genes in *Mwk* mice were not caused by the common transcription factors. Genes *Car2, Ipo5, Opn3* and *Sv2c* all appeared to have a CREB transcription factor binding site, even though *Ipo5, Opn3* and *Sv2c* were up-regulated in *Mwk* mice and *Car2* was down-regulated. In Chapter 4, western blot experiments showed increase in phosphorylated CREB (active form of CREB) levels in *Mwk* whole cerebellar lysates starting at P21. However, in the cerebellum P-CREB was expressed in Purkinje cells as well as granule cells. Therefore it was not clear whether the increase of P-CREB did occur in Purkinje cells. The fact that the up-regulated genes as well as a down-regulated gene from the microarray study have a predicted CREB transcription factor binding site does not help us understand, whether P-CREB levels are changed in Purkinje cells and whether it affects the expression of genes in the *Mwk* mice.

Table 6-5. Transcription factors that have potential binding sites in the chosen gene set. Potential binding sites are identified using the Transcription Element Search System (TESS). Transcription factors that are unique to a particular age and present in all genes in that age are shown in **blue**.

P11 change			P14 change		P18 change
↑	↑	↑	↓	↓	↑
Ipo5	Opn3	Sv2c	Car2	Stk17b	Cntn3
alpha-CBF	alpha-CBF	alpha-CBF	alpha-CBF	alpha-CBF	-
-	alpha-CP1	alpha-CP1	-	alpha-CP1	-
alpha-IRP	alpha-IRP	alpha-IRP	alpha-IRP	alpha-IRP	-
AP-1	AP-1	-	AP-1	-	-
AP-2	-	AP-2	AP-2	-	-
box 4	box 4	box 4	box 4	box 4	-
c-Jun	**c-Jun**	**c-Jun**	-	-	-
-	-	c-Myc	-	-	c-Myc
-	c-Myb	-	c-Myb	c-Myb	-
C/EBP	-	C/EBP	-	-	-
CAAT	-	-	-	CAAT	-
CAC-binding pro	CAC-binding pro	CAC-binding pro	CAC-binding pro	CAC-binding pro	-
CACCC-binding f	CACCC-binding f	CACCC-binding f	CACCC-binding f	CACCC-binding f	CACC-binding f
CBF-B	CBF-B	CBF-B	CBF-B	CBF-B	-
CCAAT-binding f	CCAAT-binding f	CCAAT-binding f	CCAAT-binding f	CCAAT-binding f	-
CDP	CDP	CDP	CDP	CDP	-
-	-	CELF	-	-	CELF
CIIS1	CIIS1	-	-	-	CIIS1
-	core	-	-	core	-
CP1	CP1	CP1	CP1	CP1	-
CP2	CP2	CP2	CP2	CP2	-
CREB	CREB	CREB	CREB	-	-
CTF	CTF	CTF	CTF	CTF	-
D	-	D	D	D	-
-	DBP	-	-	DBP	-
-	enhancer	-	-	enhancer	-
-	-	-	F2F	-	F2F
Fral	Fral	-	-	-	-
gammaCAC2	gammaCAC2	gammaCAC2	gammaCAC2	gammaCAC2	gammaCAC2
GATA-1	-	-	-	-	GATA-1
GGTGG	-	-	GGTGG	-	-
-	GG-II, GG-I	GG-II, GG-I	-	GG-II, GG-I	-
GR	GR	GR	GR	GR	GR
GT-I	GT-I	GT-I	GT-I	-	-
H1TF2	H1TF2	H1TF2	H1TF2	H1TF2	-
H4TF-1	-	H4TF-1	-	-	H4TF-1
H4TF-2	H4TF-2	H4TF-2	H4TF-2	H4TF-2	H4TF-2
-	-	-	HiNF-A	HiNF-A	HiNF-A
-	-	HNF-1	HNF-1	-	HNF-1
-	kappaY factor	-	-	kappaY factor	-
MAZ	MAZ	MAZ	-	MAZ	-

LF-A1	LF-A1	LF-A1	-	LF-A1	-
NF-1	NF-1	NF-1	NF-1	NF-1	NF-1
NF-1/L	NF-1/L	NF-1/L	NF-1/L	-	-
NF-E	NF-E	NF-E	NF-E	NF-E	-
NF-E2	NF-E2	NF-E2	NF-E2	NF-E2	NF-E2
NF-Y	NF-Y	NF-Y	NF-Y	NF-Y	-
-	-	-	muEBP-C2	muEBP-C2	-
-	PEA3	PEA3	-	PEA3	PEA3
Pit-1	Pit-1	Pit-1	Pit-1	Pit-1	Pit-1
PTF1-beta	-	-	-	-	PTF1-beta
Sp1	Sp1	Sp1	Sp1	Sp1	Sp1
SRF	SRF	SRF	SRF	SRF	-
-	-	-	**TATA**	**TATA**	-
-	-	TBP	TBP	TBP	TBP
-	-	-	**TFE3-S**	**TFE3-S**	-
-	-	-	TFIID	TFIID	TFIID
-	-	vHNF1	vHNF1	-	vHNF1
window 4	window 4	window 5	window 4	window 4	-
-	window 5	-	window 5	-	-
-	window 9	-	-	window 9	-

Table 6-6. Transcription factors that have potential binding sites in the chosen gene set and are unique to the different genes.

Ipo5	**Opn3**	**Sv2c**	**Car2**	**Stk17b**	**Cntn3**
3' enhancer, HM	ATF	box 5	IRS	MEP-1	a-MEF2
alpha-CP1	CBF (2)	E2F	TGT3	PR	CSBP-1
B1	hexamer element	gERE, gastrin E			g
II	HiNF-C	NF-1B1			GATA-2
LyF-1	HNF-3	PER2			GATA-3
NF-E1c	Oct-01	window 10			LF-A1
					myogenin
					proximal region site
					TIN-1

A number of transcription factor binding sites common to genes that were changed at P11 and P18 are unlikely to cause changes at two different time points, as they would most likely influence the expression of genes at the same time. However, other co-factors could contribute to the expression at different time points. Some transcription factors that were unique to genes changing at P11, but not affecting all genes at P11 are C/EBP and Fral. And the only transcription factor that influenced all three genes with changed expression at P11 is c-Jun. Therefore, it is possible that up-regulation of *Ipo5, Opn3* and *Sv2c* is mediated by the c-Jun transcription factor. Transcription factors that were unique to genes down-regulated at P14 include mu-EBP/C2, TATA and TFE3-S. The normal activity of one of these transcription factors could be altered in *Mwk* mice, and could cause down-regulation of its targets.

According to TESS, none of the genes have a predicted NFAT transcription factor binding site.

Summary

The microarray analysis revealed that Purkinje cells of *Mwk* mice have alterations in their gene expression when compared to wild-type mice. A combined gene set from RMA and PLIER analysis algorithms revealed 44 genes, from which 14 genes were chosen for further analysis, due to their most uniform expression among all wild-type or all *Mwk* samples. qRT-PCR experiments were able to confirm changes in expression for six of these genes: *Car2*, *Cntn3*, *Ipo5*, *Opn3*, *Stk17b* and *Sv2c*. *In situ* hybridisation studies demonstrated that all of these genes are expressed in the Purkinje cells of the cerebellum. Expression of *Ipo5*, *Opn3* and *Sv2c* changes as early as P11, which was the earliest tested time-point. Expression of *Car2* and *Stk17b* shows change at P14. And expression of *Cntn3* demonstrates change at P18.

Discussion

The TRPC3 ion channel with a point mutation in the *Mwk* mice becomes active at lower mGluR1 agonist concentrations, while the wild-type channel remains inactive (Becker et al 2009). This likely leads to increased influx of calcium ions into the Purkinje cells, and in Chapter 4 we have shown deregulations in several Ca^{2+} signalling cascades, confirming changes in Ca^{2+} levels. Ca^{2+} signalling is important for normal neuronal function and its alterations would likely lead to transcriptional changes inside the cells (Greer & Greenberg 2008). The purpose of this work was to identify gene expression changes in Purkinje cells between the wild-type and *Mwk* mice, in order to elucidate the possible pathways that lead to abnormal dendritic development and function of the Purkinje cells.

Indeed, our microarray experiment revealed changes in gene expression between Purkinje cells of wild-type and *Mwk* mice at the age of P18, which is just prior to the dendritic abnormalities evident in *Mwk* mice *in vivo* and the onset of cerebellar ataxia.

Microarray studies of other ataxia mouse mutants

Microarray experiments have been used for other mouse models of cerebellar ataxia in order to try to elucidate pathways that lead to neurodegeneration. Some of the genes that are deregulated in other cerebellar ataxias, or their family members, are also deregulated in the *Mwk* Purkinje cells.

Spinocerebellar ataxia type 1 (SCA1) is a neurodegenerative disease caused by the expansion of a glutamine repeat in the ataxin-1 protein (Orr et al 1993). The primary line of SCA1 mouse models has 82 glutamines in its ataxin-1 protein (Ataxin-1-82Q) (Burright et al 1995). These mice display poor rotarod performance, subtle atrophy of the Purkinje cell dendrites, and gait abnormalities (Burright et al 1995; Clark et al 1997). Other mouse models of SCA1 include $Atxn1^{154Q/+}$, where Ataxin 1 protein has 154 polyglutamine repeats, and $Atxn1^{-/-}$, in which *Ataxin 1* gene is knocked

out. From microarray studies, *Ipo5* gene was found to be slightly down-regulated in Atxn1$^{-/-}$ and Atxn1$^{154Q/+}$ mice, whereas in our microarray analysis we see up-regulation of *Ipo5* in *Mwk* Purkinje cells. Also, a *Car8* gene, which is a family member of *Car2* (down-regulated *in Mwk* Purkinje cells), was identified to be down-regulated in Ataxin-1-82Q and Atxn1$^{-/-}$ mice, while *Car9* was down-regulated in Ataxin-1-82Q, Atxn1$^{-/-}$ and Atxn1$^{154Q/+}$ mice (Crespo-Barreto et al 2010; Serra et al 2004; Serra et al 2006).

Staggerer mice have a loss-of-function mutation in a gene encoding the transcription factor RORα and have very similar abnormalities in cerebellar development to the SCA1 mice (Hamilton et al 1996; Sidman et al 1962). *Car8* gene was also found down-regulated in *staggerer* mice (Gold et al 2003). Our microarray analysis revealed some ribosomal proteins that were altered in the *Mwk* mice, most of them down-regulated, but Rpl10 is up-regulated. In *staggerer* mice Rlp10a was, however, down-regulated. Zinc finger proteins were down-regulated in *Mwk* mice, and another zinc family member gene was also down-regulated in *staggerer* mice.

Interestingly, *Trpc3* gene expression is reduced in all three mouse models of SCA1, and also in *Staggerer* mice (Crespo-Barreto et al 2010; Lin et al 2000; Mitsumura et al 2011). This suggests that TRPC3, ataxin-1 and RORα could all be involved in the common pathogenesis pathway leading to cerebellar ataxia.

Another mouse model of cerebellar ataxia is SCA3, that expresses a mutant ataxin 3 with 79 glutamines (ataxin-3-Q79) and displays motor abnormalities due to neuronal dysfunction (Chou et al 2008). The dendrites of SCA3 Purkinje cells show signs of degeneration, including reduction in dendritic arborisation. In the *Mwk* mice, a proteasome 26S subunit gene was down-regulated, while other proteasome subunits were up-regulated in the SCA3 mouse model.

SCA7 is also a cerebellar ataxia disorder caused by the expansion of the polyglutamine tract in the ataxin 7 protein. Ataxin-7-Q52 mice display reduced dendritic arborisation of Purkinje cells (Chou

et al 2010). *Car2* gene is down-regulated in the SCA7 mouse model, which is consistent with our microarray results. Another gene down-regulated in the SCA7 mouse model is *Stk11*, which is a family member of *Stk17b*, which is down-regulated in the *Mwk* mice.

These observations are interesting, as they further demonstrate that different types of cerebellar ataxias could have a common signalling mechanism downstream of the mGluR1 signalling, which is described in Chapter 1.

Genes chosen from our microarray experiment for further investigation

We focused on the genes that showed the most uniform expression between the four replicates of wild-type and *Mwk* samples. The changes in six of those genes were confirmed by qRT-PCR. These genes are *Car2, Cntn3, Ipo5, Opn3, Stk17b* and *Sv2c*. Their expression in the cerebellum was studied by *in situ* hybridisation and revealed a very exclusive expression in Purkinje cells in the cerebellum for most genes. *Car2* was also expressed in the oligodendrocytes. We also performed a time-course qRT-PCR experiment, with ages P11, P14 and P18, where some genes showed alterations in expression as early as P11.

Genes up-regulated at P11

Time-course qRT-PCR experiments revealed that expression of *Ipo5, Opn3* and *Sv2c* genes is already altered at the earliest time point tested, P11.

- **Importin 5 (Ipo5)**

Expression of *Ipo5* in wild-type Purkinje cells is very low and only increases slightly at P18, whereas we see a very steep increase in the expression in *Mwk* Purkinje cells throughout the tested ages.

Ipo5 is a member of the importin beta family and is also known as RAN binding protein 5 (RanBP5), importin β3 (IMB3), or karyopherin β3 (Kpnb3). It is a nuclear import protein which

binds cargo directly through a nuclear localisation signal (Deane et al 1997; Jakel & Gorlich 1998). The transport of cargo from the cytoplasm into the nucleus by Ipo5 occurs through the nuclear core complex and is released after Ipo5 binds to the Ran^{GTP} protein, after which the importin protein is recycled back into the cytoplasm (Deane et al 1997; Jakel & Gorlich 1998). Ipo5 can therefore be found in the cytoplasm and at the nuclear rim (Yaseen & Blobel 1997). Loading and release of cargo from transport molecules is guided by the Ran^{GTP} gradient across the nuclear membrane (Gorlich & Kutay 1999). As Ran^{GTP} concentration is highest in the nucleus, transport of Ipo5 cargo can only be unidirectional into the nucleus. Ipo5 might also serve as a chaperone protein, protecting exposed basic domains of its cargo from outside interactions, while they are being imported into the nucleus (Jakel & Gorlich 1998; Jakel et al 2002).

Many proteins are known to be imported into the nucleus by Ipo5. For instance, Ipo5 transports transcription factors. These include c-Jun – a major component of the AP-1 transcription factor, which is involved in cell survival (Shaulian & Karin 2002; Waldmann et al 2007), and the p60TRP transcription regulator protein, which controls neuronal aging and survival (Heese et al 2004). Interestingly, p60TRP protein levels are down-regulated in patients suffering from Alzheimer's disease, which suggests its role in neurodegeneration. Due to interactions with c-Jun, p60TRP, and other transcription factors, Ipo5 can potentially influence gene expression, and increased *Ipo5* levels in the Purkinje cells could lead to an increase in transcription of other genes in the *Mwk* mice. Interestingly, Table 6-5 shows, that *Opn3* has a c-Jun transcription factor binding site, which could mean that increased *Ipo5* expression could be influencing increased *Opn3* expression.

Another protein that is transported by Ipo5 is p35, which is a specific activator of the Cdk5 cyclin-dependent kinase in the nervous system (Fu et al 2006). Cdk5 is not a typical cyclin-dependent kinase, as it is not involved in the cell cycle regulation. It is rather known for its involvement in a number of neural functions, such as cell signalling, synaptic plasticity, membrane transport and

neurite outgrowth (Dhavan & Tsai 2001; Nikolic et al 1996). Deregulation of Cdk5 might even contribute to Alzheimer's disease and Amyotrophic lateral sclerosis (ALS) (Dhavan & Tsai 2001; Patrick et al 1999). Cdk5 and p35 can be found both in the cytoplasm and in the nucleus (Gong et al 2003; Nikolic et al 1996). Cdk5 is imported into the nucleus via p35, from where it could influence neuronal activity, including synaptic plasticity, although the exact mechanism remains unknown (Fu et al 2006). One of its targets in the nucleus is a transcription factor MEF2 (Gong et al 2003). We have shown that *Cntn3* gene has a MEF2 transcription factor binding site, so disruptions in *Ipo5* expression could cause further transcriptional changes in Purkinje cells of *Mwk* mice.

Cdk5 knockout mice die around birth (Ohshima et al 1996). Therefore, Ohshima et al developed a *Cdk5* chimeric mouse ($cdk^{-/-} \leftrightarrow cdk^{+/+}$), which shows defects in Purkinje and granule cell migration (Ohshima et al 1999). The *Mwk* mice, however, do not display any migration defects. Also, neurite outgrowth is inhibited in dominant-negative Cdk5 cell mutants (Nikolic et al 1996). Increased levels of Ipo5 could be causing an abnormal balance in localisation of p35/Cdk5, which could affect the normal function of Cdk5, and cause a degree of inhibition of dendritic outgrowth in Purkinje cells of the *Mwk* mice.

Up-regulation of *Ipo5* very early on in the developmental stages of Purkinje cells could be the cause of the *Mwk* phenotype through further transcriptional changes, or through a mechanism of removal of vital proteins from the cytoplasm to the nucleus. Further experiments could look at the distribution of the Ipo5 protein in Purkinje cells, because it might be altered in the *Mwk* mice. Targets of Ipo5 could also be investigated further.

- **Opsin 3 (Opn3)**

Another gene that is up-regulated in *Mwk* Purkinje cells at the earliest tested time-point is *Opn3.* Expression of *Opn3* in wild-type mice at the ages P11, P14 and P18 shows a very slight increase in expression, however, in *Mwk* mice, *Opn3* is very significantly up-regulated.

Opn3 is also known as panopsin and encephalopsin. Opsins are members of the G-protein coupled receptors and function by activating G-protein and an effector enzyme and are mostly known for their role in vision (Halford et al 2001; Kumbalasiri & Provencio 2005; Terakita 2005). Opsin proteins comprise of seven families and Opn3 belongs to the encephalopsin/tmt-opsin subfamily (Terakita 2005). It is not yet clear which G protein this family is coupled to. Opn3 is a "non-classical" opsin as it has a low level of homology with other visual opsin proteins (approximately 30%) and is distributed widely throughout the organism, with high expression found in the brain and testis, and low expression levels in the heart, retina, and other organs (Blackshaw & Snyder 1999; Halford et al 2001). This is why it is likely that Opn3 has a distinctive and not yet identified function. Interestingly, the highest expression in the brain is in the Purkinje cells of the cerebellum, where they show a patterned expression from around week 3 (Blackshaw & Snyder 1999). Our *in situ* hybridisation results, however, showed equal expression in all cerebellar lobes.

Even though the exact function of Opn3 is unknown, one study implicated Opn3 in triggering vesicle exocytosis induced by light (Henkel et al 2006). What is more, it has been established that neurites grow by vesicle exocytosis into the plasma membrane (Hughes 1953; Meldolesi 2011; Pfenninger 2009; Tang 2008), and it is thought that calcium signalling, as well as rearrangements of the cytoskeleton have an important role in that process (Hsu et al 2004). Because *Mwk* mice have less arborised Purkinje cell dendrites, the proposed function of Opn3 in exocytosis is very interesting. Perhaps, there is a mechanism that prevents dendrite outgrowth through vesicles in *Mwk* mice, and therefore *Opn3* gene is being up-regulated in order to repair exocytosis. This

suggests that Opn3 could play a previously unknown role in dendritic development, particularly in the Purkinje cells of the cerebellum.

- **Synaptic vesicle glycoprotein 2c (Sv2c)**

Another gene up-regulated in the *Mwk* mice in all three ages is *Sv2c*. In wild-type Purkinje cells, expression of *Sv2c* is very low, slightly increasing at P18, in *Mwk* mice, however, the expression is continuously up-regulated and is drastically increased from P11 to P18.

SV2C is a member of the synaptic vesicle 2 (SV2) protein family. SV2 is a very conserved transmembrane glycoprotein, present on surfaces of synaptic vesicles of all vertebrates, and plays an important role in synaptic vesicle exocytosis (Buckley & Kelly 1985; Dardou et al 2011). SV2 proteins have a significant homology to bacterial sugar transporters and to other transporter types, which is why they could potentially be involved in transporting an unknown substrate into the synaptic and secretory vesicles (Bajjalieh et al 1992; Janz & Sudhof 1999). At some point they were thought to transport Ca^{2+}, but this was later disproven (Janz et al 1999; Lezzi et al 2005). Because distribution of the SV2 isoforms is not restricted to a particular neurotransmitter system, they probably do not function as neurotransmitter transporters. No other SV2 transporter activities have been identified to date (Dardou et al 2011). It has been suggested that SV2 proteins could serve as structural components of the synaptic vesicles. However, SV2 proteins are not required for the normal synapse assembly (Janz et al 1998). Also, their function in Ca^{2+} dependent endocytosis has been proposed (Chang & Sudhof 2009).

Three isoforms of SV2 exist: SV2A, SV2B and the most recently discovered SV2C (Janz et al 1998; Janz & Sudhof 1999). Among the family of SV2 proteins, SV2A has been studied most extensively, whereas little is known about SV2C. It has been proposed that all three isoforms serve a similar function (Janz et al 1998), however knockout studies show that in the absence of SV2A, other

isoforms do not rescue the phenotype, which suggests that they could, in fact, serve different functions (Janz et al 1999)

SV2C is an N-glycosylated protein with 12 transmembrane domains, concentrated on the surface of small synaptic vesicles and primarily expressed in the brain, where it shows a very restricted distribution in only a few brain areas, including low mRNA expression and strong protein expression in the Purkinje cells of the cerebellum (Dardou et al 2011; Janz & Sudhof 1999). SV2C are primarily associated with VGAT vesicles (vesicular gamma-aminobutyric acid [GABA] transporters), especially in the Purkinje cell layer, but are also present in VGlut1 vesicles (vesicular glutamate transporters) (Dardou et al 2011; Gronborg et al 2010). It has been hypothesised that SV2C could be involved in neurotransmitter release and synaptic transmission, as well as exocytosis (Dardou et al 2011; Schivell et al 2005). Its involvement in exocytosis suggests that, like Opn3, it could also be involved in the dendritic outgrowth by vesicle exocytosis. However, being a synaptic vesicle protein, SV2C would most likely be involved in the vesicle trafficking at the terminal of the Purkinje cell axon.

Dardou and colleagues mention SV2C knockout mice, however they do not discuss their phenotype and only use the mouse brain to test specificity of the antibody (Dardou et al 2011). It would be curious to investigate the effects of SV2C knock down on the development of the cerebellum. Also, it would be interesting to cross the $SV2C^{-/-}$ mouse with the *Mwk* mouse to observe whether down-regulation of SV2C would rescue the *Mwk* dendritic phenotype.

Genes down-regulated at P14

Microarray and qRT-PCR experiments showed down-regulation of two genes in the *Mwk* Purkinje cells starting at P14. These genes are *Car2* and *Stk17b*.

- **Carbonic anhydrase 2 (Car2)**

Our data demonstrates that the expression of *Car2* in the wild-type cerebellum is increasing from P11 to P18, and even though the same is happening in the *Mwk* Purkinje cells, there is significantly less expression compared to wild-type cells, starting at P14 and continuing at P18.

Car2 is a member of the carbonic anhydrase (CA) family. CAs are zinc-containing metalloenzymes that catalyse a reversible hydration of carbon dioxide: $CO_2 + H_2O \rightarrow HCO_3^- + H^+$, thus playing a major role in pH homeostasis regulation, which is important for cellular growth (Meldrum & Roughton 1933; Nogradi & Mihaly 1990; Thomas 1989). Sixteen isoforms of CAs have been identified, thirteen of which have enzymatic activity and three do not (Pan et al 2010). Because several CAs can be expressed in the same tissue, it is possible that they have different functions. Although it has been suggested that loss of one isozyme may lead to the up-regulation of another: for instance, there is increased Car4 activity in brains of Car2-deficient mice (Brion et al 1994). Human Car2 deficiency leads to renal tubular acidosis, osteopetrosis, cerebral calcification, and severe growth retardation (Sly et al 1983) and Car2-deficient mice have renal tubular acidosis (Lewis et al 1988). As with the *Mwk* mice, Car2 null mice were also generated by ENU mutagenesis (Lewis et al 1988) and no gross abnormalities in the brains of Car2 null mice have been reported (Ridderstrale & Wistrand 2000).

Car2 is the most abundant CA isozyme and is expressed in the cytoplasm of all major mammalian organs (Pan et al 2006; Sly & Hu 1995). Car2 is also the most abundant CA in the brain, although its levels of expression are much higher in colon, kidney and stomach (Pan et al 2006). In the cerebellum Car2 is expressed in the Purkinje cells and the oligodendrocytes. In the Purkinje cells it is expressed in the cell body, axons, and primary and secondary (but not tertiary) dendrites (Nogradi et al 1997). Expression of Car2 in the mouse starts around P9, peaks at P20, and after P26 starts to decline and stops being expressed by P32 (Nogradi et al 1997; Nogradi & Mihaly

1990). Interestingly, dendritic development of Purkinje cells occurs in parallel with *Car2* expression, suggesting that Car2 could play a role in their development.

Expression of Car2 was investigated in a mouse model of cerebellar ataxia – the *lurcher* mouse. *Lurcher* mice have a mutation in a cation channel GRID2, which causes a constitutively active inward current in the Purkinje cells (Zuo et al 1997). Purkinje cells of *lurcher* mice display abnormal development with less branched dendritic trees during the early phase of postnatal development and start degenerating at P10-P12, with only 10% of Purkinje cells left at P26 and disappear almost completely by three months (Caddy & Biscoe 1979). In the *lurcher* mice, Car2 protein expression is markedly reduced in the degenerating Purkinje cells, which also suggest a role of Car2 in the development of Purkinje cells. The authors propose that Car2 is required for increased rate of synaptogenesis, dendritic growth, establishment of neuronal connections and metabolic maturation. As mentioned before, Car2 levels were also down-regulated in a SCA7 mouse model of cerebellar ataxia, where ataxin protein has 52 glutamine repeats and causes cerebellar malfunction, including reduced Purkinje cell dendritic arborisation (Chou et al 2010). Therefore, reduction of *Car2* expression in the *Mwk* mice could cause abnormal development of Purkinje cell, perhaps via disturbed pH homeostasis.

- **Serine-threonine kinase 17b (Stk17b)**

Another gene that becomes down-regulated at P14 is *Stk17b*. Wild-type *Stk17b* increases in expression from P14 to P18. The *Mwk Stk17b*, however, is significantly less expressed than the wild-type *Stk17b* and is only slightly increasing in expression from P14 to P18.

Stk17b is also known as DRAK2 (DAP kinase-related apoptosis-inducing protein kinase). It is a member of the DAP (death associated protein) kinase family and is a immunoregulatory serine/threonine kinase with the highest expression levels in the lymphocytes, but is also present in the brain (McGargill et al 2004). Stk17b is a negative regulator of T cell activation, mature T cell

apoptosis and memory T cell development (Mao et al 2006; McGargill et al 2004). In the central nervous system, however, Stk17b serves an unknown function (Mao et al 2006). Expression of Stk17b can be seen in both the cytoplasm and the nucleus (Kuwahara et al 2006), which was also confirmed by our immunohistochemistry experiments. It has been shown that nuclear localisation of Stk17b, induced by UV irradiation, causes apoptosis-like cell death *in vitro* (Kuwahara et al 2006). Our results demonstrated that localisation of Stk17b was found at equal levels in the cytoplasm and the nucleus, and did not differ in *Mwk* mice at P20. It is still possible for Stk17b to localise more to the nucleus at later time points, and cause Purkinje cell death in *Mwk* mice from four months onwards.

Stk17b$^{-/-}$ mice have been generated, but only their immune system has been investigated (McGargill et al 2004). Studying the brain of the knock-out mice would be useful in order to investigate the role of Stk17b in the brain, and it would be interesting to compare it with the pathology of the *Mwk* brain. Also, Stk17b overexpression mice exist (Mao et al 2006), and it would be curious to see whether crossing them with the *Mwk* mice would rescue the dendritic phenotype of Purkinje cells.

Gene up-regulated at P18

In the wild-type Purkinje cells, expression of *Cntn3* is invariable throughout P11-P18, whereas in the *Mwk* Purkinje cells *Cntn3* expression increases from P11 to P18, and becomes significantly up-regulated at P18.

- **Contactin 3 (Cntn3)**

Cntn3 is also known as Pang (plasmacytoma-associated neuronal glycoprotein) and BIG-1 (brain-derived immunoglobulin superfamily protein 1). Cntn3 is a glycosylphosphatidylinositol-anchored membrane protein, belonging to the immunoglobulin superfamily of neuronal adhesion molecules (Yoshihara et al 1994). Highest expression levels of *Cntn3* mRNA are found in the brain,

restricted to a subset of neurons, Purkinje cells being one of them; with expression in other tissues and non-neuronal cells within the nervous system as well (Yoshihara et al 1995; Yoshihara et al 1994). Expression of Cntn3 starts at P2 and reaches its maximum in the adult brain. *In vitro* Cntn3 has been shown to have neurite outgrowth-promoting activity. It has also been proposed that Cntn3 could be involved in neuronal network maintenance and synaptic plasticity (Yoshihara et al 1995).

Even though the role of Cntn3 in the cerebellum is not yet known, other members of the contactin family have been implicated in its development (Stoeckli 2010). For example, contactin family member TAG1 is required for the maturation of granule neurons, for the pathfinding of the parallel fibres and could even be implicated in influencing Purkinje cell dendritic development via the input from parallel fibres (Baeriswyl & Stoeckli 2008; Stottmann & Rivas 1998; Wang et al 2011). Another contactin family member – F3/contactin – has also been shown to be involved in the development of granule cells (Bizzoca et al 2003; Coluccia et al 2004). This indicates that Cntn3 could also play a previously unknown function in the development of the cerebellum, and Purkinje cells in particular.

Distribution of proteins encoded by genes of interest in wild-type vs. *Mwk* cerebella

We have looked at the localisation of Stk17b in the mouse cerebellum, of wild-type and *Mwk* mice, and discovered no differences. In future experiments it would be useful to examine protein expression of the other genes, identified in the microarray experiment. If their localisation differs in *Mwk* mice, it could help us understand the mechanism behind abnormal Purkinje cell development in *Mwk* mice.

Transcription factor binding sites of the genes of interest

Identification of transcription factor binding sites for our genes of interest could help identify common regulators of the genes and could help understand the mechanism of gene deregulation.

One of the potential transcription factor binding sites that is only present in *Cntn3* is a-MEF2. Interestingly, MEF2 has been implicated in the pathogenesis of SCA1, where it has shown to be repressed by Ataxin-1 (Bolger et al 2007). Perhaps, events that take place before P18 in the *Mwk* mouse lead to the activation of MEF2, which causes increased expression of *Cntn3*. Also, MEF2 and NFAT transcription factors co-regulate gene expression, responsible for heart failure (Putt et al 2009). This indicates that Cntn3 gene expression could be also regulated by NFAT signalling. No other NFAT transcription factor binding sites were identified in this experiment.

c-Jun transcription factor has potential binding sites on all three genes up-regulated at P11: *Ipo5, Opn3* and *Sv2c*. It is activated by c-Jun N-terminal kinase (JNK), and interestingly, increased activation of JNK was observed in a mouse model of cerebellar ataxia – the *Lurcher* mouse (Repici et al 2008). *Lurcher* mice have a constitutively open cation channel GRID2 which leads to dendritic abnormalities of Purkinje cells and causes their progressive death from two weeks of age (Zuo et al 1997). *Lurcher* mice also have reduced expression of Car2, which we also see in the Purkinje cells of *Mwk* mice. So, it is possible that both *Lurcher* and *Mwk* mice display Purkinje cell dendritic abnormalities via activation of the c-Jun transcription factor, which leads to up-regulation of *Ipo5, Opn3* and *Sv2c*; and through down-regulation of *Car2*.

Several genes also have a putative CREB transcription factor binding site, but some of them are up-regulated (*Ipo5, Opn3* and *Sv2c*), and one is down-regulated (*Car2*). So it is unclear, how CREB influences transcription of these genes.

The software that allows prediction of transcription factor binding sites can give good guidance, but it is not 100% accurate. Therefore, these results need to be considered cautiously and have to be verified.

Summary

Our work has revealed that the *Mwk* mutation in the TRPC3 ion channel causes changes in gene expression in the Purkinje cells of the cerebellum, which most likely occurs due to deregulation of the Ca^{2+} signalling pathways. We have confirmed changes in expression of six genes: *Car2, Cntn3, Ipo5, Opn3, Stk17b* and *Sv2c*. Moreover, the time-course experiment revealed that expression of *Ipo5, Opn3* and *Sv2c* becomes up-regulated as early as P11 (which was the earliest time-point which was tested); expression of *Car2* and *Stk17b* becomes down-regulated after P14; and expression of *Cntn3* becomes up-regulated after P18. All of these genes are expressed in the Purkinje cells of the cerebellum, as demonstrated by our *in situ* hybridisation experiments.

Changes in expression of *Ipo5* could cause further changes in cell gene expression, as it is known to import various transcription factors into the nucleus. *Opn3* and *Sv2c* could potentially both be involved in the mechanism of neurite outgrowth by vesicle exocytosis, and changes in their expression could cause alterations in this mechanism and cause the *Mwk* phenotype of Purkinje cells. Car2 could cause alterations in pH levels of Purkinje cells. Function of Stk17b in the brain has not been established, but since it is an apoptosis-inducing kinase, it could be responsible for Purkinje cell death at a later stage; or it could serve a previously unknown function. Cntn3 could cause changes in Purkinje cell neurite outgrowth through an unknown mechanism.

Changes in expression of any of these genes could potentially be the cause of abnormal development of Purkinje cell dendrites and further studies need to be done, in order to narrow down the exact mechanism.

CHAPTER 7. General Discussion

In this thesis I have described the current work on a mouse model of cerebellar ataxia – the *Moonwalker* (*Mwk*) mouse, which has a gain-of-function mutation in a non-selective transient receptor potential canonical channel, type 3 (TRPC3).

The results obtained in this thesis have contributed to the notion that a common pathway potentially connects different types of cerebellar ataxias, and includes the ion channel TRPC3. The study of the interaction partners in combination with the study of Ca^{2+} signalling pathways has potentially revealed a mechanism downstream of Ca^{2+} influx that could contribute to the disease pathogenesis. This mechanism involves Ca^{2+}/calmodulin-dependent protein kinase IV (CaMKIV), which was not only shown to bind the wild-type TRPC3 channel, but was also shown to have reduced activity (as measured by phosphorylation levels) in *Mwk* Purkinje cells. Moreover, I have identified changes in gene expression in the Purkinje cells of *Mwk* mice, with genes *Ipo5*, *Opn3* and *Sv2c* being up-regulated as early as P11. Changes in expression of *Opn3* lead to a possibility that Purkinje cells of *Mwk* mice have a defect in the dendritic outgrowth mechanism by vesicle exocytosis. Lastly, I have optimised an effective method of laser-capture microdissection (LCM) that provides high quality RNA for further analysis.

Figure 7-1 compares signalling events that occur in the wild-type Purkinje cell with events that occur in the *Mwk* Purkinje cell, which were identified in this thesis, and lead to abnormal development of Purkinje cell dendritic tree and cerebellar ataxia.

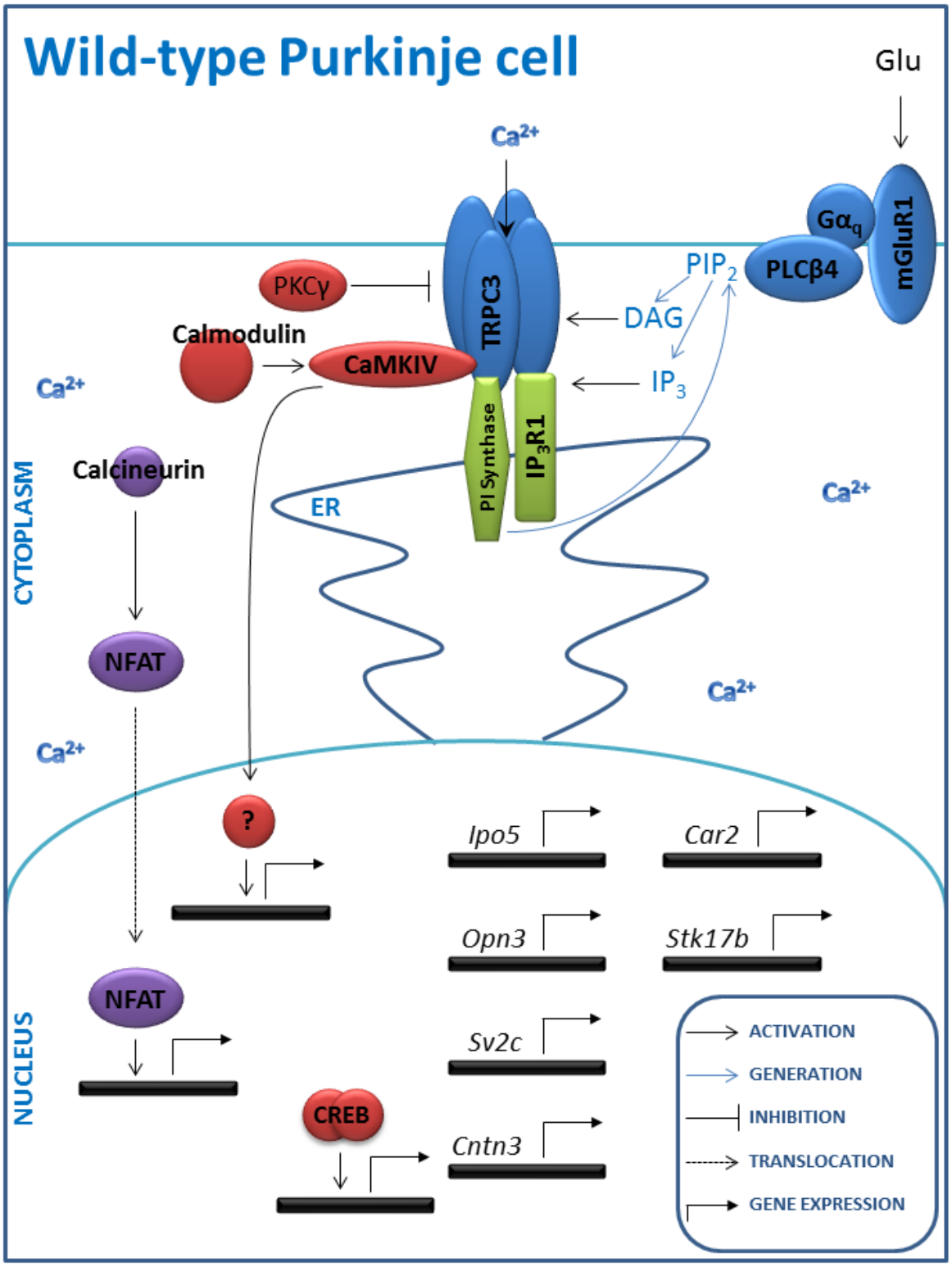
Wild-type Purkinje cell
Glu
Ca2+
Gαq
mGluR1
PLCβ4
PIP2
DAG
IP3
TRPC3
PKCγ
Calmodulin
CaMKIV
Ca2+
PI Synthase
IP3R1
Calcineurin
ER
Ca2+
CYTOPLASM
NFAT
Ca2+
?
Ipo5
Car2
Opn3
Stk17b
NFAT
Sv2c
CREB
Cntn3
NUCLEUS
ACTIVATION
GENERATION
INHIBITION
TRANSLOCATION
GENE EXPRESSION

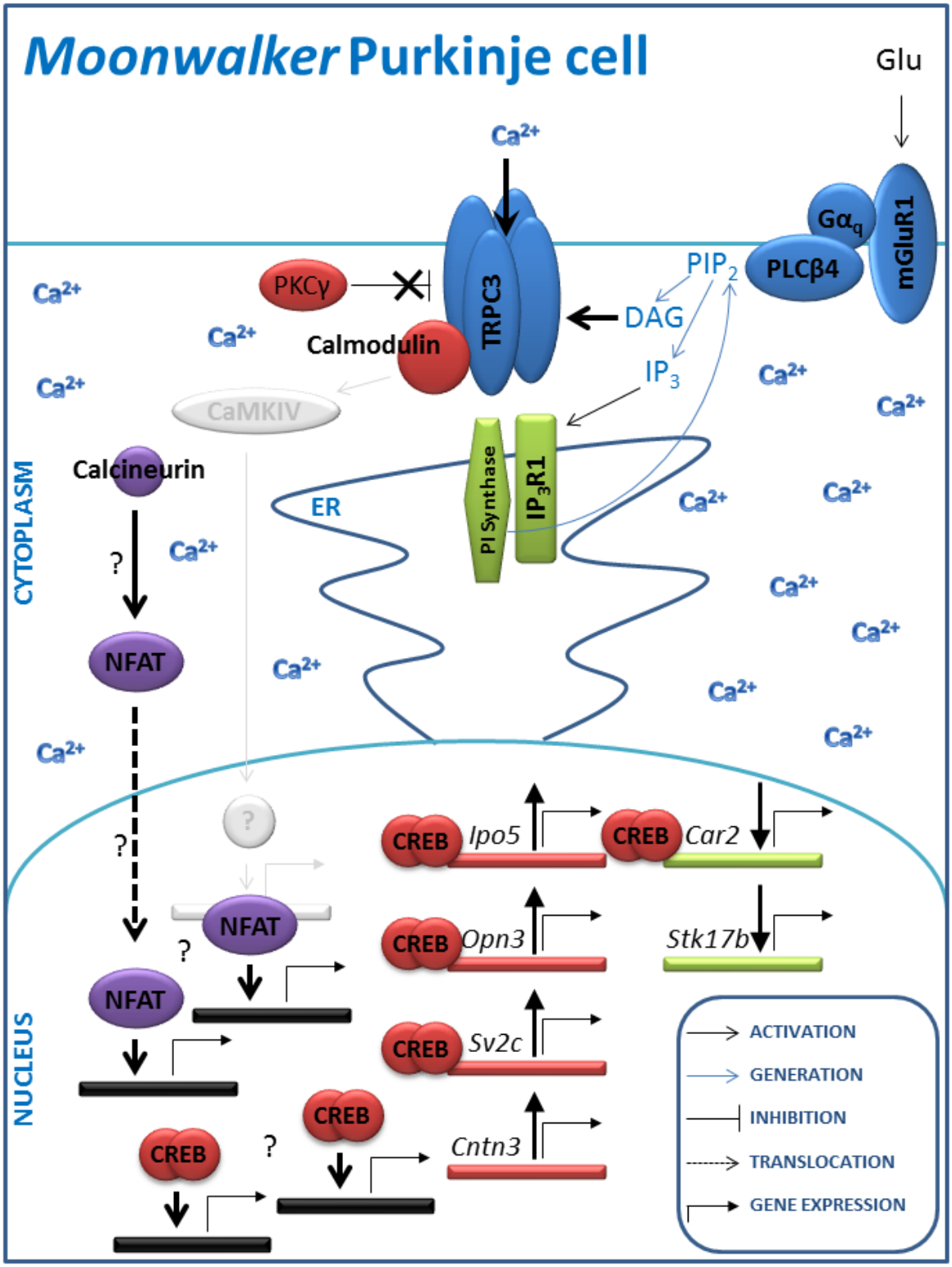
Moonwalker Purkinje cell
Glu
Ca2+
TRPC3
PKCγ
Calmodulin
CaMKIV
Calcineurin
PIP2
DAG
IP3
PLCβ4
Gαq
mGluR1
PI Synthase
IP3R1
ER
CYTOPLASM
NUCLEUS
NFAT
CREB
Ipo5
Car2
Opn3
Stk17b
Sv2c
Cntn3
ACTIVATION
GENERATION
INHIBITION
TRANSLOCATION
GENE EXPRESSION

Figure 7-1. Comparison between the events occurring in wild-type and *Moonwalker* Purkinje cells surrounding TRPC3 signalling. Wild-type Purkinje cell: TRPC3 activation can be achieved by several mechanisms. When neurotransmitter glutamate (Glu) activates mGluR1, the protein activates $G\alpha_q$, which activates PLCβ4. PIP_2 then gets cleaved by PLCβ4 to produce DAG and IP_3. These molecules generate two different activation mechanisms. One is the direct activation of TRPC3 by DAG, which causes the channel to open and allow positive ions, e.g. Ca^{2+}, to enter Purkinje cells. The other mechanism involves activation of IP_3R1 intracellular Ca^{2+} store channel by IP_3. Binding of IP_3R1 to TRPC3 through displacement of calmodulin is known to activate TRPC3. Phosphorylation of TRPC3 by PKCγ is a negative regulation mechanism which causes inactivation of TRPC3. This thesis has identified two novel interaction partners of TRPC3: PI synthase and CaMKIV. PI synthase generates PIP_2 which lies upstream of TRPC3 activation. CaMKIV is a kinase activated by calmodulin in response to rising Ca^{2+} levels and controls gene transcription, it likely lies down-stream of TRPC3 signalling. NFAT/calcineurin signalling cascade, which also controls gene transcription, is known to be activated by TRPC3 in heart and muscle, and therefore is potentially regulated by TRPC3 in Purkinje cells as well. In fact, it has been demonstrated that inability of PKCγ to phosphorylate TRPC3 causes reduction in NFAT-dependent gene expression. ***Moonwalker* Purkinje cell:** in *Mwk* Purkinje cells it was demonstrated that TRPC3 becomes more sensitive to activation. This, together with changes in activity of all Ca^{2+} signalling proteins that were tested in this thesis, strongly suggests elevated Ca^{2+} levels inside Purkinje cells of *Mwk* mice. In particular, we observed reduction in CaMKIV phosphorylation in *Mwk* mice from P21, which would reduce its activity and sequentially could cause changes in gene expression. This could be either achieved by an increased PP2A phosphatase activity, or perhaps through abnormal binding to TRPC3. For example, it is possible that *Mwk* TRPC3 cannot bind CaMKIV, and this binding might be important for its phosphorylation. Or, *Mwk* TRPC3 could have an abnormally high affinity for calmodulin, which could prevent it from activating its downstream targets. Due to a known connection between TRPC3 activation and the NFAT/calcineurin signalling pathway, it is possible that increased Ca^{2+} inside *Mwk* Purkinje cells due to abnormal function of TRPC3 could lead to changes in the NFAT/calcineurin signalling pathway. Since calcineurin is activated by Ca^{2+}, we could assume that the gene expression controlled by this pathway is increased. This, however, needs to be established. CREB is another transcription factor that was shown to have increased phosphorylation in *Mwk* cerebella. It is not, however, clear whether Purkinje cells also have an increase in CREB phosphorylation, or if it is decreased or unchanged. Increased phosphorylation would mean increased CREB-dependent gene transcription, like in the case of *Ipo5, Opn3* and *Sv2c*. These genes were all shown to be increased in expression in Purkinje cells of *Mwk* mice by microarray, and have a predicted CREB binding site in their promoters. Expression of *Cntn3* is also increased in *Mwk* Purkinje cells later in development, whereas expression of *Car2* and *Stk17b* is decreased. Changes in gene expression in *Mwk* mice likely lead to the observed abnormalities in Purkinje cell dendrites, as well as cerebellar ataxia.

Binding partners

Activity of the TRPC3 ion channel is regulated by several mechanisms. One of these requires activation of the G protein-coupled metabotropic glutamate receptor 1 (mGluR1) by glutamate (Glu). The mGluR1 activates G protein $G\alpha_q$, which activates phospholipase C β4 (PLCβ4). Active PLCβ4 generates diacylglycerol (DAG) and inositol 1,4,5-trisphosphate (IP_3) from phosphatidylinositol 4,5-bisphosphate (PIP_2). DAG directly activates TRPC3 causing its activation and opening. IP_3 activates IP_3R1 – an intracellular Ca^{2+} store channel. IP_3R1 activates TRPC3 by displacing calmodulin and binding to the same site on the channel. Protein kinase C γ (PKCγ) is a negative regulator of TRPC3 activity, as phosphorylation by PKCγ causes the channel to close. There is evidence that the S4/S5 linker of TRPC3 is subject to PKCγ phosphorylation and that the S4/S5 linker harbouring a *Mwk* mutation cannot be phosphorylated by PKCγ *in vitro* (Becker et al 2009).

Many of the proteins involved in TRPC3 activity regulation have been implicated in several cerebellar ataxias. For example, PKCγ and IP_3R1 are causes of spinocerebellar ataxias SCA14 and SCA15, respectively (Abeliovich et al 1993; van de Leemput et al 2007; Yabe et al 2003). Mutation in PKCγ in SCA14 causes Ca^{2+} homeostasis abnormalities, which are mediated by TRPC3 (Abeliovich et al 1993; Adachi et al 2008; Yabe et al 2003). Deletion or mutation in the *Ip$_3$r1* gene in SCA15 causes decreased expression of the mutated protein itself, which suggests changes in Ca^{2+} homeostasis (Bezprozvanny 2011; van de Leemput et al 2007). IP_3R1 has also been implicated in SCA2 and SCA3, where the channel interacts with mutant ataxin-2 and ataxin-3 proteins, respectively; which causes it to become overly sensitive to its activator IP_3 and results in an increased Ca^{2+} release from intracellular stores (Chen et al 2008; Liu et al 2009). Expression of IP_3R1 is also reduced in SCA1, and could contribute to the disease pathogenesis (Lin et al 2000; Serra et al 2004). Proteins $G\alpha_q$, mGluR1, and PLCβ4 that are also involved in TRPC3 activation, have been implicated in motor and coordination abnormalities in knockout studies. They all

display cerebellar ataxia, loss of long-term depression (LTD) in Purkinje cells and impairment of climbing fibres elimination (Chen et al 1995; Hashimoto et al 2001; Ichise et al 2000; Inoue et al 1998; Kano et al 1995; Kano et al 1997; Kano et al 1998; Offermanns et al 1997).

Therefore it is possible that different types of cerebellar ataxias could have the same mechanism of disease pathogenesis, and TRPC3 could be a part of that mechanism. Interestingly, expression of TRPC3, $G\alpha_q$, IP_3R1, mGluR1, PKCγ and PLCβ4 in the cerebellum is almost exclusively limited to the Purkinje cells (Baude et al 1993; Furuichi et al 1993; Huang et al 2007; Kose et al 1988; Nakamura et al 2004; Tanaka et al 2000; Watanabe et al 1998). This suggests that the common mechanism uniting these proteins could be Purkinje cell-specific and important for the disease mechanism and possibly development of these neurons in particular.

I have identified interaction partners of the TRPC3 ion channel by mass spectrometry. With all proteins identified in this study as interaction partners of TRPC3, there is a possibility that they bind to the S4/S5 linker of the protein, which is the site of *Mwk* mutation. This is because they not only bind the full length wild-type TRCP3 protein, but also bind TRPC3 without its C- and without its N-terminus *in vitro*. So, either the proteins interact with two or more distinct sites on the N- and C- termini of TRPC3, or they interact with one of the intracellular loops of TRPC3, S4/S5 linker being one of them. In case they do bind the S4/S5 linker, this potentially means that interaction with the *Mwk* TRPC3 protein could be either stronger or weaker, or even at all absent. Unfortunately, mass spectrometry is not a sensitive enough technique to detect these changes, so we do not know whether the mutation makes a difference to the affinity of binding. A way to study the interactions between the *Mwk* TRPC3 and the confirmed binding partners of the wild-type TRPC3 could be to perform the same co-immunoprecipitation (co-IP) experiments that were used to confirm interactions in this thesis, but this time to express increasingly smaller parts of the wild-type protein. If the interaction indeed occurs at the S4/S5 linker, one could try to express it with a *Mwk* mutation and repeat the co-IP experiment. This way, the part of the TRPC3 would

probably be too small to allow proper function of the channel, so it is likely that it would not cause cell death, and could still be used to determine the interaction.

In my experiments, IP_3R1 was used as a positive control, as it is a known binding partner of TRPC3, which was also confirmed by this study (Boulay et al 1999; Kiselyov et al 1999). Interestingly, we identified that IP_3R1 not only binds the C-terminus of the TRPC3 protein as has been previously established (Boulay et al 1999), but could also bind other parts of the protein. The exact interaction site on the TRPC3 protein needs to be further analysed, because our data demonstrated that, along with binding to the C-terminus of TRPC3, IP_3R1 could also bind anywhere between the first amino acid of the N-terminus up to the last intracellular loop of the protein. If the binding occurs at the S4/S5 linker of the TRPC3 protein, it is possible that the interaction strength between TRPC3 and IP_3R1 could be altered. As Ca^{2+} entry through TRPC3 channels could activate a Ca^{2+} release from the stores through the IP_3R1 channel (Berridge 1998), changes in their interaction affinity could be the cause of the putative Ca^{2+} homeostasis alterations inside Purkinje cells.

Phosphatidylinositol (PI) synthase is another protein identified as an interaction partner of wild-type TRPC3. PI synthase is an enzyme upstream of IP_3 and DAG generation, which are the two molecules involved in TRPC3 activation (Hofmann et al 1999; Mikoshiba 2011a), so it can be involved in TRPC3 activation regulation. Moreover, binding between TRPC3 and PIP_2 – a product of PI synthase activity – might be required for TRPC3 to remain at the plasma membrane (Soboloff et al 2007). So any changes in the binding between PI synthase and the *Mwk* TRPC3 could contribute to the gain-of-function of the mutated TRPC3 channel.

The study also revealed that CaMKIV interacts with wild-type TRPC3, which is a previously unreported interaction. Moreover, when I studied levels of phosphorylation (hence, activation) of some of the key Ca^{2+} signalling proteins, it was discovered that CaMKIV phosphorylation is reduced in *Mwk* Purkinje cells. Reduced phosphorylation of CaMKIV in *Mwk* mice could possibly

be due to its abnormal interaction with the mutated TRPC3 protein. TRPC3 is known to bind calmodulin – an activator of the Ca^{2+}/calmodulin (CaM) signalling cascade, which includes CaMKIV (Tang et al 2001). This suggests that activation of the CaM signalling cascade by Ca^{2+} might require a formation of a protein complex with TRPC3. If, for example, CaMKIV cannot bind the *Mwk* TRPC3, this could prevent its phosphorylation. As well as possible abnormalities in binding to CaMKIV, *Mwk* TRPC3 could have changes in binding affinity to calmodulin. Calmodulin is bound to TRPC3 when the channel is un-stimulated. In the presence of Ca^{2+}, calmodulin is displaced by IP_3R1, which causes TRPC3 activation (Tang et al 2001). It is possible that calmodulin might remain bound to the *Mwk* TRPC3 even when the channel becomes activated, hence its inability to move could prevent it from activating its downstream targets, i.e. CaMKIV.

Results of the study of TRPC3 interaction partners provides more evidence in support of a common signalling pathway possibly connecting several cerebellar ataxias, and includes $G\alpha_q$ protein, IP_3R1, mGluR1, PLCβ4, and PKCγ. Moreover, studies of the *Mwk* mice demonstrate that this signalling pathway could be responsible not only for the correct function of the Purkinje cells, but also for the proper development of their dendrites. Events that occur downstream of the common signalling pathway, which are important for Purkinje cell function and development, have not been identified. The results presented in this study suggest that CaMKIV could be involved in that pathway. Below I also describe which other signalling pathways are affected in *Mwk* mice due to likely changes in intracellular [Ca^{2+}].

Calcium signalling

I examined the activity of some of the key Ca^{2+} signalling proteins by looking at their levels of phosphorylation. The results revealed that all investigated proteins have abnormal levels of phosphorylation, which strongly implies that *Mwk* mice have alterations in Ca^{2+} levels inside Purkinje cells. Therefore, the suggestion that behavioural changes in TRPC3 knockout mice could

be due to altered Ca^{2+} signalling could be true (Hartmann & Konnerth 2009). Because TRPC3 is a gain-of-function mutation, it is logical to assume that Purkinje cells have an increased Ca^{2+} influx.

Phosphorylation levels of Ca^{2+}/calmodulin-dependent protein kinase type II (CaMKII), cyclic-AMP response element binding protein (CREB) and extracellular signal regulated kinase (ERK) are increased in *Mwk* cerebella, meaning that their activity is enhanced; whereas phosphorylation of CaMKIV is potentially decreased, so its activity is likely reduced.

The increase in CaMKII and ERK phosphorylation in the cerebella of *Mwk* mice occurs after the dendritic tree of Purkinje cells is fully developed. Hence, even though this confirms that Ca^{2+} homeostasis inside Purkinje cells is altered, CaMKII and ERK pathways are probably not responsible for the abnormal development of Purkinje cell dendrites. However, other studies have shown that expression of CaMKII and ERK in the cerebellum occurs in both Purkinje and granule cells (Jia et al 2007). Therefore, any subtle changes in early onset phosphorylation levels in Purkinje cells could be disguised by normal expression in granule cells.

Phosphorylation of CaMKIV, on the other hand, is potentially down-regulated in the *Mwk* cerebella as early as P21. Interestingly, in the cerebellum, the phosphorylated form of CaMKIV is only expressed in the Purkinje cells; hence the subtle down-regulation that is observed in whole cerebellar lysates by western blot likely happens in Purkinje cells. Even though it is not what you would initially expect from a cell with increased Ca^{2+} levels, there is a possible explanation, which does not depend on the binding of TRPC3 to CaMKIV as discussed earlier. In a typical cell, after a rise in Ca^{2+} concentration, activity of CaMKIV increases, but despite calcium levels remaining high, CaMKIV activity returns to basal levels soon after (Park & Soderling 1995). This deactivation of CaMKIV occurs due to the de-phosphorylation by a protein serine/threonine phosphatase 2A (PP2A) (Westphal et al 1998). Interestingly, it has been shown that induced expression of TRPC1 causes an increase in PP2A phosphatase activity through elevated intracellular calcium levels (Marasa et al 2008). Therefore, increased levels of intracellular Ca^{2+} that likely occur in Purkinje

cells of *Mwk* mice could induce the activity of PP2A, which in turn could cause increased de-phosphorylation of CaMKIV. To test for a possible increase in PP2A activity in *Mwk* mice, one could inhibit it and observe whether it makes a difference to the phosphorylation levels of CaMKIV.

Mice lacking CaMKIV display motor and coordination abnormalities, and a reduced number and immature development of Purkinje cells (Ahn et al 1999; Ho et al 2000; Ribar et al 2000). This information, together with our results, suggests that CaMKIV acts downstream of TRPC3 to regulate the dendritic development of Purkinje cells.

Another protein with altered phosphorylation starting at P21, is CREB, which is a transcription factor, regulated by CaMKIV, as well as other kinases. But unlike CaMKIV, phosphorylation of CREB is up-regulated in the whole cerebellar lysates of *Mwk* mice. However, the phosphorylated CREB is not only expressed in the Purkinje cells, but is also expressed in the granule cells of the cerebellum, which are the most abundant neurons of the brain. The up-regulation in CREB phosphorylation could therefore come from granule cells, as a secondary response to abnormal development of Purkinje cells, while in Purkinje cells it could be down-regulated (as in CaMKIV knockout mice (Ho et al 2000)) or unchanged. If it is up-regulated in Purkinje cells, this could be facilitated by another kinase, as CREB has several upstream regulators, including CaMKII and ERK. So the reduced activity of CaMKIV does not necessarily influence the activation of CREB in *Mwk* mice.

The only way to test how CaMKII, CREB and ERK phosphorylation is altered in *Mwk* Purkinje cells, would be to separate Purkinje cells and granule cells. Even though laser-capture microdissection has been previously used for protein experiments, too many cells would need to be dissected for an accurate experiment, making it excessively time-consuming, and hence, not feasible. As an alternative, the localisation of P-CREB in the nucleus of Purkinje cells could be compared to the perikaryon localisation. Nuclear expression would suggest that CREB is influencing transcription.

Although preliminary experiments showed no differences (roughly 1:1 ratio between expression in perikaryon and cytoplasm in wild-type and *Mwk* Purkinje cells), more samples could be tested, as well as more time points.

Changes in activity of Ca^{2+} signalling cascades likely lead to changes in cell transcription, which has been demonstrated in this thesis.

Microarray

The microarray experiment revealed that Purkinje cells of *Mwk* mice have gene transcription changes. I confirmed expression changes in six genes: *Car2, Cntn3, Ipo5*, *Opn3*, *Stk17b* and *Sv2c*. The genes that show increase in their expression as early as P11 are *Ipo5*, *Opn3* and *Sv2c*, and are therefore postulated to play a role in disease onset in the *Mwk* mouse.

Importin 5 (Ipo5) is a nuclear import protein, which is known to carry transcription factors into the nucleus, and is therefore able to influence transcription (Deane et al 1997; Jakel & Gorlich 1998; Waldmann et al 2007). Along with transcription factors, it can carry many other proteins, one of them being p35, which is an activator of Cdk5 cyclin-dependent kinase (Fu et al 2006). Interestingly, Cdk5 is known for its involvement in neurite outgrowth (Dhavan & Tsai 2001; Nikolic et al 1996). Increased levels of Ipo5 could be causing more p35/Cdk5 translocation into the nucleus, which could alter the normal function of Cdk5, and cause inhibition of neurite outgrowth.

Synaptic vesicle glycoprotein 2c (Sv2c) plays a role in synaptic vesicle exocytosis (Dardou et al 2011). Interestingly, Sv2c is known to interact with a vesicular Ca^{2+} sensor synaptotagmin 1 (Schivell et al 1996; Schivell et al 2005), which was identified in our mass spectrometry experiment as a potential binding partner of TRPC3. SV2 proteins are essential for trafficking of synaptotagmin to the synaptic vesicles in order to control vesicle fusion (Yao et al 2010). If synaptotagmin, indeed, interacts with TRPC3, it is possible that the mechanism of TRPC3 insertion

into the plasma membrane upon activation could be different in *Mwk* mice due to increased Sv2c expression.

Opsin 3 (Opn3) has a low level of homology with visual opsin proteins and is highly expressed in the brain, with the highest expression in Purkinje cells (Blackshaw & Snyder 1999; Halford et al 2001). The function of Opn3 remains largely unknown, but one study implicated it in triggering vesicle exocytosis induced by light (Henkel et al 2006). This function of Opn3 is very interesting, as dendrites are known to grow by vesicle exocytosis, with Ca^{2+} signalling being involved in this process (Hsu et al 2004; Hughes 1953; Pfenninger 2009). So the *Mwk* Purkinje cells could have an altered mechanism of dendritic growth by vesicle exocytosis which does not allow proper extension and arborisation of the dendritic trees.

Mechanism of neurite outgrowth requires continuous addition of new membrane to the extending dendrite through fusion of vesicles with the plasma membrane at the point of growth (Hughes 1953; Meldolesi 2011; Pfenninger 2009; Tang 2008). This process is likely regulated by another mechanism (Pfenninger 2009), and perhaps normal function of TRPC3 could be involved in it. The *Mwk* mice displaying a less branched dendritic tree could have a defect in the mechanism of neurite outgrowth regulation, and so the up-regulation of *Opn3* gene expression could be the cause of that.

A point to note is that CREB transcription factor has a predicted binding site at the promoters of all three genes up-regulated at P11 (*Ipo5, Opn3* and *Sv2c*), suggesting that it could be responsible for their increased expression. However, *Car2*, which is down-regulated in *Mwk* Purkinje cells at P14, also has a predicted CREB binding site. The decrease in *Car2* expression could nevertheless be dependent on a number of transcription cofactors, not CREB alone. Unfortunately, these predictions do not help us understand the activity levels of CREB transcription factor in *Mwk* Purkinje cells.

Laser-capture microdissection

Lastly, during this work, I have developed an effective, reliable and consistent method for collecting cells of interest using the laser-capture microdissection (LCM) technique. The RNA integrity number (RIN) of the microdissected cells is of high quality, averaging around RIN~7. The success of this method depends on the addition of an RNase inhibitor to all water-containing ethanol dilutions, which prevents the water activating endogenous RNases in the sample and consequently preserves the good quality of RNA. I believe that this method can be successfully used to obtain high quality RNA from different cell types with reliable results, which is very difficult to achieve with the LCM technique.

Future experiments

Expression of candidate genes in Purkinje cells in organotypic slice cultures would be useful to investigate the molecular mechanism of dendritic development of Purkinje cells. Organotypic slice cultures have been used extensively to study development and function of the cerebellum (Kapfhammer 2004). Using this technique, it is possible to preserve the structure of the cerebellum for a long time *in vitro* (Tanaka 2009). Also, intact Purkinje cell can be maintained within a slice and show good survival (Kapfhammer 2004). This means that the process of dendritic development of Purkinje cells can be effectively studied using this method. So, the genes that were confirmed to be altered in the Purkinje cells of the *Mwk* mice should be transduced with a virus or knocked down with microRNA in the Purkinje cells of wild-type and *Mwk* cerebellar slices. The genes that were up-regulated in *Mwk* Purkinje cells (*Cntn3, Ipo5, Opn3* and *Sv2c*) should be transduced into the wild-type cerebellar slices in order to observe whether they produce a *Mwk* phenotype. The same genes should be knocked down in the *Mwk* cerebellar slices to see whether this rescues the dendritic phenotype. For the genes down-regulated in the *Mwk* Purkinje cells (*Car2* and *Stk17b*), the opposite should be performed. I believe these

experiments would be crucial for the determination of the exact pathway downstream of TRPC3 signalling that leads to the abnormal development of Purkinje cell dendrites.

The changes in expression of *Opn3,* revealed in the microarray analysis, could cause a defective mechanism of dendritic extension via vesicle exocytosis. To test for these defects, one could examine the vesicles in the Purkinje cells of wild-type and *Mwk* mice. The vesicles can be labelled using a BODIPY-ceramide, which is a fluorescent lipid derivative and is a membrane marker; its fluorescent colour is dependent on the concentration of lipids (Pfenninger et al 2003). These experiments would reveal whether there is a reduction in the number of vesicles used for dendritic membrane extension in *Mwk* Purkinje cells, whether their distribution is different, or if they are smaller in size.

Another important experiment would be to further investigate the nuclear factor of activated T-cells (NFAT) signalling pathway because it is known to be controlled by TRPC3 activity in heart and muscle (Bush et al 2006). Moreover, a recent report demonstrated that co-transfecting cells with wild-type and *Mwk* TRPC3 at a 3:1 ratio could be tolerated by the cells (Poteser et al 2011), so this technique could be used to compare NFAT localisation inside the cells transfected with wild-type TRPC3 only and cells transfected with 3:1 ratio of wild-type to *Mwk* TRPC3. In fact, the paper by Poteser et al demonstrates that NFATc1-dependent transcription is silenced in a TRPC3 transfected cardiac muscle cell line when PKCγ is unable to phosphorylate the channel (Poteser et al 2011). This suggests that Purkinje cells of *Mwk* mice could have a decreased NFAT-dependent transcription, since the S4/S5 linker is a likely site for PKCγ phosphorylation. However, it is also possible that NFAT activity increases due to elevated Ca^{2+} influx and this is what preliminary results by Dr Esther Becker suggest. I have looked at whether the six genes identified in the microarray experiment have a predicted NFAT binding site in their promoter; however, none of them seem to have an NFAT binding site according to the prediction tool that I used. Other prediction tools could be used to look for the NFAT binding site. Also, one could investigate

whether any other genes identified in the microarray experiment could have a predicted NFAT binding site.

Furthermore, even though recent unpublished data by Dr Esther Becker has demonstrated that there are no differences between the expression levels of TRPC3 on the plasma membrane of wild-type and *Mwk* cerebella when un-stimulated, it is still worth investigating whether the stimulation of mGluR1 by its agonist (S)-3,5-dihydroxyphenylglycine (DHPG) at different concentrations changes that. This experiment could reveal whether the mechanism of TRCP3 translocation to the plasma membrane is changed in *Mwk* mice.

Conclusions

In this thesis I have investigated the interaction partners of TRPC3; have looked at the levels of activation of important Ca^{2+} signalling proteins in the cerebella of wild-type and *Mwk* mice; and have examined the differences in gene expression in the Purkinje cells of *Mwk* mice, which were extracted using an optimised laser-capture microdissection technique. My work has revealed that CaMKIV likely lies downstream of TRPC3 activation and Ca^{2+} influx, which could be the pathway responsible for the normal development of Purkinje cell dendrites. It could also be part of the putative common mechanism among several cerebellar ataxias. The microarray analysis was performed using samples obtained by a newly-optimised and reliable LCM method, providing high quality RNA. It demonstrated changes in gene expression of *Mwk* Purkinje cells, which could partly be caused by reduction in CaMKIV activity. Increased expression of *Opn3* in *Mwk* Purkinje cells could lead to an altered mechanism of dendritic outgrowth by vesicle exocytosis, which needs to be investigated further. Work in this thesis depicts TRPC3 as a possible target for cerebellar ataxia treatment.

References

Abeliovich A, Paylor R, Chen C, Kim JJ, Wehner JM, Tonegawa S (1993) Pkc-Gamma Mutant Mice Exhibit Mild Deficits in Spatial and Contextual Learning. *Cell* 75:1263-1271

Adachi N, Kobayashi T, Takahashi H, Kawasaki T, Shirai Y, Ueyama T, Matsuda T, Seki T, Sakai N, Saito N (2008) Enzymological Analysis of Mutant Protein Kinase C Gamma Causing Spinocerebellar Ataxia Type 14 and Dysfunction in Ca(2+) Homeostasis. *Journal of Biological Chemistry* 283:19854-19863

Ahn S, Ginty DD, Linden DJ (1999) A Late Phase of Cerebellar Long-Term Depression Requires Activation of Camkiv and Creb. *Neuron* 23:559-568

Aiba A, Kano M, Chen C, Stanton ME, Fox GD, Herrup K, Zwingman TA, Tonegawa S (1994) Deficient Cerebellar Long-Term Depression and Impaired Motor Learning in Mglur1 Mutant Mice. *Cell* 79:377-388

Altman J, Anderson WJ (1972) Experimental Reorganization of Cerebellar Cortex .1. Morphological Effects of Elimination of All Microneurons with Prolonged X-Irradiation Started at Birth. *J. Comp. Neurol.* 146:355-&

Ambudkar IS, Ong HL (2007) Organization and Function of Trpc Channelosomes. *Pflugers Arch.* 455:187-200

Anderson KA, Kane CD (1998) Ca2+/Calmodulin-Dependent Protein Kinase Iv and Calcium Signaling. *Biometals* 11:331-343

Antonsson B (1997) Phosphatidylinositol Synthase from Mammalian Tissues. *Biochimica Et Biophysica Acta-Lipids and Lipid Metabolism* 1348:179-186

Baeriswyl T, Stoeckli ET (2008) Axonin-1/Tag-1 Is Required for Pathfinding of Granule Cell Axons in the Developing Cerebellum. *Neural Dev.* 3

Bajjalieh SM, Peterson K, Shinghal R, Scheller RH (1992) Sv2 a Brain Synaptic Vesicle Protein Homologous to Bacterial Transporters. *Science (Washington D C)* 257:1271-1273

Banks RE, Dunn MJ, Forbes MA, Stanley A, Pappin D, Naven T, Gough M, Harnden P, Selby PJ (1999) The Potential Use of Laser Capture Microdissection to Selectively Obtain Distinct Populations of Cells for Proteomic Analysis - Preliminary Findings. *Electrophoresis* 20:689-700

Bantscheff M, Schirle M, Sweetman G, Rick J, Kuster B (2007) Quantitative Mass Spectrometry in Proteomics: A Critical Review. *Anal. Bioanal. Chem.* 389:1017-1031

Barmack NH, Qian ZY, Yoshimura J (2000) Regional and Cellular Distribution of Protein Kinase C in Rat Cerebellar Purkinje Cells. *J. Comp. Neurol.* 427:235-254

Batchelor AM, Garthwaite J (1993) Novel Synaptic Potentials in Cerebellar Purkinje-Cells - Probable Mediation by Metabotropic Glutamate Receptors. *Neuropharmacology* 32:11-20

Baude A, Nusser Z, Roberts JDB, Mulvihill E, McIlhinney RAJ, Somogyi P (1993) The Metabotropic Glutamate-Receptor (Mglur1-Alpha) Is Concentrated at Perisynaptic Membrane of Neuronal Subpopulations as Detected by Immunogold Reaction. *Neuron* 11:771-787

Becker EBE, Olivera PL, Glitsch MD, Banks GT, Achilli F, Hardy A, Nolan PM, Fisher EMC, Davies KE (2009) A Point Mutation in Trpc3 Causes Abnormal Purkinje Cell Development and Cerebellar Ataxia in Moonwalker Mice. *Proc. Natl. Acad. Sci. U. S. A.* 106:6706-6711

Belmont L, Mitchison T, Deacon HW (1996) Catastrophic Revelations About Op18/Stathmin. *Trends Biochem.Sci.* 21:197-198

Bennett MK, Calakos N, Scheller RH (1992) Syntaxin - a Synaptic Protein Implicated in Docking of Synaptic Vesicles at Presynaptic Active Zones. *Science* 257:255-259

Bennett MK, Garciaarraras JE, Elferink LA, Peterson K, Fleming AM, Hazuka CD, Scheller RH (1993) The Syntaxin Family of Vesicular Transport Receptors. *Cell* 74:863-873

Berglund EO, Murai KK, Fredette B, Sekerkova G, Marturano B, Weber L, Mugnaini E, Ranscht B (1999) Ataxia and Abnormal Cerebellar Microorganization in Mice with Ablated Contactin Gene Expression. *Neuron* 24:739-750

Berridge MJ (1993) Inositol Trisphosphate and Calcium Signaling. *Nature* 361:315-325

Berridge MJ (1995) Calcium Signaling and Cell-Proliferation. *Bioessays* 17:491-500

Berridge MJ (1998) Neuronal Calcium Signaling. *Neuron* 21:13-26

Bezprozvanny I (2009) Calcium Signaling and Neurodegenerative Diseases. *Trends in Molecular Medicine* 15:89-100

Bezprozvanny I (2011) Role of Inositol 1,4,5-Trishosphate Receptors in Pathogenesis of Huntington's Disease and Spinocerebellar Ataxias. *Neurochem. Res.* 36:1186-1197

Bitoun E, Finelli MJ, Oliver PL, Lee S, Davies KE (2009) Af4 Is a Critical Regulator of the Igf-1 Signaling Pathway During Purkinje Cell Development. *J. Neurosci.* 29:15366-15374

Bizzoca A, Virgintino D, Lorusso L, Buttiglione M, Yoshida L, Polizzi A, Tattoli M, Cagiano R, Rossi F, Kozlov S, Furley A, Gennarini G (2003) Transgenic Mice Expressing F3/Contactin from the Tag-1 Promoter Exhibit Developmentally Regulated Changes in the Differentiation of Cerebellar Neurons. *Development* 130:29-43

Blackshaw S, Snyder SH (1999) Encephalopsin: A Novel Mammalian Extraretinal Opsin Discretely Localized in the Brain. *J. Neurosci.* 19:3681-3690

Blaeser F, Ho N, Prywes R, Chatila TA (2000) Ca2+-Dependent Gene Expression Mediated by Mef2 Transcription Factors. *Journal of Biological Chemistry* 275:197-209

Bolger TA, Zhao X, Cohen TJ, Tsai CC, Yao TP (2007) The Neurodegenerative Disease Protein Ataxin-1 Antagonizes the Neuronal Survival Function of Myocyte Enhancer Factor-2. *Journal of Biological Chemistry* 282:29186-29192

Bollimuntha S, Singh BB, Shavali S, Sharma SK, Ebadi M (2005) Trpc1-Mediated Inhibition of 1-Methyl-4-Phenylpyridinium Ion Neurotoxicity in Human Sh-Sy5y Neuroblastoma Cells. *Journal of Biological Chemistry* 280:2132-2140

Bonner RF, EmmertBuck M, Cole K, Pohida T, Chuaqui R, Goldstein S, Liotta LA (1997) Cell Sampling - Laser Capture Microdissection: Molecular Analysis of Tissue. *Science* 278:1481-&

Boulay G, Brown DM, Qin N, Jiang MS, Dietrich A, Zhu MX, Chen ZG, Birnbaumer M, Mikoshiba K, Birnbaumer L (1999) Modulation of Ca(2+) Entry by Polypeptides of the Inositol 1,4,5-Trisphosphate Receptor (Ip3r) That Bind Transient Receptor Potential (Trp): Evidence for Roles of Trp and Ip3r in Store Depletion-Activated Ca(2+) Entry. *Proc. Natl. Acad. Sci. U. S. A.* 96:14955-14960

Boulton TG, Nye SH, Robbins DJ, Ip NY, Radziejewska E, Morgenbesser SD, Depinho RA, Panayotatos N, Cobb MH, Yancopoulos GD (1991) Erks - a Family of Protein-Serine Threonine Kinases That Are Activated and Tyrosine Phosphorylated in Response to Insulin and Ngf. *Cell* 65:663-675

Brion LP, Suarez C, Zhang H, Cammer W (1994) Up-Regulation of Carbonic-Anhydrase Isozyme-Iv in Cns Myelin of Mice Genetically Deficient in Carbonic-Anhydrase-Ii. *Journal of Neurochemistry* 63:360-366

Buchholz JN, Behringer EJ, Pottorf WJ, Pearce WJ, Vanterpool CK (2007) Age-Dependent Changes in Ca2+ Homeostasis in Peripheral Neurones: Implications for Changes in Function. *Aging Cell* 6:285-296

Buckley K, Kelly RB (1985) Identification of a Transmembrane Glycoprotein Specific for Secretory Vesicles of Neural and Endocrine-Cells. *J. Cell Biol.* 100:1284-1294

Burgin KE, Waxham MN, Rickling S, Westgate SA, Mobley WC, Kelly PT (1990) Insitu Hybridization Histochemistry of Ca-2+ Calmodulin-Dependent Protein-Kinase in Developing Rat-Brain. *J. Neurosci.* 10:1788-1798

Burright EN, Clark HB, Servadio A, Matilla T, Feddersen RM, Yunis WS, Duvick LA, Zoghbi HY, Orr HT (1995) Sca1 Transgenic Mice - a Model for Neurodegeneration Caused by an Expanded Cag Trinucleotide Repeat. *Cell* 82:937-948

Bush EW, Hood DB, Papst PJ, Chapo JA, Minobe W, Bristow MR, Olson EN, McKinsey TA (2006) Canonical Transient Receptor Potential Channels Promote Cardiomyocyte Hypertrophy through Activation of Calcineurin Signaling. *Journal of Biological Chemistry* 281:33487-33496

Bustin SA (2002) Quantification of Mrna Using Real-Time Reverse Transcription Pcr (Rt-Pcr): Trends and Problems. *Journal of Molecular Endocrinology* 29

Caddy KWT, Biscoe TJ (1979) Structural and Quantitative Studies on the Normal C3h and Lurcher Mutant Mouse. *Philosophical Transactions of the Royal Society of London Series B-Biological Sciences* 287:167-&

Capecchi MR (1989) Altering the Genome by Homologous Recombination. *Science* 244:1288-1292

Catterall WA (1995) Structure and Function of Voltage-Gated Ion Channels. *Annu. Rev. Biochem.* 64:493-531

Cayouette S, Boulay G (2007) Intracellular Trafficking of Trp Channels. *Cell Calcium* 42:225-232

Celio MR (1990) Calbindin-D-28k and Parvalbumin in the Rat Nervous-System. *Neuroscience* 35:375-475

Chang WP, Sudhof TC (2009) Sv2 Renders Primed Synaptic Vesicles Competent for Ca(2+)-Induced Exocytosis. *J. Neurosci.* 29:883-897

Chawla S, Hardingham GE, Quinn DR, Bading H (1998) Cbp: A Signal-Regulated Transcriptional Coactivator Controlled by Nuclear Calcium and Cam Kinase Iv. *Science* 281:1505-1509

Chen C, Kano M, Abeliovich A, Chen L, Bao SW, Kim JJ, Hashimoto K, Thompson RF, Tonegawa S (1995) Impaired Motor Coordination Correlates with Persistent Multiple Climbing Fiber Innervation in Pkc Gamma Mutant Mice. *Cell* 83:1233-1242

Chen X, Tang TS, Tu HP, Nelson O, Pook M, Hammer R, Nukina N, Bezprozvanny I (2008) Deranged Calcium Signaling and Neurodegeneration in Spinocerebellar Ataxia Type 3. *J. Neurosci.* 28:12713-12724

Choi DW (1988) Calcium-Mediated Neurotoxicity - Relationship to Specific Channel Types and Role in Ischemic Damage. *Trends in Neurosciences* 11:465-469

Chou AH, Chen CY, Chen SY, Chen WJ, Chen YL, Weng YS, Wang HL (2010) Polyglutamine-Expanded Ataxin-7 Causes Cerebellar Dysfunction by Inducing Transcriptional Dysregulation. *Neurochemistry International* 56:329-339

Chou AH, Yeh TH, Ouyanglc P, Chen YL, Chen SY, Wang HL (2008) Polyglutamine-Expanded Ataxin-3 Causes Cerebellar Dysfunction of Sca3 Transgenic Mice by Inducing Transcriptional Dysregulation. *Neurobiology of Disease* 31:89-101

Chuaqui RF, Bonner RF, Best CJM, Gillespie JW, Flaig MJ, Hewitt SM, Phillips JL, Krizman DB, Tangrea MA, Ahram M, Linehan WM, Knezevic V, Emmert-Buck MR (2002) Post-Analysis Follow-up and Validation of Microarray Experiments. *Nature Genet.* 32:509-514

Clapham DE (1995) Calcium Signaling. *Cell* 80:259-268

Clapham DE (2003) Trp Channels as Cellular Sensors. *Nature* 426:517-524

Clapham DE (2007) Calcium Signaling. *Cell* 131:1047-1058

Clark HB, Burright EN, Yunis WS, Larson S, Wilcox C, Hartman B, Matilla A, Zoghbi HY, Orr HT (1997) Purkinje Cell Expression of a Mutant Allele of Sca1 in Transgenic Mice Leads to Disparate Effects on Motor Behaviors, Followed by a Progressive Cerebellar Dysfunction and Histological Alterations. *J. Neurosci.* 17:7385-7395

Clement-Ziza M, Munnich A, Lyonnet S, Jaubert F, Besmond C (2008) Stabilization of Rna During Laser Capture Microdissection by Performing Experiments under Argon Atmosphere or Using Ethanol as a Solvent in Staining Solutions. *Rna-a Publication of the Rna Society* 14:2698-2704

Coluccia A, Tattoli M, Bizzoca A, Arbia S, Lorusso L, De Benedictis L, Buttiglione M, Cuomo V, Furley A, Gennarini G, Cagiano R (2004) Transgenic Mice Expressing F3/Contactin Transient Axonal Glycoprotein Promoter Developmentally Regulated Deficits of the from the Undergo Cerebellar Function. *Neuroscience* 123:155-166

Crabtree GR, Olson EN (2002) Nfat Signaling: Choreographing the Social Lives of Cells. *Cell* 109:S67-S79

Crabtree GR, Schreiber SL (2009) Snapshot: Ca(2+)-Calcineurin-Nfat Signaling. *Cell* 138

Crespo-Barreto J, Fryer JD, Shaw CA, Orr HT, Zoghbi HY (2010) Partial Loss of Ataxin-1 Function Contributes to Transcriptional Dysregulation in Spinocerebellar Ataxia Type 1 Pathogenesis. *Plos Genetics* 6

Dardou D, Dassesse D, Cuvelier L, Deprez T, De Ryck M, Schiffmann SN (2011) Distribution of Sv2c Mrna and Protein Expression in the Mouse Brain with a Particular Emphasis on the Basal Ganglia System. *Brain Res.* 1367:130-145

Davisson MT, Bronson RT, Tadenev ALD, Motley WW, Krishnaswamy A, Seburn KL, Burgess RW (2011) A Spontaneous Mutation in Contactin 1 in the Mouse. *PLoS One* 6

Deane R, Schafer W, Zimmermann HP, Mueller L, Gorlich D, Prehn S, Ponstingl H, Bischoff FR (1997) Ran-Binding Protein 5 (Ranbp5) Is Related to the Nuclear Transport Factor Importin-Beta but Interacts Differently with Ranbp1. *Molecular and Cellular Biology* 17:5087-5096

Dhavan R, Tsai LH (2001) A Decade of Cdk5. *Nature Reviews Molecular Cell Biology* 2:749-759

Durr A (2010) Autosomal Dominant Cerebellar Ataxias: Polyglutamine Expansions and Beyond. *Lancet Neurol.* 9:885-894

Eder P, Poteser M, Groschner K. 2007. Trpc3: A Multifunctional, Pore-Forming Signalling Molecule

Transient Receptor Potential (Trp) Channels. ed. V Flockerzi, B Nilius, pp. 77-92: Springer Berlin Heidelberg

EmmertBuck MR, Bonner RF, Smith PD, Chuaqui RF, Zhuang ZP, Goldstein SR, Weiss RA, Liotta LA (1996) Laser Capture Microdissection. *Science* 274:998-1001

Erondu NE, Kennedy MB (1985) Regional Distribution of Type-Ii Ca-2+ Calmodulin-Dependent Protein-Kinase in Rat-Brain. *J. Neurosci.* 5:3270-3277

Exton JH (1996) Regulation of Phosphoinositide Phospholipases by Hormones, Neurotransmitters, and Other Agonists Linked to G Proteins. *Annu. Rev. Pharmacol. Toxicol.* 36:481-509

Fend F, Emmert-Buck MR, Chuaqui R, Cole K, Lee J, Liotta LA, Raffeld M (1999) Immuno-Lcm: Laser Capture Microdissection of Immunostained Frozen Sections for Mrna Analysis. *American Journal of Pathology* 154:61-66

Fink CC, Bayer KU, Myers JW, Ferrell JE, Schulman H, Meyer T (2003) Selective Regulation of Neurite Extension and Synapse Formation by the Beta but Not the of Isoform of Camkii. *Neuron* 39:283-297

Fleige S, Pfaffl MW (2006) Rna Integrity and the Effect on the Real-Time Qrt-Pcr Performance. *Molecular Aspects of Medicine* 27:126-139

Fletcher CF, Lutz CM, Osullivan TN, Shaughnessy JD, Hawkes R, Frankel WN, Copeland NG, Jenkins NA (1996) Absence Epilepsy in Tottering Mutant Mice Is Associated with Calcium Channel Defects. *Cell* 87:607-617

Frey N, McKinsey TA, Olson EN (2000) Decoding Calcium Signals Involved in Cardiac Growth and Function. *Nat. Med.* 6:1221-1227

Frey N, Olson EN (2003) Cardiac Hypertrophy: The Good, the Bad and the Ugly. *Annu. Rev. Physiol.* 65:45-79

Fu XR, Choi YK, Qu DN, Yu Y, Cheung NS, Qi RZ (2006) Identification of Nuclear Import Mechanisms for the Neuronal Cdk5 Activator. *Journal of Biological Chemistry* 281:39014-39021

Fujishima K, Horie R, Mochizuki A, Kengaku M (2012) Principles of Branch Dynamics Governing Shape Characteristics of Cerebellar Purkinje Cell Dendrites. *Development* 139:3442-3455

Furuichi T, Simonchazottes D, Fujino I, Yamada N, Hasegawa M, Miyawaki A, Yoshikawa S, Guenet JL, Mikoshiba K (1993) Widespread Expression of Inositol 1,4,5-Trisphosphate Receptor Type-1 Gene (Insp3r1) in the Mouse Central-Nervous-System. *Receptors & Channels* 1:11-24

Furuya S, Ono K, Hirabayashi Y (1995) Sphingolipid Biosynthesis Is Necessary for Dendrite Growth and Survival of Cerebellar Purkinje-Cells in Culture. *Journal of Neurochemistry* 65:1551-1561

Futatsugi A, Nakamura T, Yamada MK, Ebisui E, Nakamura K, Uchida K, Kitaguchi T, Takahashi-Iwanaga H, Noda T, Aruga J, Mikoshiba K (2005) Ip3 Receptor Types 2 and 3 Mediate Exocrine Secretion Underlying Energy Metabolism. *Science* 309:2232-2234

Gaudilliere B, Konishi Y, de la Iglesia N, Yao GI, Bonni A (2004) A Camkii-Neurod Signaling Pathway Specifies Dendritic Morphogenesis. *Neuron* 41:229-241

Gennarini G, Cibelli G, Rougon G, Mattei MG, Goridis C (1989) The Mouse Neuronal Cell-Surface Protein-F3 - a Phosphatidylinositol-Anchored Member of the Immunoglobulin Superfamily Related to Chicken Contactin. *J. Cell Biol.* 109:775-788

Gennarini G, Durbec P, Boned A, Rougon G, Goridis C (1991) Transfected F3 F11 Neuronal Cell-Surface Protein Mediates Intercellular-Adhesion and Promotes Neurite Outgrowth. *Neuron* 6:595-606

Ghez C, Thach WT (2000) The cerebellum. In Kendel ER, Schwartz JH, Jessell TM *Principles of Neural Science,* Fourth Edition, New York, Elsevier, 832-852

Ghosh A, Greenberg ME (1995) Calcium Signaling in Neurons - Molecular Mechanisms and Cellular Consequences. *Science* 268:239-247

Ginty DD (1997) Calcium Regulation of Gene Expression: Isn't That Spatial? *Neuron* 18:183-186

Glitsch MD (2010) Activation of Native Trpc3 Cation Channels by Phospholipase D. *Faseb J.* 24:318-325

Going JJ, Lamb RF (1996) Practical Histological Microdissection for Pcr Analysis. *Journal of Pathology* 179:121-124

Gold DA, Baek SH, Schork NJ, Rose DW, Larsen DD, Sachs BD, Rosenfeld MG, Hamilton BA (2003) Ror Alpha Coordinates Reciprocal Signaling in Cerebellar Development through Sonic Hedgehog and Calcium-Dependent Pathways. *Neuron* 40:1119-1131

Goldowitz D, Hamre K (1998) The Cells and Molecules That Make a Cerebellum. *Trends Neurosci.* 21:375-382

Goldsworthy SM, Stockton PS, Trempus CS, Foley JF, Maronpot RR (1999) Effects of Fixation on Rna Extraction and Amplification from Laser Capture Microdissected Tissue. *Molecular Carcinogenesis* 25:86-91

Gong XM, Tang XL, Wiedmann M, Wang XM, Peng JM, Zheng D, Blair LAC, Marshall J, Mao ZX (2003) Cdk5-Mediated Inhibition of the Protective Effects of Transcription Factor Mef2 in Neurotoxicity-Induced Apoptosis. *Neuron* 38:33-46

Gorlich D, Kutay U (1999) Transport between the Cell Nucleus and the Cytoplasm. *Annual Review of Cell and Developmental Biology* 15:607-660

Gradin HM, Marklund U, Larsson N, Chatila TA, Gullberg M (1997) Regulation of Microtubule Dynamics by Ca2+/Calmodulin-Dependent Kinase Iv Gr-Dependent Phosphorylation of Oncoprotein 18. *Molecular and Cellular Biology* 17:3459-3467

Greer PL, Greenberg ME (2008) From Synapse to Nucleus: Calcium-Dependent Gene Transcription in the Control of Synapse Development and Function. *Neuron* 59:846-860

Greka A, Navarro B, Oancea E, Duggan A, Clapham DE (2003) Trpc5 Is a Regulator of Hippocampal Neurite Length and Growth Cone Morphology. *Nat. Neurosci.* 6:837-845

Gronborg M, Pavlos NJ, Brunk I, Chua JJE, Munster-Wandowski A, Riedel D, Ahnert-Hilger G, Urlaub H, Jahn R (2010) Quantitative Comparison of Glutamatergic and Gabaergic Synaptic Vesicles Unveils Selectivity for Few Proteins Including Mal2, a Novel Synaptic Vesicle Protein. *J. Neurosci.* 30:2-12

Grueber WB, Sagasti A (2010) Self-Avoidance and Tiling: Mechanisms of Dendrite and Axon Spacing. *Cold Spring Harbor Perspectives in Biology* 2

Gugger OS, Hartmann J, Birnbaumer L, Kapfhammer JP (2012) P/Q-Type and T-Type Calcium Channels, but Not Type 3 Transient Receptor Potential Cation Channels, Are Involved in Inhibition of Dendritic Growth after Chronic Metabotropic Glutamate Receptor Type 1 and Protein Kinase C Activation in Cerebellar Purkinje Cells. *Eur. J. Neurosci.* 35:20-33

Gundlfinger A, Kapfhammer JP, Kruse F, Leitges M, Metzger F (2003) Different Regulation of Purkinje Cell Dendritic Development in Cerebellar Slice Cultures by Protein Kinase C Alpha and Beta. *Journal of Neurobiology* 57:95-109

Ha S, Redmond L (2008) Erk Mediates Activity Dependent Neuronal Complexity Via Sustained Activity and Creb-Mediated Signaling. *Dev. Neurobiol.* 68:1565-1579

Halford S, Freedman MS, Bellingham J, Inglis SL, Poopalasundaram S, Soni BG, Foster RG, Hunt DM (2001) Characterization of a Novel Human Opsin Gene with Wide Tissue Expression and Identification of Embedded and Flanking Genes on Chromosome 1q43. *Genomics* 72:203-208

Hamilton BA, Frankel WN, Kerrebrock AW, Hawkins TL, FitzHugh W, Kusumi K, Russell LB, Mueller KL, vanBerkel V, Birren BW, Kruglyak L, Lander ES (1996) Disruption of the Nuclear Hormone Receptor Ror Alpha in Staggerer Mice. *Nature* 379:736-739

Hamori J. 1969. *Development of Synaptic Organization in the Partially Agranular and in the Trans Neuronally Atrophied Cerebellar Cortex*. 845-858 pp.

Hara K, Shiga A, Nozaki H, Mitsui J, Takahashi Y, Ishiguro H, Yomono H, Kurisaki H, Goto J, Ikeuchi T, Tsuji S, Nishizawa M, Onodera O (2008) Total Deletion and a Missense Mutation of Itpr1 in Japanese Sca15 Families. *Neurology* 71:547-551

Hartmann J, Dragicevic E, Adelsberger H, Henning HA, Sumser M, Abramowitz J, Blum R, Dietrich A, Freichel M, Flockerzi V, Birnbaumer L, Konnerth A (2008) Trpc3 Channels Are Required for Synaptic Transmission and Motor Coordination. *Neuron* 59:392-398

Hartmann J, Henning HA, Konnerth A (2011) Mglur1/Trpc3-Mediated Synaptic Transmission and Calcium Signaling in Mammalian Central Neurons. *Cold Spring Harbor Perspectives in Biology* 3

Hartmann J, Konnerth A (2005) Determinants of Postsynaptic Ca2+ Signaling in Purkinje Neurons. *Cell Calcium* 37:459-466

Hartmann J, Konnerth A (2009) Mechanisms of Metabotropic Glutamate Receptor-Mediated Synaptic Signalling in Cerebellar Purkinje Cells. *Acta Physiol.* 195:79-90

Hashimoto K, Miyata M, Watanabe M, Kano M (2001) Roles of Phospholipase C Beta 4 in Synapse Elimination and Plasticity in Developing and Mature Cerebellum. *Mol. Neurobiol.* 23:69-82

Hashimoto T, Ase K, Sawamura S, Kikkawa U, Saito N, Tanaka C, Nishizuka Y (1988) Postnatal-Development of a Brain-Specific Subspecies of Protein Kinase-C in Rat. *J. Neurosci.* 8:1678-1683

Hatten ME, Heintz N (1995) Mechanisms of Neural Patterning and Specification in the Developing Cerebellum. *Annu. Rev. Neurosci.* 18:385-408

He ZH, Jia CX, Feng SJ, Zhou KC, Tai YL, Bai X, Wang YZ (2012) Trpc5 Channel Is the Mediator of Neurotrophin-3 in Regulating Dendritic Growth Via Camkii Alpha in Rat Hippocampal Neurons. *J. Neurosci.* 32:9383-9395

Heese K, Yamada T, Akatsu H, Yamamoto T, Kosaka K, Nagai Y, Sawada T (2004) Characterizing the New Transcription Regulator Protein P60trp. *Journal of Cellular Biochemistry* 91:1030-1042

Helme-Guizon A, Davis S, Israel M, Lesbats B, Mallet J, Laroche S, Hicks A (1998) Increase in Syntaxin 1b and Glutamate Release in Mossy Fibre Terminals Following Induction of Ltp in the Dentate Gyrus: A Candidate Molecular Mechanism Underlying Transsynaptic Plasticity. *Eur. J. Neurosci.* 10:2231-2237

Hendelman WJ, Aggerwal AS (1980) The Purkinje Neuron .1. A Golgi-Study of Its Development in the Mouse and in Culture. *J. Comp. Neurol.* 193:1063-1079

Henkel AW, Upmann I, Bartl CR, Bonsch D, Reichardt C, Maier JM, Nurnberger M, Umstatter R, Reulbach U, Kornhuber J, Wiltfang J (2006) Light-Induced Exocytosis in Cell Development and Differentiation. *Journal of Cellular Biochemistry* 97:1393-1406

Herrup K, Wilczynski SL (1982) Cerebellar Cell Degeneration in the Leaner Mutant Mouse. *Neuroscience* 7:2185-2196

Hibi M, Shimizu T (2012) Development of the Cerebellum and Cerebellar Neural Circuits. *Dev. Neurobiol.* 72:282-301

Hicks A, Davis S, Rodger J, HelmeGuizon A, Laroche S, Mallet J (1997) Synapsin I and Syntaxin 1b: Key Elements in the Control of Neurotransmitter Release Are Regulated by Neuronal Activation and Long-Term Potentiation in Vivo. *Neuroscience* 79:329-340

Hirai H, Launey T (2000) The Regulatory Connection between the Activity of Granule Cell Nmda Receptors and Dendritic Differentiation of Cerebellar Purkinje Cells. *J. Neurosci.* 20:5217-5224

Hisatsune C, Kuroda Y, Akagi T, Torashima T, Hirai H, Hashikawa T, Inoue T, Mikoshiba K (2006) Inositol 1,4,5-Trisphosphate Receptor Type-1 in Granule Cells, Not in Purkinje Cells, Regulates the Dendritic Morphology of Purkinje Cells through Brain-Derived Neurotrophic Factor Production. *J. Neurosci.* 26:10916-10924

Ho N, Liauw JA, Blaeser F, Wei F, Hanissian S, Muglia LM, Wozniak DF, Nardi A, Arvin KL, Holtzman DM, Linden DJ, Zhuo M, Muglia LJ, Chatila TA (2000) Impaired Synaptic Plasticity and Camp Response Element-Binding Protein Activation in Ca2+/Calmodulin-Dependent Protein Kinase Type Iv/Gr-Deficient Mice. *J. Neurosci.* 20:6459-6472

Hoeflich KP, Ikura M (2002) Calmodulin in Action: Diversity in Target Recognition and Activation Mechanisms. *Cell* 108:739-742

Hofmann T, Obukhov AG, Schaefer M, Harteneck C, Gudermann T, Schultz G (1999) Direct Activation of Human Trpc6 and Trpc3 Channels by Diacylglycerol. *Nature* 397:259-263

Hofmann T, Schaefer M, Schultz G, Gudermann T (2002) Subunit Composition of Mammalian Transient Receptor Potential Channels in Living Cells. *Proc. Natl. Acad. Sci. U. S. A.* 99:7461-7466

Holland NT, Smith MT, Eskenazi B, Bastaki M (2003) Biological Sample Collection and Processing for Molecular Epidemiological Studies. *Mutation Research-Reviews in Mutation Research* 543:217-234

Houlden H, Johnson J, Gardner-Thorpe C, Lashley T, Hernandez D, Worth P, Singleton AB, Hilton DA, Holton J, Revesz T, Davis MB, Giunti P, Wood NW (2007) Mutations in Ttbk2, Encoding a Kinase Implicated in Tau Phosphorylation, Segregate with Spinocerebellar Ataxia Type 11. *Nature Genet.* 39:1434-1436

Hsu SC, TerBush D, Abraham M, Guo W (2004) The Exocyst Complex in Polarized Exocytosis. *International Review of Cytology - a Survey of Cell Biology, Vol. 233* 233:243-265

Huang WC, Young JS, Glitsch MD (2007) Changes in Trpc Channel Expression During Postnatal Development of Cerebellar Neurons. *Cell Calcium* 42:1-10

Hughes A (1953) The Growth of Embryonic Neurites - a Study on Cultures of Chick Neural Tissues. *Journal of Anatomy* 87:150-&

Ichise T, Kano M, Hashimoto K, Yanagihara D, Nakao K, Shigemoto R, Katsuki M, Aiba A (2000) Mglur1 in Cerebellar Purkinje Cells Essential for Long-Term Depression, Synapse Elimination, and Motor Coordination. *Science* 288:1832-1835

Inoue T, Kato K, Kohda K, Mikoshiba K (1998) Type 1 Inositol 1,4,5-Trisphosphate Receptor Is Required for Induction of Long-Term Depression in Cerebellar Purkinje Neurons. *J. Neurosci.* 18:5366-5373

Isaacs AM, Oliver PL, Jones EL, Jeans A, Potter A, Hovik BH, Nolan PM, Vizor L, Glenister P, Simon AK, Gray IC, Spurr NK, Brown SDM, Hunter AJ, Davies KE (2003) A Mutation in Af4 Is

Predicted to Cause Cerebellar Ataxia and Cataracts in the Robotic Mouse. *J. Neurosci.* 23:1631-1637

Ito M. 1984. *The Cerebellum and Neural Control*. XVII+580P pp.

Ito M (2002) Historical Review of the Significance of the Cerebellum and the Role of Purkinje Cells in Motor Learning. *Annals of the New York Academy of Sciences* 978:273-288

Jakel S, Gorlich D (1998) Importin Beta, Transportin, Ranbp5 and Ranbp7 Mediate Nuclear Import of Ribosomal Proteins in Mammalian Cells. *Embo Journal* 17:4491-4502

Jakel S, Mingot JM, Schwarzmaier P, Hartmann E, Gorlich D (2002) Importins Fulfil a Dual Function as Nuclear Import Receptors and Cytoplasmic Chaperones for Exposed Basic Domains. *Embo Journal* 21:377-386

Janz R, Goda Y, Geppert M, Missler M, Sudhof TC (1999) Sv2a and Sv2b Function as Redundant Ca2+ Regulators in Neurotransmitter Release. *Neuron* 24:1003-1016

Janz R, Hofmann K, Sudhof TC (1998) Svop, an Evolutionarily Conserved Synaptic Vesicle Protein Suggests Novel Transport Functions of Synaptic Vesicles. *J. Neurosci.* 18:9269-9281

Janz R, Sudhof TC (1999) Sv2c Is a Synaptic Vesicle Protein with an Unusually Restricted Localization: Anatomy of a Synaptic Vesicle Protein Family. *Neuroscience* 94:1279-1290

Jensen KF, Ohmstede CA, Fisher RS, Sahyoun N (1991) Nuclear and Axonal Localization of Ca2+ Calmodulin-Dependent Protein-Kinase Type-Gr in Rat Cerebellar Cortex. *Proc. Natl. Acad. Sci. U. S. A.* 88:2850-2853

Jia YC, Zhou J, Tai YL, Wang YZ (2007) Trpc Channels Promote Cerebellar Granule Neuron Survival. *Nat. Neurosci.* 10:559-567

Johnson GL, Lapadat R (2002) Mitogen-Activated Protein Kinase Pathways Mediated by Erk, Jnk, and P38 Protein Kinases. *Science* 298:1911-1912

Kamme F, Salunga R, Yu JX, Tran DT, Zhu J, Luo L, Bittner A, Guo HQ, Miller N, Wan J, Erlander M (2003) Single-Cell Microarray Analysis in Hippocampus Ca1: Demonstration and Validation of Cellular Heterogeneity. *J. Neurosci.* 23:3607-3615

Kano M, Hashimoto K, Chen C, Abeliovich A, Aiba A, Kurihara H, Watanabe M, Inoue Y, Tonegawa S (1995) Impaired Synapse Elimination During Cerebellar Development in Pkc Gamma Mutant Mice. *Cell* 83:1223-1231

Kano M, Hashimoto K, Kurihara H, Watanabe M, Inoue Y, Aiba A, Tonegawa S (1997) Persistent Multiple Climbing Fiber Innervation of Cerebellar Purkinje Cells in Mice Lacking Mglur1. *Neuron* 18:71-79

Kano M, Hashimoto K, Watanabe M, Kurihara H, Offermanns S, Jiang HP, Wu YP, Jun K, Shin HS, Inoue Y, Simon MI, Wu DQ (1998) Phospholipase C Beta 4 Is Specifically Involved in Climbing Fiber Synapse Elimination in the Developing Cerebellum. *Proc. Natl. Acad. Sci. U. S. A.* 95:15724-15729

Kapfhammer JP (2004) Cellular and Molecular Control of Dendritic Growth and Development of Cerebellar Purkinje Cells. *Progress in Histochemistry and Cytochemistry* 39:131-182

Kar P, Nelson C, Parekh AB (2011) Selective Activation of the Transcription Factor Nfat1 by Calcium Microdomains near Ca2+ Release-Activated Ca2+ (Crac) Channels. *Journal of Biological Chemistry* 286:14795-14803

Kim JY, Zeng WZ, Kiselyov K, Yuan JP, Dehoff MH, Mikoshiba K, Worley PF, Muallem S (2006) Homer 1 Mediates Store- and Inositol 1,4,5-Trisphosphate Receptor-Dependent Translocation and Retrieval of Trpc3 to the Plasma Membrane. *Journal of Biological Chemistry* 281:32540-32549

Kiselyov K, Kim JY, Zeng WZ, Muallem S (2005) Protein-Protein Interaction and Functiontrpc Channels. *Pflugers Arch.* 451:116-124

Kiselyov K, Mignery GA, Zhu MX, Muallem S (1999) The N-Terminal Domain of the Ip3 Receptor Gates Store-Operated Htrp3 Channels. *Mol. Cell* 4:423-429

Kiselyov K, Xu X, Mozhayeva G, Kuo T, Pessah I, Mignery G, Zhu X, Birnbaumer L, Muallem S (1998) Functional Interaction between Insp(3) Receptors and Store-Operated Htrp3 Channels. *Nature* 396:478-482

Knight MA, Kennerson ML, Anney RJ, Matsuura T, Nicholson GA, Salimi-Tari P, Gardner RJM, Storey E, Forrest SM (2003) Spinocerebellar Ataxia Type 15 (Sca15) Maps to 3p24.2-3pter: Exclusion of the Itpr1 Gene, the Human Orthologue of an Ataxic Mouse Mutant. *Neurobiology of Disease* 13:147-157

Koeppen AH (2005) The Pathogenesis of Spinocerebellar Ataxia. *Cerebellum* 4:62-73

Koh S, Yamamoto A, Inoue A, Inoue Y, Akagawa K, Kawamura Y, Kawamoto K, Tashiro Y (1993) Immunoelectron Microscopic Localization of the Hpc-1 Antigen in Rat Cerebellum. *Journal of Neurocytology* 22:995-1005

Kolch W (2000) Meaningful Relationships: The Regulation of the Ras/Raf/Mek/Erk Pathway by Protein Interactions. *Biochem. J.* 351:289-305

Konnerth A, Dreessen J, Augustine GJ (1992) Brief Dendritic Calcium Signals Initiate Long-Lasting Synaptic Depression in Cerebellar Purkinje-Cells. *Proc. Natl. Acad. Sci. U. S. A.* 89:7051-7055

Konradi C (2005) Gene Expression Microarray Studies in Polygenic Psychiatric Disorders: Applications and Data Analysis. *Brain Research Reviews* 50:142-155

Kordasiewicz HB, Thompson RM, Clark HB, Gomez CM (2006) C-Termini of P/Q-Type Ca2+ Channel A1a Subunits Translocate to Nuclei and Promote Polyglutamine-Mediated Toxicity. *Human Molecular Genetics* 15:1587-1599

Kornhauser JM, Cowan CW, Shaywitz AJ, Dolmetsch RE, Griffith EC, Hu LS, Haddad C, Xia ZG, Greenberg ME (2002) Creb Transcriptional Activity in Neurons Is Regulated by Multiple, Calcium-Specific Phosphorylation Events. *Neuron* 34:221-233

Kose A, Saito N, Ito H, Kikkawa U, Nishizuka Y, Tanaka C (1988) Electron-Microscopic Localization of Type-I Protein Kinase-C in Rat Purkinje-Cells. *J. Neurosci.* 8:4262-4268

Kouchi Z, Igarashi T, Shibayama N, Inanobe S, Sakurai K, Yamaguchi H, Fukuda T, Yanagi S, Nakamura Y, Fukami K (2011) Phospholipase C Delta 3 Regulates Rhoa/Rho Kinase Signaling and Neurite Outgrowth. *Journal of Biological Chemistry* 286:8459-8471

Kube DM, Savci-Heijink CD, Lamblin AF, Kosari F, Vasmatzis G, Cheville JC, Connelly DP, Klee GG (2007) Optimization of Laser Capture Microdissection and Rna Amplification for Gene Expression Profiling of Prostate Cancer. *Bmc Molecular Biology* 8

Kumbalasiri T, Provencio I (2005) Melanopsin and Other Novel Mammalian Opsins. *Experimental Eye Research* 81:368-375

Kuwahara H, Nakamura N, Kanazawa H (2006) Nuclear Localization of the Serine/Threonine Kinase Drak2 Is Involved in Uv-Induced Apoptosis. *Biol. Pharm. Bull.* 29:225-233

Lefebvre JL, Kostadinov D, Chen WSV, Maniatis T, Sanes JR (2012) Protocadherins Mediate Dendritic Self-Avoidance in the Mammalian Nervous System. *Nature* 488:517-+

Leung YM, Kang YH, Gao XD, Xia FZ, Xie HL, Sheu L, Tsuk S, Lotan I, Tsushima RG, Gaisano HY (2003) Syntaxin 1a Binds to the Cytoplasmic C Terminus of Kv2.1 to Regulate Channel Gating and Trafficking. *Journal of Biological Chemistry* 278:17532-17538

Lewis SE, Erickson RP, Barnett LB, Venta PJ, Tashian RE (1988) N-Ethyl-N-Nitrosourea Induced Null Mutation at the Mouse Car-2 Locus - an Animal-Model for Human Carbonic Anhydrase-Ii Deficiency Syndrome. *Proc. Natl. Acad. Sci. U. S. A.* 85:1962-1966

Lezzi M, Theander S, Janz R, Loze C, Wollheim CB (2005) Sv2a and Sv2c Are Not Vesicular Ca2+ Transporters but Control Glucose-Evoked Granule Recruitment. *J. Cell Sci.* 118:5647-5660

Li HS, Xu XZS, Montell C (1999) Activation of a Trpc3-Dependent Cation Current through the Neurotrophin Bdnf. *Neuron* 24:261-273

Li J, Gu X, Ma Y, Calicchio ML, Kong D, Teng YD, Yu L, Crain AM, Vartanian TK, Pasqualini R, Arap W, Libermann TA, Snyder EY, Sidman RL (2010a) Nna1 Mediates Purkinje Cell Dendritic Development Via Lysyl Oxidase Propeptide and Nf-[Kappa]B Signaling. *Neuron* 68:45-60

Li JX, Gu XS, Ma YH, Calicchio ML, Kong D, Teng YD, Yu LL, Crain AM, Vartanian TK, Pasqualini R, Arap W, Libermann TA, Snyder EY, Sidman RL (2010b) Nna1 Mediates Purkinje Cell Dendritic Development Via Lysyl Oxidase Propeptide and Nf-Kappa B Signaling. *Neuron* 68:45-60

Li Y, Jia YC, Cui K, Li N, Zheng ZY, Wang YZ, Yuan XB (2005) Essential Role of Trpc Channels in the Guidance of Nerve Growth Cones by Brain-Derived Neurotrophic Factor. *Nature* 434:894-898

Lin X, Antalffy B, Kang D, Orr HT, Zoghbi HY (2000) Polyglutamine Expansion Down-Regulates Specific Neuronal Genes before Pathologic Changes in Sca1. *Nat. Neurosci.* 3:157-163

Liu J, Ernst SA, Gladycheva SE, Lee YYF, Lentz SI, Ho CS, Li QW, Stuenkel EL (2004) Fluorescence Resonance Energy Transfer Reports Properties of Syntaxin1a Interaction with Munc18-1 in Vivo. *Journal of Biological Chemistry* 279:55924-55936

Liu J, Tang TS, Tu HP, Nelson O, Herndon E, Huynh DP, Pulst SM, Bezprozvanny I (2009) Deranged Calcium Signaling and Neurodegeneration in Spinocerebellar Ataxia Type 2. *J. Neurosci.* 29:9148-9162

Liu XB, Bandyopadhyay BC, Singh BB, Groschner K, Ambudkar IS (2005) Molecular Analysis of a Store-Operated and 2-Acetyl-Sn-Glycerol-Sensitive Non-Selective Cation Channel. *Journal of Biological Chemistry* 280:21600-21606

Lockwich T, Pant J, Makusky A, Jankowska-Stephens E, Kowalak JA, Markey SP, Ambudkar IS (2008) Analysis of Trpc3-Interacting Proteins by Tandem Mass Spectrometry. *Journal of Proteome Research* 7:979-989

Lonze BE, Ginty DD (2002) Function and Regulation of Creb Family Transcription Factors in the Nervous System. *Neuron* 35:605-623

Lopez-Revilla R, Soto-Zarate C, Ridaura C, Chavez-Duenas L, Paul D (2004) Progressive Paralysis Associated with Diffuse Astrocyte Anaplasia in Delta 202 Mice Homozygous for a Transgene Encoding the Sv40 T Antigen. *Neuropathology* 24:30-37

Lorenzon NM, Lutz CM, Frankel WN, Beam KG (1998) Altered Calcium Channel Currents in Purkinje Cells of the Neurological Mutant Mouse Leaner. *J. Neurosci.* 18:4482-4489

Lynch G, Larson J, Kelso S, Barrionuevo G, Schottler F (1983) Intracellular Injections of Egta Block Induction of Hippocampal Long-Term Potentiation. *Nature* 305:719-721

Malenka RC, Kauer JA, Zucker RS, Nicoll RA (1988) Postsynaptic Calcium Is Sufficient for Potentiation of Hippocampal Synaptic Transmission. *Science* 242:81-84

Manto MU (2005) The Wide Spectrum of Spinocerebellar Ataxias (Scas). *Cerebellum* 4:2-6

Mao JN, Qiao XY, Luo HY, Wu JP (2006) Transgenic Drak2 Overexpression in Mice Leads to Increased T Cell Apoptosis and Compromised Memory T Cell Development. *Journal of Biological Chemistry* 281:12587-12595

Marasa BS, Xiao L, Rao JN, Zou TT, Liu L, Wang J, Bellavance E, Turner DJ, Wang JY (2008) Induced Trpc1 Expression Increases Protein Phosphatase 2a Sensitizing Intestinal Epithelial Cells to Apoptosis through Inhibition of Nf-Kappa B Activation. *Am. J. Physiol.-Cell Physiol.* 294:C1277-C1287

Marchenko SM, Thomas RC (2006) Nuclear Ca2+ Signalling in Cerebellar Purkinje Neurons. *Cerebellum* 5:36-42

Matilla-Duenas A (2008) The Highly Heterogeneous Spinocerebellar Ataxias: From Genes to Targets for Therapeutic Intervention. *Cerebellum* 7:97-100

Matsuyama Z, Wakamori M, Mori Y, Kawakami H, Nakamura S, Imoto K (1999) Direct Alteration of the P/Q-Type Ca2+ Channel Property by Polyglutamine Expansion in Spinocerebellar Ataxia 6. *The Journal of neuroscience : the official journal of the Society for Neuroscience* 19:RC14

Matus A (2000) Actin-Based Plasticity in Dendritic Spines. *Science* 290:754-758

McAllister AK, Lo DC, Katz LC (1995) Neurotrophins Regulate Dendritic Growth in Developing Visual-Cortex. *Neuron* 15:791-803

McGargill MA, Wen BG, Walsh CM, Hedrick SM (2004) A Deficiency in Drak2 Results in a T Cell Hypersensitivity and an Unexpected Resistance to Autoimmunity. *Immunity* 21:781-791

Meldolesi J (2011) Neurite Outgrowth: This Process, First Discovered by Santiago Ramon Y Cajal, Is Sustained by the Exocytosis of Two Distinct Types of Vesicles. *Brain Research Reviews* 66:246-255

Meldrum NI, Roughton FJW (1933) Carbonic Anhydrase. Its Preparation and Properties. *Jour Physiol* 80:113-142

Mellstrom B, Naranjo JR (2001) Mechanisms of Ca2+-Dependent Transcription. *Curr. Opin. Neurobiol.* 11:312-319

Metzger F (2010) Molecular and Cellular Control of Dendrite Maturation During Brain Development. *Current molecular pharmacology* 3:1-11

Metzger F, Kapfhammer JP (2000) Protein Kinase C Activity Modulates Dendritic Differentiation of Rat Purkinje Cells in Cerebellar Slice Cultures. *Eur. J. Neurosci.* 12:1993-2005

Miale IL, Sidman RL (1961) Autoradiographic Analysis of Histogenesis in Muse Cerebellum. *Exp. Neurol.* 4:277-&

Mieczkowski J, Tyburczy ME, Dabrowski M, Pokarowski P (2010) Probe Set Filtering Increases Correlation between Affymetrix Genechip and Qrt-Pcr Expression Measurements. *Bmc Bioinformatics* 11

Mikoshiba K (2011a) Role of Ip3 Receptor in Development. *Cell Calcium* 49:331-340

Mikoshiba K (2011b) Role of Ip(3) Receptor in Development. *Cell Calcium* 49:331-340

Minichiello L, Klein R (1996) Trkb and Trkc Neurotrophin Receptors Cooperate in Promoting Survival of Hippocampal and Cerebellar Granule Neurons. *Genes Dev.* 10:2849-2858

Mitsumura K, Hosoi N, Furuya N, Hirai H (2011) Disruption of Metabotropic Glutamate Receptor Signalling Is a Major Defect at Cerebellar Parallel Fibre-Purkinje Cell Synapses in Staggerer Mutant Mice. *J. Physiol.-London* 589:3191-3209

Morales S, Diez A, Puyet A, Camello PJ, Camello-Almaraz C, Bautista JM, Pozo MJ (2007) Calcium Controls Smooth Muscle Trpc Gene Transcription Via the Camk/Calcineurin-Dependent Pathways. *Am. J. Physiol.-Cell Physiol.* 292:C553-C563

Morara S, Van der Want JJL, De Weerd H, Provini L, Rosina A (2001) Ultrastructural Analysis of Climbing Fiber-Purkinje Cell Synaptogenesis in the Rat Cerebellum. *Neuroscience* 108:655-671

Muller HJ (1932) Further Studies on the Nature and Causes of Gene Mutations. *Proceedings of the Sixth International Congress of Genetics, Ithaca, New York.* 1:213-255

Nagendran T, Hardy LR (2011) Calcium/Calmodulin-Dependent Protein Kinase Iv Mediates Distinct Features of Basal and Activity-Dependent Dendrite Complexity. *Neuroscience* 199:548-562

Nakamura M, Sato K, Fukaya M, Araishi K, Aiba A, Kano M, Watanabe M (2004) Signaling Complex Formation of Phospholipase C Beta 4 with Metabotropic Glutamate Receptor Type 1 Alpha and 1,4,5-Trisphosphate Receptor at the Perisynapse and Endoplasmic Reticulum in the Mouse Brain. *Eur. J. Neurosci.* 20:2929-2944

Nakayama H, Wilkin BJ, Bodi I, Molkentin JD (2006) Calcineurin-Dependent Cardiomyopathy Is Activated by Trpc in the Adult Mouse Heart. *Faseb J.* 20:1660-1670

Negulescu PA, Shastri N, Cahalan MD (1994) Intracellular Calcium-Dependence of Gene-Expression in Single T-Lymphocytes. *Proc. Natl. Acad. Sci. U. S. A.* 91:2873-2877

Nguyen T, Di Giovanni S (2008) Nfat Signaling in Neural Development and Axon Growth. *Int. J. Dev. Neurosci.* 26:141-145

Nikolic M, Dudek H, Kwon YT, Ramos YFM, Tsai LH (1996) The Cdk5/P35 Kinase Is Essential for Neurite Outgrowth During Neuronal Differentiation. *Genes Dev.* 10:816-825

Nogradi A, Jonsson N, Walker R, Caddy K, Carter N, Kelly C (1997) Carbonic Anhydrase Ii and Carbonic Anhydrase-Related Protein in the Cerebellar Cortex of Normal and Lurcher Mice. *Developmental Brain Research* 98:91-101

Nogradi A, Mihaly A (1990) Light Microscopic Histochemistry of the Postnatal-Development and Localization of Carbonic-Anhydrase Activity in Glial and Neuronal Cell-Types of the Rat Central-Nervous-System. *Histochemistry* 94:441-447

Nolan PM, Peters J, Strivens M, Rogers D, Hagan J, Spurr N, Gray IC, Vizor L, Brooker D, Whitehill E, Washbourne R, Hough T, Greenaway S, Hewitt M, Liu XH, McCormack S, Pickford K, Selley R, Wells C, Tymowska-Lalanne Z, Roby P, Glenister P, Thornton C, Thaung C, Stevenson JA, Arkell R, Mburu P, Hardisty R, Kiernan A, Erven H, Steel KP, Voegeling S, Guenet JL, Nickols C, Sadri R, Naase M, Isaacs A, Davies K, Browne M, Fisher EMC, Martin J, Rastan S, Brown SDM, Hunter J (2000a) A Systematic, Genome-Wide, Phenotype-Driven Mutagenesis Programme for Gene Function Studies in the Mouse. *Nature Genet.* 25:440-443

Nolan PM, Peters J, Vizor L, Strivens M, Washbourne R, Hough T, Wells C, Glenister P, Thornton C, Martin J, Fisher E, Rogers D, Hagan J, Reavill C, Gray I, Wood J, Spurr N, Browne M, Rastan S, Hunter J, Brown SDM (2000b) Implementation of a Large-Scale Enu Mutagenesis Program: Towards Increasing the Mouse Mutant Resource. *Mamm. Genome* 11:500-506

Nuoffer C, Balch WE (1994) Gtpases - Multifunctional Molecular Switches Regulating Vesicular Traffic. *Annu. Rev. Biochem.* 63:949-990

Offermanns S, Hashimoto K, Watanabe M, Sun W, Kurihara H, Thompson RF, Inoue Y, Kano M, Simon MI (1997) Impaired Motor Coordination and Persistent Multiple Climbing Fiber Innervation of Cerebellar Purkinje Cells in Mice Lacking G Alpha Q. *Proc. Natl. Acad. Sci. U. S. A.* 94:14089-14094

Ohkawa N, Fujitani K, Tokunaga E, Furuya S, Inokuchi K (2007) The Microtubule Destabilizer Stathmin Mediates the Development of Dendritic Arbors in Neuronal Cells. *J. Cell Sci.* 120:1447-1456

Ohmstede CA, Jensen KF, Sahyoun NE (1989) Ca-2+/Calmodulin-Dependent Protein-Kinase Enriched in Cerebellar Granule Cells - Identification of a Novel Neuronal Calmodulin-Dependent Protein-Kinase. *Journal of Biological Chemistry* 264:5866-5875

Ohshima T, Gilmore EC, Longenecker G, Jacobowitz DM, Brady RO, Herrup K, Kulkarni AB (1999) Migration Defects of Cdk5(-/-) Neurons in the Developing Cerebellum Is Cell Autonomous. *J. Neurosci.* 19:6017-6026

Ohshima T, Ward JM, Huh CG, Longenecker G, Veeranna, Pant HC, Brady RO, Martin LJ, Kulkarni AB (1996) Targeted Disruption of the Cyclin-Dependent Kinase 5 Gene Results in Abnormal Corticogenesis, Neuronal Pathology and Perinatal Death. *Proc. Natl. Acad. Sci. U. S. A.* 93:11173-11178

Oliver PL, Davies KE (2005) Analysis of Human Neurological Disorders Using Mutagenesis in the Mouse. *Clin. Sci.* 108:385-397

Orr HT (2012) Cell Biology of Spinocerebellar Ataxia. *J. Cell Biol.* 197:167-177

Orr HT, Chung MY, Banfi S, Kwiatkowski TJ, Servadio A, Beaudet AL, McCall AE, Duvick LA, Ranum LPW, Zoghbi HY (1993) Expansion of an Unstable Trinucleotide Cag Repeat in Spinocerebellar Ataxia Type-1. *Nature Genet.* 4:221-226

Ortiz J, Harris HW, Guitart X, Terwilliger RZ, Haycock JW, Nestler EJ (1995) Extracellular Signal-Regulated Protein-Kinases (Erks) and Erk Kinase (Mek) in Brain - Regional Distribution and Regulation by Chronic Morphine. *J. Neurosci.* 15:1285-1297

Palkovits M, Leranth C, Gorcs T, Young WS (1987) Corticotropin-Releasing Factor in the Olivocerebellar Tract of Rats - Demonstration by Light-Microscopic and Electron-Microscopic Immunohistochemistry and Insitu Hybridization Histochemistry. *Proc. Natl. Acad. Sci. U. S. A.* 84:3911-3915

Pan PW, Leppilampi M, Pastorekova S, Pastorek J, Waheed A, Sly WS, Parkkila S (2006) Carbonic Anhydrase Gene Expression in Ca Ii-Deficient (Car2(-/-)) and Ca Ix-Deficient (Car9(-/-)) Mice. *J. Physiol.-London* 571:319-327

Pan PW, Waheed A, Sly WS, Parkkila S (2010) Carbonic Anhydrases in the Mouse Harderian Gland. *Journal of Molecular Histology* 41:411-417

Park IK, Soderling TR (1995) Activation of Ca2+/Calmodulin-Dependent Protein Kinase (Cam-Kinase) Iv by Cam-Kinase Kinase in Jurkat T Lymphocytes. *Journal of Biological Chemistry* 270:30464-30469

Parks DR, Herzenberg LA (1984) Fluorescence-Activated Cell Sorting - Theory, Experimental Optimization, and Applications in Lymphoid-Cell Biology. *Methods in Enzymology* 108:197-241

Patrick GN, Zukerberg L, Nikolic M, de la Monte S, Dikkes P, Tsai LH (1999) Conversion of P35 to P25 Deregulates Cdk5 Activity and Promotes Neurodegeneration. *Nature* 402:615-622

Pawelczyk T, Matecki A (1999) Phospholipase C-Delta 3 Binds with High Specificity to Phosphatidylinositol 4,5-Bisphosphate and Phosphatidic Acid in Bilayer Membranes. *Eur. J. Biochem.* 262:291-298

Perez-Branguli F, Muhaisen A, Blasi J (2002) Munc 18a Binding to Syntaxin 1a and 1b Isoforms Defines Its Localization at the Plasma Membrane and Blocks Snare Assembly in a Three-Hybrid System Assay. *Molecular and Cellular Neuroscience* 20:169-180

Perez-Novo CA, Claeys C, Speleman F, Van Cauwenberge P, Bachert C, Vandesompele J (2005) Impact of Rna Quality on Reference Gene Expression Stability. *Biotechniques* 39:52-+

Pfenninger KH (2009) Plasma Membrane Expansion: A Neuron's Herculean Task. *Nat. Rev. Neurosci.* 10:251-261

Pfenninger KH, Laurino L, Peretti D, Wang XX, Rosso S, Morfini G, Caceres A, Quiroga S (2003) Regulation of Membrane Expansion at the Nerve Growth Cone. *J. Cell Sci.* 116:1209-1217

Piedras-Renteria ES, Watase K, Harata N, Zhuchenko O, Zoghbi HY, Lee CC, Tsien RW (2001) Increased Expression of Alpha(1a) Ca2+ Channel Currents Arising from Expanded Trinucleotide Repeats in Spinocerebellar Ataxia Type 6. *J. Neurosci.* 21:9185-9193

Piochon C, Irinopoulou T, Brusciano D, Bailly Y, Mariani J, Levenes C (2007) Nmda Receptor Contribution to the Climbing Fiber Response in the Adult Mouse Purkinje Cell. *J. Neurosci.* 27:10797-10809

Poteser M, Graziani A, Rosker C, Eder P, Derler I, Kahr H, Zhu MX, Romanin C, Groschner K (2006) Trpc3 and Trpc4 Associate to Form a Redox-Sensitive Cation Channel - Evidence for Expression of Native Trpc3-Trpc4 Heteromeric Channels in Endothelial Cells. *Journal of Biological Chemistry* 281:13588-13595

Poteser M, Schleifer H, Lichtenegger M, Schernthaner M, Stockner T, Kappe CO, Glasnov TN, Romanin C, Groschner K (2011) Pkc-Dependent Coupling of Calcium Permeation through Transient Receptor Potential Canonical 3 (Trpc3) to Calcineurin Signaling in Hl-1 Myocytes. *Proc. Natl. Acad. Sci. U. S. A.* 108:10556-10561

Przedborski S, Tieu K, Perier C, Vila M (2004) Mptp as a Mitochondrial Neurotoxic Model of Parkinson's Disease. *J. Bioenerg. Biomembr.* 36:375-379

Puram SV, Kim AH, Ikeuchi Y, Wilson-Grady JT, Merdes A, Gygi SP, Bonni A (2011) A Camkii Beta Signaling Pathway at the Centrosome Regulates Dendrite Patterning in the Brain. *Nat. Neurosci.* 14:973-U958

Putney JW (2005) Physiological Mechanisms of Trpc Activation. *Pflugers Arch.* 451:29-34

Putt ME, Hannenhalli S, Lu Y, Haines P, Chandrupatla HR, Morrisey EE, Margulies KB, Cappola TP (2009) Evidence for Coregulation of Myocardial Gene Expression by Mef2 and Nfat in Human Heart Failure. *Circ.-Cardiovasc. Genet.* 2:212-U222

Rakic P, Sidman RL (1973) Organization of Cerebellar Cortex Secondary to Deficit of Granule Cells in Weaver Mutant Mice. *J. Comp. Neurol.* 152:133-161

Ramsey IS, Delling M, Clapham DE. 2006. An Introduction to Trp Channels. In *Annu. Rev. Physiol.*, pp. 619-647

Redmond L, Kashani AH, Ghosh A (2002) Calcium Regulation of Dendritic Growth Via Cam Kinase Iv and Creb-Mediated Transcription. *Neuron* 34:999-1010

Repici M, Zanjani HS, Gautheron V, Borsello T, Dusart I, Mariani J (2008) Specific Jnk Inhibition by D-Jnki1 Protects Purkinje Cells from Cell Death in Lurcher Mutant Mouse. *Cerebellum* 7:534-538

Restituito S, Thompson RM, Eliet J, Raike RS, Riedl M, Charnet P, Gomez CM (2000) The Polyglutamine Expansion in Spinocerebellar Ataxia Type 6 Causes a Beta Subunit-Specific Enhanced Activation of P/Q-Type Calcium Channels in Xenopus Oocytes. *J. Neurosci.* 20:6394-6403

Ribar TJ, Rodriguiz RM, Khiroug L, Wetsel WC, Augustine GJ, Means AR (2000) Cerebellar Defects in Ca2+/Calmodulin Kinase Iv-Deficient Mice. *J. Neurosci.* 20:art. no.-RC107

Riccio A, Medhurst AD, Mattei C, Kelsell RE, Calver AR, Randall AD, Benham CD, Pangalos MN (2002) Mrna Distribution Analysis of Human Trpc Family in Cns and Peripheral Tissues. *Brain research. Molecular brain research* 109:95-104

Ridderstrale Y, Wistrand PJ (2000) Membrane-Associated Carbonic Anhydrase Activity in the Brain of Ca Ii-Deficient Mice. *Journal of Neurocytology* 29:263-269

Robinson MJ, Cobb MH (1997) Mitogen-Activated Protein Kinase Pathways. *Curr. Opin. Cell Biol.* 9:180-186

Rodriguez-Santiago M, Mendoza-Torres M, Jimenez-Bremont JF, Lopez-Revilla R (2007) Knockout of the Trcp3 Gene Causes a Recessive Neuromotor Disease in Mice. *Biochem. Biophys. Res. Commun.* 360:874-879

Rogers DC, Fisher EMC, Brown SDM, Peters J, Hunter AJ, Martin JE (1997) Behavioral and Functional Analysis of Mouse Phenotype: Shirpa, a Proposed Protocol for Comprehensive Phenotype Assessment. *Mamm. Genome* 8:711-713

Rosenberg P, Hawkins A, Stiber J, Shelton JM, Hutcheson K, Bassel-Duby R, Shin DM, Yan Z, Williams RS (2004) Trpc3 Channels Confer Cellular Memory of Recent Neuromuscular Activity. *Proc. Natl. Acad. Sci. U. S. A.* 101:9387-9392

RuizMontasell B, Aguado F, Majo G, Chapman ER, Canals JM, Marsal J, Blasi J (1996) Differential Distribution of Syntaxin Isoforms 1a and 1b in the Rat Central Nervous System. *Eur. J. Neurosci.* 8:2544-2552

Saito N, Kikkawa U, Nishizuka Y, Tanaka C (1988) Distribution of Protein Kinase-C-Like Immunoreactive Neurons in Rat-Brain. *J. Neurosci.* 8:369-382

Saito S, Sakagami H, Tonosaki A, Kondo H (1998) Localization of Mrnas for Cdp-Diacylglycerol Synthase and Phosphatidylinositol Synthase in the Brain and Retina of Developing and Adult Rats. *Brain research. Developmental brain research* 110:21-30

Sakamoto H, Mezaki Y, Shikimi H, Ukena K, Tsutsui K (2003) Dendritic Growth and Spine Formation in Response to Estrogen in the Developing Purkinje Cell. *Endocrinology* 144:4466-4477

Sakamoto H, Ukena K, Tsutsui K (2002) Dendritic Spine Formation in Response to Progesterone Synthesized De Novo in the Developing Purkinje Cell in Rats. *Neurosci. Lett.* 322:111-115

Salin H, Maurin Y, Davis S, Laroche S, Mallet J, Dumas S (2002) Spatio-Temporal Heterogeneity and Cell-Specificity of Long-Term Potentiation-Induced Mrna Expression in the Dentate Gyrus in Vivo. *Neuroscience* 110:227-236

Schilling K, Dickinson MH, Connor JA, Morgan JI (1991) Electrical-Activity in Cerebellar Cultures Determines Purkinje-Cell Dendritic Growth-Patterns. *Neuron* 7:891-902

Schivell AE, Batchelor RH, Bajjalieh SM (1996) Isoform-Specific, Calcium-Regulated Interaction of the Synaptic Vesicle Proteins Sv2 and Synaptotagmin. *Journal of Biological Chemistry* 271:27770-27775

Schivell AE, Mochida S, Kensel-Hammes P, Custer KL, Bajjalieh SM (2005) Sv2a and Sv2c Contain a Unique Synaptotagmin-Binding Site. *Molecular and Cellular Neuroscience* 29:56-64

Schrenk K, Kapfhammer JP, Metzger F (2002) Altered Dendritic Development of Cerebellar Purkinje Cells in Slice Cultures from Protein Kinase C Gamma-Deficient Mice. *Neuroscience* 110:675-689

Schutze K, Lahr G (1998) Identification of Expressed Genes by Laser-Mediated Manipulation of Single Cells. *Nature Biotechnology* 16:737-742

Schwartz PM, Borghesani PR, Levy RL, Pomeroy SL, Segal RA (1997) Abnormal Cerebellar Development and Foliation in Bdnf-/- Mice Reveals a Role for Neurotrophins in Cns Patterning. *Neuron* 19:269-281

Selvaraj S, Sun Y, Watt JA, Wang S, Lei S, Birnbaumer L, Singh BB (2012) Neurotoxin-Induced Er Stress in Mouse Dopaminergic Neurons Involves Downregulation of Trpc1 and Inhibition of Akt/Mtor Signaling. *Journal of Clinical Investigation* 122:1354-1367

Selvaraj S, Watt JA, Singh BB (2009) Trpc1 Inhibits Apoptotic Cell Degeneration Induced by Dopaminergic Neurotoxin Mptp/Mpp+. *Cell Calcium* 46:209-218

Seo J, Hoffman EP (2006) Probe Set Algorithms: Is There a Rational Best Bet? *Bmc Bioinformatics* 7

Serra HG, Byam CE, Lande JD, Tousey SK, Zoghbi HY, Orr HT (2004) Gene Profiling Links Sca1 Pathophysiology to Glutamate Signaling in Purkinje Cells of Transgenic Mice. *Human Molecular Genetics* 13:2535-2543

Serra HG, Duvick L, Zu T, Carlson K, Stevens S, Jorgensen N, Lysholm A, Burright E, Zoghbi HY, Clark HB, Andresen JM, Orr HT (2006) Ror Alpha-Mediated Purkinje Cell Development Determines Disease Severity in Adult Sca1 Mice. *Cell* 127:697-708

Shaulian E, Karin M (2002) Ap-1 as a Regulator of Cell Life and Death. *Nat. Cell Biol.* 4:E131-E136

Shedden K, Chen W, Kuick R, Ghosh D, Macdonald J, Cho KR, Giordano TJ, Gruber SB, Fearon ER, Taylor JMG, Hanash S (2005) Comparison of Seven Methods for Producing Affymetrix Expression Scores Based on False Discovery Rates in Disease Profiling Data. *Bmc Bioinformatics* 6

Sheng ZH, Westenbroek RE, Catterall WA (1998) Physical Link and Functional Coupling of Presynaptic Calcium Channels and the Synaptic Vesicle Docking/Fusion Machinery. *J. Bioenerg. Biomembr.* 30:335-345

Shevchenko A, Tomas H, Havlis J, Olsen JV, Mann M (2006) In-Gel Digestion for Mass Spectrometric Characterization of Proteins and Proteomes. *Nature Protocols* 1:2856-2860

Shibata D, Hawes D, Li ZH, Hernandez AM, Spruck CH, Nichols PW (1992) Specific Genetic-Analysis of Microscopic Tissue after Selective Ultraviolet-Radiation Fractionation and the Polymerase Chain-Reaction. *American Journal of Pathology* 141:539-543

Shimada A, Mason CA, Morrison ME (1998) Trkb Signaling Modulates Spine Density and Morphology Independent of Dendrite Structure in Cultured Neonatal Purkinje Cells. *J. Neurosci.* 18:8559-8570

Sidman RL, Lane PW, Dickie MM (1962) Staggerer, a New Mutation in Mouse Affecting Cerebellum. *Science* 137:610-&

Simone NL, Bonner RF, Gillespie JW, Emmert-Buck MR, Liotta LA (1998) Laser-Capture Microdissection: Opening the Microscopic Frontier to Molecular Analysis. *Trends in Genetics* 14:272-276

Simons K, Zerial M (1993) Rab Proteins and the Road Maps for Intracellular-Transport. *Neuron* 11:789-799

Singh BB, Lockwich TP, Bandyopadhyay BC, Liu XB, Bollimuntha S, Brazer SC, Combs C, Das S, Leenders AGM, Sheng ZH, Knepper MA, Ambudkar SV, Ambudkar IS (2004) Vamp2-Dependent Exocytosis Regulates Plasma Membrane Insertion of Trpc3 Channels and Contributes to Agonist-Stimulated Ca2+ Influx. *Mol. Cell* 15:635-646

Sirzen-Zelenskaya A, Zeyse J, Kapfhammer JP (2006) Activation of Class I Metabotropic Glutamate Receptors Limits Dendritic Growth of Purkinje Cells in Organotypic Slice Cultures. *Eur. J. Neurosci.* 24:2978-2986

Slepnev VI, De Camilli P (2000) Accessory Factors in Clathrin-Dependent Synaptic Vesicle Endocytosis. *Nat. Rev. Neurosci.* 1:161-172

Sly WS, Hewettemmett D, Whyte MP, Yu YSL, Tashian RE (1983) Carbonic Anhydrase-Ii Deficiency Identified as the Primary Defect in the Autosomal Recessive Syndrome of Osteopetrosis

with Renal Tubular-Acidosis and Cerebral Calcification. *Proceedings of the National Academy of Sciences of the United States of America-Biological Sciences* 80:2752-2756

Sly WS, Hu PY (1995) Human Carbonic-Anhydrases and Carbonic-Anhydrase Deficiencies. *Annu. Rev. Biochem.* 64:375-401

Soboloff J, Spassova M, Hewavitharana T, He LP, Luncsford P, Xu W, Venkatachalam K, van Rossum D, Patterson RL, Gill DL. 2007. Trpc Channels: Integrators of Multiple Cellular Signals. In *Handbook of Experimental Pharmacology*, ed. V Flockerzi, B Nilius, pp. 575-591: Springer-Verlag Berlin, Heidelberger Platz 3, D-14197 Berlin, Germany

Soderling TR (1999) The Ca2+-Calmodulin-Dependent Protein Kinase Cascade. *Trends Biochem.Sci.* 24:232-236

Soderling TR, Stull JT (2001) Structure and Regulation of Calcium/Calmodulin-Dependent Protein Kinases. *Chemical Reviews* 101:2341-2351

Sotelo C (2004) Cellular and Genetic Regulation of the Development of the Cerebellar System. *Prog. Neurobiol.* 72:295-339

Sotelo C, Dusart I (2009) Intrinsic Versus Extrinsic Determinants During the Development of Purkinje Cell Dendrites. *Neuroscience* 162:589-600

Spatkowski G, Schilling K (2003) Postnatal Dendritic Morphogenesis of Cerebellar Basket and Stellate Cells in Vitro. *J. Neurosci. Res.* 72:317-326

Stagljar I, Korostensky C, Johnsson N, te Heesen S (1998) A Genetic System Based on Split-Ubiquitin for the Analysis of Interactions between Membrane Proteins in Vivo. *Proc. Natl. Acad. Sci. U. S. A.* 95:5187-5192

Stoeckli ET (2010) Neural Circuit Formation in the Cerebellum Is Controlled by Cell Adhesion Molecules of the Contactin Family. *Celll Adhes. Migr.* 4:523-526

Stottmann RW, Rivas RJ (1998) Distribution of Tag-1 and Synaptophysin in the Developing Cerebellar Cortex: Relationship to Purkinje Cell Dendritic Development. *J. Comp. Neurol.* 395:121-135

Sudhof TC (1995) The Synaptic Vesicle Cycle - a Cascade of Protein-Protein Interactions. *Nature* 375:645-653

Sudhof TC (2004) The Synaptic Vesicle Cycle. *Annu. Rev. Neurosci.* 27:509-547

Sun PQ, Enslen H, Myung PS, Maurer RA (1994) Differential Activation of Creb by Ca2+/Calmodulin-Dependent Protein-Kinases Type-Ii and Type-Iv Involves Phosphorylation of a Site That Negatively Regulates Activity. *Genes Dev.* 8:2527-2539

Swinny JD, Kalicharan D, Gramsbergen A, Van der Want JJL (2002) The Localisation of Urocortin in the Adult Rat Cerebellum: A Light and Electron Microscopic Study. *Neuroscience* 114:891-903

Swinny JD, Metzger F, Ijkema-Paassen J, Gounko NV, Gramsbergen A, van der Want JJL (2004) Corticotropin-Releasing Factor and Urocortin Differentially Modulate Rat Purkinje Cell Dendritic Outgrowth and Differentiation in Vitro. *Eur. J. Neurosci.* 19:1749-1758

Tai YL, Feng SJ, Du WL, Wang YZ (2009) Functional Roles of Trpc Channels in the Developing Brain. *Pflugers Arch.* 458:283-289

Tai YL, Feng SJ, Ge RL, Du WL, Zhang XX, He ZH, Wang YZ (2008) Trpc6 Channels Promote Dendritic Growth Via the Camkiv-Creb Pathway. *J. Cell Sci.* 121:2301-2307

Takechi H, Eilers J, Konnerth A (1998) A New Class of Synaptic Response Involving Calcium Release in Dendritic Spines. *Nature* 396:757-760

Takemura M, Mishima T, Wang Y, Kasahara J, Fukunaga K, Ohashi K, Mizuno K (2009) Ca(2+)/Calmodulin-Dependent Protein Kinase Iv-Mediated Lim Kinase Activation Is Critical for Calcium Signal-Induced Neurite Outgrowth. *Journal of Biological Chemistry* 284:28554-28562

Tanaka J, Nakagawa S, Kushiya E, Yamasaki M, Fukaya M, Iwanaga T, Simon MI, Sakimura K, Kano M, Watanabe M (2000) Gq Protein Alpha Subunits G Alpha Q and G Alpha 11 Are

Localized at Postsynaptic Extra-Junctional Membrane of Cerebellar Purkinje Cells and Hippocampal Pyramidal Cells. *Eur. J. Neurosci.* 12:781-792

Tanaka M (2009) Dendrite Formation of Cerebellar Purkinje Cells. *Neurochem. Res.* 34:2078-2088

Tanaka M, Duncan RS, McClung N, Yannazzo J-AS, Hwang S-Y, Marunouchi T, Inokuchi K, Koulen P (2006a) Homer Proteins Control Neuronal Differentiation through Ip3 Receptor Signaling. *FEBS Lett.* 580:6145-6150

Tanaka M, Yanagawa Y, Obata K, Marunouchi T (2006b) Dendritic Morphogenesis of Cerebellar Purkinje Cells through Extension and Retraction Revealed by Long-Term Tracking of Living Cells in Vitro. *Neuroscience* 141:663-674

Tanaka S, Kabayama H, Enomoto M, Saito N, Mikoshiba K (2011) Inositol 1, 4, 5-Trisphosphate Receptor Interacts with the Snare Domain of Syntaxin 1b. *Journal of Physiological Sciences* 61:221-229

Tang BL (2008) Emerging Aspects of Membrane Traffic in Neuronal Dendrite Growth. *Biochim. Biophys. Acta-Mol. Cell Res.* 1783:169-176

Tang J, Lin YK, Zhang ZM, Tikunova S, Birnbaumer L, Zhu MX (2001) Identification of Common Binding Sites for Calmodulin and Inositol 1,4,5-Trisphosphate Receptors on the Carboxyl Termini of Trp Channels. *Journal of Biological Chemistry* 276:21303-21310

Taroni F, DiDonato S (2004) Pathways to Motor Incoordination: The Inherited Ataxias. *Nat. Rev. Neurosci.* 5:641-655

Terakita A (2005) The Opsins. *Genome Biology* 6

Thomas RC (1989) Cell-Growth Factors - Bicarbonate and Phi Response. *Nature* 337:601-601

Toru S, Murakoshi T, Ishikawa K, Saegusa H, Fujigasaki H, Uchihara T, Nagayama S, Osanai M, Mizusawa H, Tanabe T (2000) Spinocerebellar Ataxia Type 6 Mutation Alters P-Type Calcium Channel Function. *Journal of Biological Chemistry* 275:10893-10898

Trebak M, Hempel N, Wedel BJ, Smyth JT, Bird GS, Putney JW (2005) Negative Regulation of Trpc3 Channels by Protein Kinase C-Mediated Phosphorylation of Serine 712. *Mol. Pharmacol.* 67:558-563

Usowicz MM, Sugimori M, Cherksey B, Llinas R (1992) P-Type Calcium Channels in the Somata and Dendrites of Adult Cerebellar Purkinje-Cells. *Neuron* 9:1185-1199

Vaillant AR, Zanassi P, Walsh GS, Aumont A, Alonso A, Miller FD (2002) Signaling Mechanisms Underlying Reversible, Activity-Dependent Dendrite Formation. *Neuron* 34:985-998

van de Leemput J, Chandran J, Knight MA, Holtzclaw LA, Scholz S, Cookson MR, Houlden H, Gwinn-Hardy K, Fung HC, Lin X, Hernandez D, Simon-Sanchez J, Wood NW, Giunti P, Rafferty I, Hardy J, Storey E, Gardner RJM, Forrest SM, Fisher EMC, Russell JT, Cai H, Singleton AB (2007) Deletion at Itpr1 Underlies Ataxia in Mice and Spinocerebellar Ataxia 15 in Humans. *Plos Genetics* 3:1076-1082

Vannier B, Peyton M, Boulay G, Brown D, Qin N, Jiang MS, Zhu X, Birnbaumer L (1999) Mouse Trp2, the Homologue of the Human Trpc2 Pseudogene Encodes Mtrp2, a Store Depletion-Activated Capacitative Ca2+ Entry Channel. *Proc. Natl. Acad. Sci. U. S. A.* 96:2060-2064

Vannier B, Zhu X, Brown D, Birnbaumer L (1998) The Membrane Topology of Human Transient Receptor Potential 3 as Inferred from Glycosylation-Scanning Mutagenesis and Epitope Immunocytochemistry. *Journal of Biological Chemistry* 273:8675-8679

Vazquez G, Wedel BJ, Trebak M, Bird GS, Putney JW (2003) Expression Level of the Canonical Transient Receptor Potential 3 (Trpc3) Channel Determines Its Mechanism of Activation. *Journal of Biological Chemistry* 278:21649-21654

Venkatachalam K, Montell C. 2007. Trp Channels. In *Annu. Rev. Biochem.*, pp. 387-417

Venkatachalam K, Zheng F, Gill DL (2003) Regulation of Canonical Transient Receptor Potential (Trpc) Channel Function by Diacylglycerol and Protein Kinase C. *Journal of Biological Chemistry* 278:29031-29040

Vig PJS, Subramony SH, McDaniel DO (2001) Calcium Homeostasis and Spinocerebellar Ataxia-1 (Sca-1). *Brain Res. Bull.* 56:221-225

Vincent J, Legrand C, Rabie A, Legrand J (1982) Effects of Thyroid Hormone on Synaptogenesis in the Molecular Layer of the Developing Rat Cerebellum. *Journal de physiologie* 78:729-738

Voogd J, Glickstein M (1998) The Anatomy of the Cerebellum. *Trends Neurosci.* 21:370-375

Wagner ML, Tamm LK (2001) Reconstituted Syntaxin1a/Snap25 Interacts with Negatively Charged Lipids as Measured by Lateral Diffusion in Planar Supported Bilayers. *Biophysical Journal* 81:266-275

Wakamori M, Yamazaki K, Matsunodaira H, Teramoto T, Tanaka I, Niidome T, Sawada K, Nishizawa Y, Sekiguchi N, Mori E, Mori Y, Imoto K (1998) Single Tottering Mutations Responsible for the Neuropathic Phenotype of the P-Type Calcium Channel. *Journal of Biological Chemistry* 273:34857-34867

Waldmann I, Walde S, Kehlenbach RH (2007) Nuclear Import of C-Jun Is Mediated by Multiple Transport Receptors. *Journal of Biological Chemistry* 282:27685-27692

Wan Y, Kurosaki T, Huang XY (1996) Tyrosine Kinases in Activation of the Map Kinase Cascade by G-Protein-Coupled Receptors. *Nature* 380:541-544

Wang W, Karagogeos D, Kilpatrick DL (2011) The Effects of Tag-1 on the Maturation of Mouse Cerebellar Granule Neurons. *Cell. Mol. Neurobiol.* 31:351-356

Wang Y, Tang BL (2006) Snares in Neurons - Beyond Synaptic Vesicle Exocytosis (Review). *Molecular Membrane Biology* 23:377-384

Watanabe M, Nakamura M, Sato K, Kano M, Simon MI, Inoue Y (1998) Patterns of Expression for the Mrna Corresponding to the Four Isoforms of Phospholipase C Beta in Mouse Brain. *Eur. J. Neurosci.* 10:2016-2025

Waterman SA (2000) Voltage-Gated Calcium Channels in Autonomic Neuroeffector Transmission. *Prog. Neurobiol.* 60:181-210

Wayman GA, Lee YS, Tokumitsu H, Silva A, Soderling TR (2008) Calmodulin-Kinases: Modulators of Neuronal Development and Plasticity. *Neuron* 59:914-931

Wayman GA, Tokumitsu H, Davare MA, Soderling TR (2011) Analysis of Cam-Kinase Signaling in Cells. *Cell Calcium* 50:1-8

Wedel BJ, Vazquez G, McKay RR, Bird GS, Putney JW (2003) A Calmodulin/Inositol 1,4,5-Trisphosphate (Ip3) Receptor-Binding Region Targets Trpc3 to the Plasma Membrane in a Calmodulin/Ip3 Receptor-Independent Process. *Journal of Biological Chemistry* 278:25758-25765

Westenbroek RE, Sakurai T, Elliott EM, Hell JW, Starr TVB, Snutch TP, Catterall WA (1995) Immunochemical Identification and Subcellular-Distribution of the Alpha(1a) Subunits of Brain Calcium Channels. *J. Neurosci.* 15:6403-6418

Westphal RS, Anderson KA, Means AR, Wadzinski BE (1998) A Signaling Complex of Ca2+-Calmodulin-Dependent Protein Kinase Iv and Protein Phosphatase 2a. *Science* 280:1258-1261

Wojda U, Salinska E, Kuznicki J (2008) Calcium Ions in Neuronal Degeneration. *Iubmb Life* 60:575-590

Wong ROL, Ghosh A (2002) Activity-Dependent Regulation of Dendritic Growth and Patterning. *Nat. Rev. Neurosci.* 3:803-812

Wu GY, Cline HT (1998) Stabilization of Dendritic Arbor Structure in Vivo by Camkii. *Science* 279:222-226

Xu PY, Bai L, Tian W, Xu T (2005) Direct Interaction with Syntaxin 1a Defines the Intracellular Localization of Munc18a. *Progress in Biochemistry and Biophysics* 32:31-36

Yabe I, Sasaki H, Chen DH, Raskind WH, Bird TD, Yamashita I, Tsuji S, Kikuchi S, Tashiro K (2003) Spinocerebellar Ataxia Type 14 Caused by a Mutation in Protein Kinase C Gamma. *Arch. Neurol.* 60:1749-1751

Yamauchi T (2005) Neuronal Ca2+/Calmodulin-Dependent Protein Kinase Ii - Discovery, Progress in a Quarter of a Century, and Perspective: Implication for Learning and Memory. *Biol. Pharm. Bull.* 28:1342-1354

Yamazaki H, Nozaki H, Onodera O, Michikawa T, Nishizawa M, Mikoshiba K (2011) Functional Characterization of the P1059l Mutation in the Inositol 1,4,5-Trisphosphate Receptor Type 1 Identified in a Japanese Sca15 Family. *Biochem. Biophys. Res. Commun.* 410:754-758

Yang B, Steegmaier M, Gonzalez LC, Scheller RH (2000) Nsec1 Binds a Closed Conformation of Syntaxin1a. *J. Cell Biol.* 148:247-252

Yao J, Nowack A, Kensel-Hammes P, Gardner RG, Bajjalieh SM (2010) Cotrafficking of Sv2 and Synaptotagmin at the Synapse. *J. Neurosci.* 30:5569-5578

Yaseen NR, Blobel G (1997) Cloning and Characterization of Human Karyopherin Beta 3. *Proc. Natl. Acad. Sci. U. S. A.* 94:4451-4456

Yoshihara Y, Kawasaki M, Tamada A, Nagata S, Kagamiyama H, Mori K (1995) Overlapping and Differential Expression of Big-2, Big-1, Tag-1, and F3 - 4 Members of an Axon-Associated Cell-Adhesion Molecule Subgroup of the Immunoglobulin Superfamily. *Journal of Neurobiology* 28:51-69

Yoshihara Y, Kawasaki M, Tani A, Tamada A, Nagata S, Kagamiyama H, Mori K (1994) Big-1 - a New Tag-1 F3-Related Member of the Immunoglobulin Superfamily with Neurite Outgrowth-Promoting Activity. *Neuron* 13:415-426

Zhang ZM, Tang JS, Tikunova S, Johnson JD, Chen ZG, Qin N, Dietrich A, Stefani E, Birnbaumer L, Zhu MX (2001) Activation of Trp3 by Inositol 1,4,5-Trisphosphate Receptors through Displacement of Inhibitory Calmodulin from a Common Binding Domain. *Proc. Natl. Acad. Sci. U. S. A.* 98:3168-3173

Zhu X, Jiang MS, Peyton M, Boulay G, Hurst R, Stefani E, Birnbaumer L (1996) Trp, a Novel Mammalian Gene Family Essential for Agonist-Activated Capacitative Ca2+ Entry. *Cell* 85:661-671

Zhuang ZP, Bertheau P, Emmertbuck MR, Liotta LA, Gnarra J, Linehan WM, Lubensky IA (1995) A Microdissection Technique for Archival DNA Analysis of Specific Cell-Populations in Lesions Less-Than-1 Mm in Size. *American Journal of Pathology* 146:620-625

Zhuchenko O, Bailey J, Bonnen P, Ashizawa T, Stockton DW, Amos C, Dobyns WB, Subramony SH, Zoghbi HY, Lee CC (1997) Autosomal Dominant Cerebellar Ataxia (Sca6) Associated with Small Polyglutamine Expansions in the Alpha(1a)-Voltage-Dependent Calcium Channel. *Nature Genet.* 15:62-69

Zieg J, Greer PL, Greenberg ME (2008) Snapshot: Ca(2+)-Dependent Transcription in Neurons. *Cell* 134

Zoghbi HY, Orr HT (2000) Glutamine Repeats and Neurodegeneration. *Annu. Rev. Neurosci.* 23:217-247

Zuo J, DeJager PL, Takahashi KA, Jiang WN, Linden DJ, Heintz N (1997) Neurodegeneration in Lurcher Mice Caused by Mutation in Delta 2 Glutamate Receptor Gene. *Nature* 388:769-773

Appendix A. Mass Spectrometry Results

Immunoprecipitation using α TRPC3 antibody to precipitate proteins from wild-type and *Moonwalker* cerebella with and without calcium in the buffer.
Proteins that had their family members in the negative control are shown in grey.

Wild-type

CODE	PROTEIN	SCORE	MATCHES	% COVER
Q9CQV8	14-3-3 protein beta/alpha	68	3	45.5
P62259	14-3-3 protein epsilon	72	3	32.2
P68510	14-3-3 protein eta	54	2	51.6
P61982	14-3-3 protein gamma	50	2	39.3
O70456	14-3-3 protein sigma	51	2	11.7
P68254	14-3-3 protein theta	51	2	14.7
P63101	14-3-3 protein zeta/delta	99	5	39.6
P16330	2~,3~-cyclic-nucleotide 3~-phosphodiesterase; Short=CNPase	90	2	24.8
P47857	6-phosphofructokinase, muscle type	53	1	24.5
Q8BWN8	Acyl-coenzyme A thioesterase 4	35	0	12.6
Q03265	ATP synthase subunit alpha, mitochondrial	177	7	43.9
Q9CQQ7	ATP synthase subunit b, mitochondrial	42	0	14.5
P56480	ATP synthase subunit beta, mitochondrial	239	6	46.3
Q9DB20	ATP synthase subunit O, mitochondrial	81	3	53.5
O70133	ATP-dependent RNA helicase A	42	0	12
Q9WV92	Band 4.1-like protein 3	36	0	15.2
O08664	B-cell CLL/lymphoma 7 protein family member C	32	0	6.5
P14211	Calreticulin	30	0	19.7
Q70KF4	Cardiomyopathy-associated protein 5	23	0	8.8
Q8VDP6	CDP-diacylglycerol--inositol 3-phosphatidyltransferase; AltName: Full=Phosphatidylinositol synthase; Short=PI synthase;	55	1	10.3
O54804	Choline kinase alpha	45	1	17.4
Q8BYH8	Chromodomain-helicase-DNA-binding protein 9; Short=CHD-9	22	0	12

Q68FD5	Clathrin heavy chain 1	38	0	18.4
Q60771	Claudin-11	32	0	6.8
Q9CQF3	Cleavage and polyadenylation specificity factor subunit 5	33	0	14.5
Q9D4V3	Coiled-coil domain-containing protein 83	43	1	16.1
Q8VBV7	COP9 signalosome complex subunit 8	25	0	12.9
Q8BH44	Coronin-2B	71	1	24.8
Q9CZ13	Cytochrome b-c1 complex subunit 1, mitochondrial	47	0	16.7
Q9DB77	Cytochrome b-c1 complex subunit 2, mitochondrial	50	1	12.4
Q9CR68	Cytochrome b-c1 complex subunit Rieske	41	0	23
P00405	Cytochrome c oxidase subunit 2	41	0	23.3
P12787	Cytochrome c oxidase subunit 5A, mitochondrial	43	0	19.9
Q9JHU4	Cytoplasmic dynein 1 heavy chain 1	30	0	14.3
Q3V1L4	Cytosolic purine 5~-nucleotidase	26	0	8.8
P59764	Dedicator of cytokinesis protein 4	26	0	11.5
Q8R1A4	Dedicator of cytokinesis protein 7	33	0	10.2
P31001	Desmin	43	1	15.1
O55111	Desmoglein-2	44	1	15
Q99LC5	Electron transfer flavoprotein subunit alpha, mitochondrial	22	0	10.5
P10126	Elongation factor 1-alpha 1	44	1	14.7
Q8BFR5	Elongation factor Tu, mitochondrial	32	0	13.3
Q80XI3	Eukaryotic translation initiation factor 4 gamma 3	33	0	12.5
P97825	Hematological and neurological expressed 1 protein;	44	1	8.4
Q60668	Heterogeneous nuclear ribonucleoprotein D0; Short=hnRNP D0	36	0	24.5
O35737	Heterogeneous nuclear ribonucleoprotein H; Short=hnRNP H	42	0	33
P70333	Heterogeneous nuclear ribonucleoprotein H2; Short=hnRNP H2	33	0	15.8
Q8R081	Heterogeneous nuclear ribonucleoprotein L; Short=hnRNP L	43	0	26.3
Q7TMK9	Heterogeneous nuclear ribonucleoprotein Q; Short=hnRNP Q	35	0	6.6
O88569	Heterogeneous nuclear ribonucleoproteins A2/B1; Short=hnRNP A2/B1	70	1	22.7
O15347	High mobility group protein B3	52	1	6.5
Q61190	Interleukin-10 receptor subunit beta	33	0	12.9

Q61771	Kinesin-like protein KIF3B	42	1	15.8
O35066	Kinesin-like protein KIF3C	42	1	12.8
P14733	Lamin-B1	120	3	30.6
P21619	Lamin-B2	62	1	16.3
P98158	Low-density lipoprotein receptor-related protein 2; Short=LRP-2	46	4	1.1
Q6P1G2	Lysine-specific demethylase 2B	32	0	21.7
P97820	Mitogen-activated protein kinase kinase kinase kinase 4	32	0	12.7
Q8NB16	Mixed lineage kinase domain-like protein	54	2	2.3
Q8R003	Muscleblind-like protein 3	38	0	8.2
Q66X05	NACHT, LRR and PYD domains-containing protein 4F	23	0	15
Q91VD9	NADH-ubiquinone oxidoreductase 75 kDa subunit, mitochondrial	43	2	4
P13595	Neural cell adhesion molecule 1; Short=NCAM-1	72	1	13.1
P35802	Neuronal membrane glycoprotein M6-a; Short=M6a	42	1	27.3
P15331	Peripherin	62	1	8.6
Q9R0K7	Plasma membrane calcium-transporting ATPase 2; Short=PMCA2	56	1	18.9
Q8K1R3	Polyribonucleotide nucleotidyltransferase 1, mitochondrial	36	0	9.8
Q69ZP3	Probable hydrolase PNKD	28	0	15.6
O35129	Prohibitin-2	38	0	11
Q9QUM9	Proteasome subunit alpha type-6	52	2	15
O55234	Proteasome subunit beta type-5	44	1	9.8
P08003	Protein disulfide-isomerase A4	60	1	8.9
P09103	Protein disulfide-isomerase	43	0	27.5
Q9JJ28	Protein flightless-1 homolog	50	1	10.9
Q61644	Protein kinase C and casein kinase substrate in neurons protein 1	61	2	21.8
Q8BXR6	Protein pellino homolog 3; Short=Pellino-3	31	0	5.2
Q5SW75	Protein phosphatase Slingshot homolog 2	30	0	10.6
P50114	Protein S100-B	31	0	16.3
O35286	Putative pre-mRNA-splicing factor ATP-dependent RNA helicase DHX15	61	2	15.2
P63011	Ras-related protein Rab-3A	37	0	25.9
Q8K0T0	Reticulon-1	51	1	9.1

Q9ES97	Reticulon-3	38	0	14.6
Q9D6X6	Serine protease 23	35	0	16.5
Q8BKX6	Serine/threonine-protein kinase SMG1	21	0	12.2
Q6NZL8	Signal peptide, CUB and EGF-like domain-containing protein 1	19	0	16.9
P62305	Small nuclear ribonucleoprotein E; Short=snRNP-E	28	0	25
P14094	Sodium/potassium-transporting ATPase subunit beta-1	28	0	12.2
P84104	Splicing factor, arginine/serine-rich 3	65	1	37.2
Q3T106	Splicing factor, arginine/serine-rich 7;	74	4	9.8
Q80TB8	Synaptic vesicle membrane protein VAT-1 homolog-like	54	1	22.8
P46096	Synaptotagmin-1	110	2	20
Q8BYI9	Tenascin-R	32	0	8.1
P01831	Thy-1 membrane glycoprotein	38	0	34
Q9EPQ8	Transcription factor 20	24	0	13.6
Q64152	Transcription factor BTF3	34	0	33.8
P42669	Transcriptional activator protein Pur-alpha	58	1	25.5
O35295	Transcriptional activator protein Pur-beta	31	0	13
Q3UQ41	Transmembrane protease serine 11A	36	0	9.3
Q8BMS1	Trifunctional enzyme subunit alpha, mitochondrial	39	0	20.3
Q8R0S4	Voltage-dependent L-type calcium channel subunit beta-4; Short=CAB4	24	0	15.8
Q9Z1G4	V-type proton ATPase 116 kDa subunit a isoform 1	36	0	21.1
Q4U4S6	Xin actin-binding repeat-containing protein 2	22	0	17
O88799	Zonadhesin	29	0	14.9

Moonwalker

CODE	PROTEIN	SCORE	MATCHES	% COVER
Q9CQV8	14-3-3 protein beta/alpha	63	1	15.9
P62259	14-3-3 protein epsilon	63	1	21.6
P68510	14-3-3 protein eta	87	1	50.8
Q04917	14-3-3 protein eta	137	6	17.1
P61982	14-3-3 protein gamma	66	1	20.2
O70456	14-3-3 protein sigma	63	1	10.9
P68254	14-3-3 protein theta	84	2	33.5
P63101	14-3-3 protein zeta/delta	110	3	45.3
P16330	2~,3~-cyclic-nucleotide 3~-phosphodiesterase; Short=CNPase	153	8	17.1
O88444	Adenylate cyclase type 1	37	0	15.1
P12236	ADP/ATP translocase 3	87	8	21.8
P61164	Alpha-centractin	44	1	8.5
Q91ZB0	Alpha-protein kinase 2	38	0	12.9
P17426	AP-2 complex subunit alpha-1	49	1	17.9
P17427	AP-2 complex subunit alpha-2	49	1	13.1
Q9DBG3	AP-2 complex subunit beta	42	0	19.1
Q03265	ATP synthase subunit alpha, mitochondrial	183	4	31.8
Q9CQQ7	ATP synthase subunit b, mitochondrial	35	1	20.3
P56480	ATP synthase subunit beta, mitochondrial	213	5	45.2
Q9DCX2	ATP synthase subunit d, mitochondrial	36	0	30.4
Q9DB20	ATP synthase subunit O, mitochondrial	64	1	65.3
A7YWC4	ATPase family AAA domain-containing protein 3	65	2	4.8
Q8K440	ATP-binding cassette sub-family A member 8-B	29	0	10.3
Q62167	ATP-dependent RNA helicase DDX3X	104	2	18.7
Q9WV92	Band 4.1-like protein 3	46	1	16
Q8R5C5	Beta-centractin	44	1	14.6
Q9D023	Brain protein 44	38	0	24.4

P08414	Calcium/calmodulin-dependent protein kinase type IV; Short=CaMKIV	78	2	4.7
P14211	Calreticulin	40	0	27.2
Q8C196	Carbamoyl-phosphate synthase [ammonia], mitochondrial	30	0	9.1
Q8VDP6	CDP-diacylglycerol--inositol 3-phosphatidyltransferase; AltName: Full=Phosphatidylinositol synthase; Short=PI synthase;	42	0	13.6
A2AL36	Centriolin	53	1	21.8
Q6IPU0	Centromere protein P	75	1	3.5
Q58A65	C-Jun-amino-terminal kinase-interacting protein 4	28	0	11.6
Q68FD5	Clathrin heavy chain 1	40	0	16.3
Q60771	Claudin-11	32	0	6.8
Q9CQF3	Cleavage and polyadenylation specificity factor subunit 5	33	0	19.8
Q9QZE5	Coatomer subunit gamma	48	1	16.7
Q9QXK3	Coatomer subunit gamma-2	48	1	15.6
A6NC98	Coiled-coil domain-containing protein 88B	46	2	0.6
O35658	Complement component 1 Q subcomponent-binding protein, mitochondrial	56	3	15.1
P12960	Contactin-1	31	0	14.6
Q9JMB8	Contactin-6	38	0	8.9
Q9DA19	Corepressor interacting with RBPJ 1	27	0	15.3
Q8BH44	Coronin-2B	60	1	26.2
Q04447	Creatine kinase B-type	32	0	8.1
Q8VE73	Cullin-7	46	1	4.3
Q6ZQ38	Cullin-associated NEDD8-dissociated protein 1	53	1	13.7
Q9CZ13	Cytochrome b-c1 complex subunit 1, mitochondrial	67	2	19
Q38RU1	Cytochrome c oxidase subunit 2	63	4	23.3
B0VYY2	Cytochrome c oxidase subunit 5A, mitochondrial	65	4	21.3
Q9JHU4	Cytoplasmic dynein 1 heavy chain 1	30	0	12.7
Q8BUR4	Dedicator of cytokinesis protein 1	37	0	10.1
O35098	Dihydropyrimidinase-related protein 4; Short=DRP-4	49	1	15.4
P25206	DNA replication licensing factor MCM3	31	0	9.6
Q9D0M5	Dynein light chain 2, cytoplasmic	32	0	44.9

Q99LC5	Electron transfer flavoprotein subunit alpha, mitochondrial	22	0	4.8
P10126	Elongation factor 1-alpha 1	37	0	16.9
P62631	Elongation factor 1-alpha 2	37	0	8.4
Q8R0W0	Epiplakin	49	1	4.9
Q9QZD9	Eukaryotic translation initiation factor 3 subunit I	38	0	10.2
P43006	Excitatory amino acid transporter 2	53	1	18.2
O35544	Excitatory amino acid transporter 4	29	0	11.4
O08795	Glucosidase 2 subunit beta	51	2	4.2
Q9Z2X1	Heterogeneous nuclear ribonucleoprotein F; Short=hnRNP F	47	1	19.8
A5A6M3	Heterogeneous nuclear ribonucleoprotein G; Short=hnRNP G	51	2	5.1
Q8VHV7	Heterogeneous nuclear ribonucleoprotein H; Short=hnRNP H	94	5	20.7
Q6AY09	Heterogeneous nuclear ribonucleoprotein H2; Short=hnRNP H2	69	3	12.5
Q8R081	Heterogeneous nuclear ribonucleoprotein L; Short=hnRNP L	46	6	11.8
O88569	Heterogeneous nuclear ribonucleoproteins A2/B1; Short=hnRNP A2/B1	40	0	13
O35594	Intraflagellar transport protein 81 homolog	30	0	33.4
P14733	Lamin-B1	172	3	33.8
P21619	Lamin-B2	95	1	16.4
P19137	Laminin subunit alpha-1	30	0	13.2
Q91WC3	Long-chain-fatty-acid--CoA ligase 6	42	0	15.4
Q99PU5	Long-chain-fatty-acid--CoA ligase ACSBG1	65	1	14.3
Q9JJF3	Lysine-specific demethylase NO66	38	0	16.7
Q9QXZ0	Microtubule-actin cross-linking factor 1	23	0	13.4
O70583	Midline-1	49	1	3.7
Q9QUS6	Midline-2	49	1	18.6
Q9DCS9	NADH dehydrogenase [ubiquinone] 1 beta subcomplex subunit 10	29	0	48.3
Q9D6J6	NADH dehydrogenase [ubiquinone] flavoprotein 2, mitochondrial	56	1	13.7
Q91VD9	NADH-ubiquinone oxidoreductase 75 kDa subunit, mitochondrial	78	2	32.5
P13595	Neural cell adhesion molecule 1; Short=NCAM-1	75	1	9.7
P06837	Neuromodulin	50	1	7.5
Q9WV84	Nucleoside diphosphate kinase, mitochondrial	38	0	9.7

Q9CZ30	Obg-like ATPase 1	42	0	12.4
Q8BJI1	Orphan sodium- and chloride-dependent neurotransmitter transporter NTT4	45	1	10.9
P15331	Peripherin	98	3	14.7
Q9Z210	Peroxisomal membrane protein 11B	48	1	13.5
Q6PF93	Phosphatidylinositol 3-kinase catalytic subunit type 3; =PI3-kinase type 3	44	1	14.9
O70362	Phosphatidylinositol-glycan-specific phospholipase D; Short=PI-G PLD	40	0	4.3
Q9R0K7	Plasma membrane calcium-transporting ATPase 2; Short=PMCA2	37	0	14.9
Q9QXS1	Plectin-1	26	0	15.8
Q9WVJ0	Potassium voltage-gated channel subfamily H member 3	38	0	3.4
P59111	Potassium voltage-gated channel subfamily H member 8	35	0	12.2
Q8CFS6	Potassium voltage-gated channel subfamily V member 2	27	0	7.5
O88705	Potassium/sodium hyperpolarization-activated cyclic nucleotide-gated channel 3	25	0	6.2
Q921N6	Probable ATP-dependent RNA helicase DDX27	35	0	19.3
P49722	Proteasome subunit alpha type-2	68	1	20.1
Q9Z2U1	Proteasome subunit alpha type-5	32	0	13.3
O09061	Proteasome subunit beta type-1	40	0	37.5
P08003	Protein disulfide-isomerase A4	57	1	14.7
P05307	Protein disulfide-isomerase	90	3	4.7
Q9JJ28	Protein flightless-1 homolog	85	2	16.2
Q61644	Protein kinase C and casein kinase substrate in neurons protein 1	42	0	29
Q9D281	Protein Noxp20	32	0	5.4
P56565	Protein S100-A1	65	1	45.7
P50114	Protein S100-B	48	1	16.3
A9CB34	Protein SFI1 homolog	45	2	1.7
Q8BG89	Protein ZNF365	25	0	7.1
O35286	Putative pre-mRNA-splicing factor ATP-dependent RNA helicase DHX15	52	1	13.1
Q1RMR4	Ras-related protein Rab-15	60	2	10.4

Q2HJH2	Ras-related protein Rab-1B	60	2	10.9
Q5R615	Ras-related protein Rab-33B	60	2	9.2
Q5U316	Ras-related protein Rab-35	60	2	10.9
P05714	Ras-related protein Rab-4A	60	2	10.3
P35279	Ras-related protein Rab-6A	60	2	13
Q9WUK4	Replication factor C subunit 2	49	1	22.6
Q8K0T0	Reticulon-1	38	0	5.5
Q5DTW2	Scm-like with four MBT domains protein 2	44	1	15.1
Q91WA6	Sharpin	27	0	5.5
Q9QZC1	Short transient receptor potential channel 3; Short=TrpC3	28	0	12.2
O75044	SLIT-ROBO Rho GTPase-activating protein 2	48	1	1.1
P62305	Small nuclear ribonucleoprotein E; Short=snRNP-E	40	0	58.7
P62317	Small nuclear ribonucleoprotein Sm D2; Short=Sm-D2	48	1	74.6
P06583	Sodium/potassium-transporting ATPase subunit beta-1	73	3	12.2
Q3SZR8	Splicing factor, arginine/serine-rich 3	70	5	31.1
Q3T106	Splicing factor, arginine/serine-rich 7	53	5	9.8
Q9CW03	Structural maintenance of chromosomes protein 3; Short=SMC-3	35	0	27
A2AVA0	Sushi, von Willebrand factor type A, EGF and pentraxin domain-containing protein 1	28	0	6.4
P46096	Synaptotagmin-1	150	4	27.8
Q9R0N5	Synaptotagmin-5	50	1	21.2
P01831	Thy-1 membrane glycoprotein	38	0	41.4
Q9Z0U1	Tight junction protein ZO-2	43	1	15
Q01853	Transitional endoplasmic reticulum ATPase	36	0	20.7
Q3UQ41	Transmembrane protease serine 11A	36	0	14.7
Q9EQN3	TSC22 domain family protein 4	29	0	16.5
Q9CQI7	U2 small nuclear ribonucleoprotein B~~	43	1	8
Q91W67	Ubiquitin-like protein 7	38	0	5.3
Q5SYL3	UPF0378 protein KIAA0100	38	0	9.6
Q6NZP2	Vasculin-like protein 1	25	0	26.2
Q9CRC0	Vitamin K epoxide reductase complex subunit 1	45	1	21.7

Q9Z1G4	V-type proton ATPase 116 kDa subunit a isoform 1	39	1	17
Q29048	V-type proton ATPase catalytic subunit A	86	4	9.4
Q91V09	WD repeat-containing protein 13	27	0	17.7
Q8VHI6	Wiskott-Aldrich syndrome protein family member 3	30	0	7.4
Q5GH64	XK-related protein 7	26	0	6.6
Q61329	Zinc finger homeobox protein 3	36	0	9.8

Wild-type + Calcium

CODE	PROTEIN	SCORE	MATCHES	% COVER
Q9CQV8	14-3-3 protein beta/alpha	59	2	39
P62259	14-3-3 protein epsilon	122	6	58
O70456	14-3-3 protein sigma	49	2	9.7
P68254	14-3-3 protein theta	117	9	34
Q8K2J0	1-phosphatidylinositol-4,5-bisphosphate phosphodiesterase delta-3; Short=PLC-delta-3;	23	0	11
O35593	26S proteasome non-ATPase regulatory subunit 14	39	0	14
Q60597	2-oxoglutarate dehydrogenase, mitochondrial	70	10	14
P10852	4F2 cell-surface antigen heavy chain	39	0	14
O35381	Acidic leucine-rich nuclear phosphoprotein 32 family member A	56	3	13
P40124	Adenylyl cyclase-associated protein 1	31	0	24
P57780	Alpha-actinin-4	27	0	14
Q9QYC0	Alpha-adducin	36	0	21
P17182	Alpha-enolase	56	1	39
Q9DB05	Alpha-soluble NSF attachment protein	30	0	38
Q7TQF7	Amphiphysin	39	0	23
O35643	AP-1 complex subunit beta-1	51	1	23
Q9DBG3	AP-2 complex subunit beta	54	1	24
Q9DCX2	ATP synthase subunit d, mitochondrial	107	13	59
Q91VR2	ATP synthase subunit gamma, mitochondrial	113	7	26
O08664	B-cell CLL/lymphoma 7 protein family member C	29	0	16
P21550	Beta-enolase	42	0	15
P12658	Calbindin	46	1	5.7
Q63810	Calcineurin subunit B type 1	50	1	5.9
P35564	Calnexin	39	0	22
P28651	Carbonic anhydrase-related protein	55	2	9.6

Q8CIS0	Caspase recruitment domain-containing protein 11	44	1	17
Q9JKC6	Cell cycle exit and neuronal differentiation protein 1	37	0	19
Q6IRU5	Clathrin light chain B	35	0	37
P18760	Cofilin-1	23	0	13
Q9D5W4	Coiled-coil domain-containing protein 81	27	0	25
Q9CR68	Cytochrome b-c1 complex subunit Rieske, mitochondrial	70	1	22
P00405	Cytochrome c oxidase subunit 2	45	9	28
Q9D0M3	Cytochrome c1, heme protein, mitochondrial	45	1	19
O88487	Cytoplasmic dynein 1 intermediate chain 2	32	0	4.7
Q8CDP0	Cytosolic carboxypeptidase 3	21	0	14
Q3V1L4	Cytosolic purine 5~-nucleotidase	33	0	6.8
P10518	Delta-aminolevulinic acid dehydratase	42	0	24
Q8CFK6	DENN domain-containing protein 1C	30	0	9.2
Q6ZQJ5	DNA2-like helicase	22	0	18
Q8CJ67	Double-stranded RNA-binding protein Staufen homolog 2	44	1	24
Q9Z0Y1	Dynactin subunit 3	38	0	28
Q8BZ98	Dynamin-3; EC=3.6.5.5	68	2	24
Q60900	ELAV-like protein 3	34	0	18
P10126	Elongation factor 1-alpha 1	52	4	8.7
Q9D8N0	Elongation factor 1-gamma	52	1	9.8
Q8BFR5	Elongation factor Tu	39	0	35
P47753	F-actin-capping protein subunit alpha-1	62	4	16
P47754	F-actin-capping protein subunit alpha-2	78	1	54
Q6PDJ6	F-box only protein 42	26	0	5.9
A2AMT1	Filensin	23	0	13
P17183	Gamma-enolase	105	9	26
Q9CWZ7	Gamma-soluble NSF attachment protein	53	1	37
P63216	Guanine nucleotide-binding protein G(I)/G(S)/G(O) subunit gamma-3	37	0	23
P62874	Guanine nucleotide-binding protein G(I)/G(S)/G(T) subunit beta-1	57	1	18
P62880	Guanine nucleotide-binding protein G(I)/G(S)/G(T) subunit beta-2	57	1	13

Q61011	Guanine nucleotide-binding protein G(I)/G(S)/G(T) subunit beta-3	33	0	19
P29387	Guanine nucleotide-binding protein subunit beta-4	57	1	17
P49312	Heterogeneous nuclear ribonucleoprotein A1; Short=hnRNP A1	51	1	20
Q9Z2X1	Heterogeneous nuclear ribonucleoprotein F; Short=hnRNP F	49	1	24
O35737	Heterogeneous nuclear ribonucleoprotein H; Short=hnRNP H	45	1	21
P70333	Heterogeneous nuclear ribonucleoprotein H2; Short=hnRNP H2	45	1	17
Q9D0E1	Heterogeneous nuclear ribonucleoprotein M; Short=hnRNP M	50	2	43
Q8VEK3	Heterogeneous nuclear ribonucleoprotein U; Short=hnRNP U	46	1	18
O08528	Hexokinase-2	50	1	19
P63158	High mobility group protein B1	40	0	46
P30681	High mobility group protein B2	40	0	23
Q8C0N1	Kinesin-like protein KIF2B	26	0	15
P16125	L-lactate dehydrogenase B chain	55	2	30
Q9CR62	Mitochondrial 2-oxoglutarate/malate carrier protein	27	0	34
Q791V5	Mitochondrial carrier homolog 2	43	4	17
Q99LC3	NADH dehydrogenase [ubiquinone] 1 alpha subcomplex subunit 10, mitochondrial	84	2	38
Q9CPP6	NADH dehydrogenase [ubiquinone] 1 alpha subcomplex subunit 5	48	2	23
Q9DCJ5	NADH dehydrogenase [ubiquinone] 1 alpha subcomplex subunit 8	43	0	53
Q9DCS9	NADH dehydrogenase [ubiquinone] 1 beta subcomplex subunit 10	64	1	57
Q9D6J6	NADH dehydrogenase [ubiquinone] flavoprotein 2, mitochondrial	64	2	35
Q8BK30	NADH dehydrogenase [ubiquinone] flavoprotein 3, mitochondrial	28	0	21
Q9DCT2	NADH dehydrogenase [ubiquinone] iron-sulfur protein 3, mitochondrial	70	6	29
Q9CXZ1	NADH dehydrogenase [ubiquinone] iron-sulfur protein 4, mitochondrial	68	2	9.1
Q8K3J1	NADH dehydrogenase [ubiquinone] iron-sulfur protein 8, mitochondrial	58	2	9.4
P35802	Neuronal membrane glycoprotein M6-a	65	1	26
Q61171	Peroxiredoxin-2	30	0	22

Q9R0K7	Plasma membrane calcium-transporting ATPase 2; Short=PMCA2	54	1	17
Q61206	Platelet-activating factor acetylhydrolase IB subunit beta	46	2	11
Q61990	Poly(rC)-binding protein 2	32	0	11
P29341	Polyadenylate-binding protein 1	55	1	30
O35129	Prohibitin-2	89	2	44
P49722	Proteasome subunit alpha type-2	59	1	33
Q9Z2U1	Proteasome subunit alpha type-5	56	1	44
O09061	Proteasome subunit beta type-1	66	7	28
Q9R1P1	Proteasome subunit beta type-3	151	4	48
P99026	Proteasome subunit beta type-4	38	1	30
P28063	Proteasome subunit beta type-8	27	0	23
O88952	Protein lin-7 homolog C	37	0	18
Q9QYX7	Protein piccolo	25	0	10
P50114	Protein S100-B	31	0	33
Q9EQU5	Protein SET	48	1	15
Q9JJ26	Pyrin	33	0	21
P47708	Rabphilin-3A	45	1	22
P61027	Ras-related protein Rab-10	49	1	23
P35283	Ras-related protein Rab-12	49	1	28
Q91V41	Ras-related protein Rab-14	49	1	33
Q8K386	Ras-related protein Rab-15	49	1	23
P62821	Ras-related protein Rab-1A	49	1	14
Q9D1G1	Ras-related protein Rab-1B	49	1	14
Q923S9	Ras-related protein Rab-30	49	1	13
O35963	Ras-related protein Rab-33B	49	1	28
Q6PHN9	Ras-related protein Rab-35	49	1	15
Q9JKM7	Ras-related protein Rab-37	49	1	23
Q8BHD0	Ras-related protein Rab-39A	49	1	18
Q8BHC1	Ras-related protein Rab-39B	49	1	25
P63011	Ras-related protein Rab-3A	49	5	16

Q9CZT8	Ras-related protein Rab-3B	49	1	27
P62823	Ras-related protein Rab-3C	49	1	40
P35276	Ras-related protein Rab-3D	49	5	16
Q8CG50	Ras-related protein Rab-43	49	1	18
P56371	Ras-related protein Rab-4A	49	1	36
Q91ZR1	Ras-related protein Rab-4B	49	1	16
P35279	Ras-related protein Rab-6A	49	1	38
P61294	Ras-related protein Rab-6B	49	1	25
P55258	Ras-related protein Rab-8A	49	1	26
P61028	Ras-related protein Rab-8B	49	5	16
O08899	Regulator of G-protein signaling 4	39	0	49
Q9ES97	Reticulon-3	49	1	9.8
P97363	Serine palmitoyltransferase 2	28	0	18
P63330	Serine/threonine-protein phosphatase 2A catalytic subunit alpha isoform	59	1	26
P48453	Serine/threonine-protein phosphatase 2B catalytic subunit beta isoform	53	1	11
P97470	Serine/threonine-protein phosphatase 4 catalytic subunit	29	0	9.8
O35655	Serine/threonine-protein phosphatase with EF-hands 1	32	0	21
Q8BTK5	SET and MYND domain-containing protein 4	27	0	11
Q8C0T5	Signal-induced proliferation-associated 1-like protein 1; Short=SIPA1-like protein 1	21	0	15
Q80TE4	Signal-induced proliferation-associated 1-like protein 2; Short=SIPA1-like protein 2	21	0	11
Q810C1	SLIT and NTRK-like protein 1	55	1	13
P62315	Small nuclear ribonucleoprotein Sm D1	43	1	56
P61957	Small ubiquitin-related modifier 2	40	0	42
Q8R191	Synaptogyrin-3	40	0	21
Q62277	Synaptophysin	40	0	19
O09117	Synaptophysin-like protein 1	32	0	23
P60879	Synaptosomal-associated protein 25	52	1	69
P61264	Syntaxin-1B	43	0	21

Q9DC40	Telomere length regulation protein TEL2 homolog	42	1	10
P01831	Thy-1 membrane glycoprotein	56	6	32
P63058	Thyroid hormone receptor alpha	33	0	19
A2ASS6	Titin	30	0	9.9
Q9QZ06	Toll-interacting protein	49	3	17
P62869	Transcription elongation factor B polypeptide 2	34	0	5.9
Q9CZX9	Transmembrane protein 85	29	0	20
O35900	U6 snRNA-associated Sm-like protein LSm2	36	0	12
Q8CCC3	Uncharacterized protein C12orf56 homolog	34	0	16
Q8C4P0	Uncharacterized protein KIAA1958 homolog	45	1	19
Q9QZ88	Vacuolar protein sorting-associated protein 29	35	0	30
Q9EQH3	Vacuolar protein sorting-associated protein 35	25	0	17
P63024	Vesicle-associated membrane protein 3; Short=VAMP-3	131	5	40
Q9WV55	Vesicle-associated membrane protein-associated protein A	36	0	10
Q9QY76	Vesicle-associated membrane protein-associated protein B	36	0	25
Q60931	Voltage-dependent anion-selective channel protein 3	84	9	25
Q9Z1G4	V-type proton ATPase 116 kDa subunit a isoform 1	35	0	13
P63082	V-type proton ATPase 16 kDa proteolipid subunit	27	0	12
P62814	V-type proton ATPase subunit B, brain isoform	74	1	34
Q8BXX2	Zinc finger and BTB domain-containing protein 49	50	1	7.5

***Moonwalker* + Calcium**

CODE	PROTEIN	SCORE	MATCHES	% COVER
Q9CQV8	14-3-3 protein beta/alpha	38	0	47.6
P62259	14-3-3 protein epsilon	87	2	62.4
O70456	14-3-3 protein sigma	38	0	20.6
P68254	14-3-3 protein theta	57	1	34.7
O35593	26S proteasome non-ATPase regulatory subunit 14	25	0	26.5
P10852	4F2 cell-surface antigen heavy chain	34	0	10.8
O35381	Acidic leucine-rich nuclear phosphoprotein 32 family member A	35	0	22.7
P40124	Adenylyl cyclase-associated protein 1	42	0	28.5
Q60662	A-kinase anchor protein 4	30	0	31.2
Q9JI91	Alpha-actinin-2	27	0	24.8
P17182	Alpha-enolase	34	0	25.8
P46660	Alpha-internexin	77	1	18.7
Q99JW2	Aminoacylase-1	29	0	19.6
O35643	AP-1 complex subunit beta-1	53	1	21.7
Q9DBG3	AP-2 complex subunit beta	48	1	14.8
P84091	AP-2 complex subunit mu	47	0	19.5
Q3UHJ0	AP2-associated protein kinase 1	28	0	11.2
Q9DCX2	ATP synthase subunit d, mitochondrial	72	9	64
Q99PE8	ATP-binding cassette sub-family G member 5	35	0	10.9
P28652	Calcium/calmodulin-dependent protein kinase type II subunit beta; Short=CaMKII beta	30	0	9.4
P28651	Carbonic anhydrase-related protein	36	0	14.8
Q9JM96	Cdc42 effector protein 4	23	0	12
Q8VDP6	CDP-diacylglycerol--inositol 3-phosphatidyltransferase; AltName: Full=Phosphatidylinositol synthase; Short=PI synthase;	29	0	16
Q9JKC6	Cell cycle exit and neuronal differentiation protein 1	28	0	16.1
A2AJK6	Chromodomain-helicase-DNA-binding protein 7	24	0	15.6

Q9DA73	Coiled-coil domain-containing protein 89	47	1	26.8
Q9CR68	Cytochrome b-c1 complex subunit Rieske, mitochondrial	98	2	34.7
Q38RW5	Cytochrome c oxidase subunit 2	54	11	27.8
P43024	Cytochrome c oxidase subunit 6A1, mitochondrial	42	0	35.1
Q9CPQ1	Cytochrome c oxidase subunit 6C	55	1	46.1
Q8CHS7	Dehydrogenase/reductase SDR family member 7C	25	0	27
Q8C4S8	DENN domain-containing protein 2A	28	0	10.2
O55111	Desmoglein-2	44	1	4.2
Q9D2G2	Dihydrolipoyllysine-residue succinyltransferase component of 2-oxoglutarate dehydrogenase complex, mitochondrial	41	0	22.7
Q9Z0Y1	Dynactin subunit 3	41	0	24.2
P10126	Elongation factor 1-alpha 1	51	1	24.7
Q9D8N0	Elongation factor 1-gamma	90	1	15.3
P19096	Fatty acid synthase	34	0	10.6
P17183	Gamma-enolase	51	1	28.1
A4FUP9	Glycosyltransferase 1 domain-containing protein 1	35	0	5.8
P62874	Guanine nucleotide-binding protein G(I)/G(S)/G(T) subunit beta-1	42	0	15.3
P62880	Guanine nucleotide-binding protein G(I)/G(S)/G(T) subunit beta-2	42	0	16.2
P29387	Guanine nucleotide-binding protein subunit beta-4	42	0	19.1
Q9Z2X1	Heterogeneous nuclear ribonucleoprotein F; Short=hnRNP F	44	1	20.2
O35737	Heterogeneous nuclear ribonucleoprotein H; Short=hnRNP H	86	3	37.6
P70333	Heterogeneous nuclear ribonucleoprotein H2; Short=hnRNP H2	72	3	26.9
O08528	Hexokinase-2	50	1	19.7
P70298	Homeobox protein cut-like 2	33	0	9.4
Q63ZW7	InaD-like protein	29	0	6.6
P15261	Interferon gamma receptor 1	22	0	15.1
Q6S5J6	Krev interaction trapped protein 1	27	0	10.5
P14733	Lamin-B1	34	0	28.7
P21619	Lamin-B2	34	0	21.5
Q61001	Laminin subunit alpha-5	27	0	13.8
Q3UZ39	Leucine-rich repeat flightless-interacting protein 1	44	1	19.3

P16125	L-lactate dehydrogenase B chain	43	1	17.4
Q99PU5	Long-chain-fatty-acid--CoA ligase ACSBG1	61	1	18.7
Q9ET37	Low affinity sodium-glucose cotransporter	30	0	11
P49300	Macrophage asialoglycoprotein-binding protein 1	50	1	10.5
Q99M71	Mammalian ependymin-related protein 1; Short=MERP-1;	34	0	4.9
P14404	MDS1 and EVI1 complex locus protein EVI1	31	0	20.1
Q9QYR6	Microtubule-associated protein 1A; Short=MAP-1A	32	0	7.1
P14873	Microtubule-associated protein 1B; Short=MAP-1B	32	0	11.8
Q791V5	Mitochondrial carrier homolog 2	52	1	12.9
O55236	mRNA-capping enzyme	29	0	24.1
O08539	Myc box-dependent-interacting protein 1	35	0	6.6
Q8K224	N-acetyltransferase 10	29	0	6.4
Q9CQ75	NADH dehydrogenase [ubiquinone] 1 alpha subcomplex subunit 2	64	1	14.1
Q9DCS9	NADH dehydrogenase [ubiquinone] 1 beta subcomplex subunit 10	57	1	39.2
Q9D6J6	NADH dehydrogenase [ubiquinone] flavoprotein 2, mitochondrial	76	2	41.5
Q8BK30	NADH dehydrogenase [ubiquinone] flavoprotein 3, mitochondrial	31	0	10.6
Q9DCT2	NADH dehydrogenase [ubiquinone] iron-sulfur protein 3, mitochondrial	32	0	31.9
P08553	Neurofilament medium polypeptide; Short=NF-M	43	1	23.9
P97300	Neuroplastin	42	0	23.2
Q80TM9	Nischarin	34	0	6.2
Q9WV85	Nucleoside diphosphate kinase 3	43	1	13.6
Q9D0J8	Parathymosin	47	1	10.9
Q61171	Peroxiredoxin-2	32	0	37.4
O70362	Phosphatidylinositol-glycan-specific phospholipase D; Short=PI-G PLD	43	1	5.4
Q68FH0	Plakophilin-4	28	0	9.3
Q9R0K7	Plasma membrane calcium-transporting ATPase 2; Short=PMCA2	37	0	21.6
Q91VN6	Probable ATP-dependent RNA helicase DDX41	27	0	19.8
Q8VDC0	Probable leucyl-tRNA synthetase, mitochondrial	47	1	15.5
O35129	Prohibitin-2	69	1	35.8

P49722	Proteasome subunit alpha type-2	63	1	44.4
Q9Z2U1	Proteasome subunit alpha type-5	65	1	42.3
O09061	Proteasome subunit beta type-1	80	2	41.2
Q9R1P1	Proteasome subunit beta type-3	117	6	26.8
P99026	Proteasome subunit beta type-4	25	0	29.9
Q8BJH1	Protein FAM164A	28	0	34.3
O88951	Protein lin-7 homolog B	39	0	17.4
Q0P5F3	Protein lin-7 homolog C	54	4	25.4
P50114	Protein S100-B	49	1	27.2
Q9EQU5	Protein SET	41	0	13.5
A2A690	Protein TANC2	31	0	9.3
Q64G17	Putative acidic leucine-rich nuclear phosphoprotein 32 family member C	35	0	20.3
P61027	Ras-related protein Rab-10	49	1	35.5
P35283	Ras-related protein Rab-12	49	1	31.3
Q91V41	Ras-related protein Rab-14	49	1	36.3
Q8K386	Ras-related protein Rab-15	49	1	29.2
P62821	Ras-related protein Rab-1A	49	1	35.1
Q504M8	Ras-related protein Rab-26	49	1	27.3
Q923S9	Ras-related protein Rab-30	49	1	10.8
O35963	Ras-related protein Rab-33B	49	1	23.1
Q6PHN9	Ras-related protein Rab-35	49	1	35.8
Q9JKM7	Ras-related protein Rab-37	49	1	16.6
Q8BHD0	Ras-related protein Rab-39A	49	1	29
Q8BHC1	Ras-related protein Rab-39B	49	1	23
Q4R4R9	Ras-related protein Rab-3A	60	5	20
Q9CZT8	Ras-related protein Rab-3B	49	1	26.5
P62823	Ras-related protein Rab-3C	49	1	32.2
P35276	Ras-related protein Rab-3D	49	1	27.9
Q8CG50	Ras-related protein Rab-43	49	1	9.5
P56371	Ras-related protein Rab-4A	49	1	35.7

Q91ZR1	Ras-related protein Rab-4B	49	1	25.8
P61294	Ras-related protein Rab-6B	49	1	29.8
P55258	Ras-related protein Rab-8A	49	1	27.5
P61028	Ras-related protein Rab-8B	49	1	46.9
Q9ES97	Reticulon-3	40	0	7.7
Q8JZV4	RNA-binding protein 41	25	0	28.1
O55131	Septin-7	34	0	25.7
Q76MZ3	Serine/threonine-protein phosphatase 2A 65 kDa regulatory subunit A alpha isoform	35	0	20.9
P48453	Serine/threonine-protein phosphatase 2B catalytic subunit beta isoform	33	0	12
Q8C0Y0	Serine/threonine-protein phosphatase 4 regulatory subunit 4	45	1	12.5
Q6NZL8	Signal peptide, CUB and EGF-like domain-containing protein 1	30	0	11.4
P62309	Small nuclear ribonucleoprotein G; Short=snRNP-G	52	1	43.4
P62315	Small nuclear ribonucleoprotein Sm D1; Short=Sm-D1	59	1	47.9
P62317	Small nuclear ribonucleoprotein Sm D2; Short=Sm-D2	51	1	56.8
Q9Z172	Small ubiquitin-related modifier 3; Short=SUMO-3	43	0	44.5
Q80TB8	Synaptic vesicle membrane protein VAT-1 homolog-like	47	1	11.3
Q8R191	Synaptogyrin-3	26	0	14
Q62277	Synaptophysin	39	0	22
P60879	Synaptosomal-associated protein 25; Short=SNAP-25	48	1	60.7
P46096	Synaptotagmin-1	83	5	10.9
P46097	Synaptotagmin-2	86	2	26.3
Q9R0N5	Synaptotagmin-5	48	1	18.7
P80314	T-complex protein 1 subunit beta	43	1	28.8
Q9D411	Testis-specific serine/threonine-protein kinase 4	43	1	11.9
P01831	Thy-1 membrane glycoprotein	38	0	27.8
Q9Z0U1	Tight junction protein ZO-2	20	0	13.4
P62869	Transcription elongation factor B polypeptide 2	36	0	7.6
P48301	Transcriptional enhancer factor TEF-4	29	0	16.2
Q01853	Transitional endoplasmic reticulum ATPase	53	6	6.6

Q9Y333	U6 snRNA-associated Sm-like protein LSm2	65	2	31.6
P62814	V-type proton ATPase subunit B, brain isoform	68	2	36.6
P31407	V-type proton ATPase subunit B, kidney isoform	59	4	17
Q9CR51	V-type proton ATPase subunit G 1	25	0	32.2
Q9WTT4	V-type proton ATPase subunit G 2	29	0	41.5

Appendix B. Microarray Results comparing gene expression between wild-type and *Moonwalker* Purkinje cells

Combined list for PLIER and RMA algorithms

Transcripts Cluster Id	Regulation	PLIER p-value	PLIER Fold change	PLIER WT signal	PLIER Mwk signal	RMA p-value	RMA Fold change	RMA WT signal	RMA Mwk signal	Gene Symbol
10594963	**down**	**0.0011**	**10.6**	**260**	**23**	**1.5E-04**	**8.2**	**232**	**26**	**Unc13c**
10406530	down	0.0186	7.1	367	64	-	-	-	-	Tmem167
10388033	down	0.0386	6.6	280	69	-	-	-	-	Derl2
10570432	up	-	-	-	-	2.7E-02	6.0	58	518	Snora3
10424411	**down**	**0.0459**	**5.9**	**758**	**185**	**1.4E-02**	**3.3**	**582**	**188**	**Tsg101**
10468309	down	0.0118	5.8	415	87	-	-	-	-	Sh3pxd2a
10531284	**down**	**0.0275**	**5.7**	**861**	**181**	**1.4E-02**	**3.6**	**765**	**220**	**Trmt112**
10514956	down	0.0327	5.7	603	125	-	-	-	-	Scp2
10569319	up	0.0347	5.7	136	551	-	-	-	-	Ctsd
10435769	**up**	**0.0265**	**5.6**	**88**	**405**	**3.1E-02**	**1.9**	**113**	**219**	**Zbtb20**
10360454	**up**	**0.0242**	**5.1**	**748**	**3068**	**1.4E-03**	**3.7**	**157**	**569**	**Opn3**

10489343	down	0.0424	4.9	275	49	-	-	-	-	Ptpla
10408677	down	0.0337	4.7	739	168	-	-	-	-	Lyrm4
10557644	**up**	**0.0144**	**4.5**	**153**	**699**	**4.0E-02**	**2.3**	**164**	**401**	**Fbrs**
10411274	**up**	**0.0104**	**4.4**	**229**	**910**	**1.6E-03**	**3.4**	**169**	**567**	**Sv2c**
10542959	**up**	**0.0312**	**4.2**	**86**	**298**	**1.4E-02**	**1.9**	**81**	**159**	**Bet1**
10373367	up	0.0453	4.1	306	1046	-	-	-	-	Coq10a
10535780	**down**	**0.0017**	**4.0**	**471**	**122**	**1.5E-02**	**1.5**	**149**	**97**	**Flt3**
10477006	**up**	**0.0248**	**3.9**	**56**	**252**	**1.0E-02**	**2.2**	**33**	**80**	**Nsfl1c**
10427718	down	0.0064	3.9	302	80	-	-	-	-	Brix1
10497765	down	0.0382	3.8	687	201	-	-	-	-	Dcun1d1
10600718	up	0.0499	3.7	204	629	-	-	-	-	Sec61g
10454912	**up**	**0.0213**	**3.6**	**93**	**307**	**5.7E-04**	**1.6**	**73**	**119**	**Eif4ebp3**
10556133	up	-	-	-	-	4.7E-02	3.6	35	182	Styx
10523001	up	0.0147	3.5	178	648	-	-	-	-	Mobkl1a
10470665	up	0.0277	3.4	107	374	-	-	-	-	Setx
10550022	down	0.0101	3.4	946	263	-	-	-	-	Psip1
10417070	**up**	**0.0001**	**3.2**	**452**	**1469**	**7.0E-04**	**2.5**	**312**	**798**	**Ipo5**

10452213	**up**	**0.0050**	**3.2**	**122**	**377**	**5.1E-03**	**2.0**	**74**	**145**	**Gtf2f1**
10470788	**up**	**0.0276**	**2.9**	**127**	**331**	**3.6E-02**	**1.6**	**110**	**174**	**Odf2**
10540599	down	-	-	-	-	1.6E-03	2.9	478	165	Cpne9
10409278	up	-	-	-	-	9.8E-03	2.9	106	291	Nfil3
10407543	down	0.0188	2.9	396	147	-	-	-	-	Gtpbp4
10369702	up	0.0309	2.9	154	429	-	-	-	-	Tet1
10433996	down	0.0411	2.9	551	217	-	-	-	-	Snap29
10542857	**down**	**0.0462**	**2.8**	**2117**	**845**	**3.0E-02**	**2.0**	**648**	**343**	**Far2**
10404774	up	0.0244	2.7	115	294	-	-	-	-	Hivep1
10402117	down	0.0347	2.7	335	137	-	-	-	-	Rps6ka5
10608385	up	0.0219	2.7	92	230	-	-	-	-	Sly
10520368	up	0.0348	2.6	159	442	-	-	-	-	En2
10493758	**down**	**0.0236**	**2.5**	**796**	**312**	**2.4E-02**	**2.0**	**399**	**185**	**Gatad2b**
10502191	down	-	-	-	-	3.9E-02	2.5	552	227	Ostc
10411454	up	-	-	-	-	2.3E-02	2.5	143	397	Sec61b
10426301	up	-	-	-	-	2.2E-02	2.5	271	694	Tcea1
10575302	down	0.0466	2.5	292	105	-	-	-	-	Ap1g1

10604595	up	0.0046	2.5	27	69	-	-	-	-	Mir106a
10490923	down	-	-	-	-	4.1E-02	2.4	336	118	Car2
10453231	down	-	-	-	-	3.8E-02	2.4	282	116	Slc8a1
10565514	up	-	-	-	-	2.2E-02	2.4	322	704	Tmem126a
10397189	up	0.0208	2.4	52	122	-	-	-	-	Ptgr2
10578361	up	0.0329	2.4	186	433	-	-	-	-	Asah1
10379866	up	-	-	-	-	3.4E-02	2.3	148	365	Car4
10605616	down	-	-	-	-	4.4E-02	2.3	98	37	Il1rapl1
10377982	up	0.0484	2.3	381	868	-	-	-	-	Kif1c
10566870	up	0.0377	2.3	167	365	-	-	-	-	Tmem41b
10546736	**up**	**0.0064**	**2.2**	**105**	**238**	**3.7E-03**	**1.6**	**77**	**125**	**Cntn3**
10369877	**down**	**0.0347**	**2.2**	**896**	**428**	**2.3E-02**	**1.8**	**694**	**397**	**Ube2d1**
10487267	**down**	**0.0179**	**2.2**	**1321**	**616**	**3.4E-02**	**2.1**	**1061**	**509**	**Polr2l**
10401028	**down**	**0.0265**	**2.2**	**478**	**210**	**3.8E-02**	**1.7**	**127**	**72**	**Sgpp1**
10417689	**down**	**0.0436**	**2.2**	**1094**	**541**	**2.3E-02**	**2.2**	**996**	**486**	**Psmd6**
10388465	down	-	-	-	-	2.9E-02	2.2	315	133	Doc2b
10590320	down	-	-	-	-	5.1E-03	2.2	309	132	Rpl14

10585091	up	-	-	-	-	3.8E-02	2.2	230	484	Nhp2l1
10432573	down	0.0304	2.2	201	95	-	-	-	-	Slc11a2
10420572	up	0.0437	2.2	205	450	-	-	-	-	Nupl1
10492402	down	0.0296	2.2	873	424	-	-	-	-	Kcnab1
10481868	up	0.0455	2.2	878	1798	-	-	-	-	Dnajb6
10465683	down	0.0020	2.2	749	344	-	-	-	-	Rab11b
10543904	**down**	**0.0337**	**2.1**	**1004**	**497**	**3.9E-04**	**1.6**	**305**	**191**	**Cnot4**
10523893	**down**	**0.0454**	**2.1**	**1810**	**839**	**2.3E-02**	**1.9**	**942**	**474**	**Rpl5**
10435075	**up**	**0.0426**	**2.1**	**352**	**676**	**1.8E-02**	**2.1**	**116**	**237**	**Tfrc**
10361748	down	-	-	-	-	2.1E+00	down	124	57	Fbxo30
10436402	down	-	-	-	-	2.1E+00	down	770	371	Cldnd1
10525877	down	-	-	-	-	2.1E+00	down	526	273	Zfp664
10355960	up	0.0160	2.1	497	1050	-	-	-	-	Scg2
10503161	up	0.0374	2.1	229	505	-	-	-	-	Chd7
10440314	up	0.0117	2.1	221	469	-	-	-	-	Cadm2
10438626	up	0.0229	2.1	351	695	-	-	-	-	Etv5
10404051	down	0.0295	2.1	704	331	-	-	-	-	Hist1h4d

10514985	**up**	**0.0475**	**2.0**	**216**	**406**	**5.8E-03**	**1.8**	**65**	**115**	**Zyg11b**
10441422	**down**	**0.0287**	**2.0**	**1610**	**825**	**3.7E-02**	**1.7**	**868**	**527**	**Zdhhc14**
10474915	**down**	**0.0097**	**2.0**	**1220**	**630**	**1.4E-02**	**1.7**	**811**	**484**	**Gchfr**
10574204	down	-	-	-	-	8.7E-03	2.0	223	111	Arl2bp
10434366	up	0.0384	2.0	343	673	-	-	-	-	Dvl3
10425158	**down**	**0.0183**	**1.9**	**577**	**314**	**1.9E-02**	**1.8**	**282**	**164**	**Pdxp**
10597515	down	-	-	-	-	3.2E-02	1.9	809	430	Rpl24
10491354	down	-	-	-	-	1.5E-02	1.9	142	73	Zfp639
10547830	up	-	-	-	-	3.3E-02	1.9	265	496	Tpi1
10501265	up	-	-	-	-	3.8E-02	1.9	53	108	Gnai3
10515983	down	-	-	-	-	6.4E-06	1.9	94	50	Dem1
10580331	up	-	-	-	-	3.9E-02	1.9	120	227	Vps35
10594144	up	0.0260	1.9	58	112	-	-	-	-	Bbs4
10369086	down	0.0212	1.9	411	208	-	-	-	-	Gopc
10592701	down	0.0237	1.9	123	66	-	-	-	-	Tmem136
10474516	down	0.0487	1.9	35	18	-	-	-	-	Olfr1302
10554269	down	0.0097	1.9	474	249	-	-	-	-	Abhd2

10461663	down	0.0221	1.9	803	412	-	-	-	-	Mrpl16
10503534	down	0.0144	1.9	398	213	-	-	-	-	Ccnc
10533659	up	0.0402	1.9	320	583	-	-	-	-	Clip1
10478374	down	0.0284	1.9	208	115	-	-	-	-	Gdap1l1
10407833	down	0.0285	1.9	868	485	-	-	-	-	Ggps1
10556113	**up**	**0.0393**	**1.8**	**838**	**1497**	**4.9E-03**	**1.7**	**70**	**120**	**Rbm3**
10478647	**down**	**0.0289**	**1.8**	**673**	**392**	**1.8E-03**	**1.8**	**226**	**127**	**Slc12a5**
10556463	down	-	-	-	-	4.3E-02	1.8	218	115	Arntl
10415574	up	-	-	-	-	1.1E-02	1.8	450	823	Ccni
10590791	down	-	-	-	-	2.6E-02	1.8	213	122	Birc2
10395287	up	-	-	-	-	4.4E-02	1.8	95	168	Atxn7l1
10403108	down	-	-	-	-	2.6E-02	1.8	297	161	Hmgn2
10387659	up	-	-	-	-	3.4E-02	1.8	183	334	Nlgn2
10574096	down	-	-	-	-	1.8E-02	1.8	607	351	Ap3s1
10454286	up	0.0295	1.8	1043	1864	-	-	-	-	Mapre2
10506714	down	0.0106	1.8	668	364	-	-	-	-	Lrp8
10549945	down	0.0147	1.8	122	66	-	-	-	-	Vmn1r67

10574962	up	0.0436	1.8	102	178	-	-	-	-	Nfatc3
10362829	down	0.0488	1.8	327	183	-	-	-	-	Ostm1
10457546	down	0.0306	1.8	611	356	-	-	-	-	Osbpl1a
10555460	down	0.0321	1.8	435	254	-	-	-	-	Stard10
10424370	**up**	**0.0033**	**1.7**	**671**	**1125**	**1.6E-03**	**1.5**	**112**	**171**	**Trib1**
10388884	**down**	**0.0412**	**1.7**	**1467**	**904**	**4.8E-03**	**1.7**	**963**	**569**	**Nlk**
10446656	**up**	**0.0394**	**1.7**	**259**	**448**	**2.2E-02**	**1.6**	**164**	**263**	**Lpin2**
10577544	**down**	**0.0437**	**1.7**	**777**	**478**	**3.6E-02**	**1.5**	**486**	**312**	**Polb**
10457606	down	-	-	-	-	3.8E-03	1.7	1202	686	Kctd1
10578019	up	-	-	-	-	4.3E-02	1.7	224	400	Nudc
10381345	up	-	-	-	-	3.1E-03	1.7	176	299	Psme3
10606083	up	-	-	-	-	4.7E-02	1.7	107	192	Cited1
10495285	down	-	-	-	-	3.6E-02	1.7	217	129	Sort1
10570418	up	-	-	-	-	3.1E-02	1.7	110	191	Upf3a
10595981	up	-	-	-	-	1.8E-02	1.7	167	294	Mras
10536334	down	-	-	-	-	2.1E-02	1.7	87	50	Dync1i1
10407097	up	-	-	-	-	8.0E-03	1.7	92	152	Pde4d

10485395	up	0.0447	1.7	700	1214	-	-	-	-	Trim44
10436442	down	0.0288	1.7	219	124	-	-	-	-	Fam60a
10354258	down	0.0149	1.7	299	173	-	-	-	-	Uxs1
10498415	down	0.0398	1.7	978	590	-	-	-	-	Dhx36
10474541	down	0.0277	1.7	2242	1337	-	-	-	-	Nop10
10594661	up	0.0130	1.7	837	1391	-	-	-	-	Tpm1
10399198	down	0.0266	1.7	372	218	-	-	-	-	Ncoa4
10517706	down	0.0295	1.7	695	418	-	-	-	-	Mrto4
10481711	up	0.0203	1.7	842	1383	-	-	-	-	Stxbp1
10521136	up	0.0268	1.7	269	443	-	-	-	-	Whsc1
10441107	down	0.0064	1.7	509	311	-	-	-	-	Psmg1
10544523	**up**	**0.0244**	**1.6**	**72**	**120**	**3.1E-02**	**1.6**	**37**	**62**	**Rny1**
10569886	**down**	**0.0370**	**1.6**	**1233**	**761**	**2.2E-02**	**1.6**	**694**	**434**	**Trappc5**
10455588	**down**	**0.0177**	**1.6**	**3875**	**2518**	**4.9E-03**	**1.6**	**3321**	**2132**	**Hspe1**
10600349	up	-	-	-	-	2.6E-02	1.6	320	521	Rpl10
10497149	down	-	-	-	-	6.8E-04	1.6	187	114	Wls
10579874	down	-	-	-	-	2.7E-02	1.6	371	227	Abce1

10584024	down	-	-	-	-	9.6E-03	1.6	259	160	Opcml
10455080	up	-	-	-	-	4.9E-02	1.6	75	128	Pcdhb9
10352393	down	-	-	-	-	4.2E-02	1.6	546	355	Srp9
10508182	up	-	-	-	-	1.5E-02	1.6	394	633	Psmb2
10363146	up	-	-	-	-	2.7E-02	1.6	70	110	Slc35f1
10586240	up	-	-	-	-	3.2E-02	1.6	52	87	Dennd4a
10408074	down	-	-	-	-	4.7E-02	1.6	528	325	Hist1h4h
10401181	down	-	-	-	-	2.0E-02	1.6	98	60	Rdh11
10514884	up	-	-	-	-	5.0E-02	1.6	141	230	Mrpl37
10596796	up	-	-	-	-	1.0E-02	1.6	114	184	Rbm6
10493995	down	-	-	-	-	2.8E-02	1.6	136	88	S100a10
10397085	up	-	-	-	-	3.4E-02	1.6	354	549	Rbm25
10394735	down	-	-	-	-	4.9E-02	1.6	190	123	Pdia6
10345882	down	-	-	-	-	1.6E-02	1.6	213	134	Mrps9
10547789	down	-	-	-	-	4.3E-02	1.6	553	347	Grcc10
10472418	up	0.0491	1.6	79	126	-	-	-	-	Scn9a
10357454	down	0.0439	1.6	326	207	-	-	-	-	Dars

10424746	down	0.0161	1.6	149	91	-	-	-	-	Zfp623
10491704	up	0.0012	1.6	89	144	-	-	-	-	Spata5
10463505	down	0.0083	1.6	387	237	-	-	-	-	Dpcd
10473261	up	0.0338	1.6	71	116	-	-	-	-	Fsip2
10483824	down	0.0006	1.6	50	32	-	-	-	-	Ttc30a1
10584376	up	0.0367	1.6	34	53	-	-	-	-	Olfr889
10350331	down	0.0313	1.6	490	316	-	-	-	-	Zfp281
10394690	down	0.0095	1.6	120	76	-	-	-	-	E2f6
10368999	down	0.0456	1.6	183	117	-	-	-	-	Grik2
10361007	up	0.0199	1.6	195	310	-	-	-	-	Smyd2
10444814	up	0.0294	1.6	56	87	-	-	-	-	H2-gs10
10573519	up	0.0441	1.6	179	279	-	-	-	-	Tnpo2
10356194	up	0.0196	1.6	648	1001	-	-	-	-	Trip12
10482139	down	0.0000	1.6	463	298	-	-	-	-	Pdcl
10494804	down	0.0085	1.6	795	516	-	-	-	-	Casq2
10602166	**down**	**0.0463**	**1.5**	**464**	**308**	**3.1E-02**	**1.6**	**181**	**112**	**Nxt2**
10354588	**down**	**0.0014**	**1.5**	**3649**	**2419**	**2.3E-03**	**1.7**	**1842**	**1106**	**Stk17b**

10484249	down	-	-	-	-	3.9E-02	1.5	140	92	Cwc22
10581073	down	-	-	-	-	8.9E-04	1.5	176	113	Dync1li2
10606864	up	-	-	-	-	3.2E-02	1.5	802	1237	Tceal5
10498620	down	-	-	-	-	1.0E-02	1.5	71	45	Trim59
10478495	down	-	-	-	-	4.8E-04	1.5	342	223	Dbndd2
10360460	up	-	-	-	-	8.2E-03	1.5	55	84	Chml
10438358	down	-	-	-	-	3.5E-02	1.5	361	239	Gp1bb
10581772	down	-	-	-	-	1.6E-02	1.5	440	285	Glg1
10469622	up	-	-	-	-	2.8E-02	1.5	61	95	Gpr158
10517421	down	-	-	-	-	1.9E-02	1.5	316	209	Pnrc2
10455092	up	-	-	-	-	4.6E-02	1.5	38	58	Pcdhb12
10571978	down	-	-	-	-	4.4E-02	1.5	128	83	Cbr4
10598678	down	0.0467	1.5	958	628	-	-	-	-	Usp9x
10579125	up	0.0496	1.5	51	79	-	-	-	-	Gatad2a
10586180	down	0.0303	1.5	191	122	-	-	-	-	Uchl4
10351471	up	0.0439	1.5	56	88	-	-	-	-	Uhmk1
10385283	down	0.0494	1.5	1164	739	-	-	-	-	Gabrg2

10416279	up	0.0078	1.5	63	96	-	-	-	-	Lgi3
10522430	up	0.0139	1.5	296	452	-	-	-	-	Dcun1d4
10567512	up	0.0382	1.5	35	53	-	-	-	-	Dnahc3
10428211	down	0.0285	1.5	444	295	-	-	-	-	Zfp706
10485798	down	0.0157	1.5	29	19	-	-	-	-	Olfr1307
10397377	down	0.0156	1.5	2893	1917	-	-	-	-	Ttll5
10416340	down	0.0153	1.5	696	464	-	-	-	-	Gfra2
10568629	up	0.0104	1.5	77	116	-	-	-	-	Mmp21
10498371	up	0.0097	1.5	38	58	-	-	-	-	P2ry12
10444431	up	0.0007	1.5	109	164	-	-	-	-	Prrt1
10477644	up	0.0375	1.5	205	307	-	-	-	-	Trp53inp2
10428842	up	0.0493	1.5	389	583	-	-	-	-	Rnf139
10589784	down	0.0187	1.5	135	89	-	-	-	-	Dclk3